Design, Synthesis, And Biological Evaluation of Anti-HIV and Anti-plasmodial Activities of Some Hydroxypyridinone-aminoquinoline Derivatives.

by

Tinotenda Deoleen Munapo

21016426

Research Dissertation for the Master of Science Degree in Chemistry

in the Department of Chemistry

Faculty of Science, Engineering and Agriculture

University of Venda

Thohoyandou, Limpopo Province, South Africa

Supervisor: Dr M. V Bvumbi

Co-supervisor: Dr W. A Andayi (Murang'a University of Technology, Kenya)

Declaration

I, Munapo Tinotenda Deoleen (21016426), declare that MSc dissertation titled **Design, Synthesis, And Biological Evaluation of Anti-HIV and Anti-plasmodial Activities of Some Hydroxypyridinone-aminoquinoline Derivatives** is my own work done under the supervision of **Dr M.V Bvumbi** and **Dr W.A Andayi**. This dissertation is my original work and has not been submitted for any degree at any other university or institution for examination. The dissertation does not contain other persons' writing unless specifically acknowledged and referenced accordingly. This work is being submitted for an MSc in chemistry at the University of Venda.

Signature: 

Date: 06 December 2024

Abstract

Malaria and HIV-AIDS are fatal infectious diseases. Given the overlap of their geographic distribution and resultant coinfection rates, interactions between the two diseases pose major public health problems are the most vulnerable population groups. Young children and pregnant women are the most vulnerable population groups, yet they have limited medication options because of immunocompromising. The levels of CYP3A4 in children and pregnant women is elevated and thus necessitating dose adjustments for most drugs in clinical use to achieve treatment success. Without the dose adjustment the resultant low drug bioavailability exposes pathogens to sub-optimal dosages thus fomenting drug resistance. Hydroxypyridinone-aminoquinoline (HPO-AQS) compounds which were found to be potent CYP3A4 inhibitors, could be repurposed as antimalarials and anti-HIV specifically for children and expectant mothers. Thus, the study also aims at repurposing HPO-AQS for treatment of HIV-AIDS and malaria coinfections. Despite the CYP3A4 liability of the HPO-AQs, these molecules can be repurposed for chemotherapeutic applications in cancer and HIV-AIDS where CYP3A4 inhibition is not an issue if risk and benefit analysis is carefully considered.

The rational design was based on quinoline as an antimalarial pharmacophore and iron chelation inhibition of plasmodium proliferation in addition to studies earlier done by Andayi et al. The HPO-AQS were designed in two series (kojic derivatives and maltol derivatives) in such a way that they have a chelator (HPO) linked to quinoline nucleus with varying linker lengths. Thereafter, the *in-silico* predictions were done using SwissADME. The attention of this work was focused on the predictions of lipophilicity, physicochemical properties, and CYP isoform targets. SwissADME results predicted that HPO-AQs could be developed as synthetic medical products. This has been the basis of subsequent synthesis and *in vitro* studies.

The kojic derived compounds **(1a-l)** were prepared by coupling N-(7-chloro-4-quinolinyl)-diaminoalkanes **(6a-g)** to 2-(chloromethyl)-5 (benzyloxy)-1-alkylpyridin-4-(*1H*)-ones **(3a-3c)**. The synthesis of the maltol-derived **(2a-i)** conjugates involved the Michael addition of *N*-(7-chloro-4- quinolinyl)-diaminoalkanes **(6a-g)** to 3-benzyl protected methyl maltol **(10a)** or protected ethyl maltol **(10b).** Nuclear magnetic resonance spectroscopy and Mass Spectroscopy confirmed the successful synthesis of all the target compounds. The target compounds were evaluated for their cytotoxicities, anti-HIV, antiplasmodial, anticancer and antioxidant activities *in vitro*.

A general observation on the toxicities of all the compounds, when evaluated on three different cell lines, is that maltol-derived compounds (2b and 2d) were more toxic compared to the kojic-derived compounds (**1a**, **1b**, **1f** and **1g**). With this observation, the kojic moiety counteracts the toxic effects caused by the quinoline scaffold better than the maltol moiety.

Based on the TZM-bI cells MTT assays, the most nontoxic compounds [**1b; 1e; 1f; 1g and 2b**] with relatively higher IC_{50} values, were further evaluated for anti-HIV (Reverse Transcription Inhibition and HIV Protease Activity inhibition) and antioxidant activities. The compounds with lower cytotoxicity IC_{50} values in the TZM bl cell line [**1a** and **2d**] were further evaluated for their anti-cancer properties using the Nitric Oxide Assays. In the reverse transcriptase assays, **1e** (IC_{50} = 26.2±0.19µM) and **1f** (IC_{50} = 32.90±3.79µM) were the better inhibitors whilst **1g** (IC_{50} = 56.56 ± 0.74µM) was the least inhibitor. In the protease inhibition assay, **1e** was the best inhibitor (in relation to the positive control). Of the two evaluated compounds, **1a** and **2d**, none of them produced nitric oxide as expected, as the tested compounds were not very toxic but moderately toxic in the cytotoxic assays, as observed by the cytotoxicity results. The protected HPO-AQS showed no antioxidative potential, and **1b** only showed antioxidant properties but only in high concentrations.

The antiplasmodial activities of HPO-AQS were evaluated against the chloroquine drug-sensitive (NF54) and the chloroquine drug-resistant strains (K1). These activities on the wild-type isolate, *P. falciparum* Nf54, range from moderate to very high, with some IC_{50} values below 20nM, which is comparable to the control antimalarial agents. Resistance indices analysis showed that most of the compounds had values greater than 5, except for **1a** with RI = 3.5. However, there is cross-resistance for the rest of the compounds, which can be expected of these compounds due to their 7-chloroquinoline moiety.

Keywords: Co-infection, HIV-AIDS, Malaria, Hydroxypyridinone-aminoquinolines.

Acknowledgements

First and foremost, praise, thanks, and honour unto YAHWEH, the ALMIGHTY, for HIS grace and blessings throughout my research work. Thank you for making it possible and taking me this far.

I wish to extend my heartfelt gratitude to my research supervisors (Dr M.V Bvumbi and Dr W.A Andayi) for their unwavering support and guidance throughout the completion of my MSc studies. Your collaboration efforts, outsourcing research materials and opportunities, thoughtful feedback and constant encouragement have honed my skills and enriched this thesis's quality. Thank you for allowing me to attend the Frank Warren Organic Chemistry Conference (2023) the SACI North Young Symposium; with your assistance, I managed to attend the DMPK 101 course offered by the University of Dundee (UK).

I'd also like to acknowledge the contributions of my fellow researchers and the resources provided by the Chemistry Department and the University of Venda. Special mention to Mr P. Pandelani for running NMR analyses and Mr F. Mutshaeni for providing me with laboratory resources crucial for me to do my synthesis experiments and for making it possible for me to attend the API Process Technology Day at CPT-Pharma in Pretoria.

I extend my appreciation to my fellow lab mates for assisting and entertaining me in the Drug Synthesis and Isolation/ Design, Synthesis and Biomolecular Research Group lab for constructive contributions towards this study while allowing me to build myself.

This acknowledgement extends to Dr NG Gama and Ms SK Khuzwayo, and the rest of the HIV research group at the University of Pretoria for hosting me in their HIV laboratory and teaching me how to perform the in vitro HIV assays. I would like to thank them for their time and resources that I used, for imparting knowledge, their acceptance, patience, friendship, and empathy.

Dr D Taylor and Co-workers at H3D (University of Cape Town), for performing the antiplasmodial tests against NF54 and K1 strains.

I am grateful to the National Research Foundation (NRF) for financial support.

Completing this dissertation required more than just academic support. I am deeply grateful to my family and friends for their patience, understanding, and encouragement throughout this journey. Their belief in me has been a source of emotional, physical, and spiritual strength, enabling me to tackle this challenging endeavor. Special thanks to my best friend, Ba Shammah, and Ms. A Mukwevho for their invaluable mentorship. Their steadfast support has been a constant source of motivation

Abbreviations and Acronyms

ADMET = Absorption, Distribution, Metabolism, Excretion and Toxicity

AQ = Aminoquinoline

Bn = Benzyl

CQ = Chloroquine

CYPs = cytochrome P450 isoenzymes

DCM = Dichloromethane

DMSO = Dimethyl Sulfoxide

EtOAc = Ethyl acetate

Equiv = Equivalents

FGI = Functional group interconversion

FTIR = Fourier Transformed Infrared

IC_{50} = Concentration needed to cause 50% inhibition in activity or growth

IR = Infra-Red

IUPAC = International Union of Pure and Applied Chemistry

MeOH = Methanol

$MgSO_4$ = Magnesium Sulphate

MP = Melting Point

MHz = Megahertz

NMR = Nuclear Magnetic Resonance

^{1}H NMR = Proton Nuclear Magnetic Resonance

^{13}C NMR = Carbon Nuclear Magnetic Resonance

ppm = parts per million

δ = chemical shift in ppm

J = coupling constant

s = singlet

d = doublet

t = triplet

dd = doublet of doublets

q = quintet

m = multiplet

RT = Room Temperature

TEA = Triethylamine

TLC = Thin Layer Chromatography

UV = Ultraviolet

WHO = World Health Organisation

Conference Presentations

Poster Presentations:

1. SACI North Section Young Chemists' Symposium held on the 13th of October 2023 (University of Limpopo).
2. Faculty Research Indaba and Open Day on the 23rd of November 2023 (University of Venda).
3. 16th Frank Warren Organic Chemistry Conference on the 5th of December 2023 (The Ranch Hotel, Polokwane) – 3rd Best Poster Award.
4. SACI North Section Young Chemists' Symposium held on the 25th of October 2024 (University of Venda) – 2nd Best Poster Award

Contents

Chapter 1: Background and Literature Review

According to the latest World Health Organization report (WHO 2023), HIV-AIDS has claimed 40.4 million lives ever since it's discovery. In 2022, approximately 0.6 million people died of HIV-related causes and about 1.3 million people become newly infected with HIV globally. The report also highlighted that the African region accounts for 50% of the new global HIV infections, compounding the burden of being the most affected region with 25.6 million people living with HIV[1].

The most recent WHO malaria report mentioned that malaria claimed approximately 619 000 lives in 2021 and there were 247 million new cases of malaria in 2021 compared to 245 million in 2020. The report further states that the African Region bears the heaviest malaria burden i.e. 96% of deaths globally of which 78.9% of these deaths were in children under the age of 5 years[2]. From the statistics mentioned above, it is evident, without any doubt, that malaria and HIV-AIDS are fatal infectious diseases. Even though both diseases are widespread, their distributions are most common and greatly overlap in the sub-Saharan African regions.

In malaria endemic regions, HIV-AIDS infection increases the risk of malaria infection, especially in individuals with advanced immunosuppression. That being so, malaria and HIV coinfection is common in the sub-Saharan region. Given the overlap of their geographic distribution and resultant rates of coinfection, interactions between the two diseases pose major public health problems[3].

1.1 HIV-AIDS

The human immunodeficiency virus (HIV) is a retrovirus from the lentivirus genus that causes HIV infection[4]. The virus targets the T-lymphocytes and other white blood cells with a cluster of differentiation 4 (CD4) positive T-cells receptors on their surfaces[5].

There are two main types of HIV strains, namely HIV-1 and HIV-2, as well as several related viruses that infect certain monkeys or great apes. HIV-1 has 9 strains - A, B, C, D, F, G, H, J, K, and some have sub-strains[6]. HIV-1 is found throughout the world but the B- strain is mostly found in the United States of America. HIV-2 is almost exclusively limited to West Africa[7].

HIV-1, simply put as HIV, accounts for 95% of all infections, and if left untreated prompts the progressive destruction of $CD4^+$ cells and/or failure of the immune system. The deficient immune system is prone to life-threatening infections and other diseases that ordinarily people with healthy immune systems can fight off[8][9].

This most advanced stage of HIV infection, whereby it develops into acquired immunodeficiency syndrome (AIDS) is marked by a $CD4^+$ cell count of fewer than 200 cells/microliter of blood and/or the presence of any AIDS-defining clinical conditions such as wasting syndrome due to HIV, cytomegalovirus retinitis (with loss of vision), cervical cancer, *mycobacterium tuberculosis* as defined by the Centers for Disease Control and Prevention (CDC 2014)[10].

1.1.1 Human Infection and Transmission

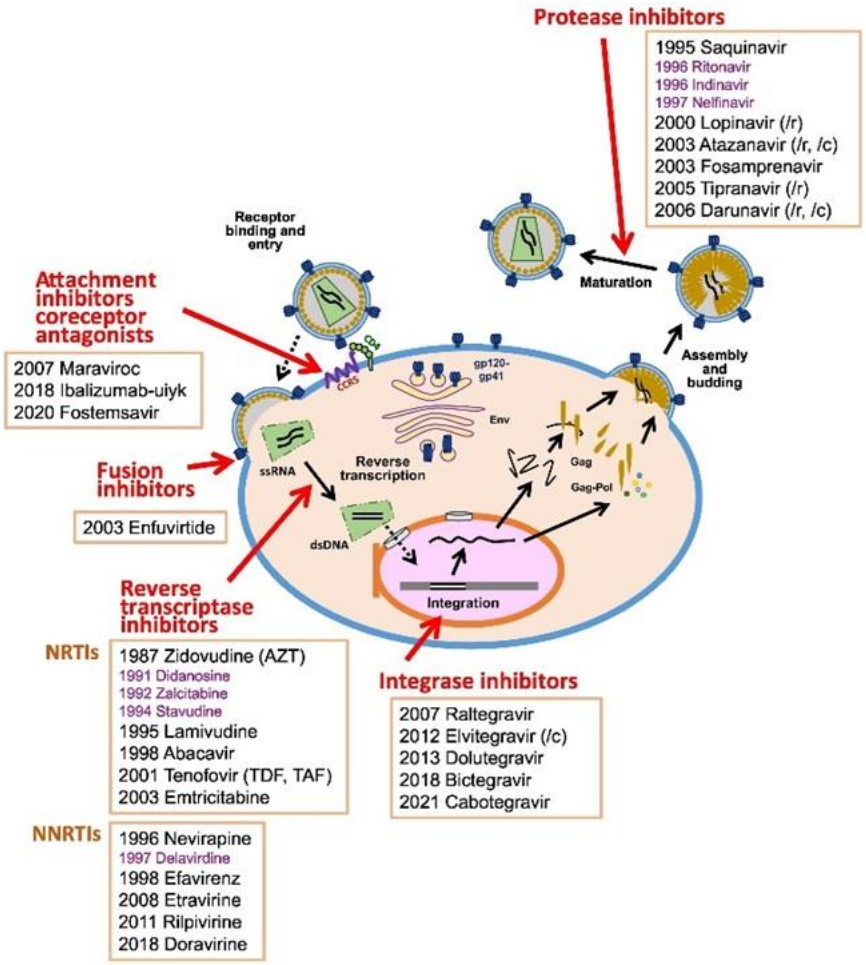

Figure 1.1: HIV life cycle and stage-specific inhibitors[11]

The HIV entry process involves a sequential and coordinated interaction between the virus and the host cell. Inside the human body, the virus grows and multiplies rapidly in stages as outlined in **Fig. 1.1** [12].

Firstly, HIV attaches to $CD4^+$ cell receptors then it fuses with the host cell. When HIV fuses with the lymphocytes[13], it deposits its cell contents (RNA, reverse transcriptase, integrase, and other viral proteins) into the host cell. The HIV genome is then integrated onto the host DNA by the integrase and with the aid of the reverse transcriptase, the cell is turned into a virus-generating factory[10][5].

The virus starts to form long-chain HIV proteins. These are the protein chains that the HIV virus uses to replicate itself and spread to other $CD4^+$ cells in the body. The new HIV RNA and proteins which will be produced by the infected $CD4^+$ cell make their way to the surface of the cell to assemble into non-infectious immature HIV[14].

Lastly, the immature HIV is released from within the infected $CD4^+$ that produced it. Being an immature HIV, it is unable to infect another $CD4^+$ cell, so another HIV enzyme known as a protease is released. The function of this enzyme is to break up the long chain proteins forming the immature HIV. Once separated they then combine and mature into the infectious form of HIV, ready to infect new cells[11][12].

Unlike the flu virus, the HIV virus is not airborne transmitted[14]. From an infected person, HIV can be transmitted through direct contact with specific body fluids such as semen, blood, vaginal secretions, and breast milk from infected people. It can also be transmitted from a mother to foetus and during delivery[15]. However, HIV cannot be transmitted through activities such as hugging, shaking hands, kissing, or even sharing personal objects, food, or water[16].

HIV is present in breastmilk and can infect the nursing infant. This infection mechanism is a major issue in third-world countries where alternatives to breastfeeding are limited[17]. Although extensive passage into breastmilk is generally thought to be an undesirable characteristic for most drugs, in third-world countries there is potential therapeutic advantage in treating HIV infected mothers with drugs that accumulate in breastmilk[18][19].

1.1.2 Signs and Symptoms of HIV

A few weeks after the inceptive infection, individuals experience flu-like symptoms and at times no symptoms at all. At this early stage, asymptomatic carriers tend to be most infectious, sadly, many will only become aware of their statuses in the extreme stages of infection[20].

When the immune system tries to fight the infection, mostly the virus retreats and hibernates in the lymph tissues. The untreated, infected individual usually remains healthy for 5 to 15, years, but the virus continues to replicate in the background, slowly obliterating the immune system[21][22]. Eventually, the body is unable to defend itself, succumbs to overwhelming opportunistic infections and develops other signs and symptoms, such as swollen lymph nodes, weight loss, fever, diarrhoea, and cough. Without treatment, they could also develop severe illnesses such as tuberculosis (TB), cryptococcal meningitis, severe bacterial infections, and cancers such as lymphomas and Kaposi's sarcoma[9][23].

1.1.3 Geographic Distribution

According to the 2023 epidemiological fact sheet published by the World Health Organization, there were about 39 million people living with HIV, 1.3 million new infections and 630 000 deaths by the end of 2022[24]. In 2020, it was reported that there were 37.7 million people living with HIV[25]. Compared with the 2021 data, when there were approximately 38 million people worldwide, the numbers are increasing[26]. The World Health Organization envisioned a worst-case scenario of 7.7 million HIV-related deaths over the next 10 years, thus an increase in the HIV infections due to HIV service disruptions during COVID-19, and the slowing public health response to HIV[22].

Figure 1.2: Global HIV prevalence and distribution. Adapted from UNAIDS 2023 estimates[27].

According to regions, the statistics were distributed as shown in **Fig. 1.2**. Not so good for Eastern and Southern Africa countries which are Ethiopia, South Sudan, Uganda, Rwanda, Burundi, Somalia, Kenya, United Republic of Tanzania, Angola, Zambia Malawi, Mozambique, Zimbabwe, Botswana, Namibia, Swaziland, Lesotho and South Africa[28]. Most of these countries also appeared on the list of top ten countries with the highest share of the global new HIV infections in 2021 (**Fig 1.3**).

According to News24's newspaper titled: 'HIV data is baffling', [https://www.news24.com/witness/news/hiv-data-is-baffling-20190529] the data that was released on the Institute of Health Metrics and Evaluation's website by the University of Washington in 2019 showed a high prevalence of HIV in adults between the ages of 15 and 49 in different parts of South Africa. UMgungundlovu had the highest HIV prevalence (29.7%) not only in South Africa but on the continent while KwaZulu-Natal as a whole had a 24% prevalence.

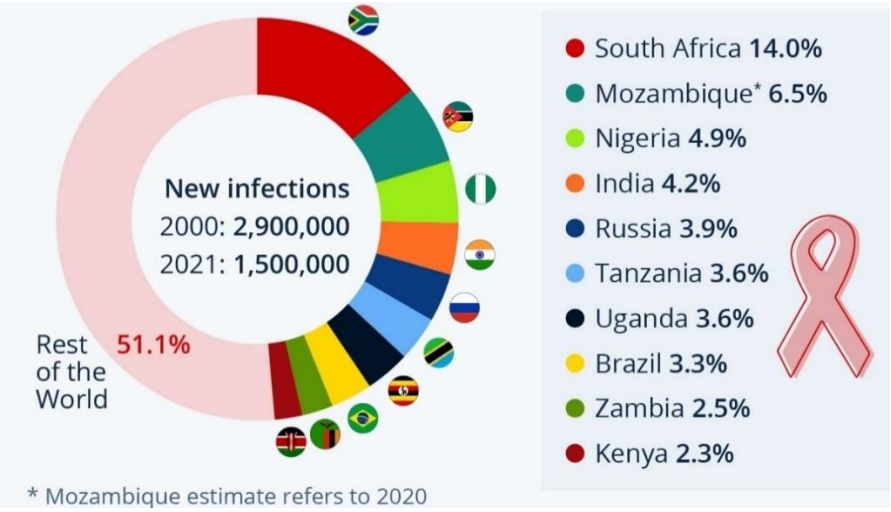

Figure 1.3: Global HIV new infections distribution[29].

Free State was second with a prevalence of 21.3%, followed by Mpumalanga with 20.9% then North West (18.6%), Eastern Cape (18.2%), Gauteng (16.7%), Limpopo (13.2%), Northern Cape (11.5%) and lastly Western Cape (10.0%). Director of the Centre for the Aids Programme of Research in South Africa (Caprisa), Professor Salim Abdool Karim, said he was unable to give a definitive answer as to why uMgungundlovu had such a high rate despite ongoing research and the fact that there is good coverage of the area in terms of treatment. It can be assumed that one of the possible reasons might be the issue of drug resistance**.**

When reporting the results of their Sixth South African National HIV Prevalence, Incidence, and Behaviour survey (SABSSM VI) on their website[30], the Human Sciences Research Council (HSRC) stated that there were about 7.8 million people living with HIV in South Africa at the end of 2022. Comparing this data with 2017, when the number was about 7.9 million, then there is light at the end of the tunnel with a possibility of eliminating HIV in South Africa. So, to reach the new proposed global 95–95–95 targets set by UNAIDS – 95% of the people living with HIV should be knowing their statuses, 95% of the infected people who know their statuses should be on treatment and 95% of people on treatment should be having a suppressed viral load. To achieve this, there is a need to redouble efforts in fighting this infectious disease[22].

1.1.4 Prevention

Several methods and interventions have proved highly effective in reducing the risk of the spread and contraction of HIV[27]. These include abstinence, use of condoms, avoiding sharing sharp objects and use of pre-exposure and post-exposure prophylaxes. According to the Centers for Disease Control and Prevention, pills such as Truvada and Descovy and vaccines such as Apretude and CAB-LA are licensed to be used as pre-exposure prophylaxes[31].

1.1.5 Treatment - Antiretroviral Therapy (ART)

Unlike other viruses, HIV is a retrovirus, and it can outmanoeuvre the host's DNA mode of replication to make its own copies thereby causing an immutable infection[10]. For this reason, it has turned out to be hard to kill. Thus, there is not cure yet for HIV/AIDS. However, with increasing access to effective HIV prevention, diagnosis, treatment, and care, including for opportunistic infections, HIV infection has become a manageable chronic health condition, enabling people living with HIV to live long and healthy lives[11].

The intention of antiretroviral therapy is to maintain suppressed plasma HIV- ribonucleic acid (RNA) levels (also called viral load) below the level of detection of sensitive HIV-RNA assays. Continued suppression of HIV- RNA can be maintained if individuals adhere to appropriate ART regimens[32].

HIV medicines protect the immune system by blocking HIV at different stages of the HIV life cycle (**Fig.1.1**), hence, their classification based on their mechanism of action is as follows:

1. **Entry/Attachment Inhibitors**

   These medicines work by blocking the virus's ability to fuse/attach to or enter healthy host cells[33]. For example, fostemsavir is an oral prodrug that is hydrolyzed to its active form temsavir (**Scheme 1**) which binds to the HIV gp120 envelope adjacent to the gp120-CD4 binding site. The binding of temsavir prevents the gp120 conformational change required for normal attachment to the CD4 receptor[34][35].

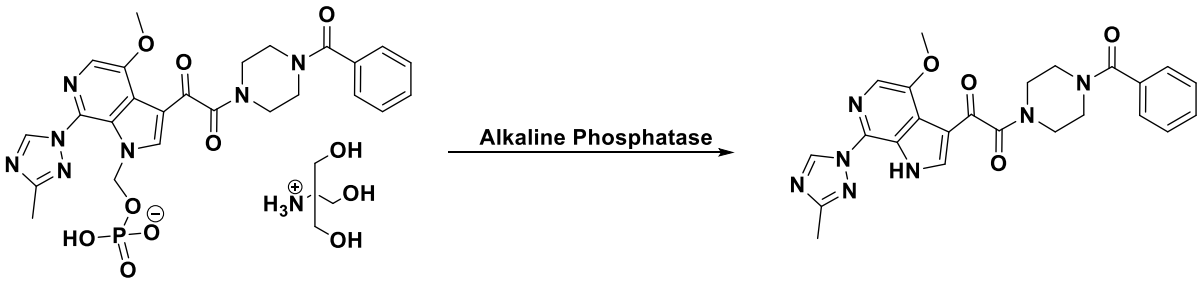

Fostemsavir

Scheme 1.1: The hydrolysis of fostemsavir.

   Enfuvirtide is another inhibitor administered as a subcutaneous injection and acts by inhibiting the fusion of the viral and the host membrane. Thus, without the means to enter the host cell, HIV cannot replicate[36].

2. **HIV- Reverse Transcriptase Inhibitors**

   There are two classes of HIV reverse transcriptase inhibitors namely **nucleoside reverse transcriptase inhibitors** (NRTIs) and **Non NRTIs.** The main difference between the two subclasses is that NRTIs act as host nucleotide decoys by attaching

to the host DNA and cause termination of the elongating HIV DNA chain whereas the NNRTIs bind directly to the HIV reverse transcriptase enzyme blocking its action. Currently, the NRTIs serve as the backbone of ART regimens. Examples are Emtricitabine, Rilpivirine and Doravirine[10][37].

3. **Integrase Inhibitors**

   This type of anti-HIV drug only binds to the integrase enzyme that is attached to the viral DNA. The binding of the integrase inhibitors to the integrase prevents the HIV complex from integrating into the host DNA. When the HIV integration process is blocked, the HIV DNA becomes a substrate for host repair enzymes that subsequently convert the HIV DNA complex into a by-product. Cabotegravir and Bictegravir are examples of integrase inhibitors already on the market[10][38].

4. **Protease inhibitors (PIs)**

   The PIs bind to the active site of the protease enzyme thereby restraining its activity. This class of drugs interfere and stops the polyprotein processing maturation process. As a result, preventing the infection of new cells[39]. The protease inhibitors do not have an effect on cells already infected with HIV (those with proviral DNA integrated into the host DNA). PIs are available as a second-line treatment in some resource-limited settings. Darunavir, Tipranavir and Fosamprenavir are examples of protease inhibitors already on the market[37].

Although the currently available drugs cannot completely kill the HIV virus, they help prevent the progression of HIV into AIDS as well as reducing the risk of HIV transmission. Of the 39 million people living with HIV globally, about 76% of them had access to ARTs in 2022[27].

1.1.6 Vaccines

As reported by the National Institutes of Health on their website[40], currently there is no licensed HIV vaccine; however, there have been about 250 clinical trials of potential vaccines. Sadly, most of the trials never went beyond phase 1 and only a few made it to the late-stage phases.

Most recently, the mosaic vaccine, a promising Janssen investigational jab known as HVTN706/HPX3002, underwent clinical trials from 2019 until October 2022[41]. The regimen was made up of a mosaic-based adenovirus vector (Ad26.Mos4.HIV) and soluble proteins (Clade C/Mosaic gp140 adjuvanted with aluminum phosphate). It was administered in four doses over twelve months, and no safety concerns with the shots were identified[42][43].

As per a notice on the Johnson and Jonhson website[44],the studies on the mosaic vaccine was discontinued. Their decision was based on their side research findings, which showed that in as much as the vaccine was safe, it was not effective against HIV; however, further studies have commenced[45]. Despite the disappointments and the setbacks, researchers are working tenaciously, looking at new technologies and strategies to design vaccines to prevent HIV. They strongly believe that an effective vaccine is still possible[41][46].

1.2 Malaria

Malaria is caused by the protozoan single-cell parasite (**Fig. 1.4**) of the *Plasmodium* genus[47]. The malaria parasite develops both in humans and in female Anopheles mosquitoes. The size and the genetic complexity of the parasite mean that each infection presents thousands of antigens to the human immune system[48].

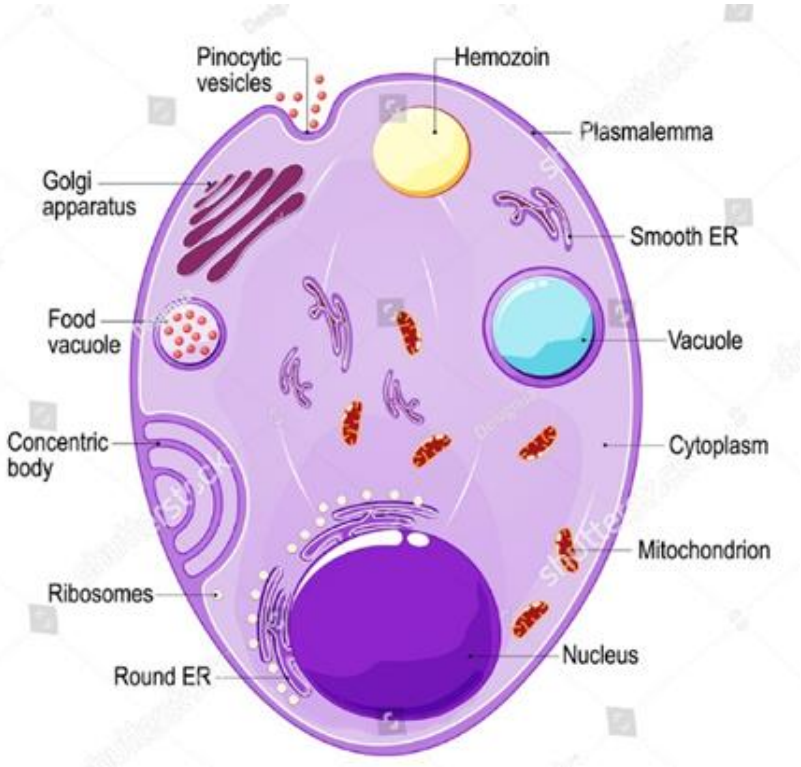

Figure 1.4: Structure of the *Plasmodium*[49].

Malaria is endemic in most tropical and subtropical regions of the world. Of the five *Plasmodium* species (*namely vivax, malariae, knowles, falciparum and ovale*) that infect humans, *plasmodium falciparum* is the most virulent and is responsible for most of the morbidity and mortality due to malaria[50][51]. Malaria is a major clinical and economic problem. The mechanism of severe malaria in *P. falciparum* infection is mainly due to cytoadherence and then sequestration of *P. falciparum* infected erythrocytes leading to

occlusion of blood flow resulting in decrease oxygen delivery to tissues and end organ damage. This disease is prevalent in less developed countries, greatly constraining socioeconomic growth[52][53].

1.2.1 Transmission

The route of transmission is mainly through infected female Anopheline mosquitoes taking a blood mead inoculating parasites to humans and infecting their erythrocytes (red blood cells)[54].

Malaria Life Cycle

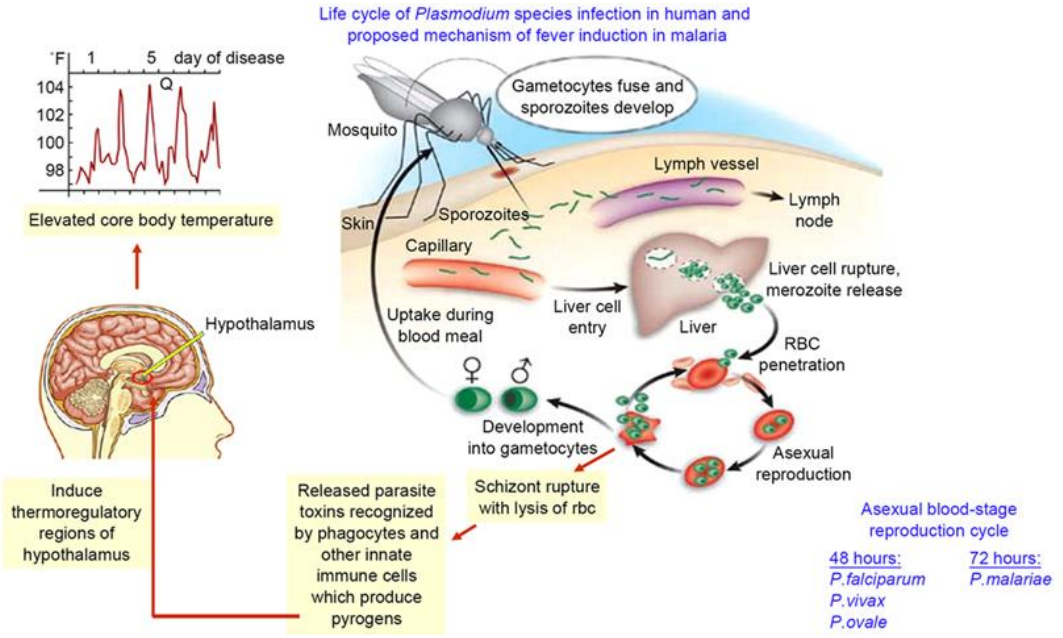

Figure 1.5: Life cycle of malaria infection in human and proposed mechanism of fever induction[55]

As the anopheles mosquito bites (**Fig. 1.5**), it injects sporozoites from its salivary glands into the dermis of the human skin. Once the sporozoites are inside the human body, they move through the blood stream to the liver where they reproduce asexually and mature into schizont. At this stage, they do not cause any sign or symptoms of infection. In mammals, after about 7 to 10 days, the parasites, in the form of merozoites, are released from the liver cells in vesicles, journey through the heart, and arrive in the lungs, where they bide within lung capillaries. The vesicles eventually disintegrate, freeing the merozoites to enter the blood phase of their development[47][52] (48)[56].

In the bloodstream, the merozoites invade red blood cells and multiply again until the cells burst. The merozoites from burst erythrocytes move to invade more uninfected erythrocytes. This cycle is repeated, causing fever each time parasites break free and invade blood cells. Some of the infected blood cells leave the cycle of asexual multiplication. Instead of

replicating, the merozoites in these cells develop into sexual forms of the parasite, called gametocytes, that circulate in the bloodstream[57][58].

When a mosquito bites an infected human, it ingests the gametocytes, which develop further into mature sex cells called gametes. The fertilized female gametes develop into actively moving ookinetes that burrow through the mosquito's midgut wall and form oocysts on the exterior surface[59].

Inside the oocyst, thousands of active sporozoites develop. The oocyst eventually bursts, releasing sporozoites into the body cavity that travel to the mosquito's salivary glands[57]. The cycle of human infection begins again when the mosquito bites another person. The parasite also changes through several life stages even while in the human host, presenting different antigens at different stages of its life cycle. Understanding which of these can be a useful target for vaccine development has been complicated. In addition, the parasite has developed a series of strategies that allow it to confuse, hide, and misdirect the human immune system[60][61].

After the incubation period, depending on different species of *Plasmodium* (*P falciparum, P vivax and P ovale infection)* to 72 hours *(P malariae*), patients often report experiencing symptoms. These symptoms manifest clinically in a spectrum; from non-specific uncomplicated symptoms of acute febrile illness, intermittent fever, chills, sweating and headache, with or without anaemia and jaundice, to severe complication with seizure, confusion, coma, renal failure, shock, acute respiratory distress syndrome and death[53][62].

Other routes of transmission in humans include blood transfusion, organ transplantation, shared use of contaminated needles or syringes, and mother-to-child transplacental or perinatal transmission[47][55]. Boudová et al. emphasized on the impact of mother-to-child transmission which is often overlooked. Pregnant women are a significant reservoir of parasite gametocytes and serious consideration and intervention strategies should be developed and implemented to help save lives against the deadly disease[63].

During the first and second pregnancies, women lack adequate immunity to variant surface proteins expressed by the parasite on the surface of infected red blood cells, thereby weakening their immune systems[64][65][66]. These proteins will then bind to the placenta, where they can hide throughout the whole gestation period. Inevitably, the fetus is susceptible to malaria infection. The risk factors of gestational malaria include low birth weight, prematurity, fetal anemia and stillbirth, thereby increasing infant mortality and in worst cases HIV co-morbidity[67][68].

1.2.2 Geographical Distribution

As reported by the World Health Organization, over the period 2000-2018, there have been a steady decrease in the number of reported cases as well as deaths that are associated with malaria.

From 2018-2022, the trends have been fluctuating but one thing that remained constant is that the WHO African region suffers the most due to the malaria epidemic. **Table 1.1** summarizes the trends of the global malaria epidemic from 2018 up until 2022 [2][69][70].

Table 1.1: Malaria epidemic trends

Year	Malaria Cases		People dying from Malaria-related causes	
	Globally	WHO African Region	Globally	WHO African Region
2018	228 million	213 million	405 000	380 700
2019	229 million	215 million	568 000	386 000
2020	245 million	230 million	627 000	599 000
2021	247 million	234 million	619 000	593 000
2022	249 million	233 million	608 000	580 000

In the past five years, the WHO African region alone has accounted for over 90% of the reported cases. Newborns, young children (5 years and below), pregnant women, immunosuppressed individuals (e.g. patients with HIV/AIDS) and non-immune travellers accounted for a greater chunk of the number of cases yearly[71].

A notable increase in the number of cases from 2019 to 2020, as well as the rebound in malaria cases and malaria-associated deaths from 2020 (**Table 1.1**), was ascribed to the negative impacts of the COVID-19 pandemic. For example, there was a disruption of services and distribution of medication due to the lockdown[2][70].

Comparing the African region to other WHO regions whose malaria incidence and mortality rates are always lower, these two groups of people come from different socio-economic statuses. In developed nations, people have easy or maybe cheap access to education. They understand the importance of building broader social networks that improve their knowledge of health behaviours and prevention techniques[72][73].

On the contrary, people from endemic African region are i) less educated ii) malnutritioned thereby compromising their immune systems iii) unemployed therefore they cannot afford to buy medication iv) poor settlement patterns and land-use changes that impel breeding habitats for mosquitoes and lastly unstable political systems (that impact the quality of infrastructure, access to primary health care, clean water, and sewage services) also contribute to how malaria has spread beyond its geographical limits. [74][75][72][76]

Malaria in South Africa

In South Africa, malaria is mainly transmitted along the international border areas and about 5 million people are at risk of contracting the disease.

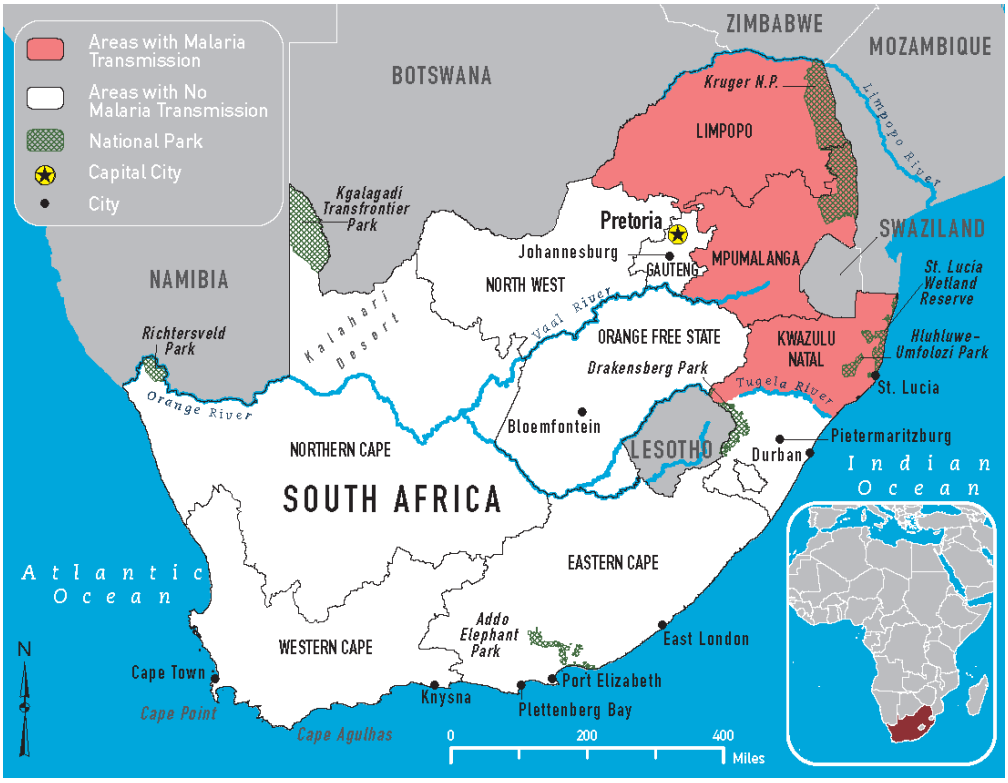

Figure 1.6: Distribution of Malaria in South Africa[77]

Malaria transmission is confined to the north-eastern border districts of Mpumalanga, Limpopo, and KwaZulu-Natal provinces (**Fig. 1.6**) [78]. Both local and international travellers are agents of spreading malaria in these areas. Very rarely is malaria contracted in the North-West and Northern Cape provinces. The transmission of malaria is seasonal. Generally, malaria cases start to rise in October, peaking in January and February and decreasing towards May. In Limpopo, malaria is more prevalent in the Mopani and Vhembe districts of the province during the rainy season[77][79].

To date, several methods and strategies have been put in place to fight malaria. These include i) prevention methods, including the use of chemoprophylaxis, and ii) treatment, including prevention of relapses of malaria[80]. In considering the type of medication, options depend on the severity and the symptoms of malaria, geographic location, age and whether one is pregnant or not[81].

1.2.3 Prevention

When combating infectious disease, prevention is an essential initial step that lays the foundation for disease control. A few preventative strategies are in place that aim to lower malaria incidences. These strategies pivot on vector control and medical prophylaxis for those at risk. The complexity and genome variability of the parasite are challenging, though the observation of acquired natural immunity after repeated exposure in a subset of patients bears optimism[23].

1. Vector control – these are either mechanical (house improvements and removal trapping), environmental (habitat manipulation and waste management), chemical (insecticide-treated bed nets and chemical repellents)[82], or biological (biological larvicides and fungi) methods used to reduce the chances of mosquito bites and malaria transmission[83][84].

2. Seasonal Malaria Chemoprevention – A strategy commonly known as chemoprophylaxis whereby a full therapeutic course of antimalarials is administered to the population in areas with seasonal transmission, aiming to prevent the disease or infection[85]. This strategy was recommended by the World Health Organization in 2012 and it has been introduced as part of national malaria control strategies in countries of the Sahel and sub-Sahel regions of West Africa[86][87].

   Malaria chemoprophylaxis is further subdivided as **i.)** Casual prophylaxis (used to prevent infection – blood stage) and ii**.)** Clinical or suppressive prophylaxis (used to inhibit parasitaemia and its symptoms – liver stage). Currently in South Africa, Atovaquone-proguanil (casual), Doxycycline and Mefloquine (clinical) are recommended to be used as chemoprophylactic options[88][80].

   There is also Intermittent Preventative Treatment (IPT) which is full course treatment is administered to infants (IPTi) and pregnant (IPTp) women, who are residing in areas of moderate to high malaria transmission areas[89].

1.2.4 Treatment

The golden age of antimalarials was ushered in by the discovery, extraction, and isolation of quinine from the bark of the cinchona tree in 1820. Following this, was the discovery and development of other natural and synthetic compounds with examples represented in **Fig. 1.7** Quinine, however, remained the mainstay of malaria treatment until the 1920s, when more effective synthetic antimalarials became available[90][91].

The drugs that were developed for the treatment and prevention of relapses of malaria can be classified according to their chemical structure and mode of action[87].

1. Classification based on their chemical structures. Some of their examples and structures are illustrated in **Fig. 1.7** These include 4-aminoquinolines, peroxides, folates, naphthoquinones, iron chelators etc.

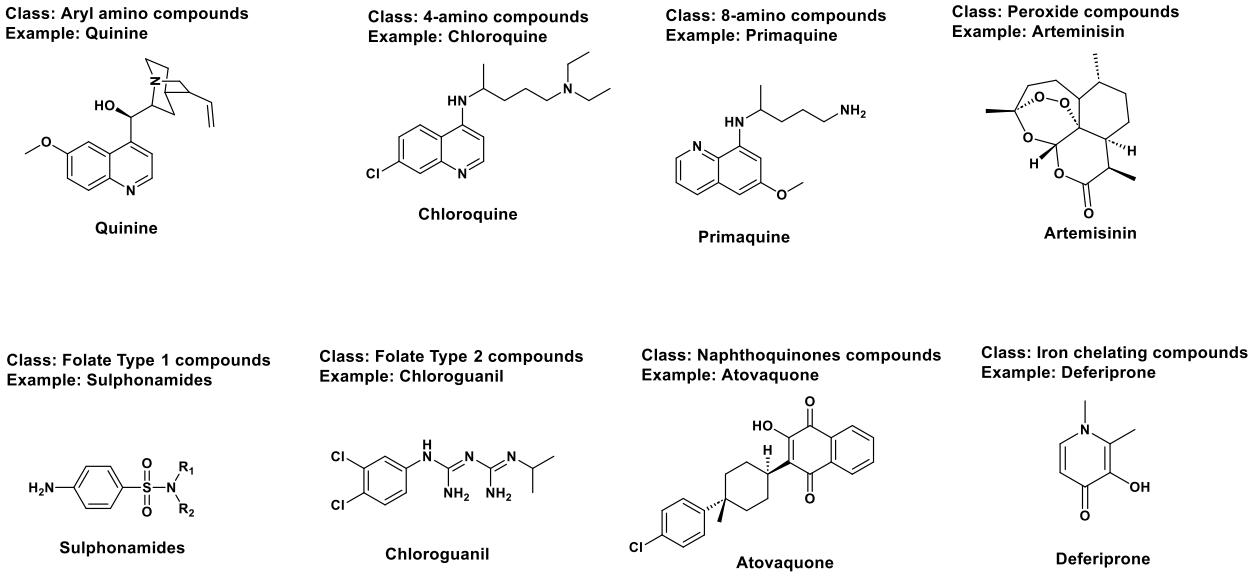

Figure 1.7: Chemical structures of some drug classes[87].

2. Classification based on their modes of action

i. **Tissue schizonticides for causal prophylaxis:** These drugs act on the primary tissue forms of the plasmodia, which, after growth within the liver, initiate the erythrocytic stage. By blocking this stage, further development of the infection can be theoretically prevented. Pyrimethamine and Primaquine have this activity. However, since it is impossible to predict the infection before clinical symptoms begin, this mode of therapy is more theoretical than practical[80][87].

ii. **Blood schizonticides:** As examples, we have chloroquine and pyrimethamine. They act on the blood stage, and in doing so, they terminate clinical attacks of malaria [92][93].

iii. **Gametocytocides:** these types of drugs destroy the gametocytes, interrupting the life cycle and preventing the transmission of the infection. Primaquine is an example of such drugs[94].

iv. **Sporontocides:** These drugs intercept the formation of oocysts in the mosquito, thereby stopping transmission. Primaquine and chloroguanide have this action[95].

v. **Tissue schizonticides for preventing relapse:** This class of drugs help to prevent relapse episodes of *P. vivax* and *P. ovale* caused malaria. They primarily target the liver stage (hypnozoites). As examples, we have primaquine and pyrimethamine[83].

As of today, no single drug with multiple target actions that interfere with all stages of the parasite's life cycle exists. Therefore, antimalarial drug doses have been formulated in such a way that a patient is prescribed with at least two different drug classes. For instance, in case of *P. vivax* and *P. ovale* infections, the treatment formulation would include blood schizonticide, a gametocytocide and a tissue schizonticide[96][88].

1.2.5 New Developments:

Tao Wu et al. reported a new class of antimalarials called imidazolopiperazines. This class of drugs acts against both asexual and sexual blood stages and the pre-erythrocytic liver stages of malarial parasites[97]. Ganaplacide, also known as KAF156, is an imidazolopiperazine that is undergoing clinical trials. It is being promoted for use in prophylaxis, treatment, and prevention of malaria transmission. In the phase II trials, it is co-administered with lumefantrine in patients (adults and children) with mild *P. falciparum* malaria. Bernhards Ogutu et al. (2023) reported that so far, the drug is being well tolerated in patients, especially in adults. However, its co-administration with lumefantrine is being evaluated further in phase II trials[98][99].

On their website page [https://clinicaltrials.gov/study/NCT04300309 Date of Access: 23 December 2023], Novartis Pharmaceuticals reported about the ongoing clinical trial, phase II evaluations of a new Artemether-lumefantrine Dispersible Tablet. These evaluations are focused on determining how effective, safe and tolerable the tablet is as well as the pharmacokinetics associated with it in infants and neonates. The patients should be weighing 5kg and with uncomplicated malaria. The studies were being conducted in five nations. There is no detailed information about the outcome of the trials yet but on the website it shows studies in Burkina Faso trials were terminated, in Zambia, Kenya and Mali they were withdrawn, and Congo they are still recruiting[100].

1.2.6 Vaccines

RTS, S/AS01 Vaccine

The first approved vaccine named RTS, S/AS01, is a product of three decades of research and development by GlaxoSmithKline (GSK) in collaboration with other research institutes[59]. This work was funded by the Gates Foundation especially during the late-stage development[101]. The vaccine is made up of genes from circumsporozoite, the outer protein of *P. falciparum*, a portion of a hepatitis B virus, as well as a chemical adjuvant to enhance the immune's response against the antigens[102].

Infection is averted by effectuating high antibody titers that obstruct the parasite from infecting the liver[103]. In late 2012, a phase III trial of RTS, S/AS01, it was found that this vaccine provided modest protection against both clinical and severe malaria in young infants[104]. Roughly about 12 months later, preliminary results of a phase III clinical trial denoted a reduction in the number of malaria cases among infants by around 25 percent and by almost 50 percent among young children, thus the vaccine was less effective for infants[59]. Three doses of vaccine plus a booster reduced the risk of clinical episodes by 26 percent over three years but offered no significant protection against severe malaria[103][105]. This translates to about 70% effectiveness in preventing malaria in children when combined with conventional antimalarial drugs[101].

In 2015, the European Medicines Agency endorsed the RTS, S vaccine on the proposition for the jab to be used to immunize six weeks to seventeen months old children outside the European Union[106][107]. In October 2021, the World Health Organization recommended the extensive use of the vaccine (under the brand name Mosquirix) in children aged five months and above. This qualified it to be the first-ever recommended malaria vaccine. The WHO then prequalified the RTS, S vaccine in July 2022[2][59][103].

According to an article issued by WHO[108], in three African countries, namely Ghana, Kenya, and Malawi, children had received at least one shot of the vaccine. The jab should be provided in a schedule of 4 doses for it to reduce severe malaria to a negligible effect. The number of countries was envisaged to increase to twelve in the next two years by adding Benin, Burkina Faso, Burundi, Cameroon, the Democratic Republic of the Congo, Liberia, Niger, Sierra Leone, and Uganda to the queue. The first doses of the vaccine were anticipated to be delivered in these nations late 2023 and rolled out early 2024[70].

R21/Matrix-M Vaccine

On the 2nd of October 2023, the World Health Organization also recommended another vaccine named R21/Matrix-M, for the prevention of malaria in children. The vaccine was developed by the University of Oxford in collaboration with Serum Institute of India, using their Matrix-M adjuvant technology[109].

Just like the RTS, S/AS01, the R21/Matrix-M jab comprises of a malaria protein from the *Plasmodium falciparum* parasite[107], a Matrix-M adjuvant and a hepatitis B virus surface antigen scaffold **(Fig. 1.8).** Both vaccines target the sporozoites. To be considered effective, both vaccines must eradicate these sporozoites prior to entry into the hepatic system. Thus, terminating the propagation of the malaria life cycle in the human host[106][107].

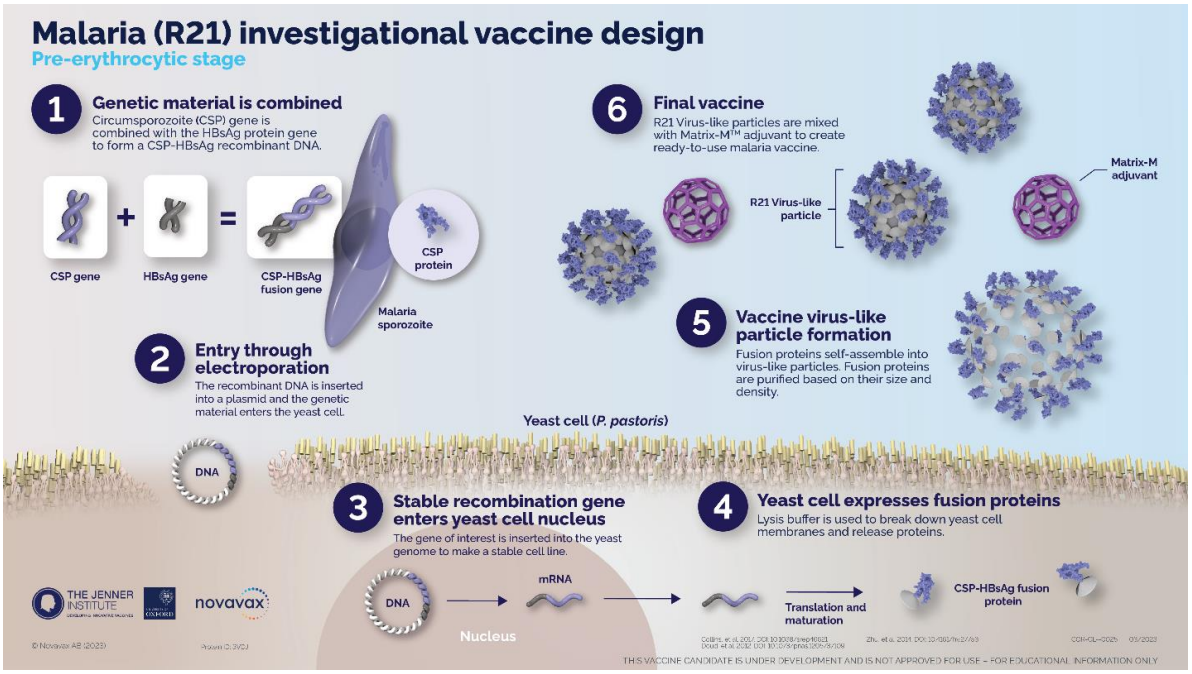

Figure 1.8: The stages in the design of the R21/Matrix-M vaccine[110].

The R21/Matrix-M R21 jab is also administered in three doses plus a booster dose which is administered one year after the third jab. It has been reported that it is more potent than Mosquirix with an efficacy of 75%[111]. A vaccinologist from the University of Oxford, who helped to develop R21 said this is because every molecule of R21 has a malaria antigen fused to it, compared with one in five molecules in the RTS,S vaccine[107][112]. With the R21/Matrix M, the world now has a vaccine that meets the WHO's target of 75% efficacy, after it gets prequalification from WHO then there will be options of two vaccines[113].

In as much as R21 is easier and less expensive to manufacture, there remains a long and rocky road to a malaria-free world. In highly endemic nations, vaccine coverage is still low even for other diseases and it's going to be difficult to make sure every child gets immunized against malaria [107].

Vaccine design strategies aim to interfere and interrupt the life cycle of the parasite at different stages. For instance, the pre-erythrocytic stage that is targeted by both the RTS, S and the R21 vaccines[114]. There are also transmission blocking vaccines that targets the sexual stages of the parasite.

They work by obstructing the maturation of the parasite inside the mosquito and the propagation of parasites to other human hosts. Currently being evaluated in clinical trials are Pfs25 and Pfs230D1[115][116]. As for blood-stage target vaccines, ChAd63 PvDBPII is the leading candidate that is still under trials[116].

1.3 Malaria and HIV-AIDS Co-Infection

The prevalence of malaria and HIV infection overlaps in most endemic regions and co-infection of these diseases have important public health implications. Geographical overlapping **(Fig.1.9)** of these diseases has generated global interest in terms of their potential interactions and an integrated control effort in most endemic regions is essential[3][23].

HIV and malaria each interact with the host's immune system, and this interaction often results in a complex activation of immune cells which cause dysfunctional levels of cytokine and antibody production. In addition, CD4+ T cells have a major role in the development and maintenance of malaria immunity, but HIV infections meddle with this immunity[117][118]. Thus, malaria co-infection with HIV triggers malaria disease progression, increases the risk of severe malaria in adults, increases risk of congenital infection and this dual infection fuels the spread of both diseases especially in sub-Saharan Africa[119][120].

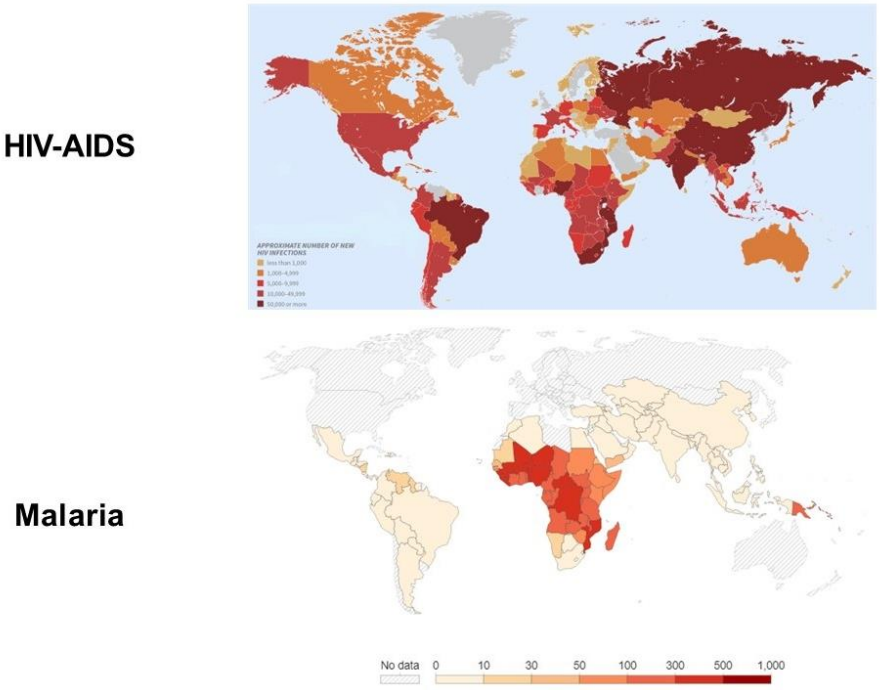

Figure 1.9: Malaria and HIV/AID are overlapping epidemics.[100][121].

Geographical overlap/co-infection of HIV-AIDS and malaria can cause therapeutic interactions (drug-drug interactions), clinical interactions and immunologic consequences[122]. Given the lack of gravidity-specific protection against malaria seen with HIV infection in pregnant women, HIV puts more pregnancies at risk for complications associated with malaria. For example, the cohort studies conducted in Cameroon showed that malaria infection during pregnancy may increase the risk of mother-to-child transmission of HIV. In pregnant women, HIV infection increases the risk of high-density *Plasmodium falciparum* infection, higher risk of maternal anaemia and low birth weight[119][3].For treatment, the use of cotrimoxazole (CTX)

prophylaxis and antiretroviral therapy (ART) in HIV-infected patients seem to provide a protective effect from malaria[123]. While infection with HIV has been associated with an increased rate of malaria treatment failure, this was due to re-infection with new malaria strains, rather than recrudescence of prior infection. Pregnant HIV-infected women and their infants are the least protected against malaria, despite being the most vulnerable population[124]

On a positive note, the antimalarial drug chloroquine has effects on HIV by inhibiting the production of infectious viral particles via impairing virus glycosylation. Chloroquine also has synergistic effects on HIV suppression when combined with the protease inhibitors (indinavir, ritonavir, and saquinavir) at concentrations achieved with prophylaxis dosing[125]. In vitro studies have also shown a synergistic effect in inhibiting the growth of malaria parasite growth when the protease inhibitors ritonavir and saquinavir are combined with and chloroquine or mefloquine[120].

1.4 Drug Metabolism

Understanding and having a good knowledge of drug metabolism, also called biotransformation, is crucial in medicinal chemistry to interpret the science of therapeutics and toxicology[126]. This knowledge will be a fundamental and very necessary tool/aid in a successful drug design and development process[127]. Put simply, drug biotransformation is a chemical alteration process that increases the hydrophilicity of the drug thereby facilitating its excretion[128].

After administration, drugs pass through the hepatic system, which is the primary site for drug metabolism. Once in the liver, enzymes convert prodrugs to active metabolites or convert active drugs to inactive forms[127]. This enzymatic catalysis is a pivotal determinant of these biotransformation processes. The class and quantity of enzymes are critical to the efficiency of biotransformation of drugs[129].

Cytochrome P450 (CYP450) enzymes are responsible for the metabolism of about 70-80% of all drugs in clinical use. CYP450 pathways are distinguished by the nature of gene sequences. That is how they are designated a family number, for example CYP1, CYP2, CYP3; then a subfamily letter [CYP1A, CYP2D, CYP3A]. Lastly, they are further differentiated by a number for the isoform or individual enzyme [CYP1A1, CYP2D6, CYP3A4][130][131].

Genetic make-up determines the rate of drug metabolism in humans. Another factor is the hepatic system's functionality which is directly proportional to age. Newborns and infants have immune systems that are not fully developed which calls for special medication formulations. As the person gets old, so does the liver's functionality deteriorate[132][133]. With a weak

hepatic system, the metabolism of drugs in adults is slow. Consequently, there will be high chances of worsening drug intolerability (side effects) and unfavourable drug-drug interactions[134] among the very young and the old. Unfortunately, negative drug interactions result in reduced drug metabolism by enzyme inhibition or increased drug metabolism by enzyme induction[135].

Induction of drug metabolizing enzymes, especially CYP3A4, can be an unwanted biochemical process for a drug candidate from a drug-drug interaction standpoint. Drug-drug interactions caused by enzyme induction result in increased clearance, and thereby decreased exposure of the main therapeutic agent(s)[136]. Inversely, CYP3A4 inhibition results in the improvement of exposure of the main therapeutic agent(s), therefore better efficacy and in most cases decreased toxicity [137].

Anti-HIV Drugs that affect the CYP3A4 enzymes

Ritonavir, Delavirdine and Nelfinavir are strong CYP3A4 inhibitors whilst Nevirapine and efavirenz are CYP3A4 inducers. As a result of this inhibition, there is a positive drug-drug interaction enabling lower dosages and less frequent dosing intervals[138][139]. A notable exposure increase was observed when ritonavir and saquinavir were co-administered to HIV-seronegative volunteers[138].

Antimalaria Drugs that affect the CYP3A4 enzymes.

It has been noted that artemisinin is a strong inducer of the CYP1A2, CYP2A6, and CYP3A4 enzymes. It accomplishes this by activating two closely related nuclear hormone receptors responsible for the transcriptional regulation of CYP enzyme expression[140].

1.5 Drug Resistance

Drug resistance defines a situation whereby pathogens, e.g parasites and viruses, are less sensitive (tolerant) and no longer respond to antimicrobial medicines that are supposed to kill them. Drug resistance decreases the efficaciousness of medication in chemotherapy. The extensiveness of drug resistance curbs the therapeutic options for medications including antimalarials and ARTs[141][142].

The use of antimicrobials inflicts selective pressure on microbes[143]. For instance, a specific antimalarial can lower or eradicate *P. malariae* parasitemia and leave out *P. falciparum* strains as survivors. By virtue of heredity, the surviving microbes impart the genetic codes for resistance to their progeny[142][144].

Ultimately, strains resistant to one specific drug can develop resistance against other medications with similar modes of action, resulting in multi-drug resistance[145].

Eggleston. K *et al.* reported some of the contributing factors to the development of drug resistance to be[142]:

i. Misuse of medication: This is the wrong use of antimicrobials and, oftentimes, the misuse of medications. For example, an antifungal is used for viral infection or even use of antibiotics in agriculture and food animals. This is not to be confused with drug repurposing, which is the intentional, research-driven process of using an approved drug to treat a different disease involving clinical studies to ensure safety and effectiveness. The aim is to broaden therapeutic uses for drugs already proven safe[146].

ii. Overuse of medication. This is the inappropriate use of prescribed medications most commonly for instant gratification. Because of ignorance, some patients assume overdosing can speed up the healing process and this is not always the case since toxicity issues will arise[147].

iii. Underuse of medication: This happens due to failure, shortage, and/or absence of drugs, leading to a patient not completing a medication course. Thus, too short period for the medication to be effective as prescribed by expects(8)[148]. Underuse often co-exists with the overuse of cheap and affordable first-line drugs[142].

Woefully, for many stubborn microbes, only a few new therapeutic agents or strategies have been developed so far. But increased awareness through education for prescribers, distributors, and patients could stimulate innovation both in drug development and diagnostics[142][149]. The initial step in drug development is understanding the mechanism of resistance and trends from structure-activity relationships[150]. In this report two drugs, chloroquine (antimalaria) and saquinavir, are used as examples to discuss the modes of action of antimalarials and anti-HIV drugs, respectively.

Chloroquine

Before the development of chloroquine resistance, this drug had been used to treat mainly *P. vivax* and *P. falciparum* infections on a broad scale for many years due to its high level of efficacy, limited toxicity, and cost-effective synthesis methods[151][152]. It was recommended to be used by young children (0-5 years) and pregnant women who are most vulnerable to malaria infection[153]. The chemical structure of chloroquine comprises of the quinoline scaffold and a diethylaminoisopentylamino side chain (**Fig.1.10**)

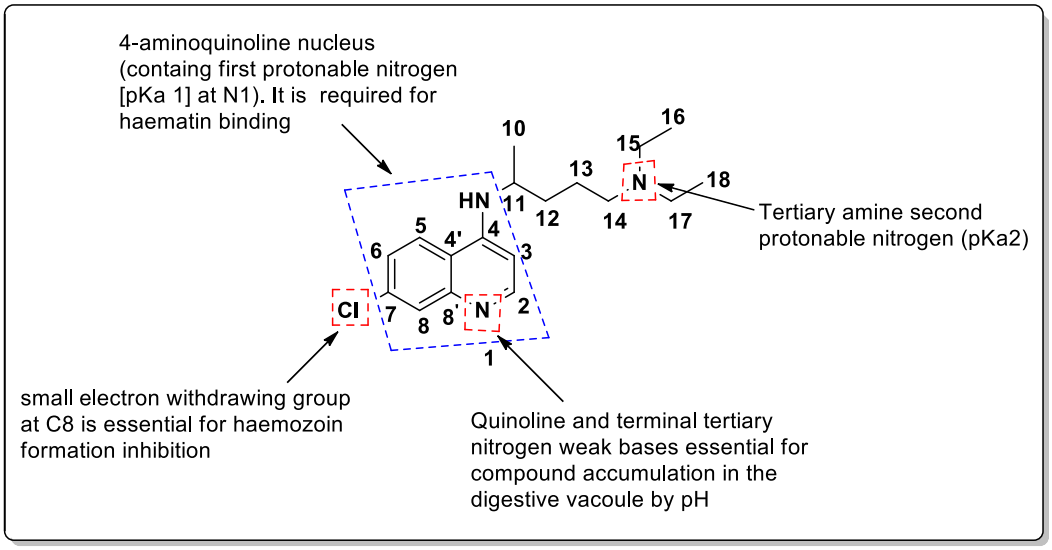

Figure 1.10: Structure-activity relationship (SAR) of Chloroquine

Mechanism of Action of Chloroquine:

The mode of action and resistance of chloroquine has not been thoroughly expounded. However, the proposed mechanism of action involves the accumulation of the chloroquine drug in the parasite's acidic digestive food vacuole either by ion trapping or heme polymerization inhibition[154][80].

Inside the human cell, *P. falciparum* feeds on amino acids. It accesses them by digesting the haemoglobin in the digestive vacuole during the intra-erythrocytic phase. As it feeds, a haemoglobin-derived iron (III) protoporphyrin IX (FeIII PPIX) complex, commonly known as haematin, is formed. Haematin is toxic to the parasite. The parasite detoxifies the haematin by converting it into haemozoin through crystallization or oxidation[155][156].

At their target site, the acidic parasite's digestive vacuole[154], 4-aminoquinoline derived drugs which are diprotic weak bases accumulates by 3 possible ways: passively diffusing across membranes; importation via an ATP-dependent transporter (active uptake) or by binding to a chloroquine accepter called ferriprotoporphyrin. As these type of drugs accumulate inside the acidic digestive vacuole they will be in protonated forms hence ion trapping. [157][158].

After further studies, in their paper, Olafson et al. referencing Egan 2003, demonstrated that quinoline antimalarials inhibit haematin crystallization through the adsorption of a drug–haematin complex on the haematin crystal surface[159].

The complexation of chloroquine to ferriprotoporphyrin IX (FPIX) results in inhibition of haemozoin formation. The free haematin interferes with the parasite detoxification processes and thereby damages the *Plasmodium* membranes by lipid peroxidation mechanism.

However, this has not been clarified yet due to the absence of unambiguous chloroquine-Fe(III) heme crystallographic data[160].

Chloroquine resistance

The major limitation to the usefulness of chloroquine is the emergence of drug-resistant strains of *P. falciparum*[151]. Aguiar et al. 2018 reported that chloroquine resistance does not involve any change to the target, which is the parasite, but involves drug efflux mechanisms[154]. Drug efflux is a mechanism in which the parasite will pump the toxic drug out of the cell. As a result of this, there is a decrease in the build-up and uptake of the drug in the parasite vacuole[161]. Resistance to chloroquine in *P. falciparum* parasites is mainly linked to mutations in the *P. falciparum* chloroquine resistance transporter (PfCRT) and to mutations in PfMDR1, the homologue of the human multidrug resistance gene MDR1. The PfCRT, and PfMDR1 facilitate resistance by interacting synergistically thereby reducing drug influx (**Fig. 1.11**)[162].

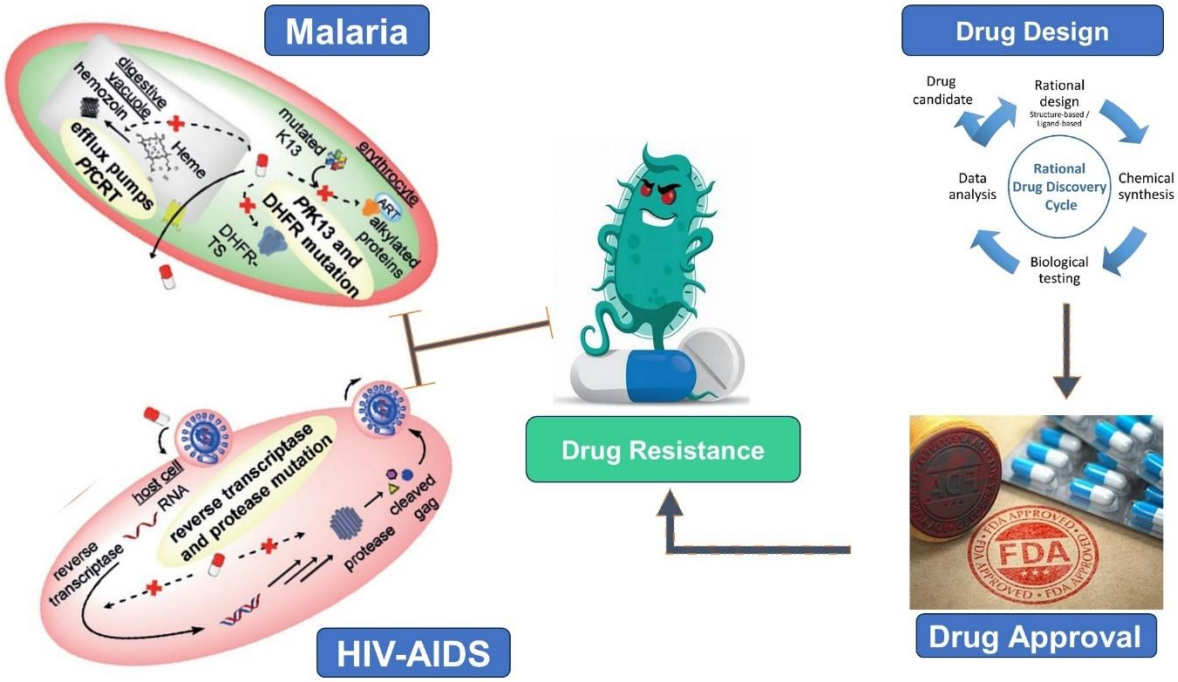

Figure 1.11 The impairment of major clinical indications due to drug resistance[163].

Saquinavir

The protease inhibitor saquinavir (**Fig. 1.12**) works by attaching itself to the HIV protease's catalytic site and preventing the cleavage of viral polyprotein precursors into mature, functional proteins, which are essential for viral replication[164].

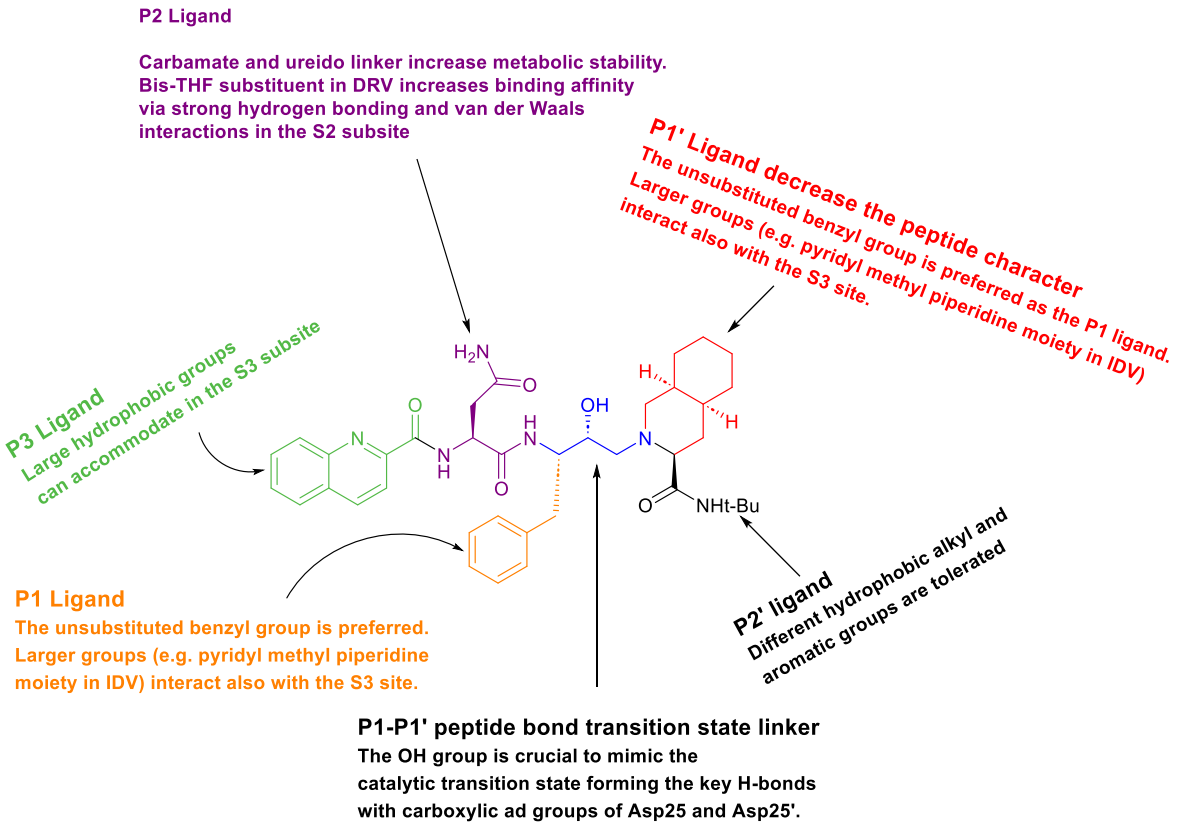

Figure 1.12 The Structure-Activity-Relationship of Saquinavir[165] .

Drug Resistance in HIV

In some patients, as the HIV viruses multiply, they also mutate. Some of these mutations even develop whilst a person is under treatment resulting in the inability of drugs to block the replication of the virus (**Fig. 1.11**)[166]. Financially unprivileged HIV positive pregnant women, when taking prevention treatment (e.g nevirapine) so as to prevent infection of their unborn babies pose to themselves the lethality of drug resistance evolvement if the unborn baby becomes infected. Another risk occurs when patients start using pre-exposure and post exposure prophylaxes while already infected with HIV [167][163].

Over the past years, a lot of research has been carried out to design better anti-HIV agents. An example is saquinavir and analysis of its structure-activity relationship to overcome resistance in HIV protease inhibitors is detailed in **Fig.1.12**.

Almost all the first protease inhibitors (PIs) to be approved by FDA had peptide-like chemical backbones and for the reason of this similarity, they suffered common problems such as low

oral bioavailability, high clearance rate, low half-life, and side effects as well. New drugs including lopinavir, atazanavir, tipranavir and darunavir were then made aiming to overcome the problems and complications associated with the previous PIs, particularly mutations that render the protease resistant[168][169].

In HIV therapy, resistance is determined by laboratory tests using a blood sample of the subject patient. Different antiretroviral formulations will then be assessed, and those found to be effective against that specific HIV strain will be prescribed as a regimen[166]. Thereafter, viral load assessment will continually be in check to monitor the efficacy of the prescribed regimen. In a case whereby the viral load is above the acceptable, that's an indication to say that the regimen prescribed is not effective, drug-resistance testing is repeated. With the new test results, experts can identify whether drug resistance is the problem and, if so, a need to change the regimen[167][166].

The widespread drug resistance has led researchers on a quest to refine the old scientific procedures to overcome resistance[167]. Combination therapy was working until the manifestation of non-complementary pharmacokinetics between different drugs. Issues like different absorption degrees and the patient's overall condition are problematic factors in fine-tuning the dosages of administered drugs to duplicate the observed *in vitro* synergy of both drugs[170].

Aided by the knowledge acquired from structure-activity relationship studies, this lack of pharmacokinetic complementarity may be overcome by conjugating pharmacophoric scaffolds to make a single hybrid antimicrobial agent[170][171]. Thus, monotherapy acquired through hybridization. It is efficient to reduce drug–drug interactions therefore facilitating the drug development process[172][173].

1.6 Hybridization as a strategy for drug discovery and development

Molecular hybridization is a rational drug design strategy that involves the conjugation of two or more existing bioactive moieties/pharmacophores[91][174]. The resultant hybrid entity should have amplified efficacy, reduced toxicity and/or exert multifactorial biological activities. Drug conjugates can be used to trigger the stability, release, or activity of drugs[175][176]. Hybrid molecules can be designed and classified based on the overlapping degree of joined scaffolds i.e fused and merged hybridizations.

Fused hybridization is the direct linkage through functional groups of each moiety, whereas merged hybrids are attained by overlapping moieties[177] as illustrated in **Fig. 1.13.** When linkers are involved, scaffolds are conjugated either by

(i) Cleavable linkers are bio-transformed at the site of action, the pro-drug strategy[178]. The most prominent role of drug conjugates is currently found in targeted delivery in which conjugation facilitates selective uptake in a specific cell type or tissue[174]. These type of linkers can be cleaved predominantly via three different mechanisms: acid-sensitive hydrazone linkers, glutathione-sensitive disulfide linkers, and protease-sensitive peptide linkers[179].

(ii) non-cleavable linkers which are non-hydrolyzable and enzymatically stable such as thioethers or maleimidocaproyl. Compared to their cleavable counterparts, they are composed of stable (esters, amides, carbamates, or disulfide) bonds that guarantee higher plasma stability and inhibit proteolytic cleavage[175][180].

The drug hybridization concept is proving to be a promising 'bullet' against the multifactorial nature of complex diseases. Currently, on the market, there are number of hybrid drugs and some candidates are still under clinical trials.

9

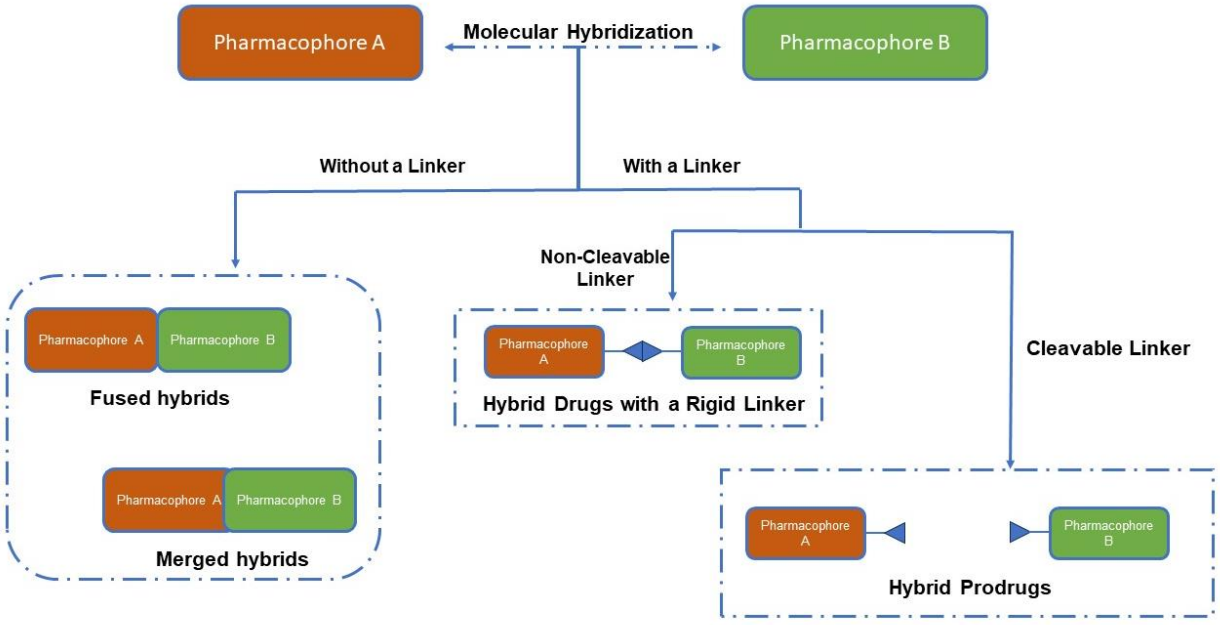

Figure 1.13: Common Strategy Templates in Hybridization[178][171]

1.6.1. Examples of hybrid drugs in clinical use

1. Brentuximab vedotin injection (**Fig 1.14**): This is an antibody-drug conjugate that works by killing cancer cells used in adults whose cancer is systemic and has failed to respond to combination chemotherapy[181].

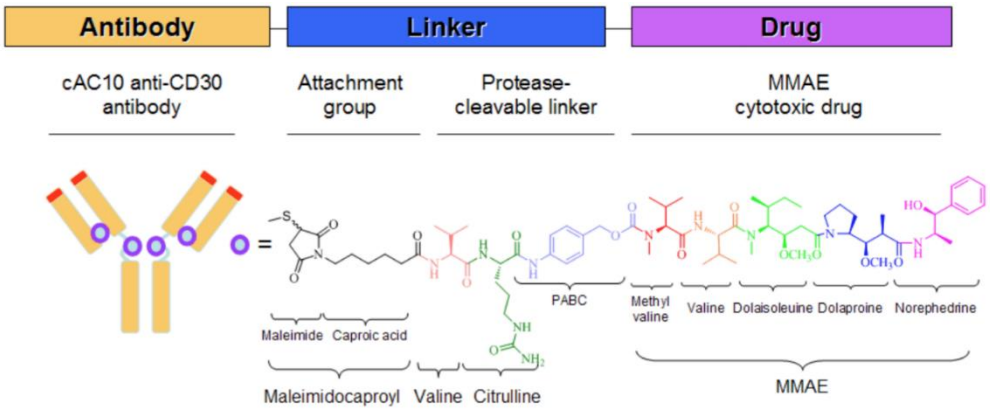

Figure 1.14: The structure of Brentuximab-Vedotin[181].

2. Trastuzumab emtansine: This is also an antibody-drug hybrid used to treat breast cancer[182] and its structure is represented in **Fig.1.15**.

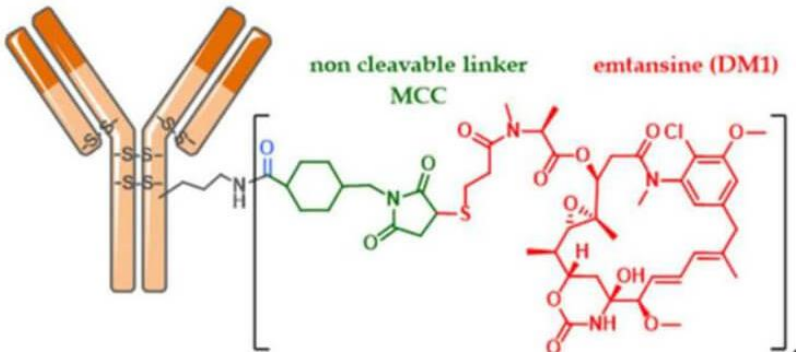

Figure 1.15: The structure of Trastuzumab-emtansine[182].

3. Dacinostat: This hybrid compounds were developed out of a non-cancer research program as reported by X.Y. Chu and co-workers in 2021 whereby they were screening a library of small compounds to find potential obesity inhibitors. In their study they discovered that dacinostat (**Fig. 1.16**) inhibited high-fat diet-induced obesity, insulin resistance, and fatty liver in mice without causing adverse effects[183].

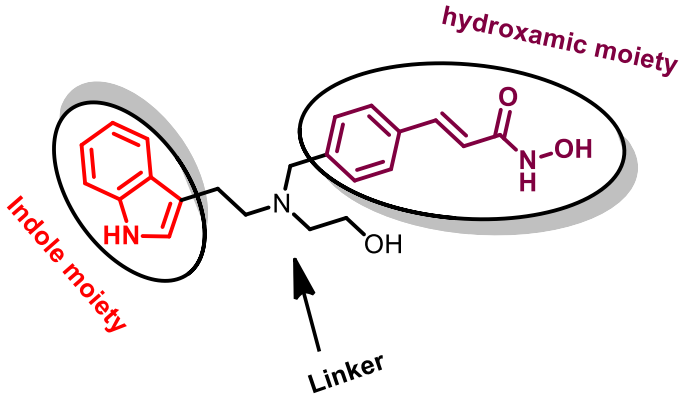

Dacinostat

Figure 1.16: Structure of Dacinostat[183].

1.6.2 Strategies for design and synthesis of hybrid drugs

For research groups that wish to pursue the conjugation route, there are several factors to be considered. This involves the selection of the right target combination and the achievement of a balanced activity towards them, while maintaining drug-like properties. The linker choice affects the overall performance of the hybrid drug thus its selection and design is key[184].

1.6.2.1 The Choice of a Linker

Drug conjugates are characterized not only by their pharmacologically active agents but also by the way they are attached to each other. The linkage influences the stability of the conjugate in the circulation, the compartment where it is activated by cleavage, and the speed of its activation[185][186]. In addition, the linker can influence the conjugates' solubility and might even alter the pharmacological potency of the pharmacophores it connects. Considering this high influence, the selection and design of a suitable linker for the desired drug conjugate is crucial. The best types of linkers will be the type of linkers that increase the polarity and hydrophilicity, thus, enhancing the solubility of the overall molecule. For example, linear chain linkers with different lengths[187][188].

Regio-chemistry of the linkage, if not well calculated, may result in negative intramolecular interactions between the biological target and the linker or even the conjugated motifs[187]. This will result in the negative impact on the efficacy and behaviour of the hybrid. The discovery of suitable positions for linker attachment might therefore require intensive studies on the structure–activity relationships[189]. Linkers thus affect how the drug binds at the active site and may further enhance activity/toxicity and vice versa.

For the current study, hydroxypyridinone-aminoquinoline (HPO-AQ) conjugates were designed in such a way that the quinoline scaffold was conjugated with hydroxypyridinone through amine linkage. According to Thelingwani et al., these linkers are cleavable as observed from their biotransformation studies[190].

1.6.3. Hydroxypyridinone-aminoquinoline hybrid drugs

In a bid to overcome chloroquine resistance by *P falciparum*, CQ like molecules, often referred to as aminoquinolines, were conjugated to iron chelating 3,4-*N*-alkyl-hydroxypyridinones[191][192] Prior to this strategy, it had been reported that combinations of 3,4-HPOs and CQ was synergistic against CQ resistant *P. falciparum*[193]. The hybrid drug under consideration can be assumed to have two moieties or scaffolds, the quinoline scaffold linked to the 3,4-*N*-alkyl-hydroxypyridinone via an *N*-alkyl-linker.

1.6.3.1 The quinoline scaffold

The quinoline motif also known as 1-aza-naphthalene or benzo[*b*]pyridine is a planar hetero-aromatic compound that is identified by the chemical formular C_9H_7N[194]. It consists of a pyridine and benzene structure fused together by a change in the state of the benzene ring with pyridine[195].

Chemically, quinoline is a tertiary amine base that can form salts in the presence of acids. Its common chemical reactions are nucleophilic and electrophilic substitutions, reactions similar to those of benzene and pyridine[196][197].

Quinoline (reported as the lead structure) and its functionalized moieties are highly essential pharmacophoric motifs with undeniable therapeutic propensity[198]. Expansive work has been done on exploring these biological properties of the functionalized quinoline scaffold and its derivatives, some of which are discussed below. The R groups can be modified to enhance antimicrobial efficacy or minimise toxicity and resistance (**Scheme 1.2**)[199].

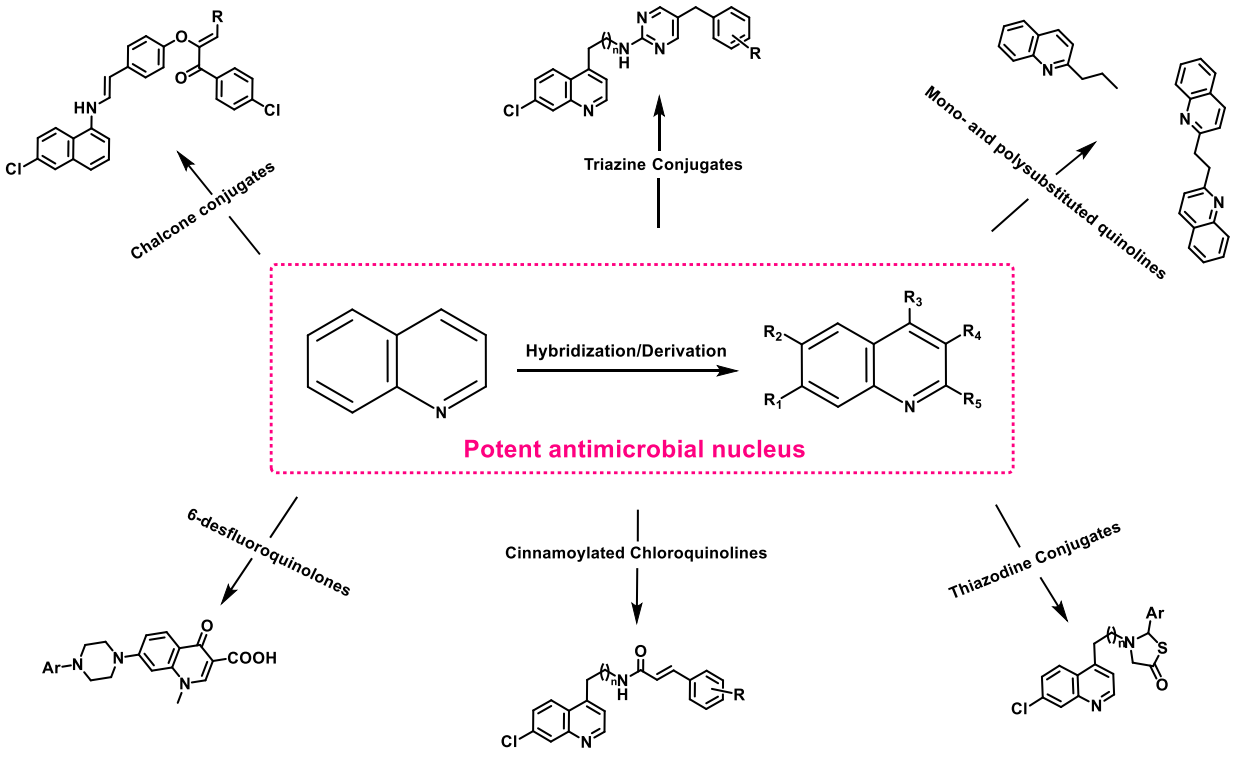

Scheme 1.2: Structures of some quinoline derivatives[194][200]

Chalcone–4–aminoquinolines conjugates tethered with keto-enamine were synthesized by Sashidhara and co-workers as potential antimalaria agents. They evaluated these compounds *in vitro* against the K1 *P. falciparum*-chloroquine resistant strain. The compounds exhibited better activities than chloroquine. The improved efficacy was associated to the substitution pattern and the number of substituents present on the phenyl ring[201].

Many researchers, including Rawat et al., explored the conjugation of 4-aminoquinoline with 1,2,3-triazine. They synthesized their compounds via the Huisgen-1,3-dipolar cycloaddition reaction of 4-azido-7-chloroquinoline with different substituted terminal alkynes. Unfortunately, none of their compounds were better than chloroquinoline when they were tested in vitro against both chloroquine-sensitive (D6) and chloroquine-resistant (W2) strains[194].

4-Aminoquinoline–cinnamic acid hybrids have also captured the interest of many researchers because of their vast biological properties including antimalarial[202] and antileishmanial[201]. Aminoquinoline-Thiozodine hybrids when tested against NF-54 strain of P. falciparum had very low IC_{50} values ranging between 0.013–0.98 mM. their structure activity relationship studies revealed that compounds with two and three carbons on the lateral side chain of 4-aminoquinoline had better activities[203].

Among others, Fakhfakh et al. and co-workers reported that mono- and poly-substituted quinolines have anti-HIV activities[201]. The Quinoline ring with NH linkage has been found to boost the inhibitory activity towards the HIV-protease. Thus quinoline/quinolone template has been identified as a potent pharmacophore and bears the potential scope for future anti-HIV drug discovery[204]. Other biological properties include anticancer, anti-inflammatory, antioxidant, antitubercular, antiprotozoal, and DNA binding [194][199].

The scaffold of interest,4,7-dichloroquinoline can be prepared by the Michael addition of acrylic acid to the chloroamine via Friedel-Crafts cyclisation (**Scheme 1.3**) Both sterically and electronically, the position next to the chlorine is slightly disfavored by the diethyl-2-oxosuccinate as it attaches to the chloroamine. Chlorination and oxidation are conveniently carried out in the same step[205].

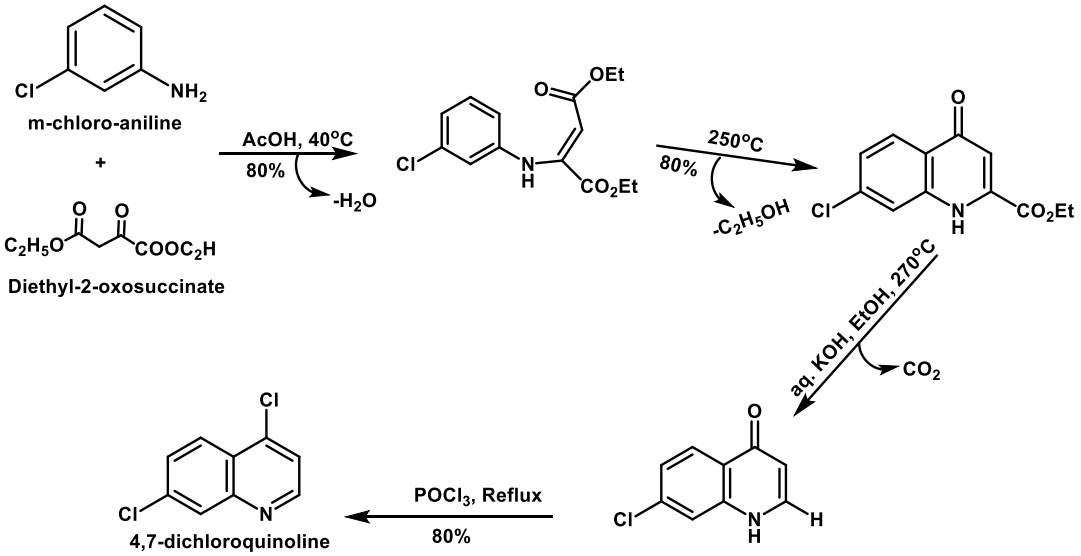

Scheme 1.3: Synthesis Scheme of 4.7-dichloroquinoline[205]

1.6.3.2. The Hydroxypyridinone Scaffold

Pyridinones are classified as six-membered heterocyclic scaffolds consisting of nitrogen, oxygen, and five carbon atoms. Despite the small size of the pyridinone, it provides five derivatizable positions possessing four hydrogen bond acceptors and a hydrogen bond donor[206]. According to the relative position between the nitrogen heteroatom and carbonyl moiety, two isomeric forms namely 2- and 4-(1H)-pyridinones exist as skeletal components **(Fig. 1.17**)[207]. However, a study on isomerization between the pyridinone and the corresponding hydroxypyridine indicates that the former form is favoured, especially in physiological conditions[208][207].

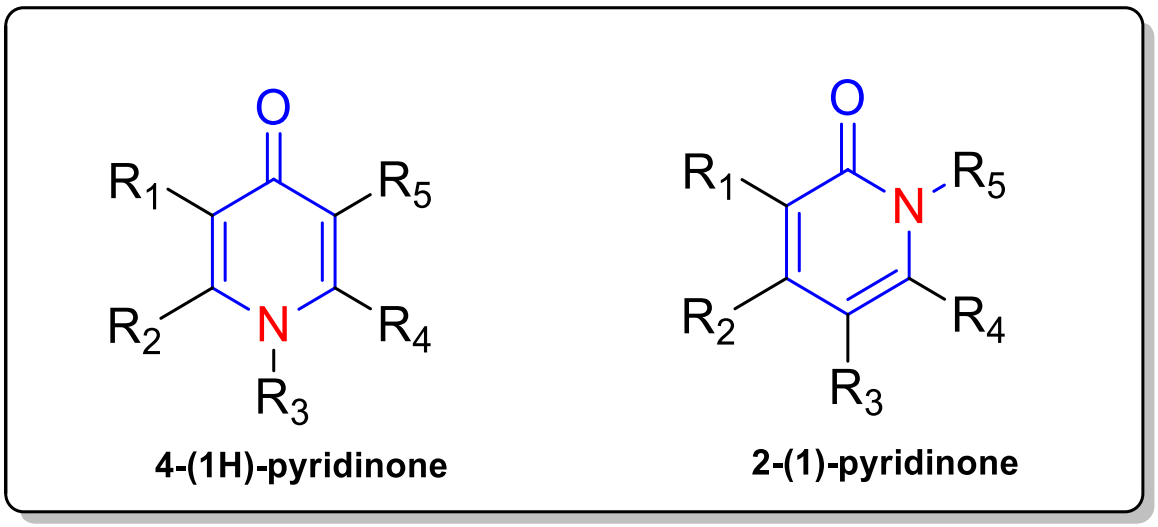

Figure 1.17: Two regio-isomeric forms of pyridinone

In recent years, pyridinone derivatives have attracted extensive attention due to their versatile agricultural, industrial and pharmaceutical applications[209]. In the pharmaceutical sector, they have managed to draw so much attention due to their various pharmacological properties. They have also stood out for their high and relatively specific iron chelation properties[206].

Motivated by the findings from the studies conducted by Xiao et al. (2006)[210] and Dias et al. (2009) [211]when 5-chloro-3-hydroxypyridin-2(1H)-one was identified as a chelating ligand. In 2013, Parhi *et al.,* reported on a series of such derivatives that inhibited the influenza A endonuclease with enhanced potency[204]. Debnath *et al.,* 2013 reported that modifications on positions 3, 4, and 6 of the pyridinone ring were crucial to improve antiviral activity. With the stated modifications, pyridinone derivatives were synthesized and evaluated using TZM-bl cell lines, and they exhibited excellent antiviral activities[212]. Also, HPOs are capable of crossing the cell membrane easily, forming additional interactions with other therapeutic targets thereby increasing the overall hydrophilicity of molecules[207].

1.6.4 Antiplasmodial Hydroxypyridinone-Aminoquinolines

Using the molecular hybridization approach, Andayi (2011) synthesized a series of 4-aminoquinoline-3-hydroxypyridin-4-one hybrid compounds as potential antimalarial agents[193][213].The hybrids were either based on kojic acid or maltol as the source of the HPO moiety and this is elaborated in **Scheme 1.4** and **Scheme 1.5**

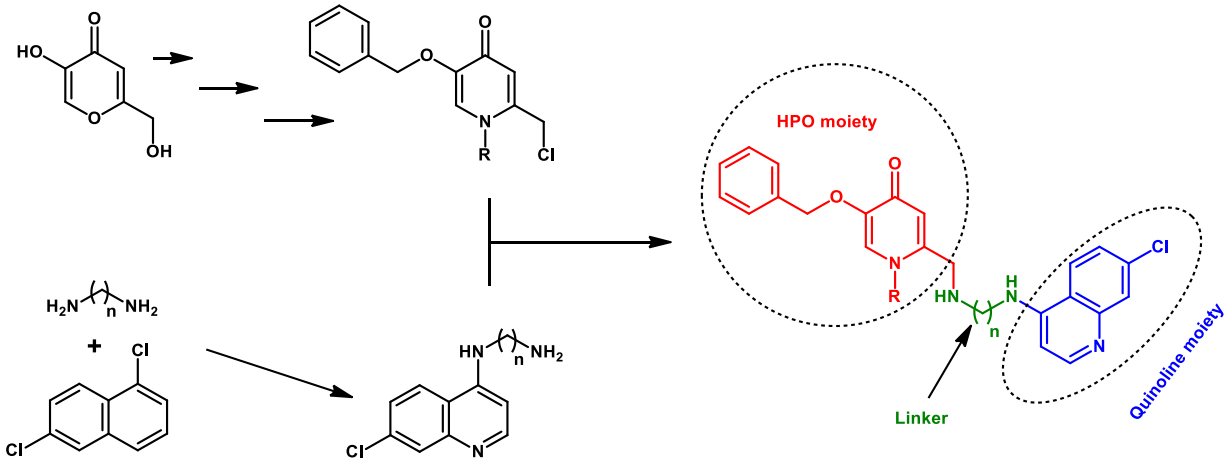

Scheme 1.4: Synthesis scheme of kojic acid derived compounds[193]

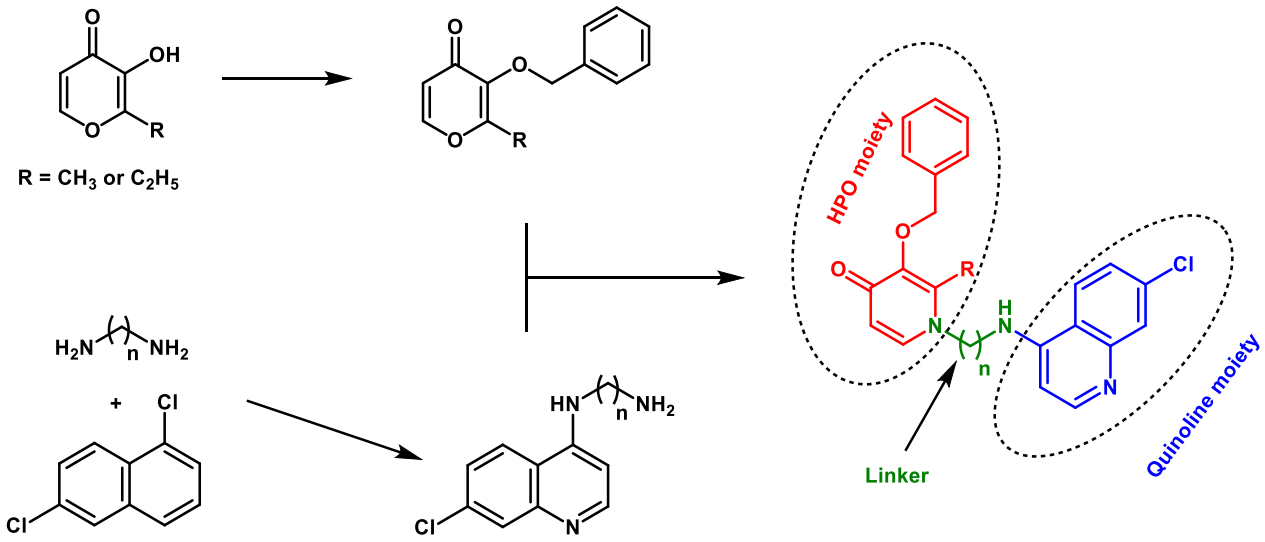

Scheme 1.5: Synthesis scheme of maltol derived compounds[193]

The synthesized compounds were evaluated for antiplasmodial activities against 3D7 (sensitive) and the K1 (resistant) strains of *P. falciparum in vitro* as well as elucidating their mechanisms of action. It was confirmed that the hybrids antiplasmodial mode of action was *via* inhibiting β-hematin formation. Unfortunately, they also showed potential to cause drug-drug interactions such that they were potent CYP3A4 inhibitors. Attempts to modify the structures to minimize the CYP3A4 inhibition were in vain[213].

Thelingwani *et al.*(2014) reported that both *in silico* and *in vitro,* hydroxypyridinone-aminoquinoline compounds are inherently CYP3A4 inhibitors irrespective of a series of structural modifications[190]. Docking studies further distinguished weak CYP3A4 inhibitors from strong inhibitors[193].

Despite the CYP3A4 liability of the HPO-AQs, these molecules can be repurposed for chemotherapeutic applications in other diseases like cancer and HIV-AIDS where CYP3A4 inhibition may not be a big issue if risk and benefit analysis are carefully considered. Therefore, in this study, a set of HPO-AQ hybrids will be synthesized and evaluated for their potential as drugs for HIV-AIDS and cancer treatment alongside management of malaria - HIV co-infections.

1.7 Problem Statement and Motivation of Study

Malaria and HIV-AIDS are fatal infectious diseases. Given the overlap of their geographic distribution and resultant coinfection rates, interactions between the two diseases pose major public health problems. To compound the situation, the causative agents of the two diseases are becoming more tolerant (resistant) to almost all currently available drugs. Also, young children and pregnant women do not have adequate medication, yet they are the most vulnerable population groups. So, there is a need to develop new agents/strategies that can cater for them and drugs with novel modes of action that can replace the old ones that have lost efficacy to resistance.

1.8 Rationale of Study

There are limited medication options for pregnant women and young children. The levels of CYP3A4 in children and pregnant women is elevated and thus necessitating dose adjustments for most drugs in clinical use to achieve treatment success. Without the dose adjustment the resultant low drug bioavailability exposes pathogens to sub-optimal dosages thus fomenting drug resistance. Hydroxypyridinone-aminoquinoline compounds which were found to be potent CYP3A4 inhibitors, could be repurposed as antimalarials specifically for children and expectant mothers.

Drug repurposing or repositioning across different types of diseases is common. Thus, the study also aims at repurposing HPO-AQS for the treatment of HIV-AIDS and malaria coinfections. Despite the CYP3A4 liability of the HPO-AQs, these molecules can be repurposed for chemotherapeutic applications in cancer and HIV-AIDS where CYP3A4 inhibition is not an issue if risk and benefit analysis is carefully considered.

1.9 Aim and Objectives of the Study

Aim

To design, synthesize, characterize and evaluate Hydroxypyridinone–aminoquinoline hybrid HPO-AQ compounds for their potential as agents against HIV-AIDS and malaria.

Objectives:

1. To design HPO-AQ molecules rationally and in silico.
2. To synthesize, purify and elucidate the structures of the synthesized compounds.
3. To test for the activities of the synthesized compounds *in vitro* antimalarial, anti-HIV and cell toxicity assays.

Chapter 2: *In-Silico* and Rational Design

The world is in dire need of new drugs with better efficacy and lower toxicities. Unfortunately, the traditional drug design and development process is long, complex, expensive, and time-consuming. The process involves 1) target identification, 2) target validation, 3) hit discovery, 4) lead optimization, and 5) preclinical/clinical development. Should the drug candidate pass all these phases, it is then approved and launched on the market. Apart from the challenges associated with target validation and hit identification, a significant number of clinical trials fail because of poor pharmacokinetics, ineffectiveness, and toxicity[214][215]. To overcome the hurdles and challenges encountered in the traditional drug design approach, modern techniques such as *in-silico* methods, also known as computer-aided drug design[215] are utilized. *In silico* techniques enables the prediction and analysis of prospective therapeutic candidates' biological activities and physicochemical[216].

2.1 Rational Design

The rational design was based on quinoline as an antimalarial pharmacophore and iron chelation inhibition of plasmodium proliferation in addition to studies earlier done by Andayi et al[192]. Just like chloroquine **(Fig. 1.10),** a lot of reports including the one published by D. D. N'Da and P.J Smith (2014), outlined the common features that influence the activity of aminoquinolines against both the sensitive and resistant strains. These features include,

i. a quinoline scaffold without any functionalization but with a halogen element at position 7 of the quinoline scaffold,
ii. a protonable nitrogen at position 1 and the other one at the end of the side chain that attaches on the 4^{th} position.
iii. the size of the chain length influences the overall antiplasmodial activities of compounds. A propyl diaminoalkane side chain was reported to be tenfold more potent than a butyl diaminoalkane side chain when evaluated against a CQ-resistant parasite strain[217][218].

All the tested compounds possess a quinoline moiety thus they only differed structurally by the linkers. These hybrids, though additionally contain a terminal hydroxypyridinone moiety, comply with these reported structural features.

Andayi *et al.* (2014) reported that the hydroxypyridinone moiety is an iron chelator thus, it is very pivotal in the design of potential antiplasmodial candidates because of the central role of iron for the rapid proliferation of the malaria parasite and the arrest of parasite growth by iron chelation.

Elevated host iron level as observed in pregnant women is a serious risk factor for human malaria. Therefore, Antimalarial drugs that can address the excess physiologic iron load problem may be beneficial to infected pregnant mothers and persons with excess physiologic iron[192][193].

The hydroxypyridinone-aminoquinoline compounds were designed in such a way that they have a chelator (HPO) linked to quinoline nucleus with varying linker length, thereafter, we moved ahead to predict the ADMET and drug-likeness of the proposed compounds using SwissADME as an *in-silico* tool.

2.2 *In Silico* Methods in Drug Design

Currently, there are two *in-silico* approaches, namely, structure-based drug design and ligand-based drug design. The availability of target protein structural information determines which approach is best to use. Ligand-based drug design is a useful method for designing molecules with properties similar to known ligands that bind to proteins, so it might be the best choice if the structure of the protein is unknown. Structure-based drug design is preferred when the structure of the protein is known[219][220].

A number of publications recommend the use of *in-silico* tools such as SwissADME as a designing tool[220][221][222]. In the present study, hydroxypyridinone-aminoquinoline compounds were designed based on the ligand-based drug approach using SwissADME. SwissADME is a screening web tool that was developed by the Swiss Institute of Bioinformatics and is freely available at www.swissadme.ch [Date of Access: 24 April 2024].

Hydroxypyridinone-aminoquinoline compounds were designed in two series namely Kojic derived derivatives **(Fig.2.1)** and Maltol derived compounds **(Fig 2.2)**. It is worth to mention that some of these compounds have been synthesized before by Andayi *et al*., and they were repurposed in this study to be used as potential anti-HIV agents.

Series One: Kojic Derived Compounds (1a-l)

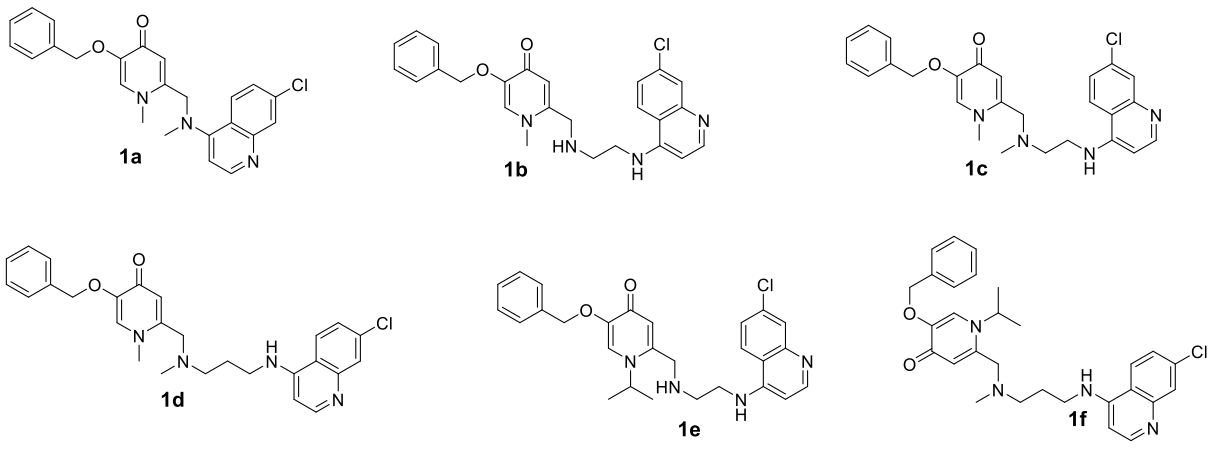

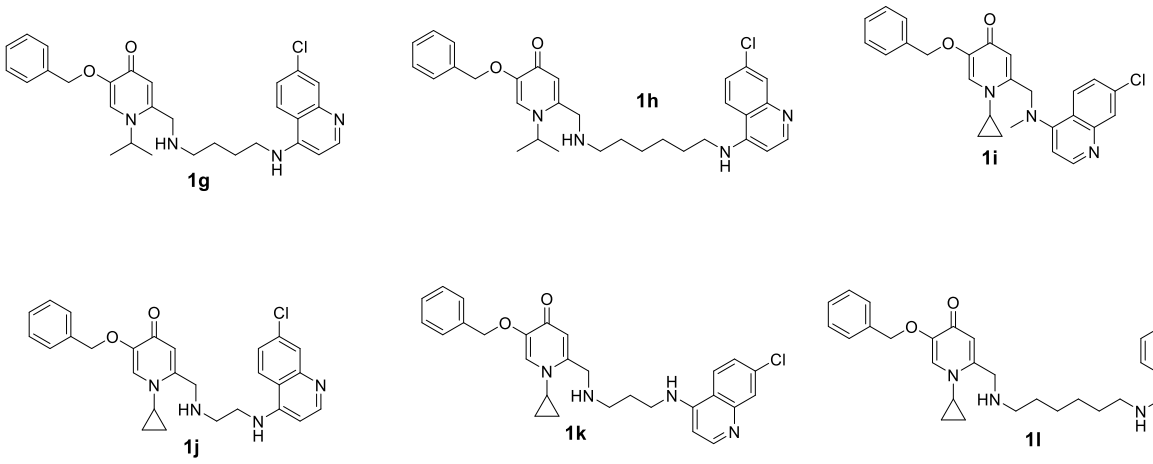

Figure 2.1: Structures of Kojic-derived compounds

Series Two: Maltol-derived compounds (2a-2h).

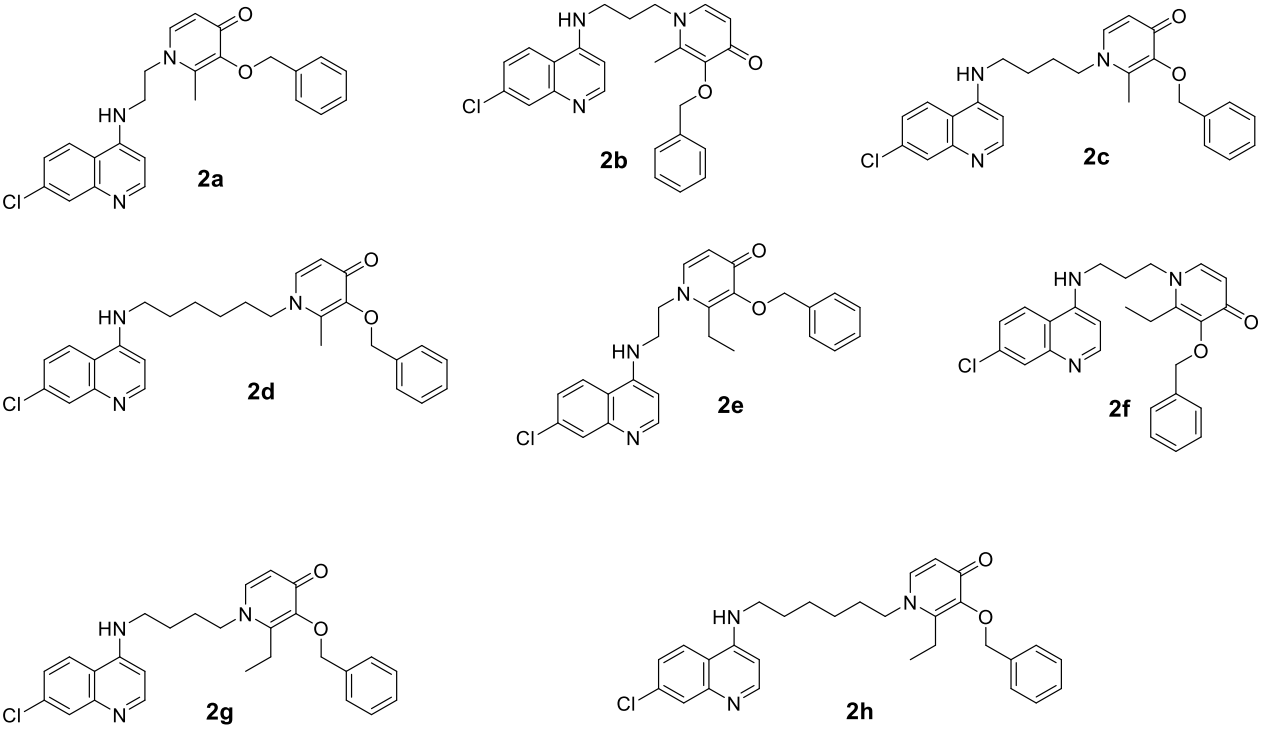

Figure 2.2: Structures of Maltol-derived compounds

2.3 SwissADME Computational Data

Important Note: Some of the raw computational data is provided in the supporting information document.

2.3.1 Physiochemical Properties

A number of physical chemical properties have been reported to be fundamental predictors of good oral bioavailability. These properties include molecular flexibility which is determined by the number of rotatable bonds, and low polar surface area or total hydrogen bond count (sum

of donors and acceptors). The number of rotatable bonds and polar surface area or hydrogen bond count tend to increase with molecular weight and may in part explain the success of the molecular weight parameter in predicting oral bioavailability. The commonly applied molecular weight cutoff is 500g/mol[223][224]. This transcribes potential good bioavailability properties for all the proposed compounds in this study as they have molecular weights not greater than 500g/mol, except for **1f** (505.05g/mol), **1g** (505.05g/mol), **1h** (533.10g/mol) and **1l** (531.10g/mol). This is because of the large number of heavy atoms present in the structures.

2.3.2 Lipophilicity

Lipophilicity (log $P_{o/w}$) reflects the affinity of a molecule for an aqueous or lipophilic environment and can be used to predict the molecules' potency, binding affinity to proteins which are mostly hydrophobic in nature. Too high lipophilicity translates to increase *in vitro* promiscuity and *in vivo* toxicity whilst low lipophilicity denotes poor ADMET (Absorption, Distribution, Metabolism, Excretion and Toxicity) properties. SwissADME have five models that aid in predicting lipophilicity and log $P_{o/w}$ is average of the values predicted by the five models[225][226].

From the data obtained from SwissADME data, it was observed that as the chain length increases, the lipophilicity values increased. From the proposed compounds, the most lipophilic compound would be with **2i** mean LogP= 6.9 and having a long carbon chain linker is a likely contributor to the high LogP value. The least lipophilic compound was derivative **1i.** It has one carbon chain linker with the predictive mean LogP= 4.712). An acceptable LogP value should be less than 5 but according to Lipinski, an ideal LogP value should be between 1.35 and 1.8 Therefore, the range of 4.712 – 6.9 is not within the acceptable range of LogP.

2.3.3 Water Solubility

Water solubility is a crucial property for potential drugs as it eases handling and formulations[227]. SwissADME predicts water solubility using two methods namely the ESOL model (ESOL Log S) and the Ali (Ali Log S) model. Khetan S.M *et. al.,* (2019), documented solubility ranges as[228]:

a) Soluble compounds: - 0 to -2
b) Moderately soluble: -2 to -4
c) Poorly soluble compounds: < -4

All the proposed compounds had Log S values within the moderately soluble to insoluble range. Compound **1i** with a Log S value of -5.19 and compound **2i** with a Log S value of -7.75. This data shows the compounds fall in category c thus poorly soluble, however this is just a prediction and actual experimental measurements will be necessary[229].

2.3.4 Pharmacokinetics

Administration, Distribution, Metabolism and Excretion behaviors of drug candidates are determined by predicting skin permeability, GI absorption, Brain-Blood Barrier Permeation, Permeability glycoprotein substrate and CYPs inhibition/induction as detailed below.

The ability of the candidate to penetrate the skin and induce toxicity denoted as the skin permeability coefficient (Log K_p value in cm/s). Negative Log K_p values suggest reduced skin penetration potential[230][231]. All the proposed compounds had coefficients within the range of -4.00 cm/s to -7.90 cm/s. This transcribes that the proposed compounds are safe and have potential to proceed to human administration stage.

Ability to diffuse across a cell membrane from a region of high concentration to low concentration (passive human gastrointestinal absorption)[232]. Gastrointestinal absorption rate is supposed to be high in both animals and humans[233]. All the proposed compounds had high gastrointestinal absorption indices. This qualify them to be good candidates. Blood-brain barrier (BBB) permeation denotes the ability of compounds to permeate the brain. Most of the compounds were predicted to be BBB substrates. It was critical to determine the brain permeability properties of the proposed compounds to determine if they won't be toxic to neurons in the brain. This could be good or bad depending on what the drug is for. I think for malaria, it is good for a compound to permeate the brain so as to cure cerebral malaria.

The permeability glycoprotein (P-gp) is the protein that transports drugs around the body system. The expression of the permeability glycoprotein in the BBB plays a pivotal role in restricting the entry of various drugs into the central nervous system. In other words, the inhibition of the permeability glycoprotein results in increased drug delivery to the brain[234].

All the proposed compounds were predicted to be P-gp substrates except for compound **1i** which foretells better absorption and distribution of these compounds. Interaction of molecules with cytochromes P450 enzymes either through inhibition or induction, especially inhibition could result in negative drug-drug interactions. Subsequently, this results in lower clearance and accumulation of the drug or its metabolites in the system thus toxicities. It is therefore vital to predict the susceptibility of which a molecule will cause consequential drug-drug interactions through inhibition of CYPs, and to determine which isoforms are affected. All the proposed compounds were predicted in SwissADME to be CYP3A4 inhibitors and some variations with CYP1A2, CYPC19, CYP2D6 isoforms[235]. CYP inhibition (specifically with CYP3A4 enzymes) experiments will be necessary to prove such predictions.

2.3.5 Drug-likeness

Drug-likeness is the qualitative measure of how the properties of a candidate molecule is similar to the existing drugs[236]. SwissADME assesses compounds based on specific requirements i.e. the Lipinski Rule of Five, Ghose filters, Veber Rules, Egans Rules, Muegges Rule and Abbots Bioavailability score.

The Lipinski Rule of Five specifies that for a molecule to qualify as a potential drug candidate it should fulfill the following: i.) molar mass of less than 500g/mol, ii.) Less than ten H-bond acceptors, iii.) Less than five H-bond bond donors and iv.) LogP<5[237].

All the proposed compounds did not violate the Lipinski Rule of Five except for **1f** (505.05g/mol), **1g** (505.05g/mol), **1h** (533.10g/mol) **and 1l** (531.10g/mol) which had molar masses greater than 500g/mol.

The Ghose Filter quantifies drug-like compounds to have[238]:

a) Log P: -0.4 to 5.6
b) Molecular Weight: 160g/mol to 480g/mol
c) Molar refractivity: 40 to 130
d) Total number of atoms: 20 to 70.

The proposed compounds had at least one Ghose violation except for **1i** has a LogP value of 4.712; Molecular weight of 419.90g/mol; Molar refractivity of 121.95 and a total number of atoms of 52.

The Veber rules qualifies compounds that have ten or less rotatable bonds and a polar surface area no greater than 140 $Å^2$. Those compounds are likely to exhibit good oral bioavailability[239]. From the SwissADME predictions, only **1l** (14 rotatable bonds) and **2g** (12 rotatable bonds) violated the Veber's rule.

The Egan rule considers compounds with 0 ≥ Topological polar surface area ≤ 132 $Å^2$ and -1≥ LogP ≤ 6 to have good bio-availabilities[240]. Pleasingly, none of the compounds violated the Egan's rule.

According to the Muegge's rule most compounds qualified to be potential drug candidates. Though a few compounds violated this rule, most of them had the stipulated preconditions that is i.) molecular Weight: 200-600g/mol ii.) LogP: -2 to 5 iii.) Polar Solar Area: ≤150 iv.) Number of rings: ≤7 vi.) Number of carbons: >4 vii.) Number of heteroatoms: >1 viii.) Number of rotatable bonds≤15 ix.) Number of H-bonds donorD≤5 x.) Number of H-bond acceptor: ≤10 [241][242]:

The Abbot Bioavailability Score predicts the likelihood of a compound to have more than 10% or 0.1 bioavailability in rats[235][232]. The predicted scores for all the compounds had 0.55 which is greater than 0.1. Should the compounds proceed to *in vivo* experiments, already we have an any idea that they will have a good bioavailability.

2.3.6 Medicinal Chemistry Friendliness

On SwissADME, these are predictions done using the PAINS model to identify problematic molecular fragments that could be toxic, medically reactive, metabolically unstable or to bear properties responsible for poor pharmacokinetics[221]. Mishra *et al.* 2019 reported that synthetic accessibility scores range from 1 (very easy) to 10 (very difficult)[222]. All the proposed compounds had synthetic scores ranging from 2-3 translating ease of synthesis.

2.4 Conclusion

The attention of this work was focused on the predictions of lipophilicity, physicochemical properties, and CYP isoform targets. The synthesis, structures, and biological potentials of these derivatives have been previously documented for our proposed compounds[213][193]. SwissADME results predicted that hydroxypyridinone-aminoquinoline compounds could be developed as synthetic medical products. This has been the basis of subsequent synthesis and *in vitro* studies (results discussed in chapters 3, 4 and 5). Accordingly, the outcomes of this research will be useful for optimizing compounds targeting malaria and HIV as well as teasing out the differences between computational predictions and actual experimental outcomes.

Chapter 3: Chemistry – Synthesis of HPO-AQs

3.1 Retrosynthetic Analyses

The hydroxypyridinone-aminoquinoline compounds synthesized in this project were designed and prepared in two distinct series: 1) Maltol-derived conjugates and 2) Kojic acid-derived conjugates. To achieve the optimal synthetic pathway for the target molecules (TM), hydroxypyridinone-aminoquinolines, several factors such as cost, simplicity, and feasibility of using various reagents and intermediates were considered. The retrosynthetic analysis of the target molecules was conducted to identify the most efficient synthetic route. Retrosynthesis involves the systematic deconstruction of the target molecule into simpler, commercially available starting materials (SMs) known as synthons. This process also includes the conversion of functional groups into other functional groups through known chemical transformations, a practice referred to as Functional Group Interconversion (FGI). By employing retrosynthesis, the target molecules were broken down into their fundamental building blocks, facilitating the identification of feasible synthetic routes based on established reactions. This approach not only streamlines the synthesis but also ensures the practicality of the proposed pathways by leveraging available reagents and intermediates. Below are the proposed retrosynthesis pathways for the hydroxypyridinone-aminoquinoline compounds, detailing the step-by-step deconstruction and subsequent reassembly into the desired target molecules[205][243][244].

3.1.1 Retrosynthesis of Kojic Acid Derived Conjugates

Starting with the target molecules (**Scheme 3.1**), specifically the kojic acid-derived conjugates, we can strategically disconnect the molecules by cleaving key carbon-nitrogen bonds. The initial disconnection yields 4-aminochloroquinolines (**6**) and the acyclic intermediate (**3)**. Further retrosynthetic analysis of the 4-aminochloroquinolines (**6**) involves cleaving another carbon-nitrogen bond, resulting in the formation of 4,7-dichloroquinoline (**9**) and diaminoalkanes (**8**). These disconnections simplify the complex target molecules into more manageable fragments. The acyclic intermediate (**3**) undergoes functional group interconversion to produce an alkylated pyridinone (**4**). This alkylated pyridinone can then be dealkylated to achieve the desired intermediate (**5**). Additionally, the benzyl-protecting group present in the molecule can be disconnected through C-O cleavage, yielding kojic acid and benzyl chloride as synthons.

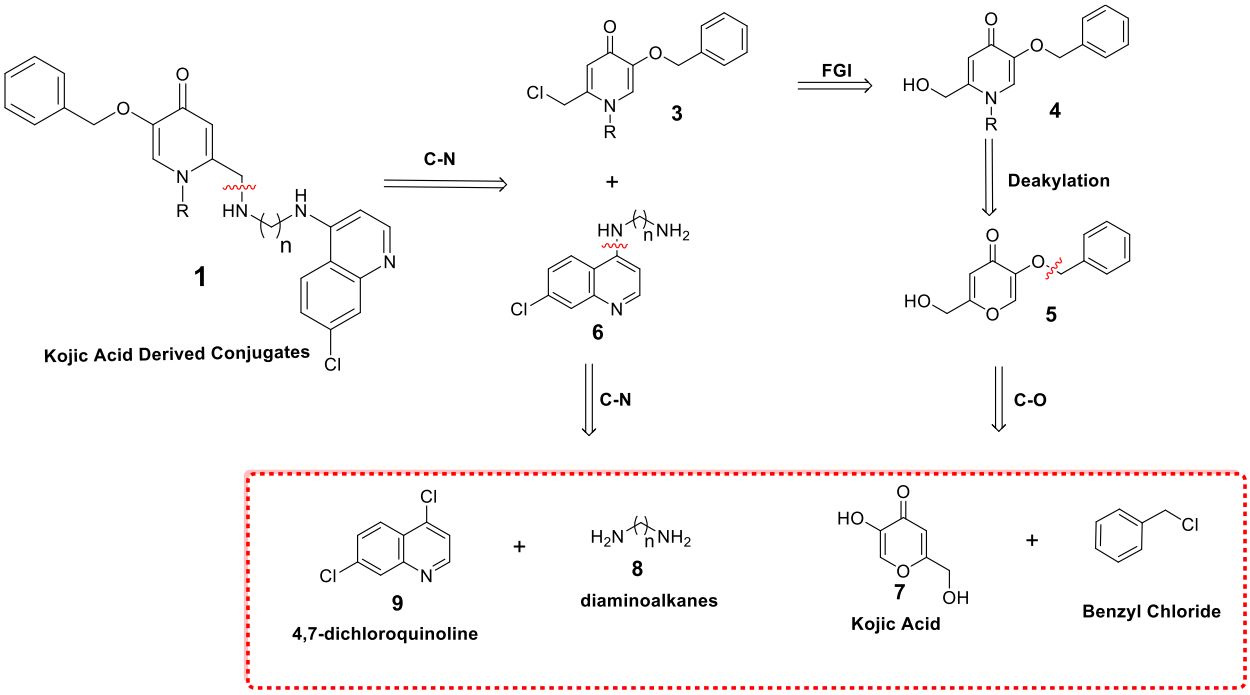

Scheme 3.1: Kojic acid derived conjugates retrosynthetic analysis

The synthons encircled in red in **Scheme 3.1** are the starting materials readily available from commercial sources. This strategic approach leverages readily accessible reagents and intermediates, streamlining the synthesis of the target molecules while ensuring cost-effectiveness and feasibility.

3.1.2 Retrosynthesis of Maltol Derived Conjugates

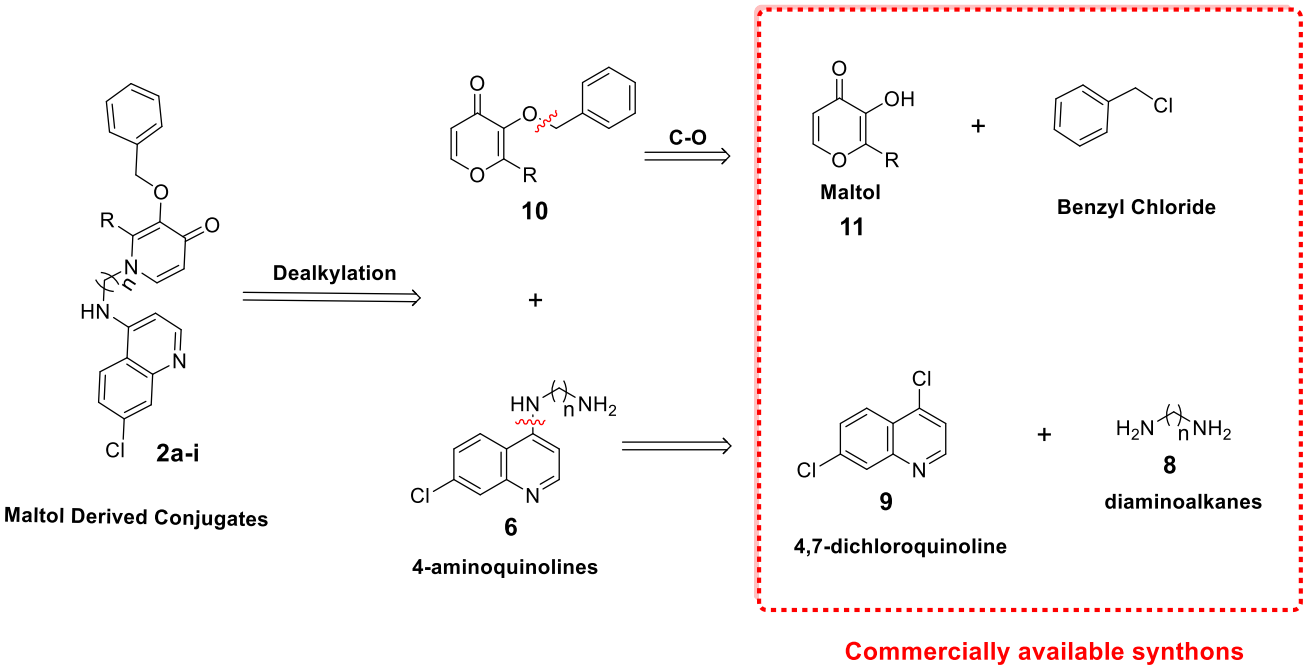

Scheme 3.2: Maltol derived conjugates retrosynthetic analysis

Starting with the target molecules, maltol derived conjugates, they could be dealkylated and disconnected to yield 4-aminochloroquinolines and the benzylated-maltols **10**. The benzyl-protecting group could be disconnected via C-O cleavage to yield kojic acid and benzyl chloride as synthons. The 4-aminochloroquinolines are cleaved via the C-N bond as indicated to 4,7-dichloroquinoline **(9)** and diaminoalkanes **(8)**. The synthons encircled in red are the starting materials which are readily available on the market.

3.2 Synthesis of Compounds

Based on the preceding retrosynthetic pathways, the target molecules were prepared as explained in detail below, starting with the commercially available synthetic precursors and/or reagents.

3.2.1 Synthetic Pathway of *N*-(7-chloroquinoline 4yl) alkyl-diamines

Guided by the previously published methods[245][246], *N*-(7-chloroquinoline 4yl) alkyl-diamines were prepared by following the schematic pathway below:

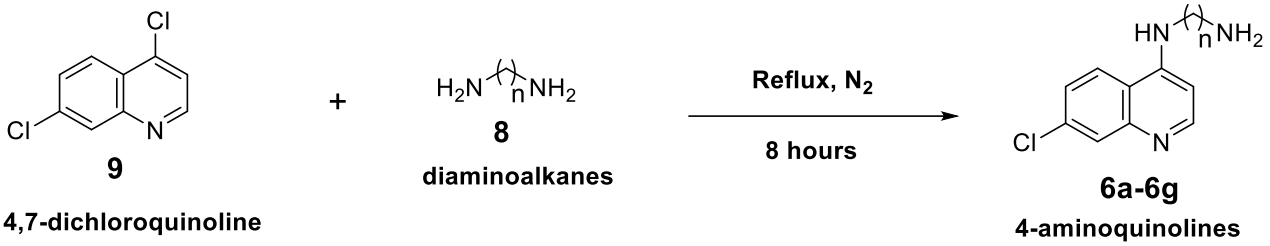

Linker in 4-aminoquinolines

6a: =methyl amine, **6b**: = 1,2 diaminoethane, **6c**: = N-metthy-1,2 diaminoethane

6d: = 1,3-diaminopropane, **6e**: = N-methyl-1,3-diaminopropane

6f: 1,4-diaminobutane, **6g**: = 1,6 diaminohexane

Scheme 3.3: General Synthesis of *N*-(7- chloroquinoline 4yl) alkyl-diamines

All the 4-aminoquinoline compounds used in this project were prepared as outlined in **Scheme 3.3,** whereby mixtures of 4,7-dichloroquinoline (1.0 equiv.) and excess different diaminoalkanes (5.0 equiv.) in neat conditions were refluxed for 8 hours while stirring under inert conditions (explained in detail in Chapter 6). The successful synthesis of 4-aminoquinolines was achieved by aromatic nucleophilic substitution at the 4th position of 4,7 dichloroquinoline with diaminoalkanes affording yellow solid compounds **6a-g** in excellent yields. The mechanism of this S_N2 reaction is depicted in **Scheme 3.4** alongside the target aminochloroquinolines.

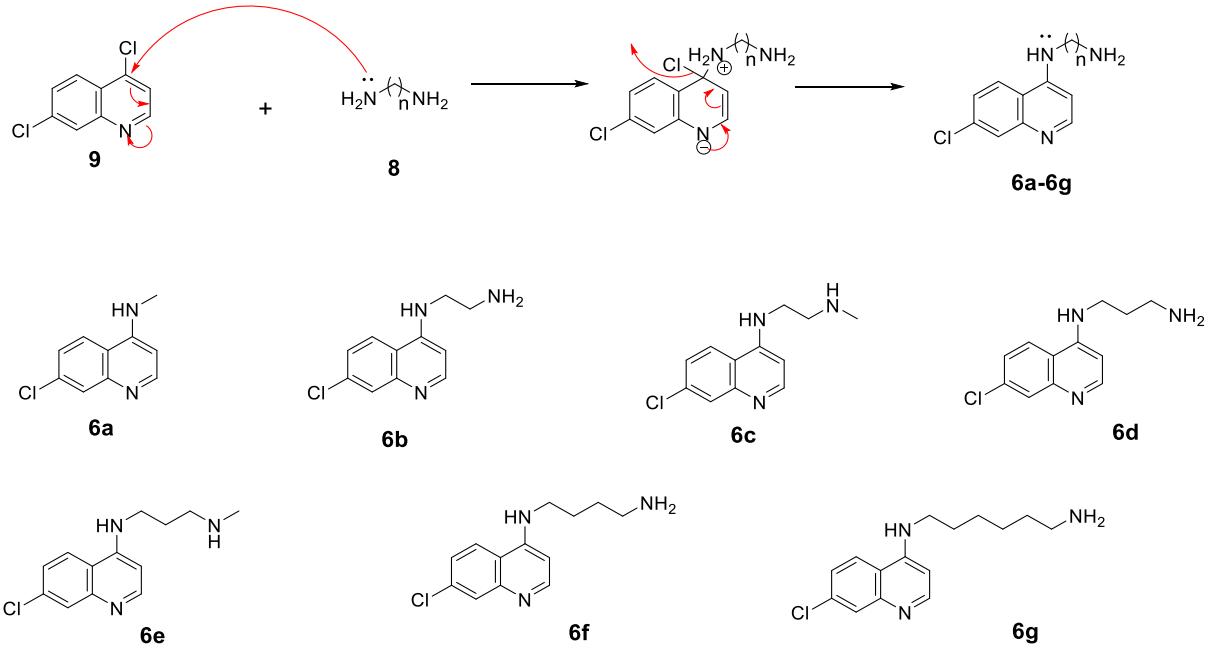

Scheme 3.4: Reaction mechanism and the seven structures of the 4-aminochloroquinoline compounds that were synthesized

According to the literature [247]–[249], ^{13}C NMR analysis of 4,7 dichloroquinoline reported the C-4 peak at around 142 ppm. After reacting the 4,7 dichloroquinoline with dialkylamines, ^{13}C NMR characterization showed that the C-4 peak appeared at around 152 ppm. The attachment of the nitrogen atom, an electronegative and a powerful electron-withdrawing element, deshielded the carbon atom and shifted it more downfield, from 142 ppm to 152 ppm. This is proof that there was a carbon-nitrogen bond formation as a result of the nucleophilic substitution reaction, confirming the success of the reactions. NMR characterization aided in elucidating the structures of all the 4-aminoquinoline compounds that were synthesized however compound **6d** was the one chosen for detailed discussion in this dissertation.

The ^{1}H NMR spectrum (**Fig. 3.1**) reveals several distinct peaks that provide insight into the compound's structural features and proton environments. The first notable peak at 8.40 ppm corresponds to H-2, which appears as a doublet due to the coupling with H-3. Similarly, H-5, resonating at 8.24 ppm, manifests as a doublet due to its interaction with H-6.

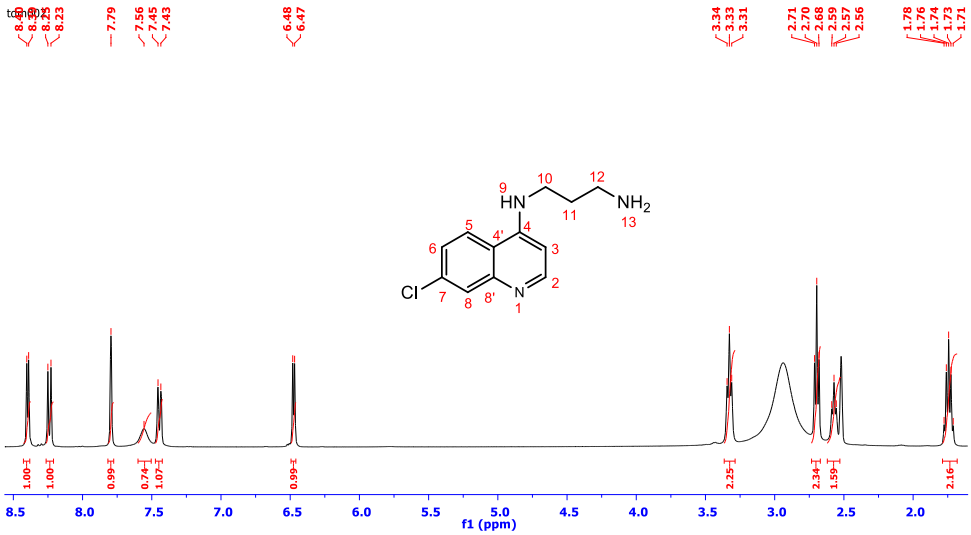

Figure 3.1: ^{1}H NMR (400 MHz, DMSO-d_6) spectrum for compound **6d**

Interestingly, H-8 at 7.79 ppm appears as a singlet, despite expectations of it forming a doublet due to meta coupling with H-6. The unexpected singlet indicates the complexity of the coupling constants or potential averaging effects from rapid proton exchange. H-9, at 7.56 ppm, exhibits a broad singlet peak. Though H-9 is adjacent to H-10, it does not show the expected splitting, likely due to rapid proton exchange, which broadens the signal and obscures the fine structure.

In NMR spectroscopy, protons attached to nitrogen or oxygen (acidic protons) exhibit unique behaviour. These protons often do not couple with adjacent protons in the aliphatic chain due to rapid exchange with the solvent or other molecules. This exchange averages out coupling interactions, resulting in broadened or sometimes completely disappeared signals, making these protons challenging to observe. The solvent used in the NMR experiment significantly influences the behaviour of these acidic protons. For instance, in deuterated solvents, exchangeable protons may be replaced by deuterium, which is not detected in standard proton NMR, further complicating the observation of coupling interactions.

Temperature and concentration also play crucial roles in the behaviour of acidic protons. Elevated temperatures increase the rate of proton exchange, broadening the signals and averaging out any couplings. Conversely, lower temperatures can reduce exchange rates, potentially revealing coupling interactions. Additionally, lower temperatures strengthen hydrogen bonds, leading to more distinct NMR signals, whereas higher temperatures weaken these bonds, increasing exchange rates and signal broadening.

Higher sample concentrations promote intermolecular interactions and proton exchange, resulting in signal broadening and reduced observable coupling. This can lead to aggregation and increased hydrogen bonding, causing complex splitting patterns and further signal

broadening. Lower concentrations mitigate these interactions, slowing exchange rates and making coupling interactions more observable, resulting in sharper NMR signals.

The proton H-6, observed at 7.44 ppm, appears as a doublet of doublets due to its coupling with both H-5 and H-8 (ortho-meta coupling). H-3, at 6.47 ppm, is a doublet due to its interaction with H-2. A triplet peak at 3.33 ppm is assigned to H-12. Theoretically, H-12 should exhibit a triplet of triplets multiplicity since it couples with two protons at position 11 and two other protons at position 13. H-10, at 2.70 ppm, appears as a triplet but is theoretically expected to be a doublet of triplets or triplet of doublets (depending on which nuclear couples first) due to the coupling with the two protons at position 11 and one proton from position 9.

H-13, resonating at 2.57 ppm, is a triplet due to coupling with the two protons from position 12. This triplet integrates for one proton; however, these are two equivalent protons. Lastly, the quintet peak assigned to H-11 results from coupling with four protons from both H-10 and H-12.

Two additional unassigned peaks are present on the spectrum. The first, a broad signal, corresponds to the moisture peak, and the second, a singlet at 2.50 ppm, is attributed to the NMR solvent DMSO used in the experiment. Eungyu Kanga *et al*. (2010) corroborated this, showing that NMR solvents consistently exhibit peaks due to moisture in addition to the residual solvent peak[250].

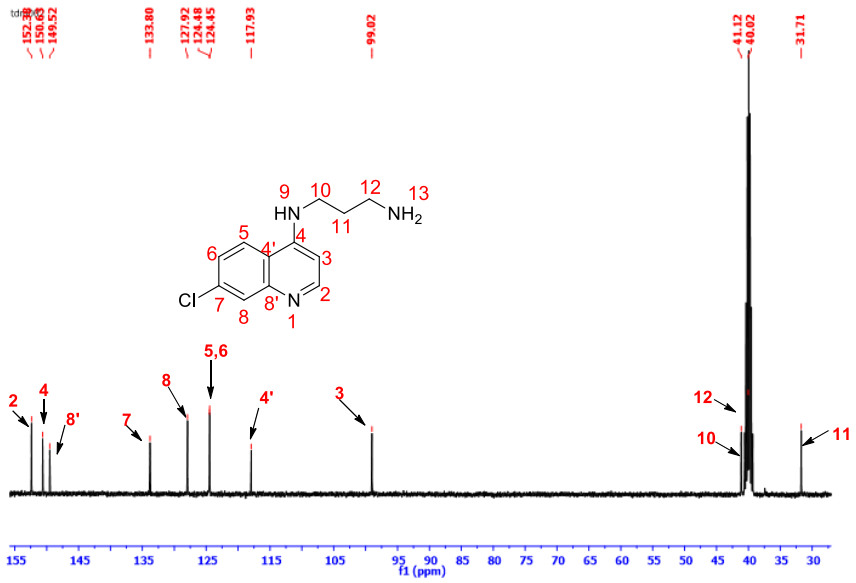

Figure 3.2: ^{13}C NMR (100 MHz, DMSO-d_6) spectrum for compound **6d**

The ^{13}C NMR spectrum (**Fig. 3.2**) provides crucial evidence confirming the successful synthesis of the target compounds. The spectrum exhibited distinct carbon peaks corresponding to the number of carbon atoms present in the molecular structure, aligning with

the expected chemical framework. The Distortionless Enhancement by Polarization Transfer (DEPT-135) experiment was employed to differentiate between various types of carbon atoms, such as methylene, methyl, and quaternary carbons.

All analyzed structures shared the quinoline scaffold, featuring nine aromatic carbon atoms. The aromatic region of the spectrum accounted for these carbons, confirming the presence of the quinoline core in each compound. The key variation across the spectra was the number of carbon peaks observed in the aliphatic region, attributable to the differing lengths of the diaminoalkane linkers (methylene carbons).

Focusing on compound **6d**, the spectrum revealed all four quaternary carbons, with their respective chemical shifts as follows: C-4 at 152.38 ppm, C-4' at 117.93 ppm, C-7 at 127.92 ppm, and C-8' at 149.52 ppm. As anticipated, these quaternary carbons did not appear in the DEPT-135 spectrum, which only shows signals for CH and CH_2 groups. The DEPT-135 spectrum also identified five methyl carbons (C-2, C-3, C-5, C-6, and C-8) as positive signals (appearing above the baseline). These peaks are characteristic of protonated carbons in the quinoline scaffold, confirming their presence. Additionally, the methylene peaks were observed below the baseline, corresponding to the aliphatic chain carbons at 41.12 ppm (C-12), 40.02 ppm (C-10), and 31.71 ppm (C-11). This detailed analysis of the ^{13}C NMR and DEPT-135 spectra underscores the successful formation of the desired compounds, highlighting the consistent presence of the quinoline core and the variable aliphatic linkers. The identification and differentiation of the various carbon types through their chemical shifts and DEPT-135 responses further validate the structural integrity and purity of the synthesized molecules.

3.2.2 Preparation of hydroxypyridinone intermediates

3.2.2.1 Protection of hydroxypyridinones

During the synthesis of hydroxypyridinone (HPO) intermediates, both maltol and kojic acid starting materials undergo nucleophilic substitution reactions. These reactions proceed through competitive carbon-oxygen bond fission pathways, which significantly influence the regioselectivity and overall yield of the desired product.

The nucleophilic substitution mechanism involves the attack of a nucleophile on an electrophilic carbon centre, leading to the cleavage of a carbon-oxygen bond. Given the nature of maltol and kojic acid, this process requires careful consideration of regioselectivity. Both starting materials contain multiple reactive hydroxyl groups, which can participate in the reaction, potentially leading to undesired side products. Protecting the competing hydroxyl groups before proceeding with the functionalization of the hydroxypyridinone core is essential to address these challenges. This selective reactivity of the hydroxyl groups during the S_N2 step of the protection process is primarily due to the differences in their electronic

environments, steric accessibility, and the nature of the protecting reagents used. The 5-position hydroxyl group is typically more nucleophilic and less sterically hindered, leading to its preferential reaction. This strategic protection enhances the regioselectivity and improves the final product's overall yield and purity. Among the various hydroxyl-protecting groups available, the benzyl (Bn) group stands out as the most favoured due to its stability under a wide range of reaction conditions. The benzyl group is robust in both acidic and basic environments, making it suitable for subsequent synthetic steps that might involve harsh conditions[251].

Benzyl protection is generally carried out using benzyl bromide (BnBr) or benzyl chloride (BnCl) in the presence of a base. The generally followed procedure involved methanol as a solvent to dissolve the starting material and the protecting reagent. Sodium hydroxide was used as a base required to deprotonate the hydroxyl groups of maltol or kojic acid, generating the corresponding alkoxide anions. The benzyl chloride was used as the protecting agent. The reaction progress was monitored using thin-layer chromatography (TLC) to ensure complete conversion of the starting material to the protected product.

3.2.2.2 Protection of Maltol

A round bottom flask containing ethyl or methyl maltol, methanol as the solvent, and sodium hydroxide (NaOH) as the base was heated to reflux before the slow, dropwise addition of benzyl chloride (BnCl) over 15 minutes to minimize fuming and effervescence. This procedure followed the synthetic pathway illustrated in **Scheme 3.5**[193][252].

The protection of maltol begins with NaOH's deprotonation of the hydroxyl group, forming the corresponding alkoxide ion - either methyl maltol-alkoxide or ethyl maltol-alkoxide. This alkoxide ion acts as a potent nucleophile, which then attacks benzyl chloride's electrophilic carbon, forming a new carbon-oxygen bond while displacing the chloride ion. This nucleophilic substitution results in the formation of benzyl ether-protected maltols (**10a** and **10b)**, where the hydroxyl group of maltol is effectively protected as a benzyl ether.

This protection enhances the molecule's stability under various reaction conditions, making it suitable for further functionalization. This protection step is crucial for the successful synthesis of hydroxypyridinones, as it prevents unwanted side reactions and ensures high regioselectivity.

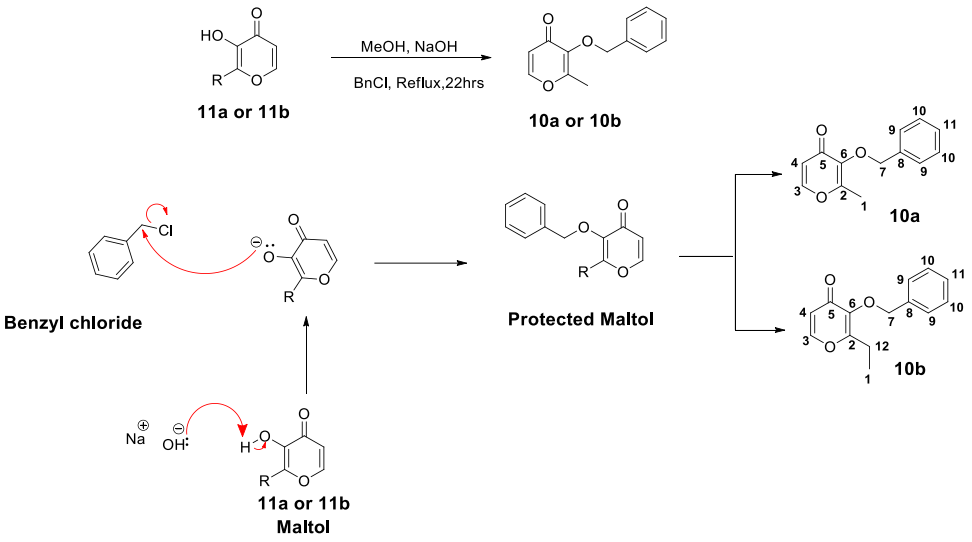

Scheme 3.5: Protection of Maltol.

Upon completion of the reaction, both desired end products, the benzyl ether-protected maltols, were obtained as yellow oils in good yields. Their structural characterization was carried out using a combination of ^{1}H NMR and ^{13}C NMR spectroscopy techniques.

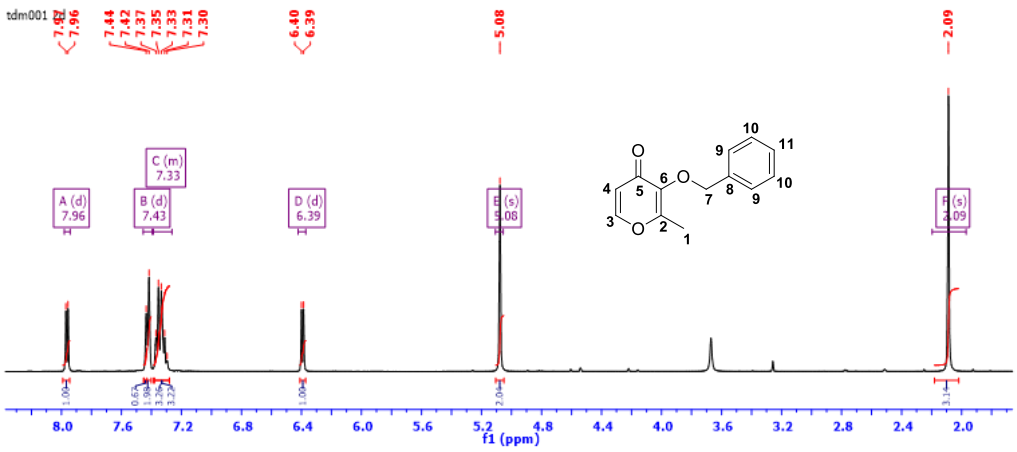

Figure 3.3: ^{1}H NMR (400 MHz, DMSO-d_6) spectrum for compound **10a**

In the ^{1}H NMR spectrum (**Fig 3.3**) of compound **10a**, the first doublet peak observed at 7.96 ppm corresponds to H-3, coupling with H-4. A doublet peak at 7.42 ppm integrates for two protons, assigned to the two equivalent protons on position 9. H-9 appears as a doublet due to coupling with the two equivalent protons on position 10. The multiplet observed in the range of 7.39–7.28 ppm is attributed to the three protons at positions 10 and 11. The theoretical doublet of doublet expected for the two protons on position 10 is not resolved due to peak

overlap with adjacent signals. H-4 resonates at 6.39 ppm as a doublet, coupled with H-3. A long singlet peak at 5.07 ppm corresponds to the two methylene protons on position 7. Finally, a singlet peak at 2.08 ppm, integrating for three protons, is assigned to the three methyl protons at position 1.

The ^{13}C NMR spectrum (**Fig 3.4**) confirmed the presence of 11 carbon signals corresponding to the structure of compound **10a**. DEPT-135 analysis further differentiated the types of carbon atoms present, providing valuable insights into their connectivity and environment. Notably, four quaternary carbons (C-2, C-6, C-5, and C-8) were expected to appear in the spectrum but did not, indicating potential chemical exchange phenomena or signal suppression under the experimental conditions.

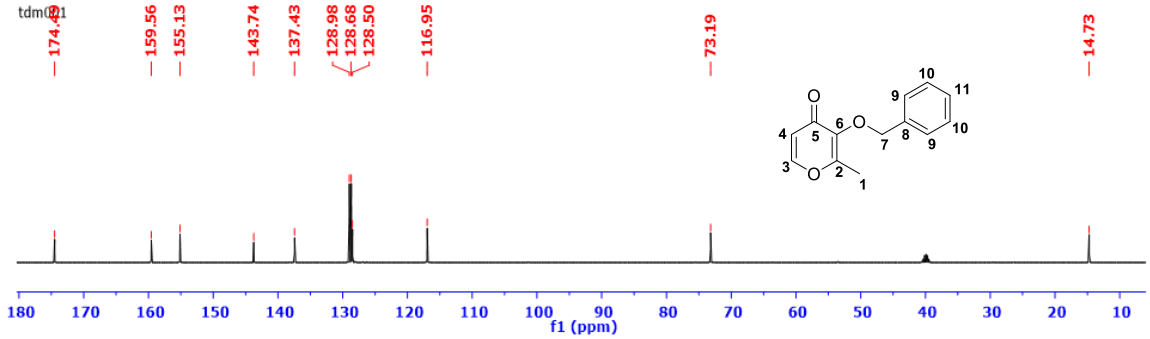

Figure 3.4: ^{13}C NMR (100 MHz, DMSO-d_6) spectrum for compound **10a**

In the case of ethyl maltol derivative **10b**, an additional methylene peak appeared at 57.84 ppm (C-12) in the ^{13}C NMR spectrum. The ^{1}H NMR spectrum showed an additional singlet peak at 4.41 ppm (H-12), which was absent in the methyl maltol counterpart. These spectral differences between methyl and ethyl maltol derivatives highlight subtle structural variations and provide essential data for the accurate characterization and differentiation of benzyl ether-protected maltols (spectra in appendix document).

3.2.2.3 Protection of Kojic Acid

In a typical preparation of benzyl-protected kojic acid, a round-bottom flask was charged with kojic acid, methanol as the solvent, and sodium hydroxide (NaOH) as the base. The mixture was heated to reflux before the slow, dropwise addition of benzyl chloride (BnCl) over 15 minutes to minimize fuming and effervescence. The reaction proceeded according to the synthetic pathway outlined in **scheme 3.6.** The first step in the protection of kojic acid is deprotonation of the hydroxyl (OH) group of kojic acid by NaOH, generating a more reactive kojic acid alkoxide ion. The kojic acid alkoxide nucleophilically attacks the electrophilic carbon

of benzyl chloride. This S_N2 reaction proceeds with the formation of a transition state and the subsequent displacement of the chloride ion. Again, the final product is the benzyl ether-protected kojic acid, where the hydroxyl group is effectively protected as a benzyl ether[193][252].

The desired product, benzyl-protected kojic acid (compound **5**), was successfully synthesized and isolated as white needle-like crystals with good yield. Comprehensive structural elucidation was carried out using ^{1}H NMR and ^{13}C NMR spectroscopy.

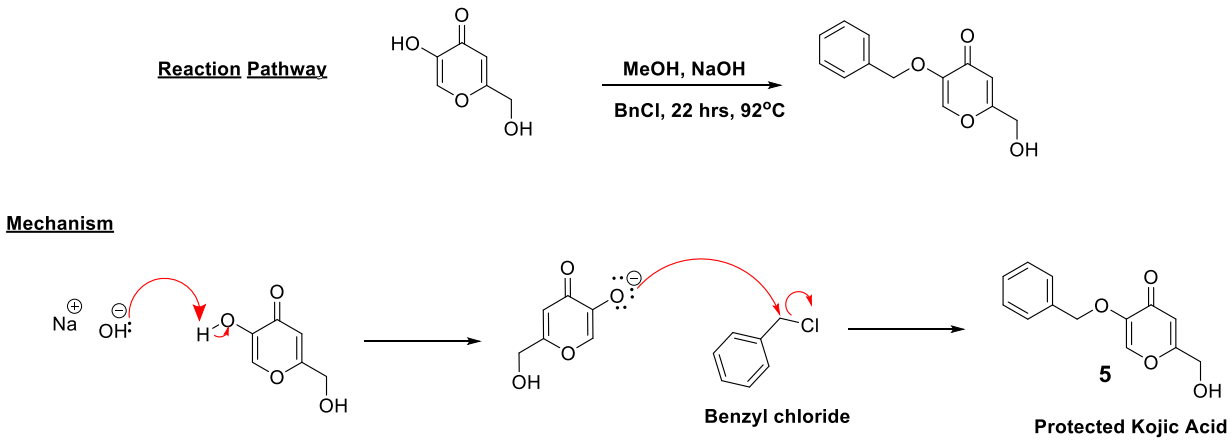

Scheme 3.6: Protection of Kojic Acid

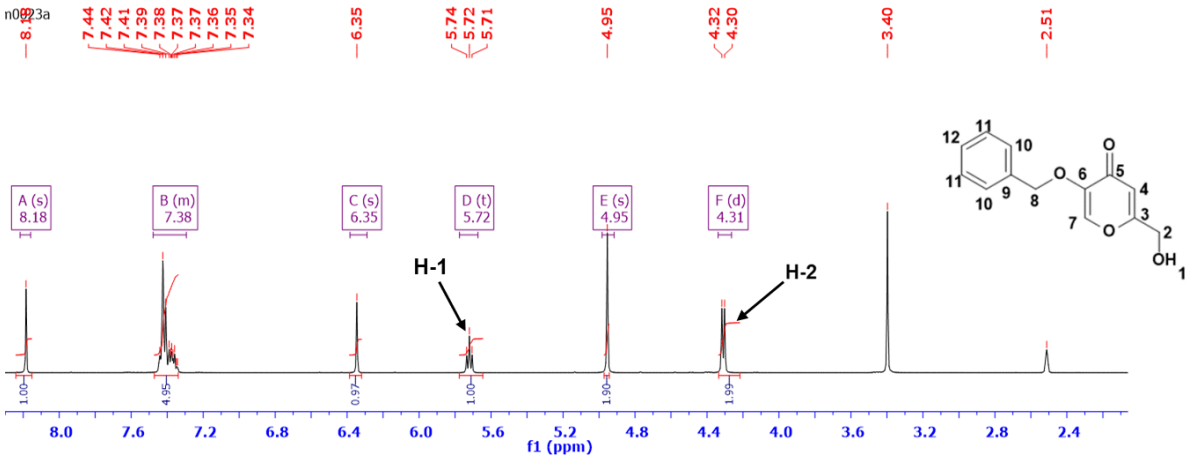

Figure 3.5: ^{1}H NMR (400 MHz, DMSO-d_6) spectrum for compound **5**

The proton NMR spectrum (**Fig. 3.5**) of benzyl-protected kojic acid provided distinct and well-resolved proton signals, confirming the integrity of the synthesized compound. The singlet peak at 8.18 ppm integrating for one proton corresponds to H-7, indicating its isolated environment without neighbouring protons for coupling. The multiplet at 7.46-7.33 ppm

integrating for five protons, is assigned to the aromatic protons of the benzyl group (H-10, H-11, and H-12). The multiplet nature reflects the complex coupling patterns typical of aromatic systems. The singlet at 6.35 ppm integrating for one proton, is assigned to H-4. The singlet nature indicates no adjacent protons for coupling, consistent with its position on the aromatic ring. The triplet peak at 5.72 ppm integrating for one proton is assigned to H-1. The triplet multiplicity arises from coupling with the two protons at position 2, following the n+1 rule for splitting patterns. A singlet at 4.95 ppm integrates two equivalent protons at position 8. The singlet nature indicates that these protons do not have adjacent protons for coupling, characteristic of methylene groups in this context. The doublet at 4.31 ppm integrating for two protons, corresponds to H-2. The doublet multiplicity is due to coupling with the single proton at position 1, showcasing a typical 1:1 coupling pattern.

The ^{13}C NMR spectrum **(Fig. 3.6)** of benzyl-protected kojic acid displayed 11 distinct carbon signals, corresponding to the carbons in the molecular structure. The DEPT-135 experiment provided further differentiation of the carbon types:

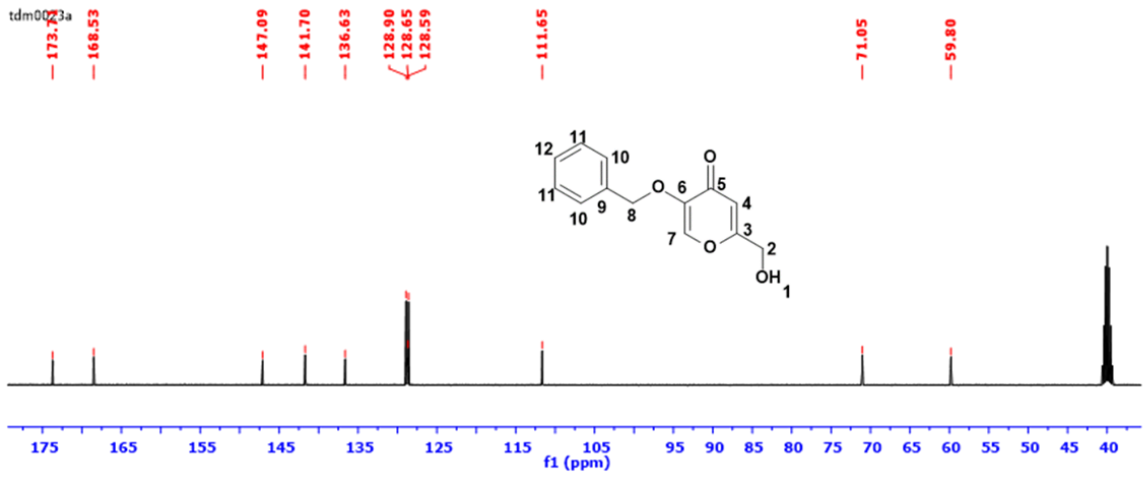

Figure 3.6: ^{13}C NMR (100 MHz, DMSO-d_6) spectrum for compound **5**

There are four quaternary carbons namely, the carbonyl carbon C-5, at 173.71 ppm which is a key feature in the kojic acid structure, C-3 at 168.53 ppm, C-6 at 147.09 ppm and C-9 at 136.63 ppm. There are two methylene carbons at 71.05 ppm (C-8) and 59.80 ppm (C-2) and five methine carbons: 141.67 ppm (C-7), 128.90 ppm (C-10), 128.65 ppm (C-11), 128.59 ppm (C-12) and 111.64 ppm (C-4).

3.2.2.4 Alkylation of the protected-kojic-acid

Alkylation is achieved *via* a double Michael addition reaction (**Scheme 3.7**). The double Michael addition involves sequential ring cleavage and ring closure. In the double Michael addition mechanism, the nucleophilic amine initially attacks the α,β-unsaturated carbonyl

system of the protected kojic acid, forming a β-amino carbonyl intermediate. This intermediate undergoes ring cleavage and intramolecular cyclization, resulting in the alkylated product. The steric hindrance of the amine significantly influences the reaction efficiency and yield.

With less bulky amines such as methylamine, isopropylamine, and cyclopropylamine, which exhibit minimal steric hindrance, facilitate efficient nucleophilic attack and subsequent cyclization. These amines result in high yields of the alkylated product due to their ease of access to the reactive sites on the protected kojic acid. Conversely, bulkier amines face steric challenges during the nucleophilic attack, leading to lower yields. The increased steric bulk hinders the approach of the amine to the electrophilic carbonyl carbon, thus reducing the efficiency of the double Michael addition. Thus, the choice of amine is crucial for optimizing the yield of the alkylated product.

Reaction Pathway

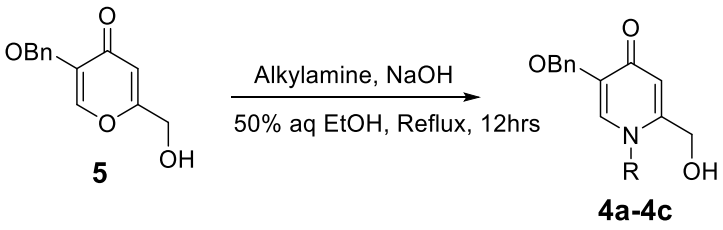

Reaction Products

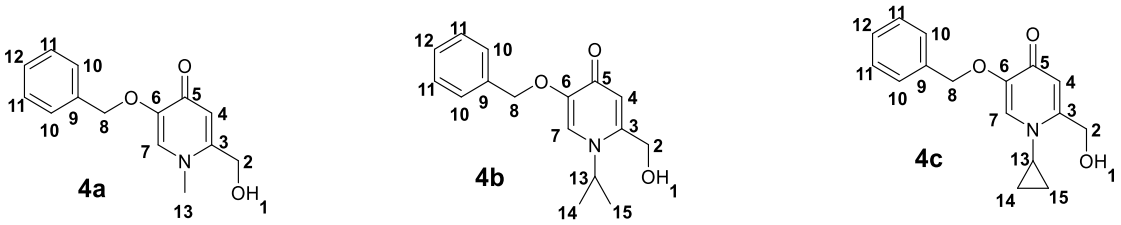

Scheme 3.7: Alkylation of the protected-kojic and reaction products

The success of the amination or alkylation reactions of benzyl-protected kojic acid was thoroughly confirmed through ^{1}H and ^{13}C NMR spectroscopic analysis. A comparative study of the NMR spectra (see appendix) of compounds **4a**, **4b**, and **4c** with the precursor compound **7** revealed significant additional peaks in the aliphatic region, indicative of successful functionalization.

^{1}H NMR Analysis

The spectrum of **4a** exhibited a new singlet peak at 3.99 ppm, integrating three protons. This peak corresponds to the methyl protons at position 13, confirming the successful alkylation. In the spectrum of **4b**, a singlet peak at 1.14 ppm was observed. This peak correlates with the

newly introduced carbon at position 13. Additionally, the methyl groups H-14 and H-15 appeared at 2.05 ppm, consistent with the expected chemical environment after alkylation. The spectrum of **4c** showed new peaks for H-13, H-14 and H-15 at 0.80 – 0.63 ppm. These overlapping signals indicate the successful incorporation of the alkyl groups. Additionally, it was observed that methylamine introduces the strongest deshielding effect on H-7, followed by cyclopropylamine and isopropylamine. This trend correlates with the electronic donating/withdrawing properties of the substituents

^{13}C NMR Analysis

The spectrum of **4a** revealed a new methyl carbon peak at 42.53 ppm, corresponding to the methyl group at position 13. This additional peak confirms the successful introduction of the methyl group during the reaction. In the spectrum of **4b**, a new carbon peak at 43.12 ppm was observed, corresponding to the newly introduced carbon at position 13. This correlates with the singlet peak in the ^{1}H NMR spectrum, further verifying the successful alkylation. Additionally, the methyl carbon peaks for H-14 and H-15 were noted. The spectrum of **4c** displayed a new peak at 22.59 ppm for the carbon at position 13, and the overlapping carbon signals for H-13 and H-14 were detected at 3.63 ppm, confirming the presence of the alkyl groups. The aromatic carbons experienced significant deshielding in the isopropylamine and cyclopropylamine derivatives compared to methylamine. This reflected the increased electron-donating or steric effects from the bulkier alkyl groups, altering the electronic density around these carbons. C-5 and C-3 show the largest downfield shifts in the isopropylamine and cyclopropylamine derivatives due to resonance or inductive effects transmitted through the structure. Minor shifts in C-10, C-11 and C-12 suggested that these carbons were less influenced by the alkyl groups directly. However, C-9 showed a more noticeable downfield shift in the isopropylamine and cyclopropylamine derivatives, indicating some degree of steric or electronic interaction.

3.2.2.5 Chlorination of the hydroxyl group

To mitigate the problem of chemoselectivity, the hydroxyl group in the alkylated protected kojic acid compounds was converted to a chloride atom, which also serves as an excellent leaving group. Compounds **4a**, **4b**, and **4c** were subjected to chlorination using thionyl chloride ($SOCl_2$) in a controlled low-temperature environment. This reaction was carried out in glass tubes immersed in an ice-acetone mixture to ensure a consistently low temperature.

Reaction Pathway

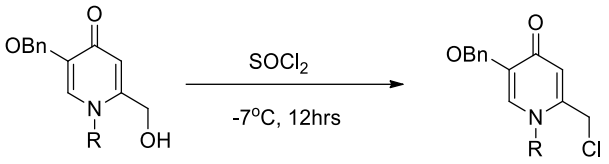

Scheme 3.8: Chlorination of the protected-kojic

The chlorination process proceeds through a nucleophilic substitution reaction (S_N2) involving thionyl chloride. The reaction initiates with the nucleophilic attack of the hydroxyl group on the sulfur atom of thionyl chloride. The lone pair of electrons on the oxygen of the hydroxyl group attacks the sulfur atom of thionyl chloride, forming a chlorosulfite ester intermediate and expelling the chloride ion forming hydrogen chloride (HCl) as a by-product.

The chlorosulfite intermediate formed undergoes a [1,2-elimination] process. The chlorine from the chlorosulfite group leaves, and a chloride ion (Cl^-) displaces the chlorosulfite group, resulting in the formation of the chlorinated products **3a**, **3b**, and **3c** as depicted in **Fig. below.** Sulfur dioxide (SO_2) and hydrogen chloride (HCl) are released as byproducts.

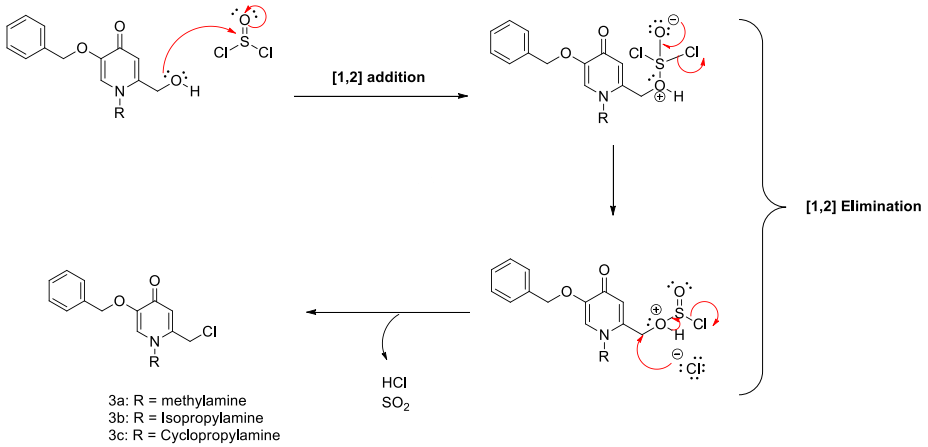

Scheme 3.9: Mechanism of the chlorination of the alkylated-protected kojic compounds

The chlorination products exhibit distinct ^1H NMR patterns, reflecting variations in their electronic environments and substituent effects. For instance, with the methylenic protons (H-2 and H-8):

Compound **3a** - H-8 at 5.21 ppm and H-2 and 4.68 ppm

Compound **3b -** H-8 at 4.96 ppm and H-2 at 4.68 ppm

Compound **3c -** H-8 at 5.08 ppm and H-2 at 4.51 ppm.

The H-8 protons showed slight downfield shifts in **3a** and **3c** compared to **3b**, reflecting subtle differences in electronic effects induced by the substituents. The H-2 protons remain consistent across all derivatives, except for a small upfield shift in **3c** likely due to steric shielding. In the carbon NMR,

Compound **3a** C-8 at 72.01 ppm and C-2 at 58.80 ppm

Compound **3b** C-8 at 71.02 ppm and C-2 and 41.60 ppm

Compound **3c** C-8 at 71.13 ppm and C-2 at 63.36 ppm

C-8 remained consistent across the derivatives, reflecting minimal electronic or steric variation. However, C-2 shows notable differences, with the **3c** derivative exhibiting the most deshielding likely due to ring strain effects.

3.3 Synthesis and Characterization of Kojic Acid Derived Conjugate Compounds

The coupling reaction of the 2-alkyl chloride intermediate of kojic acid **(3)** and the *N*-(7-chloroquinoline 4yl) alkyl-diamines **(6)** via chlorine substitution **(Scheme 3.10)** was carried out in DMF as solvent (used as solvents because they are polar aprotic and hence appropriate for solubilizing the reactants and for the S_N2 type reaction[243]) in the presence of triethylamine (Et_3N) and Na_2CO_3 as bases to optimize the neutralization of HCl which would otherwise protonate the amine and favor the reverse reaction and to optimize the deprotonation of the amine[193].

Mechanistically, the reactions begin with the base (triethylamine, Et_3N) deprotonating the amine group on the N-(7-chloroquinoline 4-yl) alkyl-diamine (**6**), generating a nucleophilic amine anion. The nucleophilic amine anion attacks the carbon attached to the chlorine atom in the 2-alkyl chloride intermediate of kojic acid (**3**). This is an S_N2 reaction, where the nucleophile displaces the leaving group (Cl) in a single step. As the nucleophilic amine attacks the carbon, the chloride ion (Cl-) is displaced, forming a new C-N bond.

Reaction Pathway

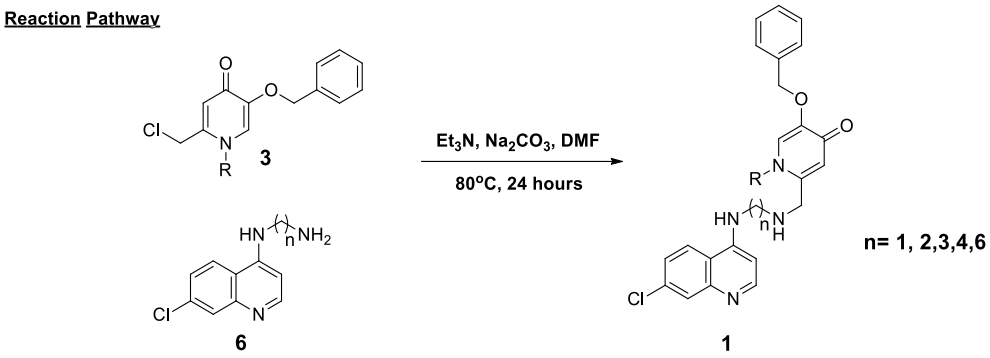

Reaction Mechanism

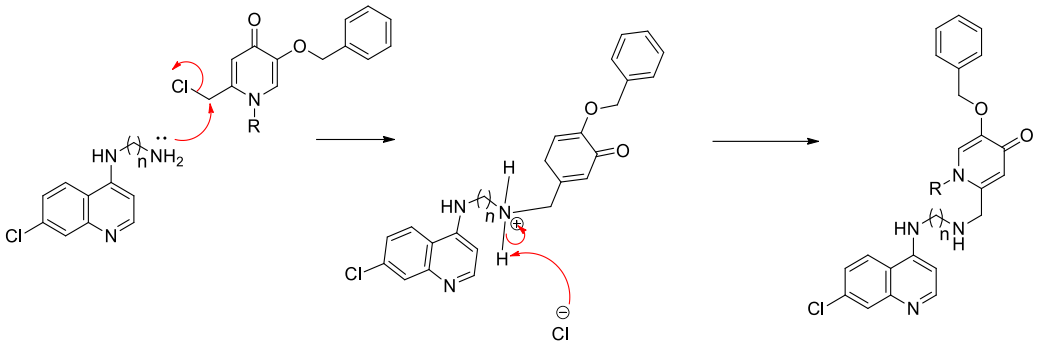

Scheme 3.10: Synthesis of Kojic acid derived conjugates

The HCl generated in the reaction is neutralized by the base (Na_2CO_3) present in the reaction mixture, preventing protonation of the amine, which would reverse the reaction. The reaction mixture was worked up, yielding the desired target compounds **(1a-l)** which were obtained in good yields. The success of the reactions was confirmed by using NMR and IR spectroscopy. Compound **1k** was the one chosen for detailed discussion and illustration in this dissertation. Compound **1k** is a product of reacting compound **6d** and **3c** as illustrated in **Scheme 3.11**. The proton NMR (**Fig.3.1**) of **6d** confirmed the presence of NH_2 (br. S, 2H at 2.57ppm). The successful synthesis (conjugating) resulted in the formation of the C-NH linkage and the abstraction of one proton in the process, leaving behind NH-12.

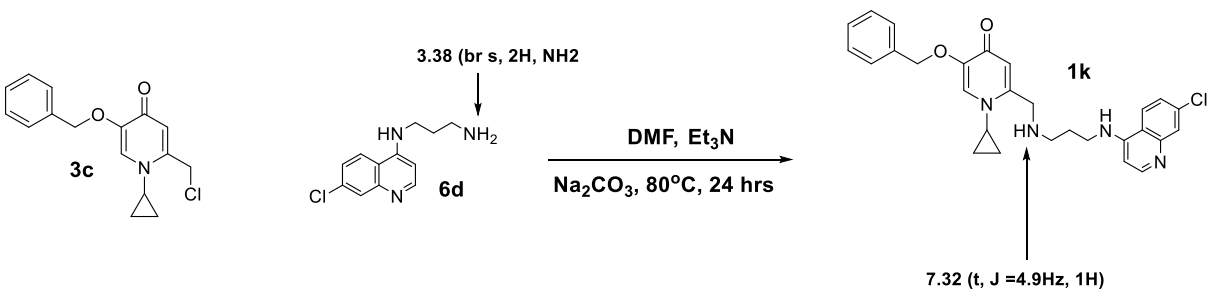

Scheme 3.11: The synthesis scheme for Compound **1k**

After the reaction, the broad signal at 3.38 ppm disappeared, and there was an emergence of a triplet peak at 8.17 ppm. Theoretically, this NH-peak is supposed to be quintet due to the four adjacent protons. As a result of conjugation, the NH-proton will be more shielded, hence, the peak moved downfield. All the other peaks were accounted for.

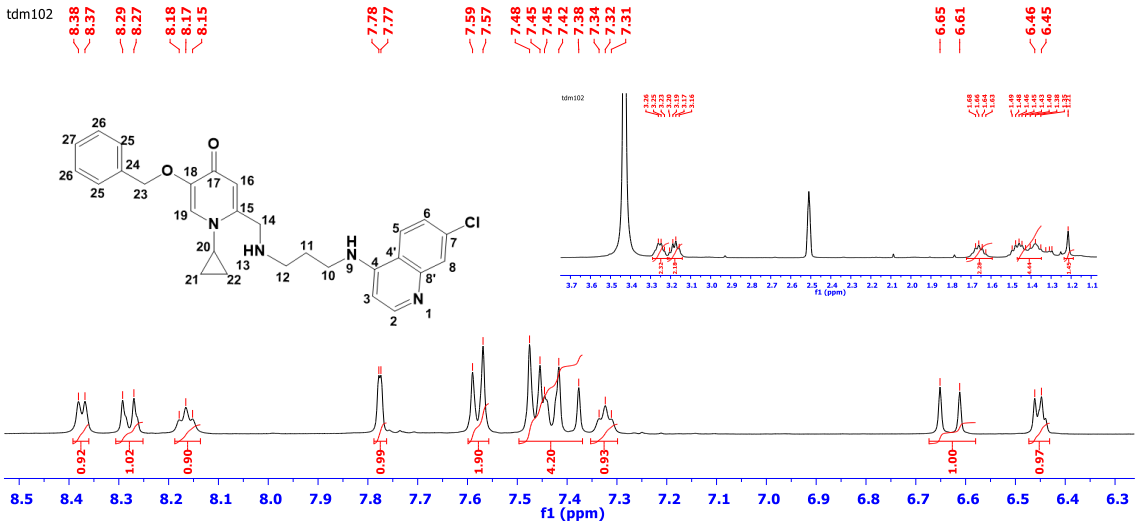

Figure 3.7: ^{1}H NMR (400 MHz, DMSO-d_6) spectrum of compound **1k**

In the proton NMR spectrum (**Fig. 3.7**), distinct peaks provided insights into the structure and environment of the protons in the molecule. The first doublet observed at 8.37 ppm is attributed to H-5, which couples with H-6, resulting in its doublet multiplicity. Similarly, H-2, resonating at 8.28 ppm, couples with H-3 to also produce a doublet. A triplet peak at 8.17 ppm is identified as NH-13, indicative of a proton in a nitrogenous environment, possibly due to its interaction with adjacent protons. H-8 appears as a doublet at 7.78 ppm, due to meta-coupling with H-6. The peaks for H-6 and H-19 overlap at 7.58 ppm, giving rise to a complex multiplicity that manifests as a doublet. Theoretically, H-6 could exhibit a doublet of a doublet multiplicity due to coupling with both H-5 and H-8, while H-19 was expected to present as a singlet. The region from 7.31 to 7.48 ppm displays a multiplet, integrating five protons, attributed to the coupling of H-25 and H-26. The triplet peak at 7.32 ppm is asigned to H-27, which couples with the two H-26 protons in a 1:2:1 ratio.

H-3 resonates as a doublet at 6.46 ppm due to its coupling with H-2. The first multiplet between 3.11 and 3.22 ppm integrates two protons on H-10, although it was expected to be a doublet of triplets due to interactions with NH-9 and H-11. H-12, at 3.18 ppm, appears as a quartet, which can be explained by its coupling with H-11 and NH-13. At 1.65 ppm, the doublet of doublets is assigned to H-11. Theoretically, this proton should exhibit a quintet multiplicity due to its interactions with H-10 and H-12. Protons H-21 and H-22, being equivalent, overlap and

result in a multiplicity in the range of 1.26 to 1.56 ppm. Lastly, the singlet peak at 1.43 ppm, integrating to one proton, is assigned to H-20. This could have been a doublet due to the two equivalent protons from the cyclopropyl group. Usually these protons that are in symmetric or equivalent environments may not exhibit expected splitting patterns due to averaging effects.

The carbon spectrum of **Fig. 3.8,** showed 26 carbons corresponding to the number of carbons in the structure.

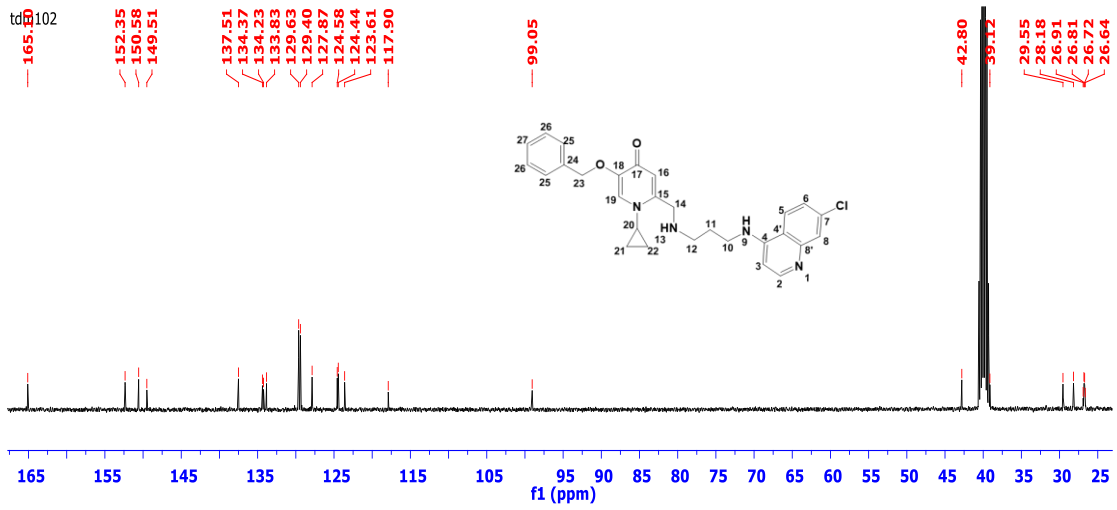

Figure 3.8: ^{13}C NMR (100 MHz, DMSO-d_6) spectrum of compound **1k**

Using DEPT-135 NMR spectroscopy, we were able to further distinguish the carbons present and elucidate the compound's framework. The spectrum revealed eight quaternary carbons at the following chemical shifts: 165.10 ppm (C-17), 150.58 ppm (C-4), 149.51 ppm (C-8'), 137.51 ppm (C-18), 134.23 ppm (C-24), 133.83 ppm (C-15), 127.87 ppm (C-7), and 117.90 ppm (C-4'). Additionally, ten methine carbons were identified: 152.35 ppm (C-2), 134.37 ppm (C-19), 129.63 ppm (C-25), 129.40 ppm (C-26, C-27), 127.87 ppm (C-8), 124.58 ppm (C-5), 124.44 ppm (C-6), 123.61 ppm (C-16), and 99.05 ppm (C-3). These chemical shifts are consistent with the presence of aromatic and aliphatic methine groups within the molecular structure. Seven methylene carbons were observed at 42.80 ppm (C-23), 39.12 ppm (C-14), 29.55 ppm (C-10), 28.18 ppm (C-12), 26.81 ppm (C-21), 26.72 ppm (C-22), and 26.64 ppm (C-11). These shifts are indicative of various aliphatic methylene groups in different chemical environments. Finally, a single methyl carbon was detected at 26.91 ppm (C-20), corresponding to a terminal methyl group in the compound. The rest of the **1a-l** compounds were elucidated using the same approach, ensuring a comprehensive analysis of their carbon frameworks and molecular structures.

3.4 Synthesis and Characterization of Maltol Derived Hybrid Compounds

The second phase of the synthesis involved the preparation of maltol-derived hybrid compounds. This synthetic procedure entailed the reaction of N-(7-chloroquinoline-4-yl) alkyl-diamines with benzylated maltol intermediates in ethanol under reflux conditions for 24 hours, as illustrated in **Scheme 3.11**. The resultant compounds were characterized by data that confirmed the successful synthesis of the target compounds **2a-i** in qualitative yields. FT-IR spectroscopy confirmed each compound's characteristic functional groups (N-H, C=O, C=N).

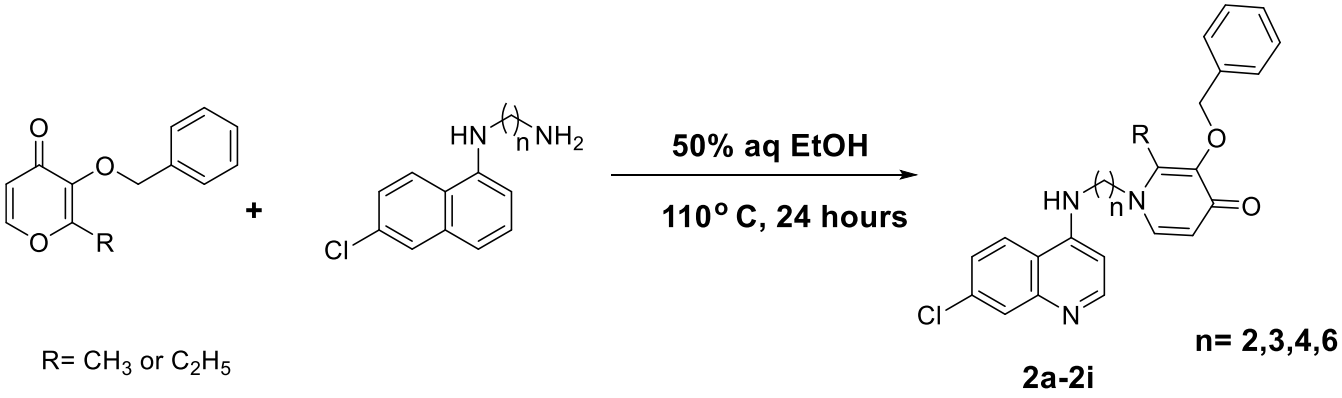

Scheme 3.11: Synthesis of Maltol derived conjugates

Literature suggests that benzylated maltols undergo amination with primary amines *via* Michael addition. The synthetic approach (**scheme 3.12**) is initiated by the deprotonation of the alpha hydrogen, generating a carbocation. This carbocation is stabilized by the electron-withdrawing groups present in the structure. The amine then attacks the carbocation, sequentially cleaving the ring. Bulky and complex amines would slow down the ring closure; however, protecting the hydroxyl group mitigated that, bringing about rapid ring closure[244].

The success of the conjugation reaction is confirmed by the disappearance of the NH_2 peak, indicating the attachment of 4-aminoquinolines to the maltol intermediate. Using compound **2b** as the discussion illustration, the success of the reaction was confirmed by the disappearance of the NH_2 peak at 2.57 ppm (**Fig. 3.1**), indicating the attachment of N1-(7-chloroquinolin-4-yl)propane-1,3-diamine (**6d**) to the methyl maltol (**10a**).

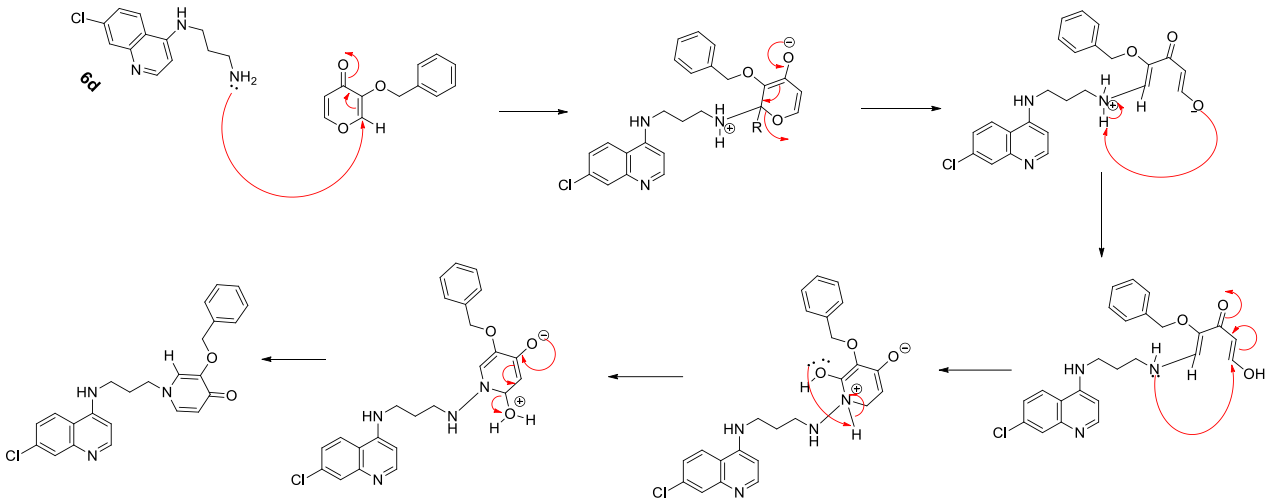

Scheme 3.12: Synthesis of **2b**

With respect to the 1D and 2D NMR spectra of the maltol-derived conjugates, compound 2b will be used as a template for discussion.

The first broad singlet peak at 9.30 ppm is assigned to NH-9 in the proton NMR spectrum. This NH proton appears as a singlet at a downfield shift (9.30 ppm), likely due to hydrogen bonding or the deshielding effects of the nearby electronegative nitrogen and aromatic rings. The lack of coupling partners explains the singlet pattern.

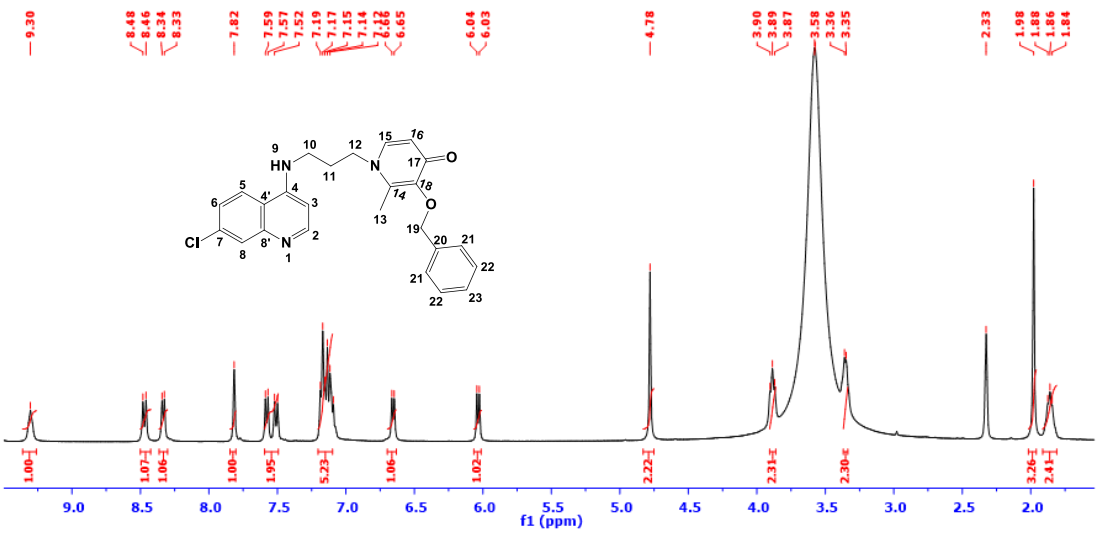

Figure 3.9: ^{1}H NMR (400 MHz, DMSO-d_6) spectrum of compound **2b**

The following next doublet peak at 8.47 ppm is assigned to H-2. This proton is deshielded by the conjugated ring system, hence giving it a chemical shift in the downfield region. The doublet pattern (J = 9.1 Hz) suggests coupling with an adjacent proton, H-3, as typical in aromatic systems with ortho coupling. H-5 at 8.33 ppm appears as a doublet with a moderate coupling constant (J = 6.8 Hz), indicating it has a neighbouring proton in an aromatic system.

This coupling pattern is consistent with the ring structure's meta or slightly longer-range coupling. The singlet peak at 7.82 ppm is assigned to H-8. It is a singlet, likely due to its position where no nearby protons are close enough to couple. Its downfield position suggests significant deshielding, possibly due to the influence of electronegative group (chlorine) or ring currents. The doublet of doublets at 7.54 ppm is assigned to H-15 and H-6. The doublet of doublets pattern arises because each proton has two coupling partners. The two sets of coupling constants are attributed and distinguished by their nearby coupling partners. A strong coupling at 27.4 Hz is influenced by the nitrogen atom in the ring, and a typical aromatic ortho coupling at 8.1 Hz. The multiplet at 7.20 – 7.10 ppm integrates five protons in the phenyl ring (benzyl group). The chemical shift and integration suggest a monosubstituted benzene ring. The multiple pattern is typical for five protons in a benzene ring with no unique substituents, as each proton experiences similar couplings.

H-3, resonating at 6.66 ppm, presents a doublet (J = 6.9 Hz) due to coupling with H-2. H-16 at 6.03 ppm couples with H-2; hence, it's a double-splitting pattern. The coupling constants of H-2, H-3, H-15 and H-16 support the point that protons near an electron-withdrawing group or double bond experience an olefinic-like deshielding effect, and their coupling constants are within 4.5-7.5 ppm. The benzylic CH_2 group appears as a singlet because it is adjacent to an aromatic ring but lacks further coupling partners, resulting in a singlet at 4.78 ppm. This position reflects partial deshielding due to the aromatic ring. H-12 is attributed to the multiplet at 3.91 – 3.86 ppm. This chemical shift suggests the CH_2 group is in a relatively deshielded environment (attached to the nitrogen atom). H-10 resonating at 3.35 ppm as a doublet. The doublet with a coupling constant of 5.1 Hz indicates coupling with the H-11 proton. The singlet at 3.18 ppm, integrating for three protons, suggests an isolated methyl group, hence assigned to H-13. H-11 couples with adjacent methylene groups, resulting in a broad multiplet around 1.91–1.81 ppm.

The carbon-13 spectrum of compound **2b** (**Fig. 3.8**) showed carbon signals correlating with the expected 23 carbons in the known structure. However, for correct and accurate elucidation of the structural framework, we utilized 2D experiments. DEPT-135 (**Fig 3.11**) analysis provided further differentiation of the types of carbon present; one methyl carbon, C-13, resonated at 12.43 ppm; four methylene carbons identified at 72.31 ppm (C-19), 50.97 ppm (C-12), 40.63 ppm (C-10), and 28.98 ppm (C-11); and ten methine carbons were discerned, including shifts at 143.83 ppm (C-2), 140.04 ppm (C-15), 128.85 ppm (C-21), 128.64 ppm (C-22), 128.28 (C-23), 127.01 ppm (C-5), 126.57 ppm (C-6), 119.90 ppm (C-8), 116.48 ppm (C-16), 99.07 ppm (C-3). Eight quaternary carbons were identified at 172.13 ppm (C-17), 155.51 ppm (C-14) ,145.75 ppm (C-4), 141.40 ppm (C-8'), 139.59 ppm (C-18), 138.11 ppm (C-20), 138.07 ppm (C-7), 116.15 ppm (C-4').

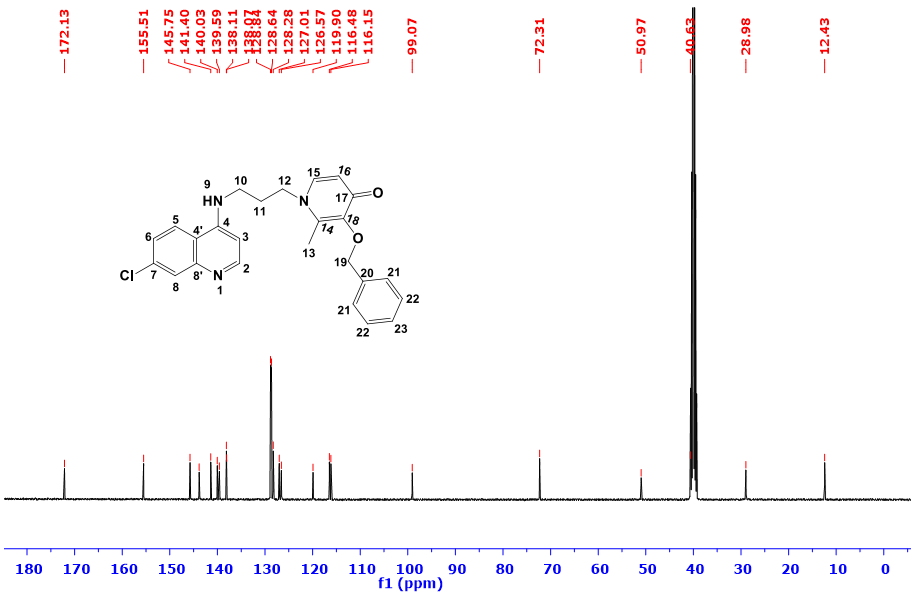

Figure 3.10: ^{13}C NMR (100 MHz, DMSO-d_6) spectrum of compound **2b**

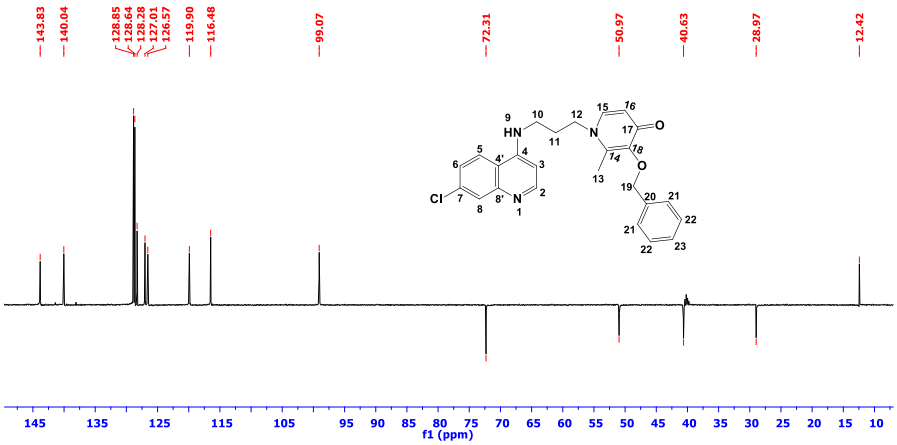

Figure 3.11: DEPT-135 NMR (100 MHz, DMSO-d_6) spectrum of compound **2b**

Correlated Spectroscopy (COSY)

COSY helps determine the signals that arise from coupling protons by providing detailed information about the spin-spin coupling between hydrogen atoms in a molecule. In a COSY spectrum, each axis represents proton chemical shifts, and cross-peaks indicate couplings between protons. This helps identify which hydrogen atoms are spin-spin coupled, facilitating the assignment of protons in crowded or overlapping spectrum regions.

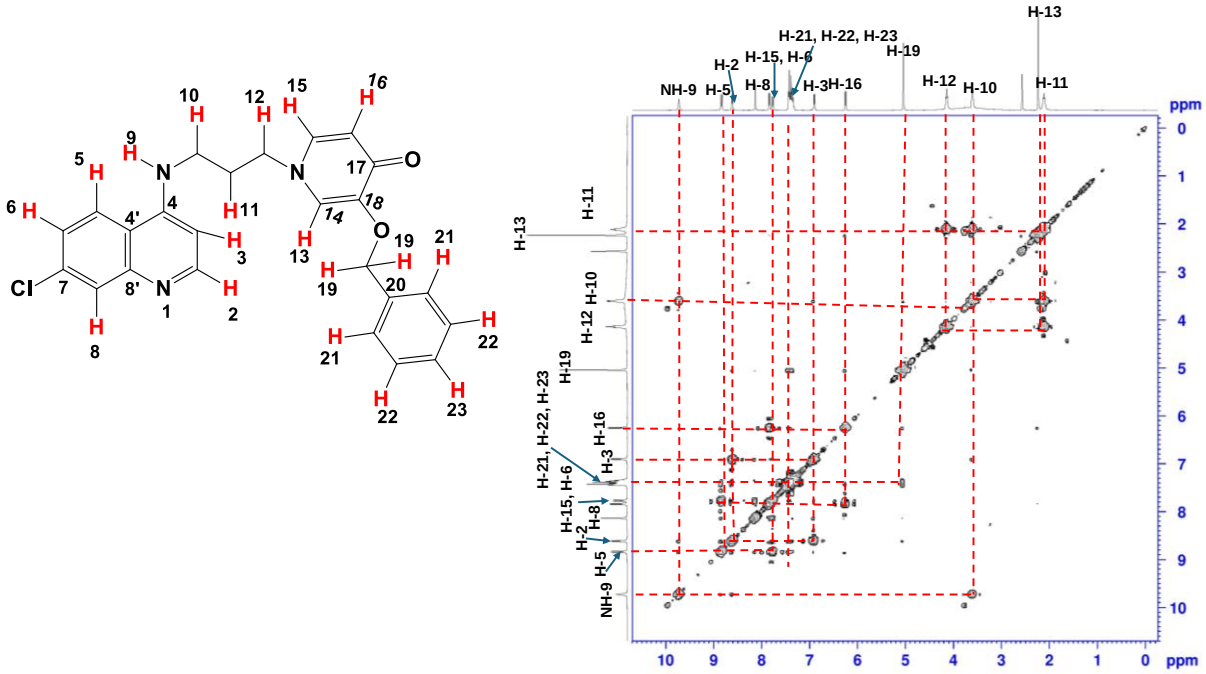

Figure 3.12: COSY NMR (400 MHz, DMSO-d_6) spectrum of compound **2b**

The NH proton does not show coupling in the 1D spectrum, as indicated by its singlet pattern (J = 0 Hz). However, the COSY spectrum shows a correlation with the H-10 protons at 3.35 ppm due to their spatial connectivity, confirming the propyl chain attachment to the NH group. The cross-peak correlations between H-2 (8.47 ppm, d, J = 9.1 Hz) and H-3 (6.66 ppm, d, J = 6.9 Hz) confirm an ortho coupling within the aromatic ring. The J value of 9.1 Hz for H-2 reflects typical ortho coupling in aromatic systems, indicating that these protons are adjacent on the ring. H-5's J value of 6.8 Hz suggests it has an ortho coupling with H-6 (7.54 ppm). H-6/H-15 at 7.54 ppm displayed two distinct J values: 27.4 Hz and 8.1 Hz. The larger J value (27.4 Hz) arose from coupling with the adjacent nitrogen, creating a very strong through-bond interaction. The 8.1 Hz coupling represents a typical ortho coupling within the ring. Cross-peaks in the COSY spectrum verified these interactions, identifying the 8.1 Hz coupling with nearby protons and the stronger coupling with an adjacent functional group. The protons of the benzyloxy group at 7.20–7.10 ppm and 4.78 ppm displayed complex splitting and overlapped as a multiplet due to typical phenyl ring couplings (ortho, meta, and para). They showed cross-peaks among themselves and with the benzylic CH_2 group at 4.78 ppm (H-19).

From the propyl linker, H-10 shows a doublet with J = 5.1 Hz, indicating coupling with the NH-9 and H-11 protons. These cross-peaks in the COSY spectrum would confirm the NH-CH_2 linkage. The relatively low J values suggest the CH_2 is next to the NH group, and this coupling is observed despite the NH's broad singlet in the 1D spectrum. This methyl proton is a singlet due to its isolation from other protons; therefore, no COSY cross-peaks were expected for this

group. The singlet confirms that it is attached to a carbon without adjacent protons. As expected, the H-11 multiplet (1.91–1.81 ppm) showed COSY cross-peaks with H-10 (3.35 ppm) and H-12 (3.91–3.86 ppm). These interactions confirm the continuity of the propyl chain. The COSY spectrum also revealed that the H-11 methylene group is coupled on both sides within the chain, consistent with its multiple pattern.

Heteronuclear Single Quantum Coherence Spectroscopy (HSQC)

The HSQC **(Fig 3.13)** spectrum provides correlations between directly bonded carbon and hydrogen atoms, helping assign carbon-proton pairs and confirm structural connectivity. By combining the provided proton, carbon, and COSY data with the HSQC correlations, we can assign protons to specific carbons and ensure accuracy in structural assignments. Below is a brief analysis of each correlation based on the spectrum.

Notably, there was no correlation for NH-9 due to the absence of a direct C-H bond. However, COSY data showing the NH-9 coupling with the CH_2 at 3.35 ppm (H-10) confirms its position next to C-10 (40.63 ppm) in the structure. The benzylic CH_2, appearing at 4.78 ppm in the proton spectrum, correlates in with C-19 at 72.31 ppm. The cross-peak between H-19 and C-19 solidifies the benzyloxy structure in the molecule. Aromatic protons H-21, H-22, and H-23 (7.20 - 7.10 ppm, m) and carbons around 128.84 - 127.01 ppm correlated**,** confirming that these carbons and protons are part of a benzene ring, consistent with a phenyl ring in the benzyloxy group. In the propyl linker region, the correlation between H-10 and C-10; H-11 (1.91–1.81 ppm, m) and C-11 (28.98 ppm) and H-12 (3.91–3.86 ppm, m) and C-12 (50.97 ppm) confirmed their respective positions. The correlation between H-13 and C-13 at 12.43 ppm confirms the methyl group. All other correlations were accounted for, as shown in **Fig 3.13.**

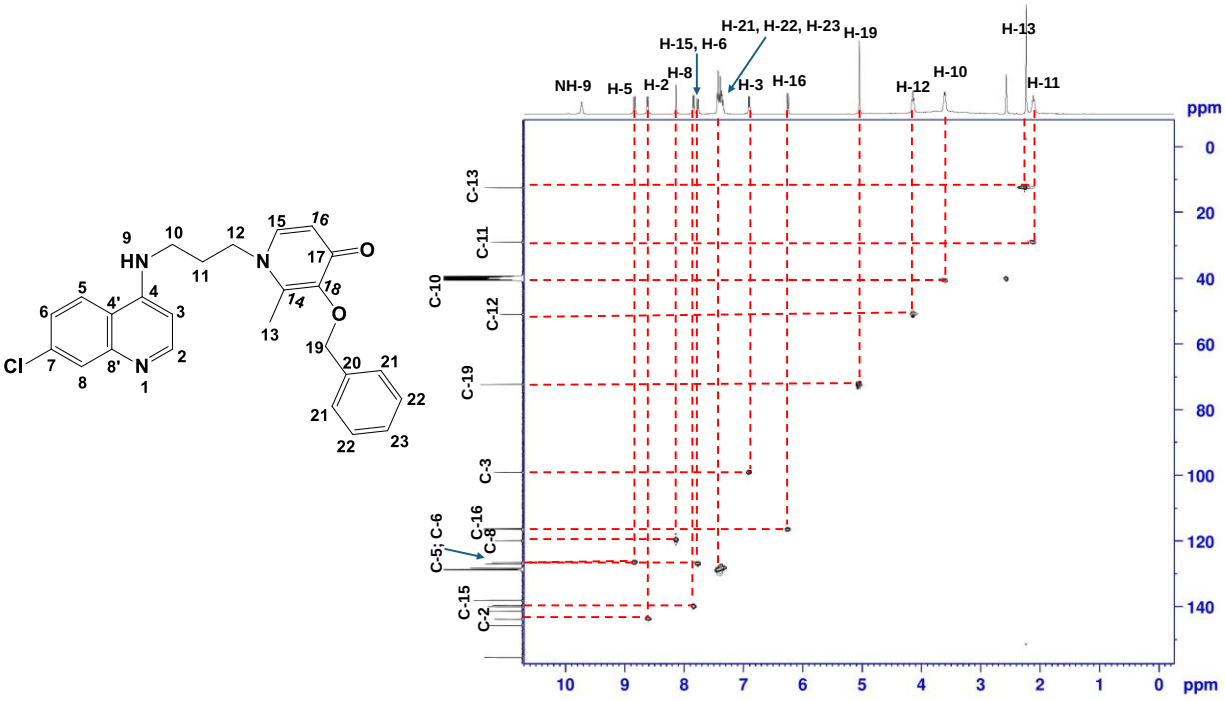

Figure 3.13: HSQC NMR (400 and 100MHz for ^{1}H and ^{13}C, DMSO-d_6) spectrum of compound **2b**

Heteronuclear Multiple Bond Correlation Spectroscopy

The HMBC spectrum reveals correlations between protons and carbons separated by two to three bonds, helping to identify longer-range connectivities that are key to confirming the skeleton of a molecule. Analyzing the spectrum below, **Fig. 3.14**, we could deduce the long-range correlations between protons in the quinoline and pyridinone rings and their neighboring carbons (though not all of them are highlighted in the spectrum) solidified the connectivity of the conjugated system. The correlations between NH-9, C-4 and C-3 as well as the correlations between H-12, C-15 and C-14 confirmed the propyl linker's orientation and continuity from NH-9 to the rest of the molecule.

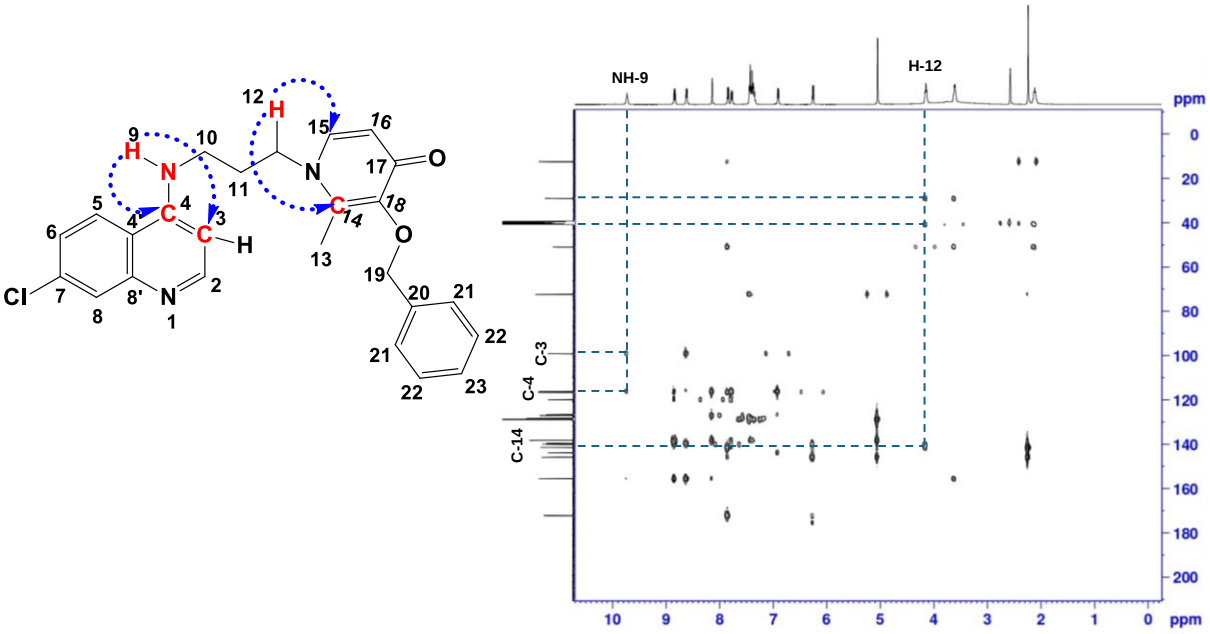

Figure 3.14: HMBC NMR (400 and 100MHz for ^{1}H and ^{13}C, DMSO-d_6) spectrum of compound **2b**

Supporting Characterization Data

The experimental melting points of the compounds are within the ranges of those obtained from the literature. Generally, the longer the hydrocarbon chain in a molecule, the higher the melting point. However, in our case, it is observed that all the short-chain linked compounds have higher melting points than the long-chain linked compounds. This is a consequence of the action of the dipole moments (see experimental section).

The difference between the obtained masses and expected masses is roughly 1g/mol. This is due to both positive and negative ionization on the molecular samples during mass analysis. In positive ionization operation, peaks corresponding to protonated analytes are observed. Apart from that, the difference between the masses is almost negligible. The mass spectrum of compound **2b** in **Fig 3.15** will serve as an example to illustrate the point mentioned above

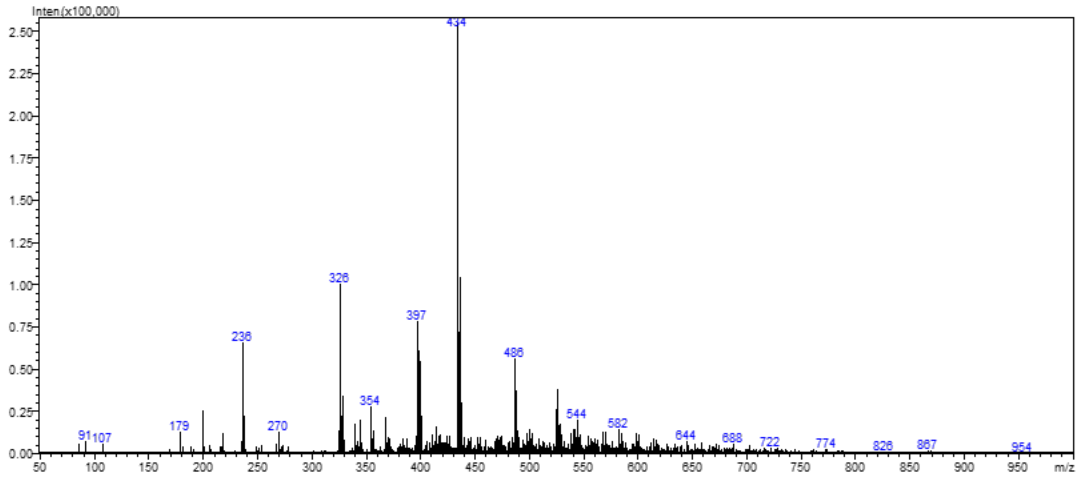

Figure 3.15: Mass Spectrum of compound **2b**

Given the structural similarities between hydroxypyridinone-aminoquinolines, several key infrared (IR) stretching vibrations or bands can be anticipated to have resembling patterns. The FTIR spectrum of compound **1k** in **Figure 3.16** will act as a representative spectrum for both kojic acid and maltol-derived conjugates.

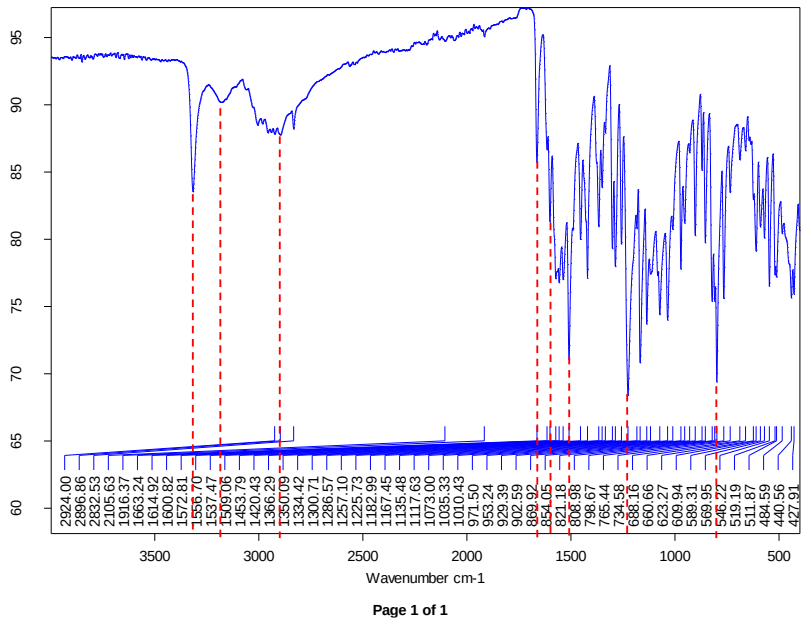

Figure 3.16: IR spectrum of compound **2b**

The amine group's N-H stretching vibrations attached to the quinoline are expected to appeared between 3300–3500 cm^{-1} as expected, with primary amines potentially displaying two peaks. The aromatic C-H stretching vibrations associated with the benzene ring in the benzyloxy group and the quinoline ring are likely to emerge between 3000–3100 cm^{-1}. For the alkyl groups, C-H stretching vibrations were observed around 2850–2960 cm^{-1}. The carbonyl

(C=O) group within the pyridinone ring, as expected, produced a strong, sharp band in the range of 1650–1750 cm^{-1}. Meanwhile, the C=C stretching vibrations of the aromatic rings (benzene and quinoline) of most target compounds occurred between 1450–1600 cm^{-1}. C-N stretching vibrations from the amino group linked to the quinoline moiety were expected around 1280–1360 cm^{-1}, and the C-O stretching in the benzyloxy group should produce a band near 1200–1300 cm^{-1}. Finally, the C-Cl bond in the 7-chloroquinoline segment is anticipated to show a frequency between 600–800 cm^{-1}, and this was observed. The identification of these functional groups was confirmed through the observed vibrations in the IR spectra, as detailed in the experimental section and the Appendix.

3.5 Conclusion

In summary, this chapter focused on the synthesis and characterization of a series of compounds derived from kojic acid and maltol. A total of 20 compounds were successfully synthesized using established methods in organic chemistry. Each compound's structure was confirmed through comprehensive analysis using ^{1}H and ^{13}C NMR spectroscopy, complemented by infrared spectroscopy (IR). The structural elucidation of the hybrid compounds was challenging due to the complexity of the proton NMR spectra and the significant overlap among carbon peaks. To overcome this, 2D NMR techniques were employed, providing crucial insights into the connectivity and arrangement of atoms within the molecule. In some compounds (e.g. **3c**, **1e** and **2h**), there was a notable duplicating of some peaks, which we suspected could be due to the excess (unreacted) intermediates that were not completely washed or a problem with the shimming and locking of the NMR instrument itself.

This study highlights the successful synthesis of kojic acid and maltol derivatives and underscores the importance of spectroscopic methods in structural characterization. By employing a combination of conventional and advanced spectroscopic techniques, this research contributes to our understanding of these compounds' chemical properties and potential applications in various fields.

Chapter 4: HIV *In-Vitro* Activity Evaluation

4.1 Background

It is known that a critical step in drug development is the biological evaluation[253]. Biological evaluations are experiments designed to estimate the potency of substances by observing their pharmacological effects on living organisms (*in vivo*) or on isolated tissues or cells (*in vitro*) and comparing the effect of these substances of unknown potency to the effect of a standard drug or compound [254][255].

Most common in modern pharmaceutical use are the *in vitro* assays. Various substances are screened based on their impact on an enzyme, receptor, site, or rate-limiting step of interest either by activation, inhibition etc. [256]. In such assays, a single point of action in each biochemical pathway is targeted, such as the role of the enzyme(s) that would have already been identified and proved by scientists[254][257].

As the experiments are conducted, the test samples are confined to a known quantity, thus the concentration is known. This is important to note since all measurements of the test sample's activities, either potency, efficacy or affinity are basically concentrations at which a defined drug effect is observed. For instance, if a compound or drug is noted to exhibit fifty percent (50%) inhibition of a specific biological activity at 5μM then the IC_{50} is taken to be 5μM. Drugs can be then compared to one another using the IC_{50} (for example if it is a cytotoxicity assay IC_{50} is the cytotoxic concentrations that killed 50% of the cells) values. By comparing IC_{50} values for different drugs, one can assess which of them is effective at lower concentrations[258]. The literature broadly categorizes IC_{50} values, acknowledging that variations in laboratory conditions and methodologies can result in differing parameters. In the study, the IC_{50} values were categorized generically as follows[259]:

(a) potent: $IC_{50} < 4$ μM

(b) very active: $IC_{50} \leq 20$ μM

(c) moderately active: $IC_{50} > 20–100$ μM

(d) weakly active: $IC_{50} > 100–1000$ μM

(e) inactive: $IC_{50} > 1000$ μM

Bioassays are also integrated with statistical methods which aid in analyzing and processing experimental results[257]. The experimental data (experimental outcome/observations) is classified as the independent variables and the known variables such as the concentrations of the test compounds are dependent variables. Independent variables only have random error whereas dependent variables have random and system errors[260]. The advantages of

modern bioassays are that they are less time-consuming, efficient, reproducible, and precise [261][262].

This chapter discusses the effects of some hydroxypyridinone-aminoquinoline compounds on cell viability (cytotoxicity), reverse transcriptase activity inhibition and HIV protease activity inhibition properties. These HIV assays corresponds to the HIV drug target stages in the lifecycle of the virus. The reverse transcriptase is for two classes of the antiretroviral agents namely **nucleoside reverse transcriptase inhibitors** (**NRTIs**) and **Non NRTIs.** The main difference between the two subclasses is that NRTIs act as host nucleotide decoys by attaching to the host DNA and cause termination of the elongating HIV DNA chain whereas the NNRTIs bind directly to the HIV reverse transcriptase enzyme blocking its action. Currently, the NRTIs serve as the backbone of ART regimens.

The HIV protease assay corresponds to the maturation stage of the viruses catalyzed by the protease enzyme. Additionally, we also evaluated the antioxidant properties and nitric oxide production properties of these compounds. The overarching goal of conducting these assays was to evaluate the potential of the HPO-AQs as anti-HIV agents. All these assays were performed by Ms Munapo under the supervision of Dr N Gama from Department of Biochemistry, Genetics, and Microbiology at University of Pretoria.

4.2. Cytotoxicity Screening Assays

One major reason why most drug candidates fail to reach the market is their toxicity in patients. Currently, cytotoxic side effects of failed drug candidates are being discovered late in the drug discovery process i.e. during clinical trials. This failure leads to the loss of large financial investments by pharmaceutical companies[263]. Though the cytotoxicity screening is crucial, it also has some limitations because the techniques developed so far are not adequately advanced to replace the animal tests. The values obtained in some cases cannot be compared because the tests are highly dependent on the parameters of the test system[264].

Such parameters can be the type of cell line, passage number of the cells, number of cells per well, volume of medium per well, growth time of a plate, concentration/volume of reagent, manufacturer of the reagent, length of incubation, reaction time, solubilization solution (if needed) even the performance of the spectrophotometer[265]. However, it is still of paramount importance to determine and/or predict a drug candidate's *in vivo* toxicity based on toxicity *in vitro* profiles. Despite all the disadvantages posed, cytotoxicity screening assays has some advantages, such as speed, reduced cost and potential for automation, and tests using human cells may be more relevant than some *in vivo* animal tests[266].

Cell-based assays are often used to screen a collection of compounds to determine if the tested molecules influence cell proliferation or show direct cytotoxic effects that eventually lead to cell death. Cell death is a desired event such as for the evaluation of anticancer agents but it is also an indicator of toxicities associated with the use of a given small molecule or the test compound's involvement in modulation of a specific pathway[267]. To guarantee success in cytotoxicity evaluations, comprehensive screening protocols must be employed. In a well-built toxicity screening procedure, different test types on different cell cultures must be performed[268]. A variety of assay methods can be used to estimate the number of viable cells, and they are classified as follows [264],

(a) dye exclusion assays – the principle is based on the concept that live cells possess intact cell membranes that exclude certain dyes, such as trypan blue, Eosin, or propidium, whereas dead cells do not[269].

(b) fluorometric assays - This assay is based on the fluorescence enhancement of propidium iodide (PI) upon binding with double-stranded nucleic acids[270].

(c) luminometric assays – an assay used to the analyze genomic DNA methylation.

(d) colorimetric assays - the principle lies in the generation of colour by chemical/biochemical reaction between target analyte and reagents. The intensity of the resulting colour can be quantified using imaging tools and processing software[271].

Regardless of the type of cell-based assay being used, it is important to know how many viable cells remain at the end of the experiment [272]. In order to determine cell proliferation, there is a need for cheap, reliable, and reproducible short-term cytotoxicity and cell viability assays[273]. It is also important to note that availability of chemicals, reagents and apparatus in the laboratory where the study is to be performed; test compounds, detection mechanisms are major considerations in selecting the assay to use.

Compared with other methods, colorimetric methods are favored because they are cheaper, easy to use and are accurate. Under colometric assays, tetrazolium reduction experiments, **MTT** [3-(4,5-dimethylthiazol-2-yl)-2,5-diphenyl-2H-tetrazolium bromide] to be specific is preferred over other methods because currently it is considered a significant advance over traditional techniques because of its sensitivity. In addition, it is a reliable indicator of cellular metabolic activities, it's rapid, versatile, quantitative, and highly reproducible with a low intratest variation between data points (±15% SD).

The MTT assay is also useful in a large-scale, antitumor drug-screening program and always allows sufficient time for cell replication, drug-induced cell death, and loss of enzymatic activity[274].

For this study, cytotoxicity of the selected compounds was evaluated on three cells lines namely human cervical carcinoma (HeLa) cells, human hepatocellular carcinoma (HepG2) cells and TZM-bl cells which are HeLa cell derivatives that were engineered to express CD4, CCR5 and CXCR4 (which makes them to be highly sensitive to HIV infection) using the MTT assay[268].

4.2.1 MTT Assay Protocol and Experimental Observations

This assay is based on the reduction of a yellow MTT salt to purple formazan crystals by metabolically active cells. The viable cells contain NAD(P)H-dependent oxidoreductase enzymes which reduce the MTT (yellow) to formazan (purple)[275].

As depicted in the cell, **Fig. 4.1** the chemical structure of MTT and formazan are illustrated inside the cell. MTT consists of a tetrazole ring core containing four nitrogen atoms (1) surrounded by three aromatic rings including two phenyl moieties (2) and one thiazolyl ring (3). Reduction of MTT results in disruption of the core tetrazole ring and the formation of formazan. Red arrows and the **"-"** sign indicate disruption of MTT reduction on the normal metabolic activity of the cells and the impeding effect of the formazan crystals (when presenting on the cell surface) on further uptake of MTT reagent by cells[265].

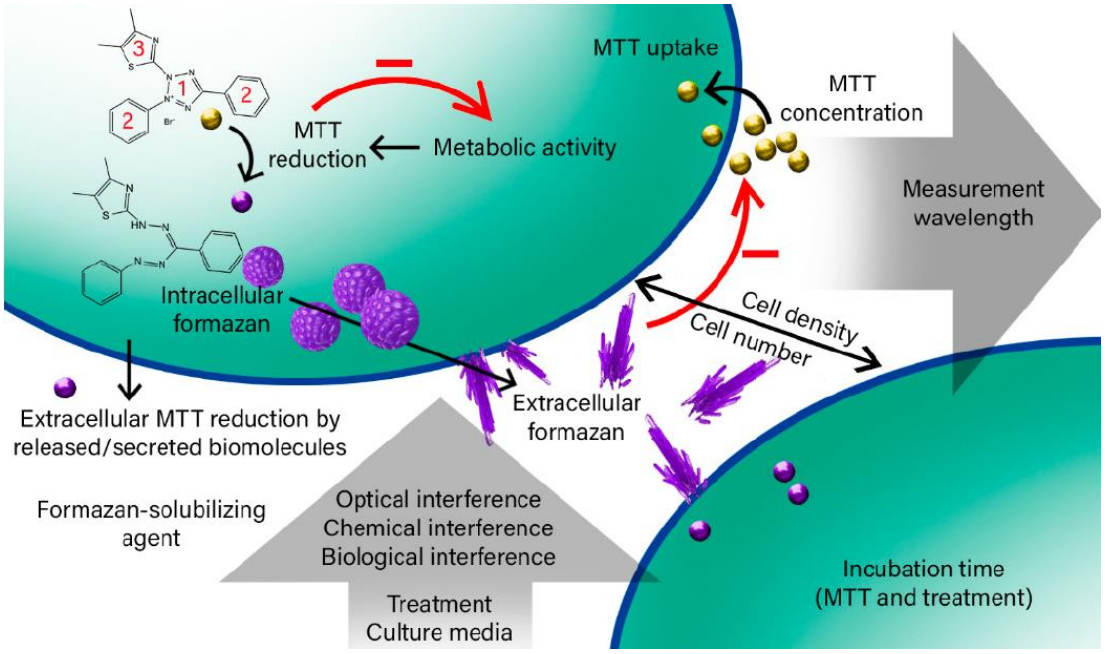

Figure 4.1: Factors affecting the final optical density measurements in the MTT[265].

Despite the inconsistences in seeding cell number, cells' supernatant removal following MTT incubation which make it difficult to compare the measured optical density value of cells between different studies, MTT assay is still commonly used and interpreted, overlooking these limitations[265].

The insoluble formazan crystals are dissolved using a solubilization solution and the resulting-coloured solution is quantified by measuring absorbance at 540 and 690 nanometers using a multi-well spectrophotometer. The darker the solution, the greater the number of viable, metabolically active cells[275].

Assay Protocol:

$1x10^5$ cells per well in 10% (Fetal Bovine Serum) FBS in Dulbecco's Modified Eagle Medium (DMEM) media [pink solution], were seeded and incubated for 24 hours in 5% carbon dioxide at 37˚C **(Fig. 4.2)**. DMEM contains many ingredients including ions (for maintaining tonicity and proper protein structure), amino acids (for protein synthesis), vitamins (to serve as enzymatic co-factors), and glucose (as a source of energy).

Figure 4.2: A picture depicting the 96 well plate with seeded cells[276].

In addition to these components, growth media are frequently supplemented with antibiotics and/or anti-mycotics to inhibit the growth of contaminating pathogenic organisms, and with acellular animal blood (serum) to provide various proteins needed for attachment and growth[277]. Serum concentrations can be varied, but typically range from about 5-20%. Finally, a buffer (often bicarbonate) must also be included to maintain proper pH, and pH indicators such as phenol red allow rapid visual assessment of pH.

The color of DMEM at its proper physiologic pH of 7.4 is orange red; the color changes at pH 7.8 to purple, at pH 7.6 to blue-red, at pH 7.0 to orange, and at pH 6.5 to yellow[277]. These inoculated cells were then treated with the test compounds **(Fig. 4.3)** and incubated for 48 hours in 5% carbon dioxide at 37°C. Cisplatin is a known antitumor drug and it was used in the MTT assay as a standard control[278].

Figure 4.4 shows how the MTT assay plates looked like after treating the cells with the selected compounds (**Fig.4.3**). In this study, only a subset of compounds was evaluated for cytotoxic potential due to resource constraints and the fact that these were the only synthesized compounds available at the time of the assays.

In the three wells that had 10% FBS media only (negative control) remained pink (the original colour of the media). This was expected as there were no viable cells that could have used the nutrients in the media nor any carbon dioxide that could have been produced in the process of respiration and other biological processes that could have resulted in the alteration of the pH. In other words, the nutrients were still there.

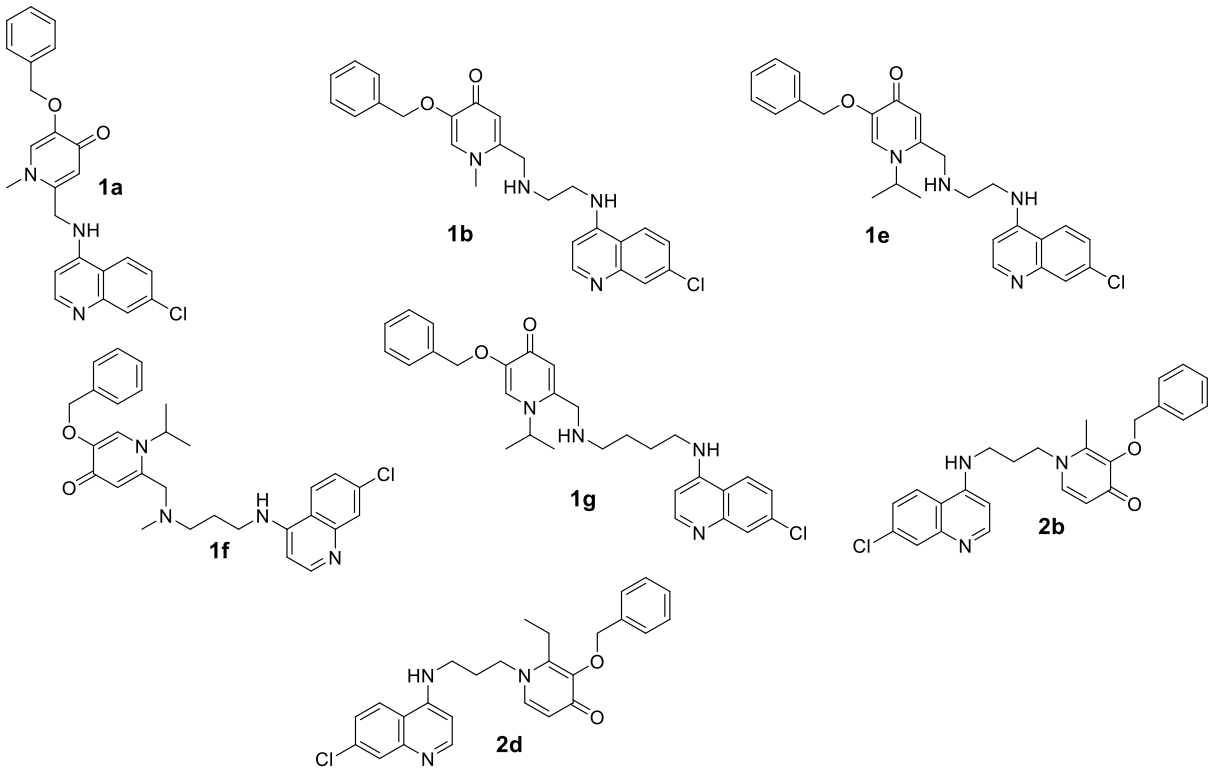

Figure 4.3: Structures of the tested compounds in the MTT assay

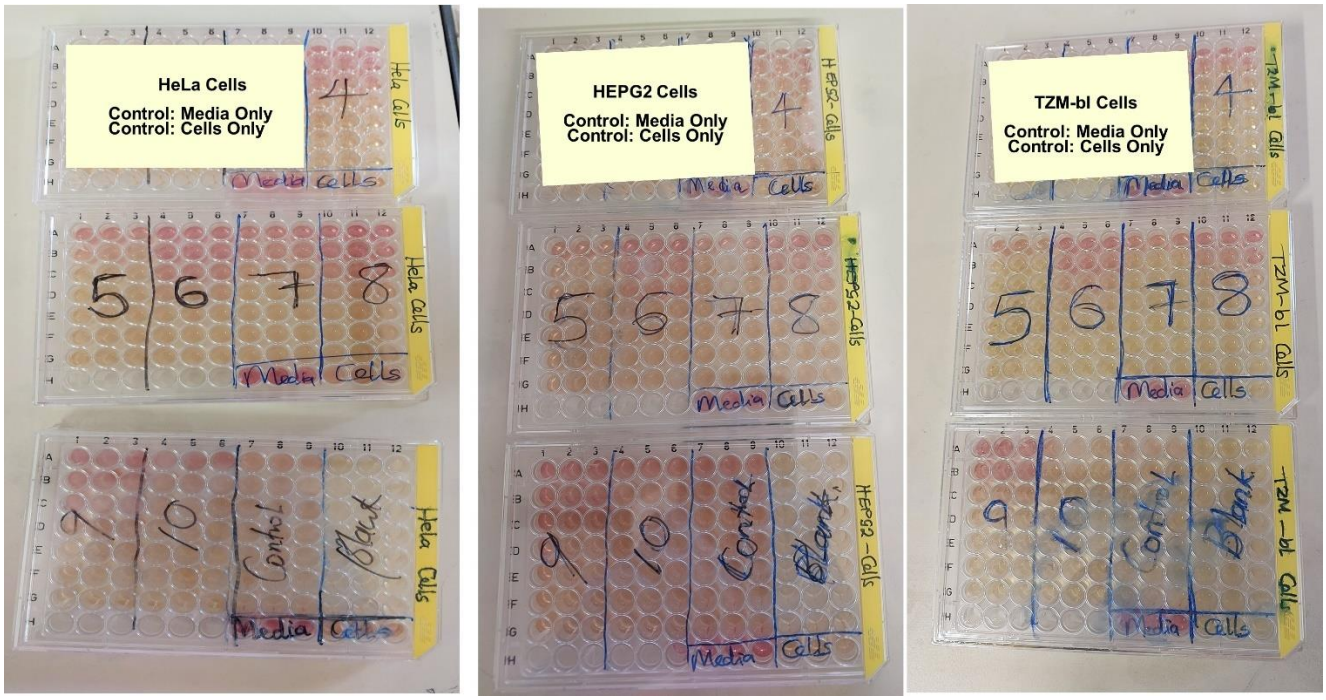

Figure 4.4: Photographs of the MTT assay plates after cell treatment with test compounds. The numbers correspond to 4.)**2b** 5.)**2e** 6.)**1e** 7.)**1g** 8.)**1b** 9.)**1f** 10.)Control = Cisplatin, Blank=Cells only

In the three wells that had untreated cells, the pink 10% FBS media turned yellow. This is because the viable cells in the wells used up all the nutrients in the media, as the cells proliferated, they produced carbon dioxide that could have been produced in the process of respiration and other biological processes that could have resulted in the alteration of the pH. Change in pH influences the colour change from pink to yellow.

The other wells that were treated with the selected hydroxypyridinone-aminoquinoline compounds had variations in colour. The first rows had the highest concentration (200μM) of the compounds. Generally, it was noted that with the highest concentration the wells remained pink. This means that the nutrients were still available and the cells no longer viable.

As the concentration decreased going down the rows to 6.25μM the pinkish colour gradually turned yellow. This indicated that the cells were still viable and present in the wells.The raw data (absorbances measured at 540nm and 690nm) was processed to calculate the percentage cell viability using the formula below. (**Note:** All the data in the appendix)

$$Percentage\ Cell\ Viabilty = \frac{Number\ of\ Viable\ Cells\ in\ each\ well}{Number\ of\ Viable\ Cells\ in\ the\ control\ well}\ x\ 100\%$$

4.2.2 Effect of HPO-AQs on HeLa cells' viability

Hela cells are derived from cervical cancer cells. They are durable, and they propagate steadily. Provided that the fundamental suitable growth conditions are met, they can divide an unlimited number of times in a laboratory cell culture plate. For this reason, Hela cells are referred to as immortal[279].

The cells were treated with different concentrations of HPO-AQs for 48 hours and cis-platin was used as the control. Overall, MTT results showed a decrease in survival of the cells in a concentration dependent manner (**Fig. 4.5).**

Generally, the cell viability of HeLa cells increased as the dose concentration decreased when treated with all the compounds including the experimental standard, cisplatin. At 200μM, all the tested compounds were more toxic than cisplatin. At 100μM, two (**1f** and **2b**) compounds showed to be less toxic as compared to the control cisplatin, while the rest were more toxic. This was shown by their percentage viabilities which were slightly greater than that of cisplatin. Notably, **1a** was comparable with cisplatin. Compound **2b** was the least toxic (highest percentage viability) compound, and **1e** was the most toxic (least percentage cell viability) at this concentration (100μM) when compared to all the tested compounds, including cisplatin. The negative percentage viability (high toxicity of compound **1e**) means that the compound lysed the cells completely causing extensive cell death and it's normalized to zero for untreated cells.

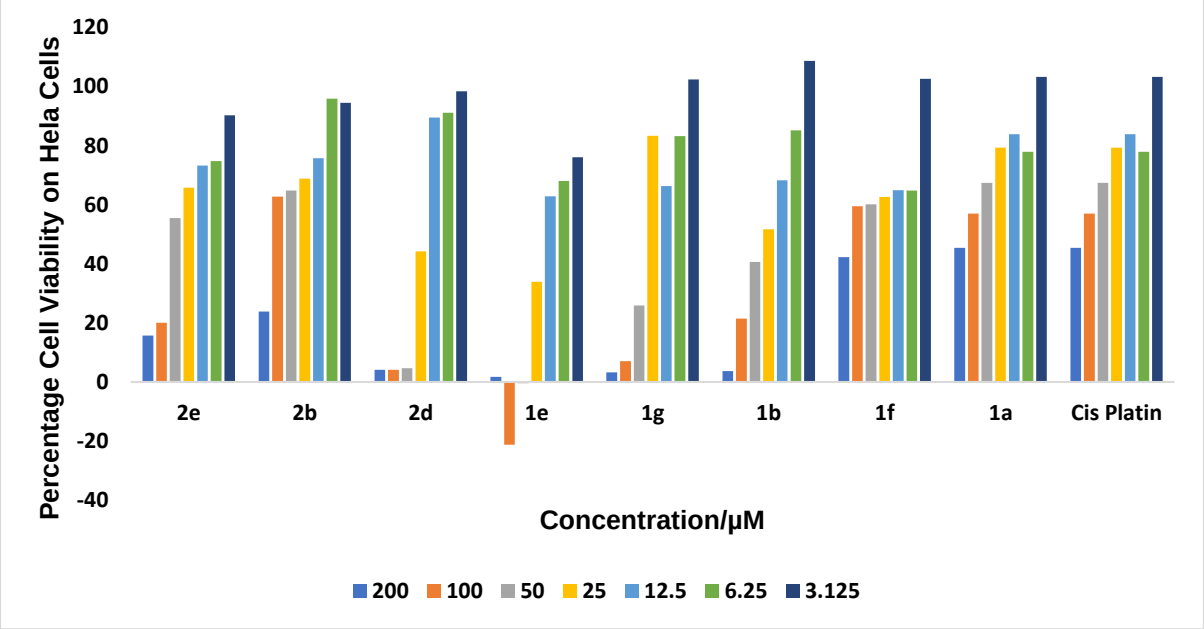

Figure 4.5: Cytotoxic effects of HPO-AQs on HeLa cells viability.

With the decreasing concentrations, the toxicity effect of all the compounds decreased hence the cell viabilities increased. Cisplatin did not cause significant cytotoxic effect at the concentration of 3.125µM with a mean percentage cell viability of 103%. Percentage viability above 100% means that the compounds could not kill the cells, rather the cells could thrive and even multiply. This translates to the compounds not being toxic at this particular concentration. The optimum dosages which caused 50% inhibition of cancer cell growth, (IC_{50}) values, were determined by GraphPad Prism analysis and results are shown in **Table 4.1**.

Table 4.1: Cell viability IC_{50} values of tested compounds in HeLa cells.

Compound	Mean IC_{50} ± SDE (µM)
1a	50.60 ± 26.40
1b	35.71 ± 10.01
1e	24.73 ± 4.74
1f	35.76 ± 12.73
1g	29.37 ± 1.475
2b	49.24 ± 20.96
2d	57.03 ± 22.06
Cis-Platin (Positive Control)	30.27 ± 8.95

Overall, all the compounds including cisplatin had IC_{50} values greater than 20µM but within the range of IC_{50} > 20–100 meaning that they were not toxic. **1e** and **1g** had lower IC_{50} values than cisplatin. Thus, they are more toxic and the rest which had higher IC_{50} values were less toxic than cisplatin. Overall **2d** was the least toxic and **1e** was the most toxic.

L. Saghaie L *et al.,* reported that the cytotoxicity of 3-hydroxypyridin-4-ones was closely related to the lipophilicity of compounds. In their studies on HeLa cells, most lipophilic compounds revealed the highest toxicity, and the more hydrophilic agent showed the less cytotoxic effect[280]. From the *in-silico* predictions, **1e** was moderately soluble which explains why its IC_{50} value is not too low neither is it high but moderately toxic even though it is the one with the least IC_{50} value.

4.2.3 Effect of HPO-AQs in HEPG2 cells' viability

The other cell lines that were used are in the MTT assay are the liver cancer cells HepG2 hepatocytes. Liver cancer is the third leading cause of cancer death worldwide[281]. There are several types of primary liver cancers namely HCC (80–90% of cases), intrahepatic cholangiocarcinoma (ICCA, 10–15% of cases), hepatoblastoma and angiosarcoma (AS). It should be noted that hepatoblastoma is the most common malignant liver tumor in children and it accounts for about 70% of cases, followed by HCC, accounting for 27%[282].

Based on cytological characteristics, HepG2 cells are the most likely tumor cells in hepatoblastoma. Also, they bear an intermediate state between normal hepatocytes and tumor cells, for which significant changes in the epigenetic regulation of nuclear and mitochondrial genes are observed [281].

As with the HeLa cells, HepG2 cells were treated with different concentrations of HPO-AQs for 48 hours. The tested compounds demonstrated significant cytotoxicity in a dose-dependent manner against the liver cancer cell lines HEPG2 as illustrated in **Fig. 4.6**.

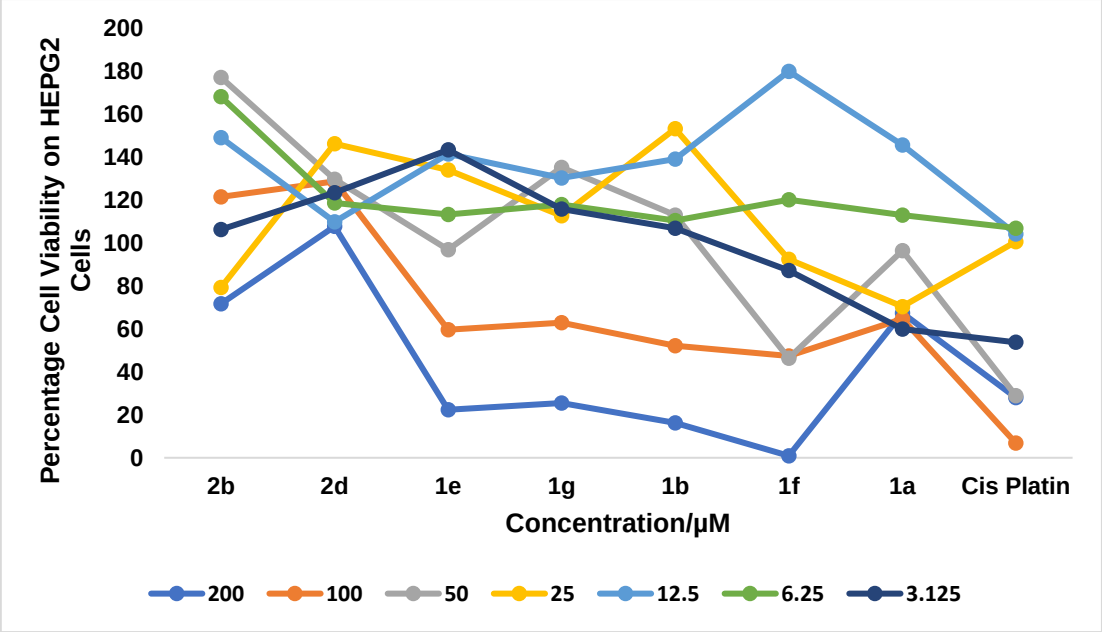

Figure 4.6: Cytotoxic effects of HPO-AQs on HEPG2 cells viability.

Comparing their trends with HeLa cells', all the tested compounds were non-toxic on HeLa cells than on HEPG2 cells (some even better than cisplatin as they had cell viabilities above 100%). With respect to HepG2 cisplatin had its highest cell viability at 6.25µM concentration which was about 106% (cell viability values above 100% generally indicate that the treated cells exhibit greater metabolic activity or proliferation compared to the untreated control) and its lowest at 100 µM which was about 6.8%. At 6.25µM, the cells could thrive in the presence of cisplatin as it was not toxic.

At 3.125µM, **1e** had the highest percentage viability which makes it to be the least toxic, followed by **2d**, **1g**, **1b**, **2b**, **1f**, **1a** and lastly cisplatin. Comparing their IC_{50} values, **2e** had the lowest followed by cisplatin **1f**, **2d**, **1e**, **1b**, **1g** and lastly **1a**.

The optimum dosages which caused 50% inhibition of cancer cell growth, (IC_{50}) values, were determined by GraphPad Prism analysis and all the compounds were not toxic (results shown in **Table 4.2**.

Table 4.2: IC_{50} values of each compound in HEPG2 cells.

Compound	Mean IC_{50} ± SDE (μM)
1a	76.78 ± 71.0
1b	57.76 ± 26.2
1e	43.06 ± 12.9
1f	34.85 ± 5.7
1g	75.57 ± 9.6
2b	41.86 ± 50.1
2d	21.18 ± 24.8
Cis-Platin (Positive Control)	26.57 ±4.9

In HEPG2 Cells, all the tested compounds had IC_{50} values greater than 20μM but within the range of IC_{50} > 20–100 meaning to say that they were not toxic.

Comparing these IC_{50} values with the HeLa cells', **2b** had a lower IC_{50} value in HEPG2 cells, and this makes it a better candidate for liver cancer treatment than as a cervical cancer agent. In particular, compound **1f**, which has an IC_{50} value of 34.85μM is slightly lower than its IC_{50} value of 35.76μM when tested in HeLa cells (a difference of 0.91μM which is almost negligible). This means that its cytotoxicity properties are almost the same whether as a cervical or hepato-cancer agent. What makes **1f** structurally unique from the other compounds is the presence of the tertiary amine group in the side chain. Probably this moiety could be important for the intake and accumulation of the drug inside the cancer cells similar to what happens in the *plasmodium*.

4.2.4 Effect of HPO-AQs in TZM-bl cells' viability

The TZM-bl cell line is derived from a HeLa cell clone that was engineered to express CD4, CCR5 and CXCR4[283]. These cells are highly permissive to infection by most strains of HIV, SIV and SHIV, including primary HIV-1 isolates and molecularly cloned Env-pseudotyped viruses[284]. The same HPO-AQs compounds with different concentrations were tested on TZM-bl cells and the MTT assay results showed an increase in survival of the cells in a concentration dependent manner.

As depicted in **Fig. 4.7**, generally, the cell viability of TZM-bl cells increased as the dose concentration decreased for most test compounds. This means that the compounds' cytotoxicity was dose dependent. Cisplatin did not cause significant cytotoxic effect at the concentration of 3.125μM with a mean percentage cell viability of 126%. However, at the lowest concentration, **1e** had the least toxicity effect on TZM-bl cells. At 50μM, **2d** had the highest cell viability and at 6.25μM **1e** was the least toxic.

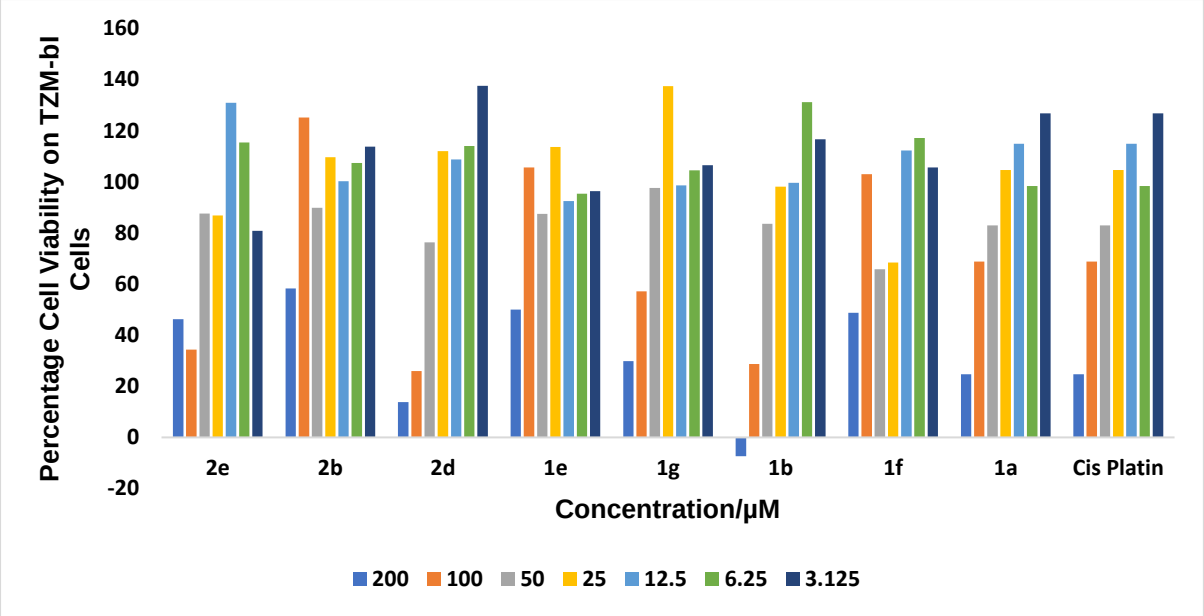

Figure 4.7: Cytotoxic effects of HPO-AQs on TZM-bl cells viability for 48 hours.

Table 4.4: Cytotoxicity/cell viability Mean IC_{50} values of the HPO-AQs in TZM-bl cells.

Compound	Mean IC_{50} ± SDE (µM)
1a	22.16 ± 4.58
1b	47.43 ± 16.9
1e	43.06 ± 14.3
1f	53.80 ± 20.1
1g	39.36 ± 4.10
2b	38.62 ± 15.2
2d	25.80 ± 20.3
Cis-Platin (Positive Control)	37.76 ± 16.8

1a and **2d** had lower IC_{50} values than cisplatin and all the other test compounds. Thus, **1a** and **2d** are the most toxic whereas **1f** was the least toxic in the TZM-bl cell line.

4.2.5 Summary

For a compound to be a good drug candidate, it must not be toxic to the normal human cells. A general observation on the toxicities of all the compounds, when evaluated on three different cell lines, is that maltol-derived compounds (**2b** and **2d**) were more toxic compared to the kojic-derived compounds (**1a, 1b, 1f and 1g**).

Based on the TZM-bl cells MTT assays, the most nontoxic compounds [**1b; 1e; 1f; 1g** and **2b**] i.e. with relatively higher IC_{50} values, were further evaluated for anti-HIV (Reverse Transcription Inhibition and HIV Protease Activity inhibition) and antioxidant activity (Free-Radical Scavenging assay).

Although the scope of the current work, focuses on HPO-AQs as potential antimalarial and anti-HIV agents, however their potential medicinal chemistry applications are not limited to only these two diseases hence they were also evaluated for anti-cancer and antioxidant properties. The data derived can be used to justify repositioning or repurposing the HPO-AQs for anti-cancer treatment. For compounds to be good anti-cancer agents they must be able to inhibit the viability of cancer cells, thus should be cytotoxic to the cancer cells. The compounds with lower cytotoxicity IC_{50} values in TZM bl cell line [**1a** and **2d**] were further evaluated for their anti-cancer properties using the Nitric Oxide (NO) Assays

4.3 Reverse Transcriptase Assay

Despite the lack of significant progress in the field of drug/vaccine development against HIV, three decades of research have emanated in various antivirals[285]. The antiviral drugs developed so far target the viral proteins, including protease, reverse transcriptase, integrase, and envelope (fusion process), or the cellular receptors involved in viral entry by inhibiting their activities[286][287].

Reverse transcriptase is an enzyme encoded from the genetic material of retroviruses that catalyzes the transcription of retrovirus ribonucleic acid (RNA) into deoxyribonucleic acid (DNA)[288]. This catalyzed transcription is the reverse process of normal cellular transcription of DNA into RNA, hence the names reverse transcriptase and retrovirus. It is central to HIV-1 infection and a major antiviral target, which makes it a biological process of great interest[289][290].

The Reverse transcriptase RT assay is used to determine the propagation of retroviruses in retrovirus-infected mammalian cells in culture. The assay is also used for *in vitro* screening for RT inhibitors[291]. Reverse transcriptase inhibitors are medications used in the management and treatment of HIV[288][292].

The reverse transcriptase colorimetric assay takes advantage of the ability of reverse transcriptase to synthesize DNA, starting from the template/primer hybrid poly (A) × $(dT)_{15}$. Biotin-labeled DNA bound to the surface of the microplate modules that is precoated with streptavidin. An antibody to digoxigenin conjugated to peroxidase (Anti-DIG-POD), is bound to the digoxigenin-labeled DNA. Afterwards the peroxidase substrate ABTS is added and the peroxidase enzyme catalyzes the cleavage of the substrate, producing a colored product as depicted in **Fig. 4.8**[293].

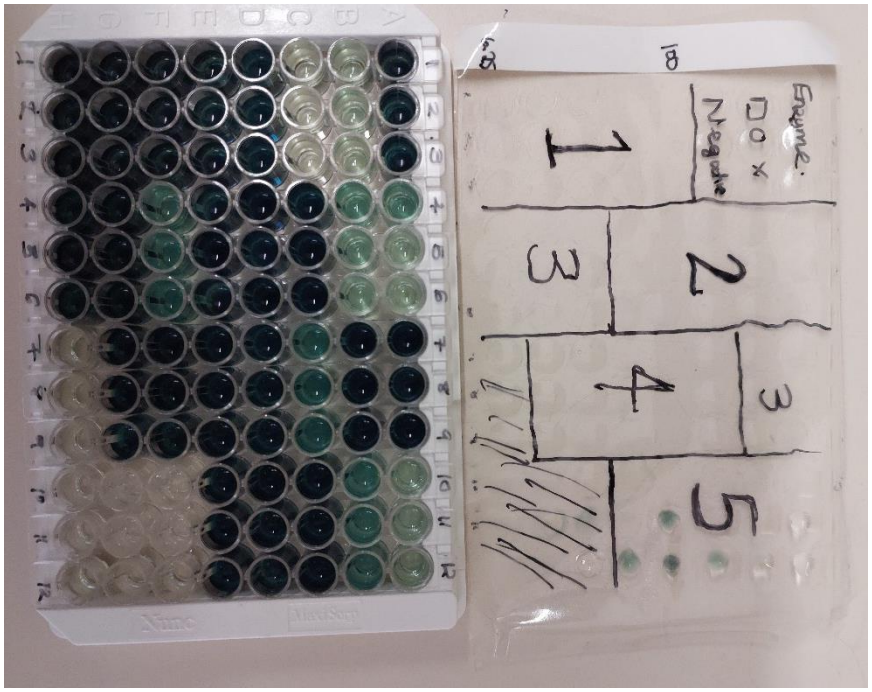

Figure 4.8: A photo of RT assay plate. The five most nontoxic compounds on TZM-bl cells were evaluated for their inhibition properties on the HIV reverse transcriptase enzyme. Numbers (1-5) were used for labelling purposes only. The numbers correspond to (1.) **2b** (2.) **1e** (3.) **1g** (4.) **1b** (5.) **1f**. The wells labelled **Enzyme** were the positive control wells**; Negative** is the negative control wells that did not contain the nucleotide. DOX wells are for control (experimental standard) .

The absorbances of the samples were determined using a microplate (ELISA) reader and they were directly correlated to the level of RT activity in the sample[293].

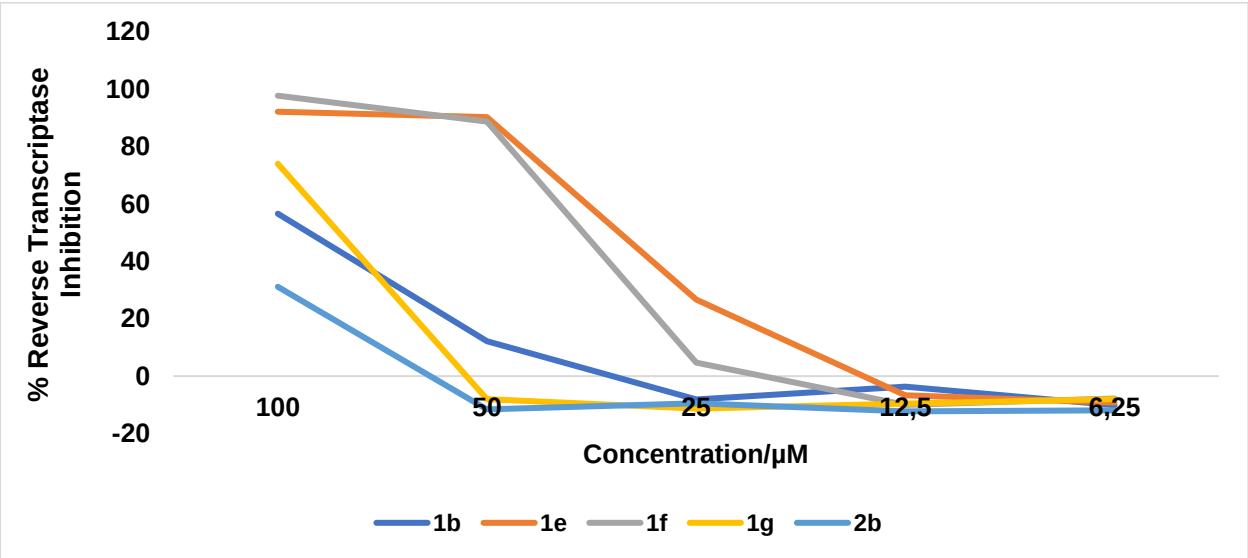

Figure 4.9: Percentage reverse transcriptase inhibition graphs

From the graphs, **Fig. 4.9**, representing the percentage inhibition, their shapes show the negative (inverse) relationship. As the concentration of the tested compounds was decreased, their inhibitory efficiency decreased.

At 100μM, **1f** could inhibit the enzyme better than the rest of the compounds. When the concentration was decreased to 50μM, **1e** inhibited the enzyme better than **1f,** whilst **1g** was the least inhibitor of them all. The compounds **1g** and **2b** could not inhibit the reverse transcription mechanism at 50μM, hence the negative inhibition.

At 25μM, **1e** and **1f** still maintained higher inhibitory properties. **1g** was overtaken by **1b**, then **1e** and lastly **2b**. As the concentration was decreased to 12.5, **1b** could inhibit the reverse transcriptase better than all the other compounds. Interestingly, **1b** could inhibit better at 12.5μM than at 25μM. In as much as the percentage inhibition for all the compounds was less than 0% (no inhibition of the enzyme) at 6.25μM, **1f** inhibited the HIV transcriptase better than the rest of the compounds.

Table 4.5: Mean IC_{50} values of each compound and their R^2 values.

Compound	Mean IC_{50} and Standard Deviation Error (μM)	R^2 Values
1b	54.13667 ± 2.68	0.983233
1e	26.30333 ± 1.76	0.998867
1f	32.90333 ± 3.79	0.992067
1g	56.56667 ± 0.74	0.995567
2b	60.50333 ± 0.19	0.956067

For qualitative comparison analyses of reverse transcriptase inhibitory properties of the five most nontoxic compounds on TZM-bl, IC_{50} values were analyzed. The IC_{50} values from the RT assay, were ranging from 26 – 60.5μM.

The IC_{50} values from the RT assay, were ranging from 26 – 60.5μM. Of the five tested compounds **1e** (IC_{50} = 26.2±0.19μM) and **1f** (IC_{50} = 32.90±3.79μM) showed the least IC_{50} values. This translated to them being the better inhibitors among the rest of the compounds. Infact **1e** was the best inhibitor while **2b** had the highest IC_{50} value (IC_{50} = 60.50 ± 0.19μM).

Table 4.6: IC_{50} values of some FDA approved RT Inhibitors

RT Inhibitor	IC_{50} values
Emtricitabine	0.0013 - 0.64 μM
Tenofovir	0.5 μM - 2.2 μM
Doravirine	0.012 – 0.014μM

In this assay, no standard or known RT inhibitor was tested together with the HPO-AQs, however, comparison was made with the IC_{50} values of some of the known RT inhibitors on the market (**Table 4.6**)[294][295][296].

The IC_{50} values of all the tested compounds were >1000 fold more than the above-mentioned commercially available drugs. This translates to these compounds being poor inhibitors of the reverse transcriptase enzyme. In this assay, the errors were minimal, this is shown by the very low standard deviation error values. R^2 values also supports this statement. Statistically, R^2 values helps us evaluate how scattered the data points are around the fitted regression line. To determine quality of R^2 the coefficients the following set points can be referred to [297],

- ≥0.91: Very good model prediction:
- 0.81 – 0.90: Fairly precise model prediction
- 0.66 – 0.80: Model prediction can only distinguish low mid-high values
- 0.50 – 0.65: More than 50% of Y variance is affected by X variance

From the RT assay data, it is clear that all the R^2 values were greater than 0.95. This shows that the model was good and the data sets for the triplicate experiments were precise.

4.4 HIV Protease Activity Assay

Therapeutic inhibition of virally encoded HIV protease is specifically targeted since the enzyme plays a critical role in processing the gag and gag-p during the maturation stage of the viral lifecycle. For this reason, the HIV protease has become an important target for HIV-AIDS chemotherapeutic agents and a key model for the development of structure-based drug design and studies of drug resistance[298][299]. Immense efforts to develop more effective HIV protease inhibitor drugs are underway[286], the reason why we are also interested in evaluating our compounds as potential protease inhibitors.

HIV-1 Protease Inhibitor Kit was devised in such a way to provide a simple and quick test suitable for high-throughput screening of HIV-1 protease inhibitors. The assay is based on the ability of active HIV-1 protease to cleave a synthetic peptide substrate to release a free fluorophore, which can be easily quantified using a fluorescence microplate reader[300]. In the presence of a HIV-1 protease inhibitor, the cleavage of the substrate is reduced/terminated, resulting in a decrease or total loss of fluorescence[301]. This simple and high-throughput adaptable assay kit can be used to screen and/or characterize potential inhibitors of HIV-1 protease[302].

For the HIV Protease inhibition assay, the five most nontoxic compounds on TZM-bl cells were evaluated for their inhibition properties on the HIV protease enzyme inhibition. The percentage inhibition data was plotted as graphs (**Fig. 4.10**) shown below.

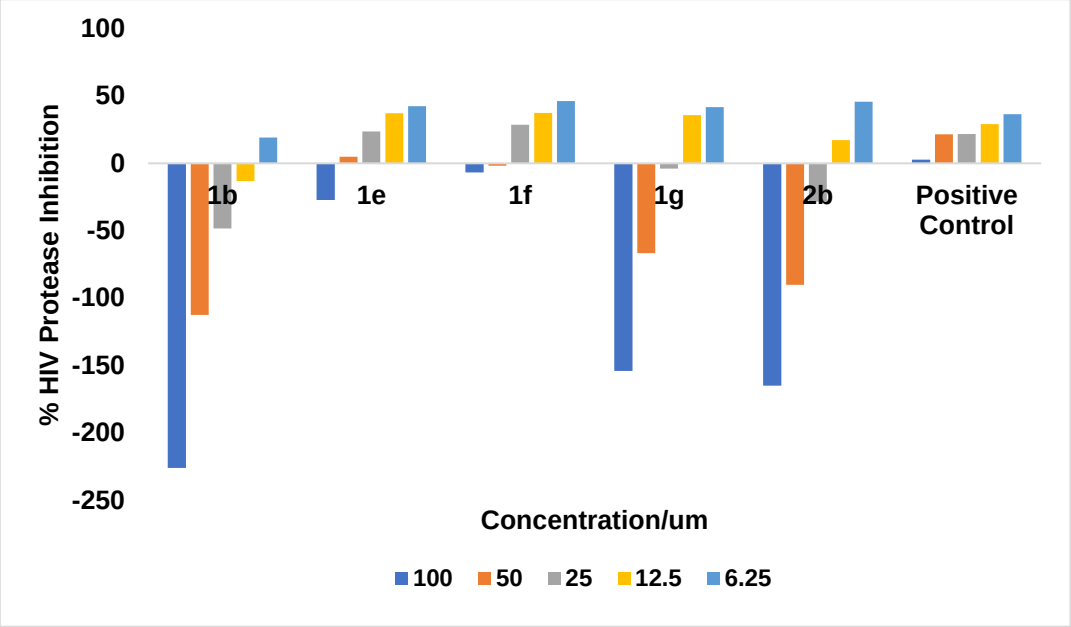

Figure 4.10: Percentage HIV protease inhibition data. [The positive control was provided with the test kit and the original name was not revealed] but it's assumed to be a protease inhibitor.

As depicted on graph shapes patterns **(Fig. 4.10),** all the compounds lost their inhibition properties in higher concentrations. The inhibition pattern was concentration dependent and similar to that observed for the positive control.

At the highest concentration of 100µM, the percentage inhibition of all the tested compounds was less than 0% and the for the positive control was only 2.69%. This translated to poor inhibition. At 50µM, the percentage inhibitions were still below zero except for **1e** (4.82%) and the positive control which had (21.82%). At 25µM, all the tested compounds exhibited improved inhibitions although **1b, 1g** and **2b** still had negative percentage inhibitions. **1e** (23.63%) and **1f** (28.65%) exhibited even better inhibition at 25µM relative to the positive control. Generally, all the tested compounds showed improved inhibition potential at 12.5µM and 6.25µM, **1b** still had the least inhibitor at 6.25 µM.

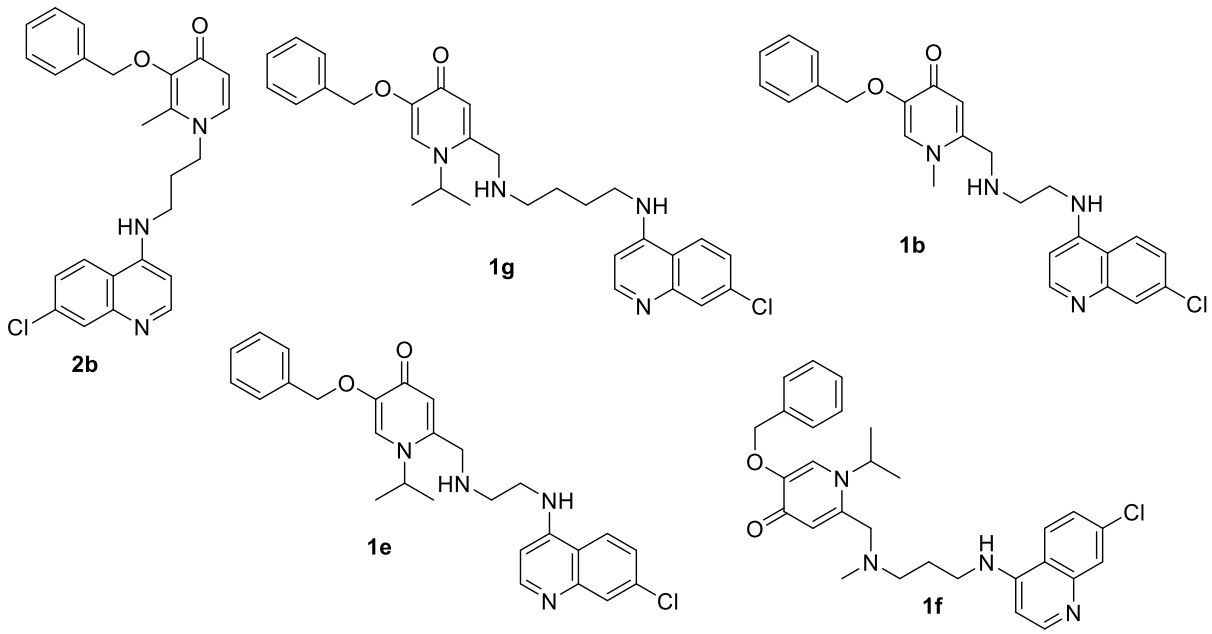

Figure 4.11: Structures of the tested compound in the protease inhibition assay

Structurally **(Fig. 4.11), 1e, 1g** and **1f** are kojic acid derived derivatives with N-isopropyl attachments. The N-methyl group lowered the inhibition properties of the compounds all together hence **1b** always had the least inhibition percentage. **1e** (two carbon chain linker) and **1f** had a three-carbon chain linker whilst **1g** had a four-carbon chain linker with 4, which is believed to have lowered its inhibition potential. Similar to **1f**, compound **2b** also had a three-carbon chain linker hence it had better inhibitory potential.

The interesting observation is that for all the tested compounds (except **1b**), at the least concentration, 6.25uM, they exhibited better inhibition properties than the positive control. Overall, **1e** was the best inhibitor (in relation to the positive control). Collectively, kojic derived compounds are better protease inhibitors than maltol derived compound.

4.5 Nitric Oxide Assay

The uncontrollable proliferation of abnormal cells anywhere in a body is a condition known as cancer. These abnormal cells are named tumors or malignant cells, and they can intrude on normal body tissues. These cancers and the abnormal cells that compose the cancer tissue are further identified by the name of the tissue that the abnormal cells originated from, for example, breast cancer, lung cancer, and colorectal cancer[303].

For cancer treatment, there is remarkable progress in the development of novel medication and therapeutic mechanisms. Currently, we have chemotherapy, radiation, hormonal, and immune therapy, which have resulted in significant clinical responses and prolongation of life, though with little complete remission. Most cytotoxic therapeutics exert their anti-tumor effect

by inducing cell death by apoptosis. The acquisition of resistance and refractoriness to conventional therapeutics remains a substantial problem.

From the review studies conducted by E. A Zaal and C.R Berkers [132], it becomes discernible that anticancer drug resistance to first-line chemotherapy is also associated with metabolic alterations. These metabolic pathways may be targeted to overcome drug resistance or to enhance the efficacy of current chemotherapy. With a better understanding of the field of cancer metabolism, the interest in exploiting the altered metabolism of cancer cells has surged the quest to find novel targets and/or agents for therapy. Many first-line chemotherapeutic agents and combinational treatments with metabolic drugs hold great promise to increase drug efficacy. It will also be good to develop compounds that specifically target the unique metabolism of cancers. Among the novel agents that have recently emerged are agents that are nitric oxide (NO) donors[304].

The toxic compounds (**1a** and **2b**) on HeLa cells were evaluated for NO production properties and the experimental data is shown in **Table 4.7** below. Method : To 50mL of the supernatants from the treated HeLa cells and nitric oxide solutions in a 96 well plate was added 50µL of 1% sulfanilamide solution and the plates were incubated at room temperature (RT) for 10mins in the dark. The plate was covered with foil paper. 50µL NED solution was added to each well and the contents were mixed well. The plates were incubated for 10minutes at RT in the dark. Again, the plate was covered with foil paper. Absorbance readings were measured at 520nm and 550nm.

Table 4.7: Percentage Nitric Oxide produced by **1a** and **2d.**

Concentration/µM	1a	2d
200	-17.3396	-17.717
100	-16.9623	-17.6855
50	-17.327	-17.6918
25	-17.0377	-17.5472
12.5	-16.7799	-17.3962
6.25	-17.1887	-17.9811
3.125	-17.2201	-17.6981

The negative values denote that all compounds did not produce nitric oxide in the assay. This is expected as the tested compounds were not very toxic but moderately toxic in the cytotoxic assays reported earlier.

4.6 Free-Radical Scavenging Assay

2,2-diphenyl-1-picrylhydrazyl (DPPH) free-radical scavenging assay

Free radicals (for example: hydroxyl radical, superoxide, hydrogen peroxide, oxygen singlet, nitric oxide radicals) are oxygen moieties that contain an unpaired electron in their atomic or molecular orbitals. They are unstable and highly reactive. To achieve atomic stability, free radicals oxidize surrounding molecules to obtain a pair of electrons[305].

In mammals, free radicals are enzymatic generated products of respiration and other metabolic functions. Equally, they play an important role in these cell-mediated activities. Excess production of free radicals consequently results in the infliction of oxidative stress on the body and can manifest in form of human health disorders including cancer. Under oxidative stress, endogenous antioxidants are not enough to deal with the increased levels of these reactive oxygen species[306]**.** Therefore, it is necessary to neutralize excess generation of free radicals[307]. Oxidative damage can be counteracted by molecules known as antioxidants.

These molecules, both natural and synthetic, are capable of inhibiting oxidation by donating electrons that can neutralize the radical formation[307]. Although synthetic antioxidants have been widely used, safety issues have been raised over time. According to S.C Lourenço et.al., there are reports indicating a link between the long-term intake of synthetic antioxidants and some ailments namely skin allergies, gastrointestinal tract problems, and in some cases increased risk of cancer. Additionally, high doses of synthetic antioxidants may cause DNA damage and induce premature senescence. Therefore, the need to replace synthetic antioxidants with natural ones has been increasing[308].

Cancer cells are always at elevated oxidative stress which affords them a survival advantage[307] and many human diseases including malaria cause increased oxidative stress therefore it is envisaged that the medicinal efficacy of HPO-AQs can be enhanced if they possess antioxidant activity. Keeping this in mind, selected HPO-AQs were evaluated for free-radical scavenging *in vitro* using the DPPH free-radical scavenging assay.

The free-radical scavenging activities of the tested compounds were estimated according to standard protocols. Various concentrations of these compounds in 100% ethanol were mixed with DPPH and the mixtures were allowed to stand for 30mins. The absorbances were measured at 492nm using a UV-VIS spectrophotometer. An equal amount of DPPH and

methanol were used as the standard and blank, respectively. The scavenging activity was calculated using the following formula:

$$Scavenging\ \% = \frac{(A_{control} - A_{sample})}{A_{Control}} x100\%$$

where $A_{control}$ is the absorbance of the DPPH alone and A_{sample} is the absorbance of DPPH along with different concentrations of the tested compounds[307]. All the assays were carried out in triplicate and average values were considered. Ascorbic acid (Vitamin C) was used as the positive standard.

As displayed in the graph (**Fig. 4.12**), all the tested HPO-AQ compounds have negative graphs except for **1b** which only showed some antioxidant potential at 100μM and 50μM. This translates to poor radical scavenging properties. It has been reported elsewhere that deprotected compounds with free metal chelating groups (OH and C=O) have antioxidant potency.

Mohammadpour et al. reported deprotected kojic derivatives which have the free chelating group) are potent antioxidants. The introduction of the methyl group lowered the antioxidant potential of their compounds. Interestingly, **1b** with a methyl group showed some antioxidant properties at a higher concentration and they lowered with decreasing concentration.

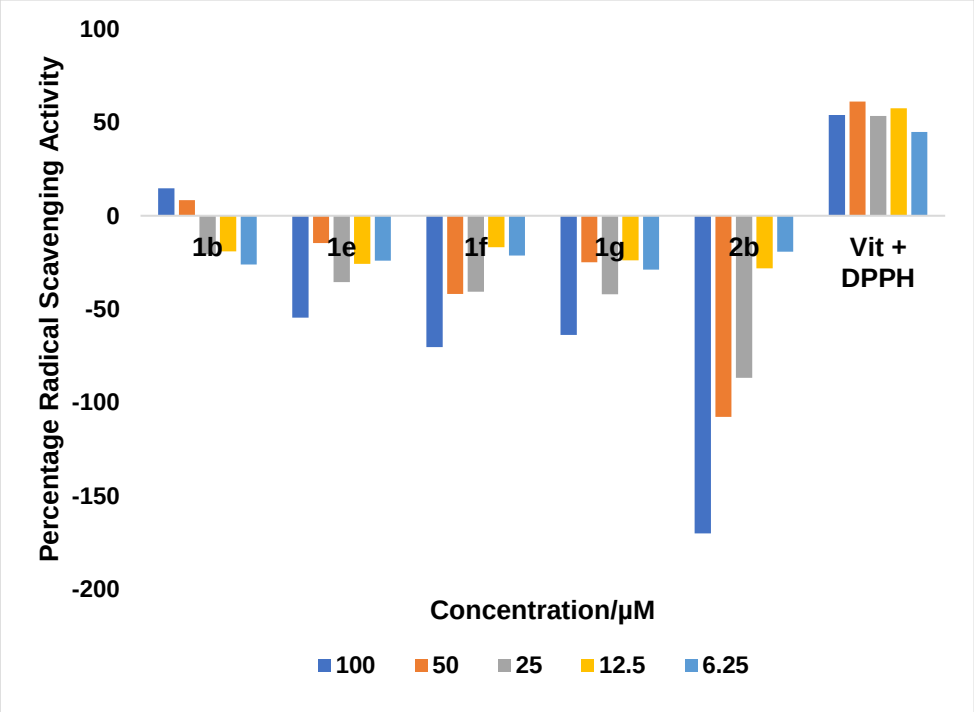

Figure 4.12: Percentage radical scavenging activity of the tested compounds

From all the work discussed above, the most common property of all the potent antioxidant compounds is the presence of the free chelating group. All the compounds that were evaluated in this current study had no free chelating group, they were benzylated which explains why they exhibited no antioxidant properties, even their IC_{50} values were all greater than 20μM except for **1b** (**Table 4.8**). However, from its R^2 value =0.00624, the model was not good and the data sets for the triplicate experiments were not precise. In future, it will be interesting to evaluate the antioxidants of the deprotected analogs, it will be beneficial in chemotherapy to have compounds that can minimizing heme-induced oxidative stress as well as acting as antimalarials and anti-HIV.

Table 4.8: Mean IC_{50} values of each compound and their R^2 values

Compound	Mean IC_{50} and Standard Deviation Error	R^2 Values
2b	31.92	0.7245
1e	4.738	0.00624
1g	50.48	0.2334
1b	25.75	0.529
1f	30.8	0.709

4.7 Conclusion

With due acknowledgement that *in vitro* studies do not always equate to *in vivo* studies but nonetheless, *in vitro* studies are considered to have an important significance at preclinical evaluation stages of drug design and development. It is advantageous to conduct *in vitro* studies prior *in vivo* as it allows insight into a compound's mode of action that might be difficult to obtain in *in vivo* experiments.

The tested compounds were moderately toxic to non-toxic. In the HeLa cells, **1e** was the most toxic, in HEPG2 cells, tdm95 was the most toxic and in TZM-bl cells, **1a** was the most toxic. A general observation on the toxicities of all the compounds when evaluated on three different cell lines is that maltol derived compounds (**2b** and **2d**) were more toxic compared to the kojic derived compounds (**1a, 1b, 1f** and **1g**). With this observation, the kojic moiety counteract the toxic effects caused by the quinoline scaffold better than the maltol moiety. The most toxic compounds were evaluated for their nitric oxide production, the negative results revealed that protected compounds showed reduced properties.

Hydroxypyridinones based compounds have been reported to show good anti-HIV potency <10μM [309]. From the structure-activity relationship studies conducted by Sirous and coworkers, they revealed that halogenating the HPO derivatives lower the cytotoxicity potentials. Also, the presence of metal-binding group (hydroxypyranone) and the properties of

the substituent on the para-position of the hydrophobic aromatic ring attached to the amide has significant effects on the antiviral inhibition. Additionally, one carbon linker's length between the amide function and the aromatic ring is more conducive to achieving optimal HIV-1 replication inhibitory activities than two carbon atoms. Besides, it was found that introducing halogen substituents, Cl and F into the benzene ring had the best metabolic stability. In the current study, overall, kojic derived compounds are better inhibitors than maltol derived compounds **1e** and **1f** showed to be the best inhibitors in both protease inhibition assays and reverse transcriptase assay.

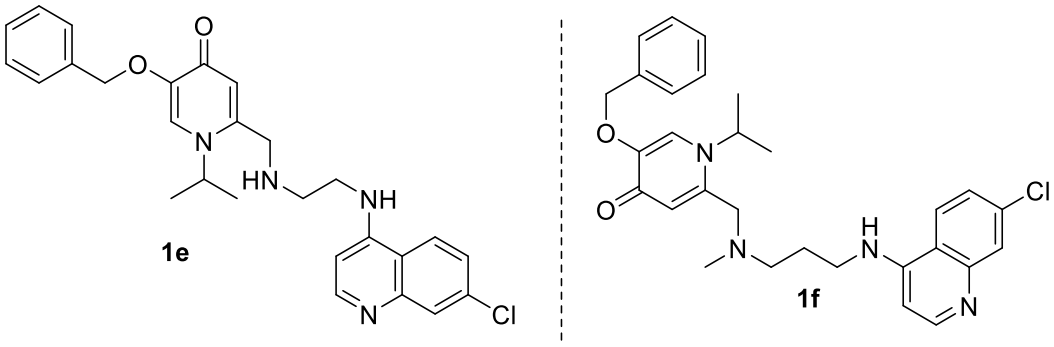

In future, **1e** and **1f** the best inhibitor in both protease inhibition assays and reverse transcriptase assay will be deprotected and modified accordingly to improve their anti-HIV and anti-oxidant potentials. It will be interesting to evaluate the antioxidants of the deprotected analogs, it will be beneficial in chemotherapy to have compounds that can minimizing heme-induced oxidative stress as well as acting as antimalarials and anti-HIV.

1b was the only compound that showed some anti-oxidant activities, but only in high concentrations.

Chapter 5: Malaria *In Vitro* Activity Evaluation

5.1 Background

The causative agent of malaria is a parasite of the genus *Plasmodium*, the most virulent strain being *Plasmodium falciparum*. Conventional chemotherapeutics involve the use of quinoline-based drugs as exemplified by chloroquine, but increased drug resistance has reduced the efficacy of these drugs [310][51]. In the quest to develop new antimalarial drugs, the antimalarial drug efficacy of potential candidates can be ascertained through four distinct methods: molecular marker studies, drug concentration measurements, *in vivo* therapeutic efficacy studies, and *in vitro* tests[311].

1. Molecular marker studies: a technique used in laboratories to search for specific genes, proteins, or other molecules that could indicate the presence of the disease or associated with drug resistance in malaria parasites. This is done using a sample of tissue, blood, or other bodily fluids[312][313].

2. Drug concentration measurements: The concentration of antimalarial medications and/or active metabolites in whole blood, plasma, or serum is measured by pharmacokinetic studies, which are used to differentiate between treatment failure brought on by antimalarial medication resistance and suboptimal drug exposure. It aids in defining actual drug resistance to various antimalarial medications. However, it needs a lot of blood samples from the patients who are receiving treatment[314][315].

3. *In vivo* therapeutic efficacy: These are preclinical studies conducted in living organism whereby compounds and their formulations are evaluated, either as a monotherapy or combination therapy. Most National Malaria Control Programs use the in vivo therapeutic efficacy study's findings as primary data to develop antimalarial drug policy, and it continues to be the gold standard for assessing the efficacy of antimalarial medications[311][316].

4. *In vitro* tests: In this type of assays, parasites are directly exposed to known concentrations of drugs and examined for inhibition of growth and maturation into schizonts. *In vitro* assays can also be used to monitor the susceptibility of the parasite by measuring the intrinsic sensitivity to different antimalarial drugs[317][318].

The ability of a substance to inhibit the growth of the *Plasmodium* parasite, which causes malaria, is known as antiplasmodial activity. The *in vitro* antiplasmodial activity of a substance is evaluated against two *Plasmodium falciparum* strains namely the chloroquine drug sensitive and the chloroquine resistant strains. The sensitive strain is susceptible to the compound that is being tested for, when they inhibited *in vitro* by a concentration of the compounds that is associated with a high possibility of therapeutic success and the resistant strains is resistant to a compounds when it is inhibited in vitro by a concentration of this drug that is associated with a great possibility of therapeutic failure.

For this study, the compounds of interest **(Fig. 5.1)** were evaluated *in vitro* against the chloroquine sensitive (CQS) clone (NF54) and the chloroquine resistant (CQR) clone(K1). The level of inhibition of growth is expressed as the mean (50%) inhibitory concentration (IC_{50}) [259]: It is worth noting that only these six compounds were selected for antiplasmodial activities because they have never been evaluated before by Andayi (2011)[193].

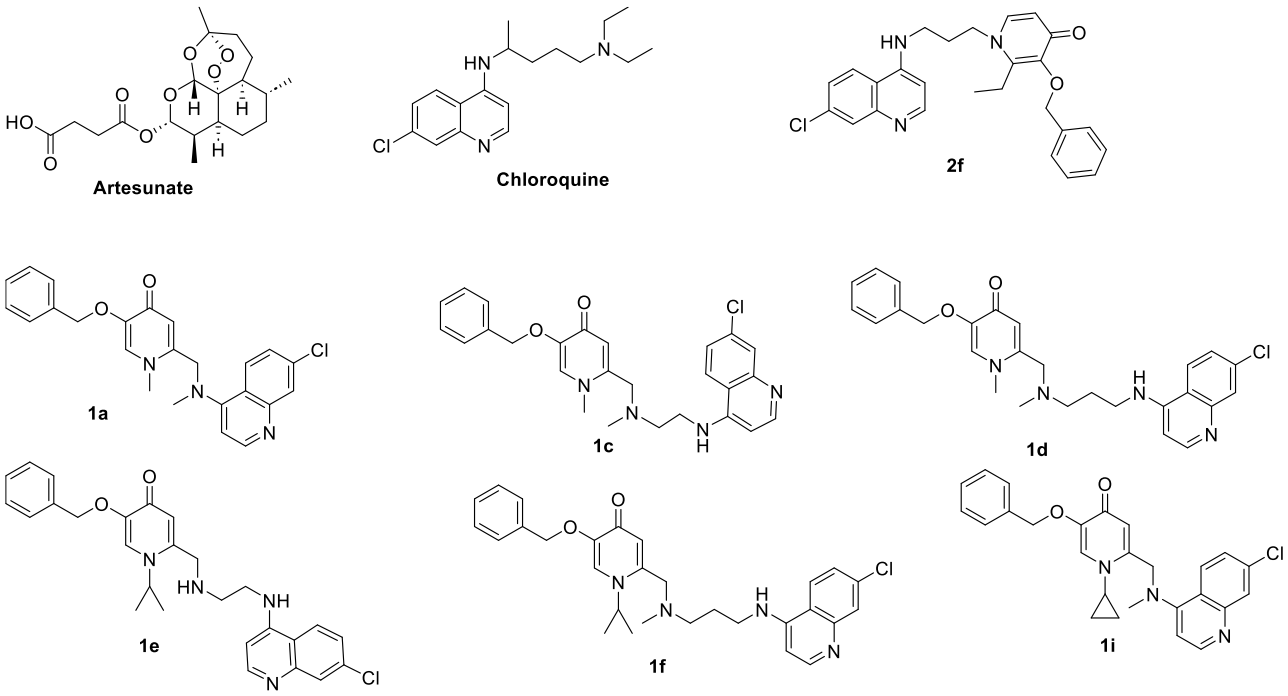

Figure 5.1: Structures of selected test compounds.

5.2 Methodology

All the *in vitro* antiplasmodial assays were performed at the H3D research center, University of Cape Town) following the protocol outlined in below (the detailed protocol can be found in Chapter 7).

A full dose response assay starting concentration of 3 µmol/L and serially diluted 2-fold in growth medium (to generate the tested concentration range) was performed for all compounds in a 96-well plate to determine the concentration inhibiting 50% of parasite growth (IC_{50} values). Two antimalarial drugs (Chloroquine and Artesunate) were used as standards/ references in all the experiments. The assay plate was incubated at 37°C for 72 hours in a sealed gas chamber under 3% O_2 and 4% CO_2, with the balance being nitrogen (N_2).

The remaining population of parasites at each concentration of the test compound was determined by comparing the absorbance of each well to the absorbance of a well containing the drug-free control. Survival was plotted against concentration, and the IC_{50} values were obtained using a non-linear dose-response curve fitting analysis via the Dotmatics software platform. The results have been summarized in **Table 5.1.**

5.3 Results and Discussion

Table 5.1:Summarized Experimental Data

HPO-Aminoquinoline hybrid	NF54	K1
	Mean IC_{50} ± SEM (nM)	**Mean IC_{50} ± SEM (nM)**
1a	625.5 ±374.5	2183.3 ± 816.7
1c	15.35 ±4.8	1273.05 ± 177.6
1d	169 ±2.2	263.1 ± 7.1
1e	33.35 ±1.5	264.15 ± 71.1
1f	15.85 ± 0.25	545.8 ±1.8
1i	2488 ±232	>3000
2f	164.1 ± 29.5	1383.2 ± 25.4
Chloroquine	7.00 ±2	232 ± 16
Artesunate	4.1 ± 0.5	4.8 ± 1

From the summarized data in **Table 5.1**, activities against the wild-type isolate *P. falciparum* Nf54 ranges from moderate to very high, with **1c** and **1f** having IC_{50} values below 20nM, which is comparable to Chloroquine, one of the control antimalarial agents. Chloroquine and artesunate are extremely active in the sensitive isolate and showed IC_{50} values of 7 nM and 4 nM respectively.

From the results in **Table 5.1** the most active compounds against CQR strain are **1d, 1e** and **1f** whereas the compounds that are most active against CQS strain are **1c, 1e** and **1f.** These compounds have shorter linkers i.e. less than three carbon atoms and the common structural features are the presence of a tertiary–N group in the linker or an iso-propyl group on the pyridinone heterocyclic N or the presence of both. Compound **1e** is the common factor in performing well against both CQR and CQS strains relative to the others.

Considering the most potent in CQS it can be noticed that structurally, **1c** (IC_{50} = 15.35nM) and **1f** (IC_{50} = 15.85nM) are similar (both have the N-isopropyl on the pyridinone heterocyclic n and a tertiary N-group in the linker) the only difference is the size of carbon chain. **1c** has two carbons whereas **1f** has three carbons. Comparing the two compounds, **1f** is more lipophilic than **1c.** It has been reported elsewhere[217] that antiplasmodial activity against the 3D7, the sensitive strain was observed to increase with increase in lipophilicity but surprisingly, **1f** is slightly more active than **1c**. However, this difference is not significant. **1e** is the third potent candidate with an IC_{50} value of 33.35nM. Its structure is similar to that of **1c** and **1f** but with no methyl group attached onto the second protonable nitrogen. That is the **1e** and **1f** have a tert-N in the linker whereas **1e** has a secondary-N group. This conversion of tertiary nitrogen to a sec-N translates to a 2-fold decline in antiplasmodial activity. This proves the importance of tertiary protonable N groups in enhancing the aminoquinoline antimalarial potency via increased food vacuolar accumulation in the *Plasmodium*.

2f with a two-carbon chain linker was the fourth most potent against CQS strain followed by **1d** was the fourth most potent against CQS strain. Structurally **1f** is similar to **1c** and **1e** except the difference of the methyl group in place of the isopropyl group. Clearly, the introduction of steric bulk at the N-alkyl group seems to enhance antiplasmodial activity against the sensitive strain. **1a** and **1i** are relatively hydrophobic however they were not really active as expected. It's interesting to note that for compound **1d**, the difference between its potency in CQR and CQS strains is significantly small (this is also seen in artesunate) and this informs its potential for further development as a molecule likely to combat both resistant and sensitive strains a kin to artesunate.

Activities against the resistant *P. falciparum* K1 strain ranged from poor to very high. Only **1d** (IC_{50} = 263.1nM) had a significantly higher antiplasmodial activity in the K1 strain comparable to chloroquine. However, the activity of compound **1e** is comparable to that of CQ with a very insignificant difference between the IC_{50} values. The rest of the compounds poorly inhibited the resistant strains. Thus, they would not be good candidates for further drug development.

5.4 Resistance Index (RI)

Resistance index (R_i) is the ratio of the IC_{50} of the resistant line to that of the parent strain. It estimates the level of resistance to be experienced the compounds of interest[319].

$$R_i = \frac{Resistant\ strain\ (K_1)\ IC_{50} value}{Sensitive\ strain\ (NF54)\ IC_{50} value}$$

The higher the Ri value, the higher the level of resistance[320];

R_i values >5, there is cross resistance.

R_i values <5 there is cross no resistance, anything <5 in this set is highlighted (**Table 5.2**).

Table 5.2: Resistance index Ratios

Compound	Resistance Index
1a	3.5
1c	8.3
1d	15.6
1e	7.9
1f	34.4
1i	ND
2f	8.4
Chloroquine	33.1
Artesunate	1.2

Resistance index equates to resistance margin which defines how much more active the compound is in the sensitive strain. On this run, chloroquine values are 7nM and 232nM, and that's about a 33x difference. And for Artesunate, the IC_{50} values are very similar in both strains (4.1 and 4.8nM) so the value is low at 1.2. All the test compounds had a better RI than CQ but higher than Artesunate.

As shown in **Table 5.2** all the compounds had values greater than 5 except for **1a** (3.5). Otherwise with the rest of the compounds there is a likelihood of cross resistance. Again, this is not a surprise because these compounds are chloroquine analogues.

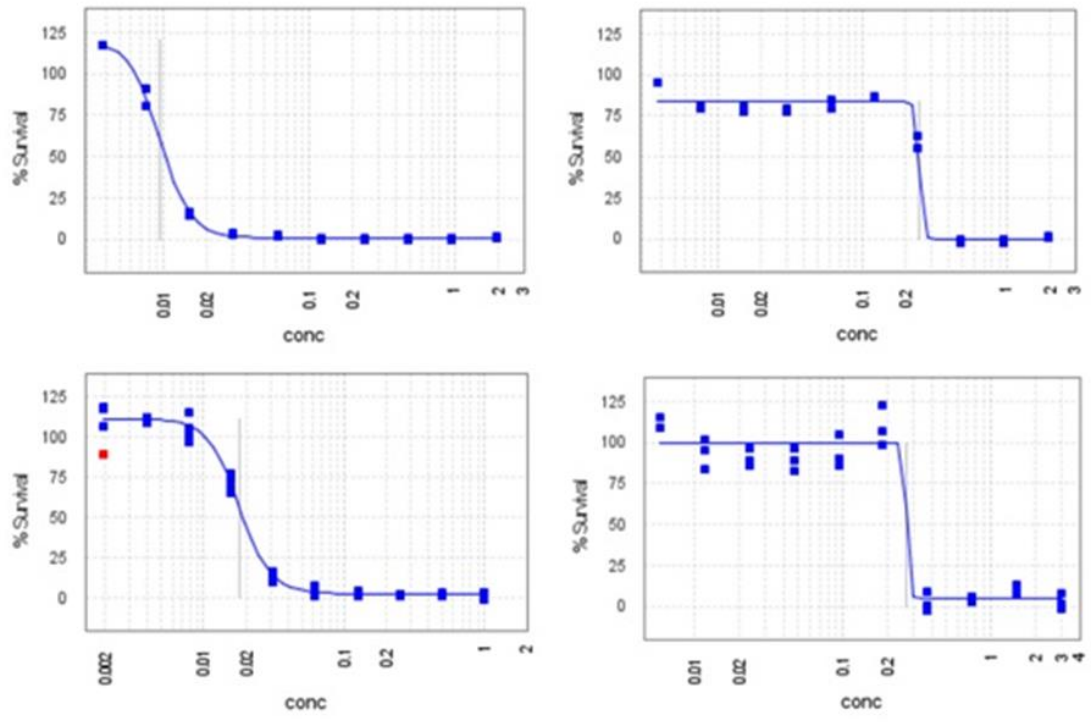

Figure 5.3: Dose-response curve of the control chloroquine diphosphate/H3D (top) and sample **1d**

(bottom) against *P. falciparum* NF54 (left) and K1 (right), showing %survival of the parasites at 10 different concentrations (in M) of each compound. Full dose response curve **(Fig 5.3)** was done for **1d** the analogue that showed the greatest potency against the resistant K1 strain. Similarly, the antiplasmodial potential of both compounds lowered as the concentrations were decreased.

5.5 Conclusion

The compounds were assayed for growth inhibition in a cell-based assay against two strains of *P. falciparum* to give a survey of the antiplasmodial activities (**Table 5.1**). Activity against the wild-type isolate *P. falciparum* NF54 ranges from moderate to very high, with some IC_{50} values below 20nM, which is comparable to both control antimalarial agents. Resistance indices analysis showed that most of the compounds had values greater than 5 except for **1a** (3.5). Otherwise with the rest of the compounds there is cross-resistance which can be expected of these compounds since they are chloroquine analogues.

Chapter 6: Conclusions and Future Work

The main aim of this study was design and synthesis of HPO-AQs and evaluate them *in vitro* for antiplasmodial and anti-HIV activities. In addition to these, cytotoxicity assays, antioxidant assays and anti-cancer assays were also done. All the compounds were characterized using ^{1}H and ^{13}C NMR spectroscopy, IR spectroscopy and melting points determination.

The anti-HIV activities of the tested compounds, overall, kojic derived compounds are better inhibitors than maltol derived compounds. **1e** and **1f** showed to be the best inhibitors in both protease inhibition assays and reverse transcriptase assay. In future, **1e** and **1f** the best inhibitor in both protease inhibition assays and reverse transcriptase assay will be deprotected and modified accordingly to improve their anti-HIV potential such that they can be dual-stage-anti-HIV agents.

When evaluated *in vitro* for their potential antiplasmodial activities, the tested HPO-AQs displayed activities ranging from moderate to very high, with some IC_{50} values below 20nM, which is comparable to chloroquine and artesunate which were both used as control antimalarial agents. The most active compounds against CQR strain were **1d, 1e** and **1f** whereas the compounds that were the most active against CQS strain are **1c, 1e** and **1f.** These exceptionally compounds have shorter linkers i.e. less than three carbon atoms and the common structural features are the presence of a tertiary–N group in the linker or an iso-propyl group on the pyridinone heterocyclic N or the presence of both. Compound **1e** is the common factor in performing well against both CQR and CQS strains relative to the others.

All the compounds had better resistance indices than CQ indicating potential to act against resistant malaria. The tertiary amine was identified to be more effective in enhancing the activity of the conjugates against the resistant strain.

The tested compounds were moderately toxic to non-toxic. In the HeLa cells, **1e** was the most toxic, in HEPG2 cells, **1f** was the most toxic and in TZM-bl cells, **1a** was the most toxic. A general observation on the toxicities of all the compounds when evaluated on three different cell lines is that maltol derived compounds (**2b** and **2d**) were more toxic compared to the kojic derived compounds (**1a, 1b, 1f** and **1g**). With this observation, the kojic moiety counteract the toxic effects caused by the quinoline scaffold better than the maltol moiety. The most toxic compounds were evaluated for their nitric oxide production, the negative results revealed that protected compounds are not good anticancer agents.

Interestingly, **1e** is one of the best performing candidates in both the antiplasmodial and anti-HIV assays but more especially on the anti-HIV assays. Future synthetic work should consider conjugates that are structurally related to compound **1e** containing both chelator and tertiary

amino groups. These types of compounds are signaling properties of potential agents of malaria and HIV/AIDS co-infection chemotherapy. In silico predictions showed that **1e** have drug-like properties with no violations. Both *in silico* and *in vitro* data showed some correlations, thus justifying the use of in silico prediction model in drug discovery of anti-infective agents.

Chapter 7: Experimental Procedures

7.1 Chemistry

Experimental techniques and Equipment Used

All reagents and starting materials utilized in this project were procured from Sigma Aldrich and were of synthesis-grade quality. These materials were used directly without further purification. To ensure optimal reaction conditions, all glassware required for setting up the reactions was thoroughly dried in an oven maintained at a temperature between 80°C and 100°C. Sample drying was performed under reduced pressure (approximately 20-30 mmHg) using a rotary evaporator. The drying temperature was carefully adjusted based on the specific solvent being removed, ensuring efficient and effective solvent evaporation without compromising the integrity of the samples.

Chromatographic separations

Thin-layer chromatography (TLC) was employed to monitor all the reactions throughout this project. The analyses were conducted using silica gel plates (Macherey-Nagel ALUGRAM Sil G/UV254 plates pre-coated with 0.25 mm silica gel 60 Å or Sigma Aldrich TLC plates). The spots were visualized by exposing the plates to ultraviolet light at 254 nm.

All synthesized compounds were purified using flash silica gel column chromatography. The silica gel was packed into columns of appropriate size for the scale of the reaction. To prepare the crude products for chromatographic separation, they were first adsorbed onto the silica gel surface. This was achieved by mixing the crude product with a small volume of ethyl acetate/methanol, followed by the addition of silica gel. Excess solvents were then removed under reduced pressure. The silica gel with the adsorbed crude product was subsequently added to the column for purification.

Spectroscopic and Physical Data

Nuclear Magnetic Resonance (NMR) spectroscopy (^{1}H NMR and ^{13}C NMR) spectra were recorded using Bruker spectrometers, specifically a 400 MHz instrument for ^{1}H NMR and a 100 MHz instrument for ^{13}C NMR. Samples were dissolved in appropriate deuterated solvents, predominantly DMSO-d_6, CD_3OD and $CDCl_3$. Chemical shifts are reported in parts per million (ppm) and are referenced relative to (upfield from) tetramethylsilane (TMS) as an internal standard or against the residual protonated solvent signal. Coupling constants (*J* values) are expressed in hertz (Hz). The following NMR abbreviations were used: *s* (singlet), *d* (doublet), *dd* (doublet of doublets), *t* (triplet), *q* (quartet), *p* (quintet), *m* (multiplet), and *br* (broad signal). Infrared spectra were obtained using a Bruker Optics Alpha FTIR spectrophotometer. Absorption maxima were reported in wavenumbers (cm^{-1}), providing insights into the

functional groups present in the synthesized compounds. The melting points of the synthesized compounds were measured using an Electrothermal 9200 Büchi LABOTEC melting point apparatus (model B-5400), utilizing capillary tubes. The melting points were reported as uncorrected values. The compounds synthesized in this project were named according to IUPAC systematic nomenclature. The structure drawings and systematic names were generated using ChemDraw Ultra 2010 (Cambridge, version 12.0.2).

Experimental Methods

All the compounds were synthesized following published procedures and in some situations with necessary modifications.

7.1.1 General Synthesis Procedure of *N*-(7- chloroquinoline 4yl) alkyl-diamines

A mixture of 4,7-dichloroquinoline (1.0 equiv.) and the corresponding diaminoalkane (5.0 equiv.) was heated under reflux for 8 hours in a nitrogen atmosphere, with continuous stirring to ensure the reaction proceeded to completion. The progress of the reaction was monitored using thin-layer chromatography (TLC). Upon completion, the reaction mixture was allowed to cool to room temperature and was subsequently poured into ice-cold water. The product precipitated out of the solution. The precipitate was then filtered, washed with water, and air-dried to obtain compounds **6a-6g**. These compounds were used in subsequent steps without further purification[245][246][321].

7.1.1.1 Synthesis of 7-chloro-*N*-methylquinolin-4-amine (6a)

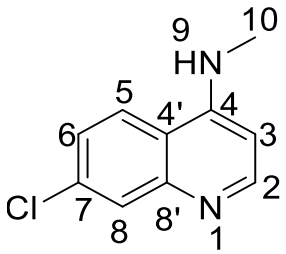

4.7-dichloroquinoline (5.00g, 25.25mmol) and methylamine (3.92g, 5.972mL, 126.23mmol) were refluxed for 8hrs under inert conditions at 165ºC while stirring to afford a creamish white solid. (4.67g, 95%).**^{1}H NMR (400 MHz, DMSO-d$_6$) δ** 8.86 (d, *J* = 4.7 Hz, 1H, H-2), 8.17 (d, *J* = 9.0 Hz, 1H, H-5), 8.13 (d, *J* = 2.1 Hz, 1H, H-8), 7.79 – 7.76 (m, 2H, NH-9, H-6), 7.75 (d, *J* = 2.1 Hz, 1H, H-3), 3.37 (s, 3H, H-10). **^{13}C NMR (101 MHz, DMSO-d$_6$) δ** 152.30 (C-2), 151.36 C-4), 149.21 C-8'), 135.81 (C-7), 127.92 (C-8), 124.67 (C-5), 124.52 (C-6), 117.84 (C-4'), 98.80 (C-3), 29.69 (C-10).

7.1.1.2 Synthesis of *N*1-(7-chloroquinolin-4-yl) ethane-1,2-diamine (6b)

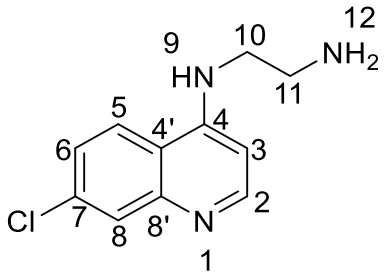

4.7-dichloroquinoline (10.00g, 50.49mmol) and 1,2-ethanediamine (15.17g, 33.71mL, 252.46mmol) were refluxed for 8hrs under inert conditions at 90º C while stirring to afford yellow solid. (4.67g, 95%). **^{1}H NMR (400 MHz, DMSO-d$_6$) δ** 8.38 (d, *J* = 4 Hz, 1H, H-2), 8.28 (d, *J* = 8.0 Hz, 1H, H-5), 7.79 (d, *J* = 2.2 Hz, 1H, H-8), 7.44 (dd, *J* = 12.0, 2.2 Hz, 1H, H-6), 7.29 (s, 1H, NH-9), 6.49 (d, *J* = 8.0 Hz, 1H, H-3), 3.26 (q, *J* = 16.0, 6.2 Hz, 2H, H-11), 2.81 (t, *J* = 12.0 Hz, 2H, H-10). **^{13}C NMR (101 MHz, DMSO-d6) δ** 152.34 (C-2), 150.79 (C-4), 149.43 (C-8'), 133.88 (C-7), 127.81 (C-8), 124.56 (C-5), 124.48 (C-6), 117.88 (C-4'), 99.16 (C-3), 46.41 (C-10), 40.46 (C-11).

7.1.1.3 Synthesis of *N*1-(7-chloroquinolin-4-yl)-N-2-methylethane-1,2-diamine (6c)

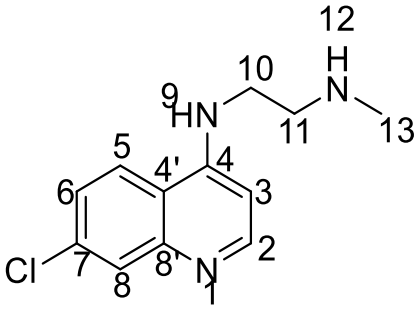

4.7-dichloroquinoline (4.00g, 20.19mmol) and N^1-methylethane-1,2-diamine (15.17g, 9.15mL, 20.19mmol) were refluxed for 8hrs under inert conditions at 90ºC while stirring to afford yellow solid. (4.67g, 95%). **^{1}H NMR (400 MHz, DMSO-d$_6$) δ** 8.40 (d, *J* = 5.4 Hz, 1H, H-2), 8.27 (d, *J* = 9.0 Hz, 1H, H-5), 7.79 (d, *J* = 2.1 Hz, 1H, H-8), 7.44 (dd, *J* = 9.0, 2.2 Hz, 1H, H-6), 7.29 (br s, 1H, NH-9), 6.51 (d, *J* = 5.5 Hz, 1H, H-3), 3.37 (t, *J* = 6.3 Hz, 2H, H-10), 2.82 (t, *J* = 6.4 Hz, 2H, H-11), 2.35 (s, 3H, H-13). **^{13}C NMR (101 MHz, DMSO-d$_6$) δ** 152.36 (C-2), 150.64 (C-4), 149.45 (C-8'), 133.89 (C-7), 127.85 (C-8), 124.59 (C-5), 124.52 (C-6), 117.92 (C-4'), 99.18 (C-3), 49.52 (C-10), 42.20 (C-11), 35.96 (C-13).

7.1.1.4 Synthesis of *N*1-(7-chloroquinolin-4-yl)propane-1,3-diamine (6d)

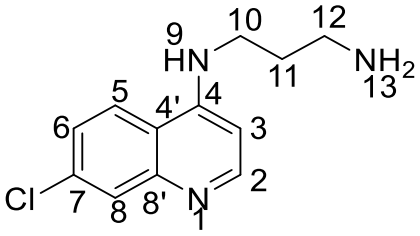

4.7-dichloroquinoline (5.00g, 25.25mmol) and 1,3-propanediamine (9.86g, 11.10mL, 126.23 mmol) were heated at 110º C under reflux for 8hrs while stirring to a creamish white solid. (2.41g, 78%). **^{1}H NMR (400 MHz, DMSO-d$_6$) δ** 8.40 (d, *J* = 5.3 Hz, 1H, H-2), 8.24 (d, *J* = 9.0 Hz, 1H, H-5), 7.79 (s, 1H, H-8), 7.56 (s, 1H, NH-9), 7.44 (d, *J* = 8.2 Hz, 1H, H-6), 6.47 (d, *J* = 5.4 Hz, 1H, H-3), 3.33 (t, *J* = 6.7 Hz, 2H, H-12), 2.70 (t, *J* = 6.4 Hz, 2H, H-10), 2.57 (t, *J* = 6.6 Hz, 1H, H-13), 1.74 (p, *J* = 6.6 Hz, 2H, H-11). **^{13}C NMR (101 MHz, DMSO-d$_6$) δ** 152.38 (C-2), 150.63 (C-4), 149.52 (C-8'), 133.80 (C-7), 127.92 (C-8), 124.48 (C-5), 124.45 (C-6), 117.93 (C-4'), 99.02 (C-3), 41.12 (C-12), 40.02 (C-10), 31.71 (C-11).

7.1.1.5 Synthesis of *N*1-(7-chloroquinolin-4-yl)-N-3-methylpropane-1,3-diamine (6e)

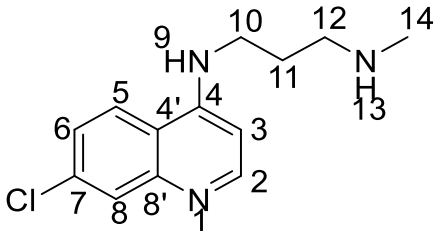

4.7-dichloroquinoline (10g, 50.49mmol) and N-methyl-1,3-propanediamine (22.25g, 26.49mL, 252.46 mmol) were heated at 110º C under reflux for 8hrs while stirring to afford yellow solid. (11.04g, 87%). **^{1}H NMR (400 MHz, DMSO-d$_6$) δ** 8.40 (d, *J* = 5.4 Hz, 1H, H-2), 8.22 (d, *J* = 9.0 Hz, 1H, H-5), 7.79 (d, *J* = 2.0 Hz, 1H, H-8), 7.57 (s, 1H, NH-9), 7.45 (dd, *J* = 9.0, 2.1 Hz, 1H, H-6), 6.46 (d, *J* = 5.4 Hz, 1H, H-3), 3.32 (d, *J* = 4.1 Hz, 2H, H-12), 2.59 (t, *J* = 6.5 Hz, 2H, H-10), 2.30 (s, 3H, H-14), 1.80 (m, 2H, H-11).**^{13}C NMR (101 MHz, DMSO-d$_6$) δ** 152.39 (C-2), 150.63 (C-4), 149.53 (C-8'), 133.79 (C-7), 127.95 (C-8), 124.47 (C-5), 124.42 (C-6), 117.93 (C-4'), 99.00 (C-3), 49.95 (C-12), 41.56 (C-10), 36.63 (C-13), 28.11 (C-11).

7.1.1.6 Synthesis of *N*1-(7-chloroquinolin-4-yl)butane-1,4-diamine (6f)

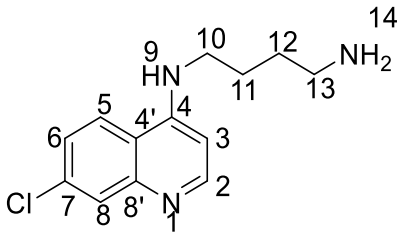

4.7-dichloroquinoline (4g, 20.20mmol) and 1,4-butanediamine (8.89g, 10.14mL, 100.98 mmol) were heated at 120º C under reflux for 8hrs while stirring to afford yellow solid. (6.04g, 72%).

^{1}H NMR (400 MHz, DMSO-d_6) δ 8.38 (d, *J* = 5.4 Hz, 1H, H-2), 8.29 (d, *J* = 9.0 Hz, 1H, H-5), 7.78 (d, *J* = 2.0 Hz, 1H, H-8), 7.71 (s, 1H, NH-9), 7.43 (dd, *J* = 9.0, 2.0 Hz, 1H, H-6), 6.45 (d, *J* = 5.4 Hz, 1H, H-3), 3.25 (t, *J* = 7.0 Hz, 2H, H-13), 2.60 (s, 2H, NH-14), 1.75 – 1.58 (m, 2H, H-10), 1.48 (m, 7.0 Hz, 2H, H-11), 0.90 – 0.71 (m, 2H, H-12). **^{13}C NMR (101 MHz, DMSO-d_6) δ** 152.35 (C-2), 150.64 (C-4), 149.49 (C-8'), 133.83 (C-7), 127.82 (C-8), 124.62 (C-5), 124.43 (C-6), 117.93 (C-4'), 99.06 (C-3), 42.79 (C-13), 41.53 (C-10), 30.69 (C-12), 25.73 (C-11).

7.1.1.7 Synthesis of *N*1-(7-chloroquinolin-4-yl) hexane-1,6-diamine (6g)

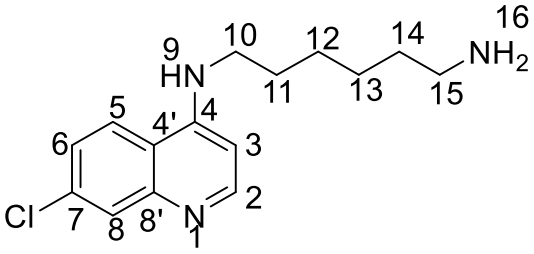

4.7 dichloroquinoline (7.61g, 38.4mmol) and 1,6 hexane-diamine (44.66g, 53.17mL, 384.32 mmol) were heated at 165º C under reflux for 8hrs while stirring to afford yellow solid. (6.04g, 57%). **^{1}H NMR (400 MHz, DMSO-d_6) δ** 8.33 (d, *J* = 5.4 Hz, 1H, H-2), 8.22 (d, *J* = 9.0 Hz, 1H, H-5), 7.73 (s, 1H, H-8), 7.31 (d, *J* = 9.0 Hz, 1H, H-6), 7.21 (br s, 1H, NH-9), 6.35 (d, *J* = 5.5 Hz, 1H, H-3), 3.27 – 3.18 (m, 2H, H-10), 3.02 (q, *J* = 12.2, 6.6 Hz, 2H, H-15), 2.54 (m, 6.9 Hz, 2H, H-14), 1.65 (m, 6.7 Hz, 2H, H-11), 1.37 (m, 6.5 Hz, 2H, H-12), 1.29 – 1.17 (m, 2H, H-13). **^{13}C NMR (101 MHz, DMSO-d_6)** δ 152.01 (C-2), 150.68 (C-4), 149.34 (C-8'), 133.99 (C- 7), 127.70 (C-8), 124.29 (C-6, C-5), 117.85 (C-4'), 98.72 (C-3), 41.84 (C-15), 33.42 (C-10), 29.52 (C-14), 28.24 (C-11), 27.06 (C-13), 26.58 (C-12).

7.1.2 Preparation of Hydroxypyridinones Intermediates

The hydroxypyridinones intermediates utilized in this projected were derived from maltol and kojic acid. The first step was to protect the pyranones (synthesis of **5**, **10a** and **10b**). Compounds **10a** and **10b** were then conjugated with different 4-aminoquinolines. The

benzylated kojic acid, **6**, was further functionalized – alkylated (**4a, 4b** and **4c**) and chlorinated (**3a, 3b** and **3c**) before conjugation with different 4-aminoquinolines.

7.1.2.1 Protection of Pyranones

A mixture of pyranone (1.0 equiv) in 50 mL of methanol (MeOH) and sodium hydroxide (NaOH) (1.5 equiv) dissolved in 5 mL of water (H2O) was heated to reflux. Once at reflux temperature, benzyl chloride (BnCl) (1.25 equiv) was added dropwise over 30 minutes. The reaction mixture was maintained at reflux (92°C) for 24 hours to ensure completion. Upon completion of the reaction, the excess solvent was removed by rotary evaporation. The resulting residue was mixed with 50 mL of distilled water and then extracted with ethyl acetate (3 x 50 mL). The organic extracts were washed twice, first with 5% NaOH solution and then with water. The combined organic layers were dried over anhydrous magnesium sulfate ($MgSO_4$), filtered, and the solvent was removed by rotary evaporation. The crude product was subjected to recrystallization from methanol, yielding the compounds **5, 10a,** and **10b**[252][193].

7.1.2.1.1 Synthesis of 3-(benzyloxy)-2-methyl-4H-pyran-4-one (10a)

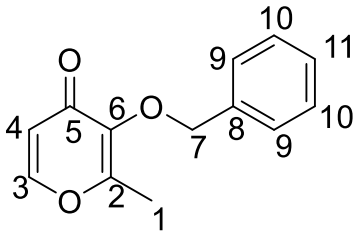

To a solution of methyl maltol (5g, 39.65mmol), NaOH (2.38g, 59.47mmol) and 50mL MeOH was added BnCl (5.72mL, 49.56mmol) dropwise over 30 minutes. The resulting mixture was stirred and refluxed at 92°C for 24 hours to afford a brown oil which was crystallized with methanol to yield white needle-like crystals (5.18g, 60.5%).**^{1}H NMR (400 MHz, DMSO-d_6) δ** 7.96 (d, *J* = 5.7 Hz, 1H, H-3), 7.43 (d, *J* = 7.4 Hz, 2H, H-9), 7.39 – 7.28 (m, 4H, H-10 and H-11), 6.39 (d, *J* = 5.7 Hz, 1H, H-4), 5.08 (s, 2H, H-7), 2.09 (s, 3H, H-1). **^{13}C NMR (101 MHz, DMSO-d_6) δ** 174.45 (C-5), 159.43 (C-2), 155.08 (C-3), 143.80 (C-6), 138.84 (C-8), 128.60 (C-11), 127.88 (C-9), 127.77 (C-10), 117.02 (C-4), 74.21 (C-7), 57.84 (C-12) 14.67 (C-1).

7.1.2.1.2 Synthesis of 3-(benzyloxy)-2-ethyl-4H-pyran-4-one (10b)

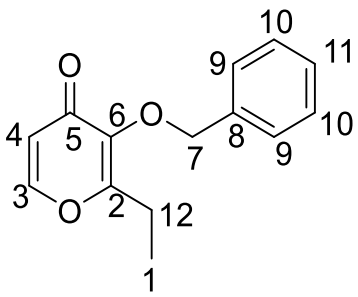

To a solution of ethyl maltol (10g, 71.35mmol), NaOH (4.28g, 107.04mmol) and 100mL MeOH was added BnCl (10.26mL, 89.20mmol) dropwise over 30 minutes. The resulting mixture was stirred and refluxed at 92°C for 24 hours to afford a brown oil which was crystallized with methanol to yield white needle-like crystals (9.8, 59.6%).**^{1}H NMR (400 MHz, DMSO-d$_6$) δ** 7.99 (d, *J* = 5.6 Hz, 1H, H-3), 7.44 (d, *J* = 8.0 Hz, 2H, H-9), 7.40 – 7.30 (m, 4H, H-10 and H-11), 6.40 (d, *J* = 5.6 Hz, 1H, H-4), 5.08 (s, 2H, H-7), 4.41 (s, 2H, H-12), 2.10 (s, 3H, H-1).**^{13}C NMR (101 MHz, DMSO-d$_6$) δ** 174.50 (C-5), 159.61 (C-2), 155.23 (C-3), 143.72 (C-6), 137.44 (C-8), 128.72 (C-9), 128.62 (C-10), 128.55 (C-11), 116.95 (C-4), 73.17 (C-7), 63.51 (C-12), 14.76 (C-1).

7.1.2.1.3 Synthesis of 5-(benzyloxy)-2-(hydroxymethyl)-4H-pyran-4-one (5)

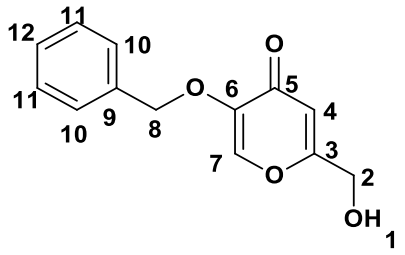

To a solution of kojic acid (4.91g, 34.55mmol), NaOH (2.07g, 51.83mmol) and 50mL MeOH was added BnCl (4.96mL, 43.18mmol) dropwise over 30 minutes. The resulting mixture was stirred and refluxed at 92°C for 24 hours to afford a brown oil. White needle-like crystals formed on cooling to room temperature and were washed in water and cold MeOH then dried under vacuum (5.27g, 66%). **^{1}H NMR (400 MHz, DMSO-d$_6$) δ** 8.18 (s, 1H, H-7), 7.46 – 7.33 (m, 5H, H-10, H-11 and H-12), 6.35 (s, 1H, H-4), 5.72 (t, *J* = 6.1 Hz, 1H, H-1), 4.95 (s, 2H, H-8), 4.31 (d, *J* = 6.0 Hz, 2H, H-2).**^{13}C NMR (101 MHz, DMSO-d$_6$) δ** 173.71 (C-5), 168.53 (C-3), 147.09 (C-6), 141.67 (C-7), 136.63 (C-9), 128.90 (C-10), 128.65 (C-11), 128.59 (C-12), 111.64 (C-4), 71.05 (C-8), 59.80 (C-2).

7.1.2.2 General Alkylation Procedure of Protected-Kojic Acid (4)

Mixtures of 2.0 equiv alkylamines and benzylated kojic acid in ethanol were refluxed in a sealed round bottomed flasks with continuous stirring to drive the reaction to completion. After the reaction was completed, the pH was adjusted to 1 (2M HCL) put in freezer for 6 hours and then washed with diethyl ether. 50mL water was added and the pH was adjusted to 9 (2M NaOH) followed by washing with water, drying over magnesium sulphate ($MgSO_4$) and excess solvent was removed by rotary evaporation[193].

7.1.2.2.1 Synthesis of 5-(benzyloxy)-2-(hydroxymethyl)-1-methylpyridin-4(1H)-one (4a)

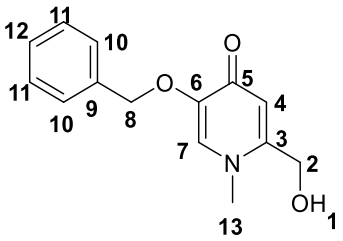

0.61mL of 40 wt. % in water methylamine (0.40g, 12.92mmol was added to a solution of **5** (1.50g, 6.46mmol) in 50mL ethanol, refluxed 70°C in a sealed tube for 12 hours to afford a brown liquid (1.2g, 76%). **^{1}H NMR (400 MHz, DMSO-d$_6$) δ** 8.69 (s, 1H, H-7), 7.44 (m, 6H, H-10, H-11, H-12, H-4), 5.20 (s, 2H, H-8), 4.68 (s, 2H, H-2), 3.99 (s, 3H, H-13). **^{13}C NMR (101 MHz, DMSO-d$_6$) δ** 162.22 (C-5), 153.29 (C-3), 144.63 (C-6), 135.88 (C-7), 132.22 (C-9), 129.04 (C-10), 128.96 (C-11), 128.72 (C-12), 111.19 (C-4), 71.94 (C-8) , 58.86 (C-2), 42.53 (C-13).

7.1.2.2.2 Synthesis of 5-(benzyloxy)-2-(hydroxymethyl)-1-isopropylpyridin-4(1H)-one (4b)

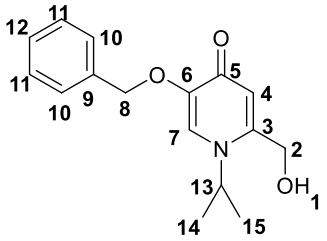

1.33mL of isopropylamine (0.92g, 15.50mmol) was added to a solution of **6** (1.8g, 7.75 mmol) in 40mL of 50% aqueous ethanol, refluxed 70°C in a sealed tube for 12 hours to afford a brown solid (2.4g, 57%). **^{1}H NMR (400 MHz, DMSO-d$_6$) δ** 8.14 (s, 1H, H-7), 7.45 – 7.26 (m, 5H, H-10, H-11, H-12), 6.30 (s, 1H, H-4), 4.90 (s, 2H, H-8), 4.26 (s, 2H, H-2), 2.05 (s, 6H, H-14, H-15), 1.14 (d, *J* = 6.5 Hz, 1H, H-13). **^{13}C NMR (101 MHz, DMSO-d$_6$) δ** 173.42 (C-5), 168.23 (C-3), 146.72 (C-6), 141.32 (C-7), 136.24 (C-9), 128.58 (C-10), 128.33 (C-11), 128.26 (C-12), 111.24 (C-4), 70.66 (C-8), 59.42 (C-2), 43.12 (C-13), 30.81 (C-14), 20.48 (C-15).

7.1.2.2.3 Synthesis of 5-(benzyloxy)-1-cyclopropyl-2-(hydroxymethyl)pyridin-4(1H)-one (4c)

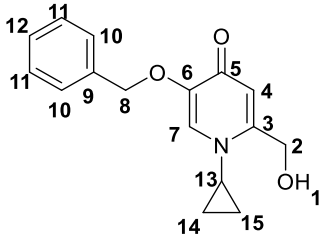

0.89mL of isopropylamine (0.74g, 89.5mmol) was added to a solution of **5** (1.5g, 6.46mmol) in 50mL ethanol, refluxed 70°C in a sealed tube for 12 hours to afford a brown needle-like crystals (1.49, 85%). **^{1}H NMR (400 MHz, DMSO-d$_6$) δ** 8.20 (s, 1H, H-7), 7.40 (d, *J* = 6.1 Hz, 5H, H-10, H-11, H-12), 6.33 (s, 1H, H-4), 4.94 (s, 2H, H-8), 4.29 (s, 2H, H-2), 0.80 – 0.63 (m, 5H, H-13, H-14, H-15). **^{13}C NMR (101 MHz, DMSO-d$_6$) δ** 173.72 (C-5), 168.65 (C-3), 147.05 (C-6), 141.65 (C-7), 136.60 (C-9), 128.90 (C-10), 128.64 (C-11), 128.59 (C-12), 111.58 (C-4), 71.02 (C-8), 59.69 (C-2), 22.59 (C-13), 3.63 (C-14, C-15).

7.1.2.3. Chlorination – Synthesis of 3

To neat cold 9.0 equiv. $SOCl_2$ below 0°C (ice/acetone mixture) in sealed glass vials, was added compounds **4a, 4b** and **4c** (1.0 equiv) respectively and stirred at room temperature for 8 hours. The brown oils formed were washed with petroleum ether and dried under vacuum to afford **3a, 3b** and **3c**[321].

7.1.2.3.1 Synthesis of 5-(benzyloxy)-2-(chloromethyl)-1-methylpyridin-4(1H)-one (3a)

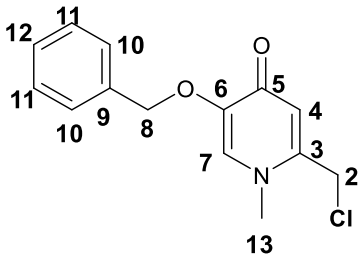

To neat cold $SOCl_2$ (13.02mL, 21.82g, 183.47mmol) below 0°C (ice/acetone mixture) in sealed glass vials, was added **4a** (5g, 20.39mmol) and stirred at room temperature for 8 hours to afford a cream paste (2.5g, 47%).**^{1}H NMR (400 MHz, DMSO-d6) δ** 8.82 (s, 1H, H-7), 7.57 (s, 1H, H-4), 7.48 (d, *J* = 7.3 Hz, 2H, H10), 7.39 (dt, *J* = 19.0, 7.0 Hz, 3H, H-11, H-12), 5.21 (s, 2H, H-8), 4.68 (s, 2H, H-2), 4.02 (s, 3H, H-13). **^{13}C NMR (101 MHz, DMSO-d6) δ** 161.53 (C-5), 153.48 (C-3), 144.40 (C-6), 135.80 (C-7), 132.43 (C-9), 129.03 (C-10), 128.96 (C-11), 128.72 (C-12), 110.94 (C-4), 72.01 (C-8), 58.80 (C-2), 42.70 (C-13).

7.1.2.3.2 Synthesis of 5-(benzyloxy)-2-(chloromethyl)-1-isopropylpyridin-4(1H)-one (3b)

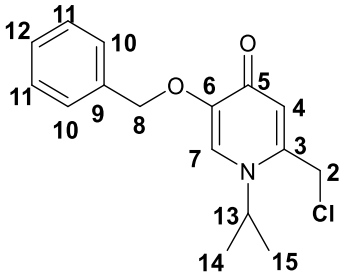

To neat cold $SOCl_2$ (5.22mL, 8.56g, 72.40mmol) below 0°C (ice/acetone mixture) in sealed glass vials, was added **4b** (2.2g, 8.04mmol) and stirred at room temperature for 8 hours to

afford a brown oil, (1.3g, 55%). **^{1}H NMR (400 MHz, DMSO-d_6) δ** 8.30 (s, 1H, H-7), 7.52 – 7.30 (m, 5H, H-10, H-11, H-12), 6.59 (s, 1H, H-4), 4.96 (s, 2H, H-8), 4.68 (s, 2H, H-2), 2.09 (s, 4H, H-14, H-15), 1.19 (d, *J* = 6.4 Hz, 1H, H-13). **^{13}C NMR (101 MHz, DMSO-d_6) δ** 173.50 (C-5), 162.30 (C-3), 147.32 (C-6), 142.10 (C-7), 136.42 (C-9), 128.93 (C-10), 128.73 (C-11), 128.64 (C-12), 114.92 (C-4), 71.02 (C-8), 41.60 (C-2), 31.14 (C-14, C-15), 20.83 (C-13).

7.1.2.3.3 Synthesis of 5-(benzyloxy)-2-(chloromethyl)-1-cyclopropylpyridin-4(1H)-one (3c)

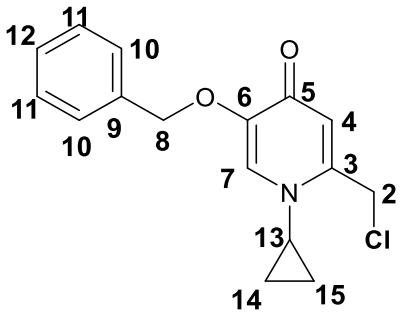

To neat cold $SOCl_2$ (3.52mL, 5.77g, 48.10mmol) below 0°C (ice/acetone mixture) in sealed glass vials, was added **4c** (1.45g, 5.34mmol) and stirred at room temperature for 8 hours to afford a brown oil, (0.79g, 51%). **^{1}H NMR (400 MHz, DMSO-d_6) δ** 7.58 (s, 1H, H-7), 7.46 – 7.14 (m, 5H, H-10, H-11, H-12), 6.27 (s, 1H, H-4)), 5.08 (s, 2H, H-8), 4.51 (s, 2H, 2H, H-2), 1.31 (d, *J* = 6.5 Hz, 1H, H-13), 1.24 – 0.99 (m, 4H, H-14, H-15). **^{13}C NMR (101 MHz, DMSO-d_6) δ** 171.81 (C-5), 148.40 (C-3), 144.12 (C-6), 142.96 (C-7), 128.81 (C-10), 128.75 (C-11), 128.49 (C-12), 118.12 (C-4), 71.13 (C-8), 63.36 (C-2), 52.08 (C-13), 22.45 (C-14, C-15).

7.1.3 General Synthesis Procedure of Kojic Acid-Derived Conjugates

To a solution of 1.0 equiv. of N-(7- chloroquinoline 4yl) alkyl-diamine **(6)** in 3mL dimethylformamide (DMF), 1.0 equiv. triethylamine (Et_3N) and 2.0 equiv. anhydrous sodium carbonate Na_2CO_3 was added to 1.0 equiv. chlorinated N-alkyl benzyl pyranones **(3)** before refluxing at 80°C for 24 hours while stirring to drive the reaction to completion. After the reaction was completed, dichloromethane (DCM) was added, the mixture was washed with water, dried over $MgSO_4$ and excess solvent was removed under reduced pressure. Target compounds were purified by column chromatography on silica gel (eluant: methanol/ethyl acetate), and excess solvent was removed by rotary evaporation. Compounds **1a-l** were synthesized using a similar procedure[193]

7.1.3.1 Synthesis of 5-(benzyloxy)-2-(((7-chloroquinolin-4-yl)(methyl)amino)methyl)-1-methylpyridin-4(1H)-one (1a)

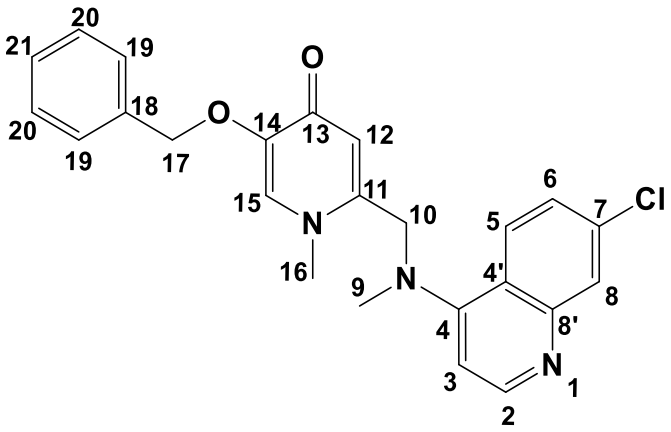

To a solution of **6a** (0.5g, 2.61mmol) in 3mL DMF, 0.36mL Et_3N (0.26g, 2.61mmol) and anhydrous Na_2CO_3 (0.28g, 5.22mmol) was added **3a** (0.69g, 3.39mmol) and refluxed at 80°C for 24 hours to yield a brown solid, $C_{24}H_{22}ClN_3O_2$: 419.90g/mol (0.7g, 69%); **mp.** 89-91°C.

^{1}H NMR (400 MHz, DMSO-d_6) δ 8.41 (d, *J* = 5.3 Hz, 1H, H-2), 8.25 (s, 1H, NH-9), 8.20 (d, *J* = 9.0 Hz, 1H, H-8), 8.09 (s, 1H, H-15), 7.80 (d, *J* = 1.7 Hz, 1H, H-6), 7.51 – 7.37 (m, 5H, H-19, H-20, H-21), 6.56 (d, *J* = 8.0 Hz, 1H, H-3), 4.19 (s, 2H, H-17), 3.39 (t, *J* = 8.6 Hz, 5H, H-10, H-16), 1.84 (s, 1H, H-9). **^{13}C NMR (101 MHz, DMSO-d_6) δ** 162.35 (C-13), 152.36 (C-2), 150.52 (C-4), 149.43 (C-8’, C-15), (133.96 (C-7, C-14), 127.89 (C-18), 124.65 (C-19), 124.48 (C-20, C-21), 124.37 (C-12), 124.32 (C-5, C-6), 117.87 (C-4’), 99.09 (C-3), 49.04 (C-17), 42.50 (C-10), 36.38 (C-16), 23.03 (C-9).

7.1.3.2 Synthesis of 5-(benzyloxy)-2-(((2-((7-chloroquinolin-4-yl)amino)ethyl)amino)methyl)-1-methylpyridin-4(1H)-one (1b)

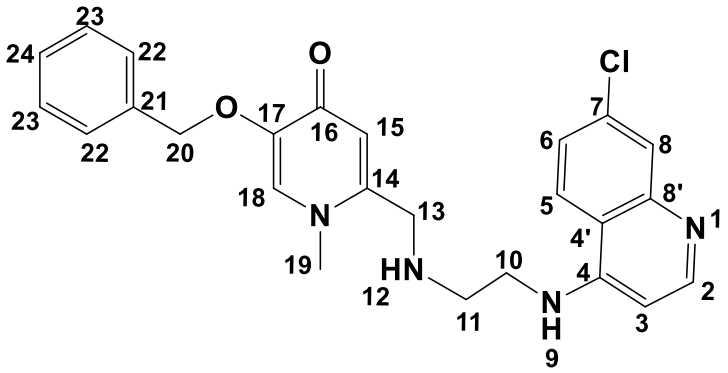

To a solution of **6b** (0.8g, 3.39mmol) in 3mL DMF, 0.47mL Et_3N (0.34g, 3.39mmol) and anhydrous Na_2CO_3 (0.72g, 6.79mmol) was added **3a** (0.89g, 3.39mmol) and refluxed at 80°C for 24 hours to yield a brown oil, $C_{25}H_{25}ClN_4O_2$: 448.94g/mol (0.98g, 62%).

^{1}H NMR (400 MHz, DMF, DMSO-d_6) δ 8.23 (d, *J* = 5.3 Hz, 1H, H-5), 8.20 (d, *J* = 9.1 Hz, 1H, H-2), 7.78 (s, 1H, H-18), 7.50 (s, 1H, H-6), 7.38 (d, *J* = 6.9 Hz, 1H, H-8), 7.33 (s, 1H), 7.20 (dd, *J* = 18.6, 8.4 Hz, 5H, H-22, H-23, H-24), 6.60 (d, *J* = 15.8 Hz, 1H, H-3), 6.42 (d, *J* = 5.4 Hz, 1H, H-15), 3.38 – 3.25 (m, 3H, H-11, NH-11), 1.88 (s, 3H, H-19), 0.62 (t, *J* = 6.3 Hz, 2H, H-10). **^{13}C NMR (101 MHz, DMF, DMSO-d6)** δ 166.32 (C-16), 152.20 (C-2), 150.58 (C-4), 149.63 (C-8'), 139.22 (C-21), 135.33 (C-17), 133.86 (C-14, C-7)), 129.57 (C-24), 129.00 (C-23), 127.85 (C-22), 124.37 (C-5), 124.16 (C-6), 122.27, 117.95 (C-15), 98.80 (C-3), 42.93 (C-20), 37.97 (C-13), 31.79 (C-11), 30.10 (C-19), 29.23 (C-10). ***V*max (KBr)** cm^{-1}**:** 3322 (N-H), 2972 (Ar C-H), 2881 (Alkyl C-H), 1549 (C=O), 1418 (C=C), 1087 (C=N), 879 (C-O), 618 (C-Cl).

7.1.3.3 Synthesis of 5-(benzyloxy)-2-(((2-((7-chloroquinolin-4-yl)amino)ethyl)(methyl)amino)methyl)-1-methylpyridin-4(1H)-one (1c)

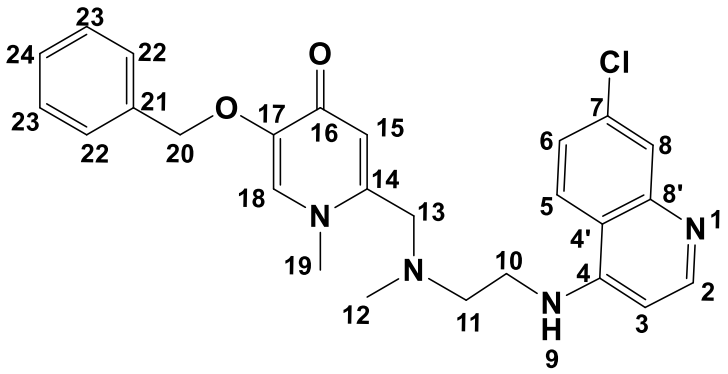

To a solution of **6c** (0.8g, 3.39mmol) in 3mL DMF, 0.47mL Et_3N (0.34g, 3.39mmol) and anhydrous Na_2CO_3 (0.72g, 6.79mmol) was added **3a** (0.89g, 3.39mmol) and refluxed at 80°C for 24 hours to yield a brown oil, $C_{26}H_{27}ClN_4O_2$: 462.97g/mol (0.98g, 62%).

^{1}H NMR (400 MHz, DMSO-d_6) δ 8.38 (d, *J* = 11.7 Hz, 2H, NH-9, H-5), 8.34 – 8.21 (m, 1H, H-2), 7.79 (d, *J* = 7.2 Hz, 1H, H-6), 7.55 – 7.13 (m, 6H, H-18,H-22, H-23, H-24), 6.49 (s, 1H, H-15), 6.10 (d, *J* = 7.4 Hz, 1H, H-3), 4.88 (s, 2H, H-20), 3.74 (s, 1H, H-13), 3.63 (s, 3H, H-19), 3.17 (s, 1H, H-11), 2.19 (s, 1H, H-10). **^{13}C NMR (101 MHz, DMSO-d_6) δ** 172.52 (C-16), 151.79 (C-2), 149.36 (C-4), 145.48 (C-8'), 141.28 (C-17), 140.19 (C-7), 138.13 (C-21), 133.90 (C-14), 128.98 (C-22), 128.65 (C-23), 128.25 (C-24), 125.11 (C-5), 124.76 (C-6), 116.66 (C-15), 99.45 (C-3), 72.46 (C-20), 63.63 (C-13), 53.47 (C-11), 42.60 (C-10), 40.82 (C-19), 12.35 (C-12). ***V*max (KBr)** cm^{-1}**:** 3314 (N-H), 2972 (Ar C-H), 2881 (Alkyl C-H), 1653 (C=O), 1418 (C=C), 1379 (C=N), 1274 (C-O), 621 (C-Cl).

7.1.3.4 Synthesis of 5-(benzyloxy)-2-(((3-((7-chloroquinolin-4-yl)amino)propyl)(methyl)amino)methyl)-1-methylpyridin-4(1H)-one (1d)

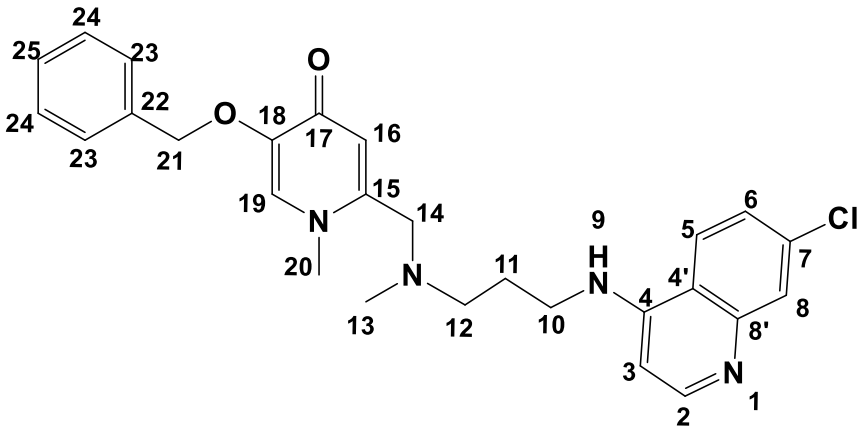

To a solution of **6e** (0.75g, 3.00mmol) in 3mL DMF, 0.42mL Et_3N (0.30g, 3.00mmol) and anhydrous Na_2CO_3 (0.63g, 6.01 mmol) was added **3a** (0.79g, 3.00mmol) and refluxed at 80°C for 24 hours to yield a brown oil, $C_{27}H_{29}ClN_4O_2$: 477.00g/mol (0.8g, 56%). **^{1}H NMR (400 MHz, DMSO-d_6) δ** 8.47 (s, 1H, NH-9), 8.35 (d, *J* = 6.8 Hz, 1H, H-5), 8.26 (s, 1H, H-2), 8.13 (s, 1H, H, H-19), 7.85 (s, 1H, H-8), 7.60 (d, *J* = 8.7 Hz, 1H, H-6), 7.47 – 7.32 (m, 5H, H-23, H-24, H-25), 6.68 (d, *J* = 6.0 Hz, 1H, H-3), 6.37 (s, 1H, H-16), 4.88 (s, 2H, H-21), 2.93 (s, 2H, H-14), 2.77 (s, 2H, H-12), 2.25 (s, 3H, H-13), 2.09 (s, 2H, H-10), 1.98 – 1.79 (m, 2H, H-11). **^{13}C NMR (101 MHz, DMSO-d_6) δ** 173.37 (C-17), 166.03 (C-4), 153.13 (C-8'), 147.06 (C-22), 141.80 (C-2), 136.55 (C-18), 136.14 (C-15), 130.83 (C-7), 128.91 (C-23), 128.68 (C-24), 128.59 (C-25), 125.77 (C-5), 125.27 (C-6), 116.73 (C-4', C-8)), 114.42 (C-16), 99.20 (C-3), 70.96 (C-21), 58.24 (C-14), 54.45 (C-12), 42.54 (C-20), 41.30 (C-14), 31.42 (C-13), 25.85 (C-11). ***V*max (KBr)** cm^{-1}**:** 3318 (N-H), 2972 (Ar C-H), 2881 (Alkyl C-H), 1652 (C=O), 1454 (C=C), 1418 (C=N), 1274 (C-O), 879 (C-Cl).

7.1.3.5 Synthesis of (benzyloxy)-2-(((2-((7-chloroquinolin-4-yl)amino)ethyl)amino)methyl)-1-isopropylpyridin-4(1H)-one (1e)

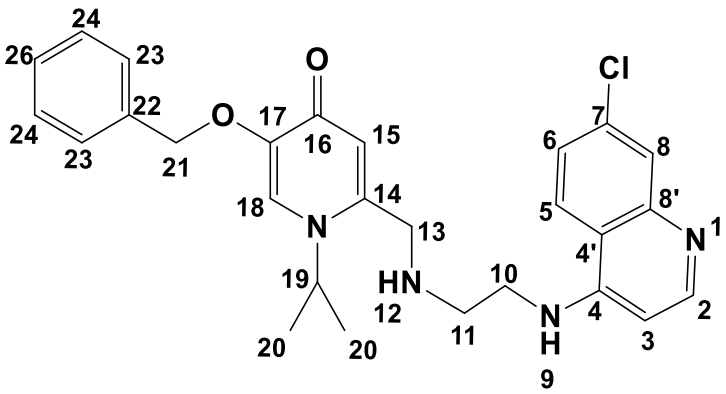

To a solution of **6b** (1.00g, 4.00mmol) in 3mL DMF, 0.56mL Et_3N (0.41g, 4.00mmol) and anhydrous Na_2CO_3 (0.85g, 8.001 mmol) was added **3b** (1.17g, 4.00mmol) and refluxed at 80°C for 24 hours to yield a brown oil, $C_{27}H_{29}ClN_4O_2$: 447.00/mol (1.08g, 53%). **^{1}H NMR (400 MHz, DMSO-d_6) δ :** NH-9; H-2, H-5, H-8, H-6, H-18, Benzyl-Protons, H-15, H-3, H-21, H-12, H-11, H-12, H-19, H-20. **^{13}C NMR (101 MHz, DMSO-d_6) δ** 163.19 (C-16), 152.13 (C-2), 150.73 (C-4), 149.32 C-14), 149.26 (C-17), 139.27 (C-21), 133.96 (C-7), 128.50 (C-23), 127.79 (C-24), 127.71 (C-25), 124.61 (C-8), 124.58 (C-18), 124.47 (C-5), 124.42 (C-6), 117.91 (C-4'), 117.88 (C-15), 99.06 (C-3), 61.94 (C-21), 55.01 (C-13), 42.10 (C-11), 34.45 (C-10), 25.84 (C-20), 25.47 (C-20). ***V*max (KBr)** cm^{-1}**:** 3322 (N-H), 2972 (Ar C-H), 2881 (Alkyl C-H), 1658 (C=O), 1419 (C=C), 1379 (C=N), 1328 (C-O), 879 (C-Cl).

7.1.3.6 Synthesis of 5-(benzyloxy)-2-(((3-((7-chloroquinolin-4-yl)amino)propyl)(methyl)amino)methyl)-1-isopropylpyridin-4(1H)-one (1f)

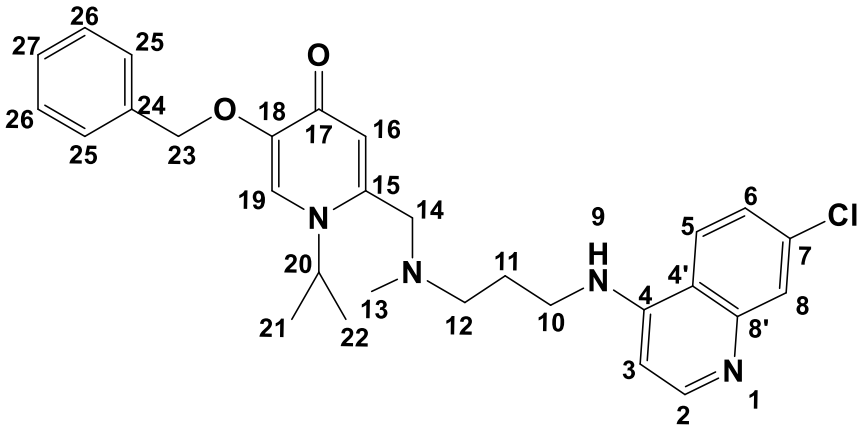

To a solution of **6e** (1.00g, 4.00mmol) in 3mL DMF, 0.56mL Et_3N (0.41g, 4.00mmol) and anhydrous Na_2CO_3 (0.85g, 8.001 mmol) was added **3b** (1.17g, 4.00mmol) and refluxed at 80°C for 24 hours to yield a brown oil, $C_{29}H_{33}ClN_4O_2$: 505.05g/mol (1.08g, 53%).**^{1}H NMR (400 MHz, DMSO-d_6) δ** 8.43 (d, *J* = 0.5 Hz, 1H, NH-9), 8.31 (dd, *J* = 12.9, 9.5 Hz, 2H, H-5, H-2), 8.03 (s, 1H, H-19), 7.82 (s, 1H, H-8), 7.70 – 7.56 (m, 1H, H-6), 7.51 (t, *J* = 10.3 Hz, 2H, H-25), 7.43 – 7.32 (m, 3H, H-26, H-27), 6.55 (d, *J* = 2.1 Hz, 1H, H-3), 6.19 (s, 1H, H-16), 4.90 (s, 2H, H-23), 3.65 (s, 2H, H-12), 3.32 – 3.24 (m, 2H, H-10), 3.17 (s, 1H, H-13), 2.93 (s, 1H, H-20), 2.77 (s, 6H, H-21, H-22). **^{13}C NMR (101 MHz, DMSO-d_6) δ** 171.79 (C-17), 151.79 (C-2), 150.96 (C-4), 148.27, 147.73, 146.21, 137.77, 134.52, 129.69 (C-25), 128.64 (C-26, C-27), 127.90, 126.19, 124.98 (C-5), 124.81 (C-6), 118.47 (C-4'), C-8), 99.44 (C-3), 70.96 (C-23), 59.05 (C-14), 54.64 (C-12), 46.75 (C-10), 41.88 (C-20), 41.61 (C-11), 34.51 (C-20), 29.20 (C-21, C-22). ***V*max (KBr)** cm^{-1}**:** 3320 (N-H), 2972 (Ar C-H), 2881 (Alkyl C-H), 1651 (C=O), 1419 (C=C), 1379 (C=N), 1326 (C-O), 879 (C-Cl).

7.1.3.7 Synthesis of 5-(benzyloxy)-2-(((4-((7-chloroquinolin-4-yl)amino)butyl)amino)methyl)-1-isopropylpyridin-4(1H)-one (1g)

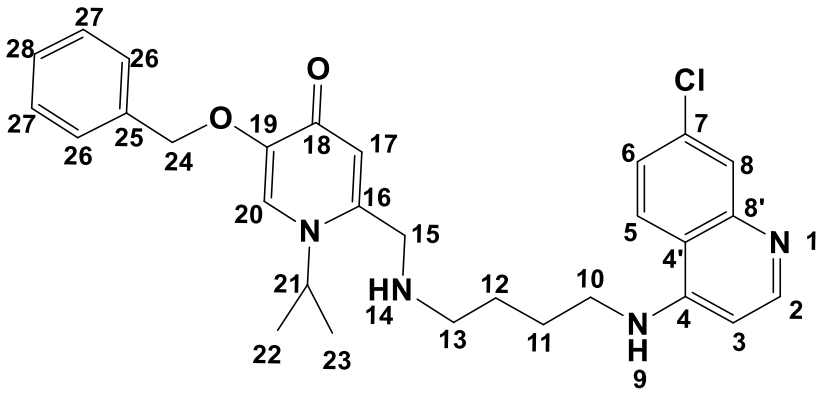

To a solution of **6f** (1.25g, 5.01mmol) in 3mL DMF, 0.70mL Et_3N (0.30g, 3.00mmol) and anhydrous Na_2CO_3 (01.06g, 5.01 mmol) was added **3b** (1.46g, 5.01mmol) and refluxed at 80°C for 24 hours to yield a brown oil, $C_{29}H_{33}ClN_4O_2$: 505.05 g/mol (1.49g, 59%). **^{1}H NMR (400 MHz, DMSO-d_6) δ** 8.41 (s, 1H, NH-9), 8.33 – 8.18 (m, 2H, H-5, H-2), 8.12 (s, 1H, H-20), 8.03 (s, 1H, H-6), 7.80 (s, 1H, H-8), 7.51 – 7.33 (m, 5H, H26, H-27, H-28), 6.49 (d, *J* = 5.1 Hz, 1H, H-3), 6.39 (s, 1H, H-17), 4.88 (s, 2H), 3.31 (d, *J* = 5.7 Hz, 2H, H-13), 2.93 (s, 1H, H-10), 2.77 (s, 1H, H-14), 2.24 (s, 6H, H-22, H-23), 2.09 (s, 2H, H-1), 2.00 – 1.75 (m, 4H, H-11, H-12). **^{13}C NMR (101 MHz, DMSO-d_6) δ** 173.52 (C-18), 152.12 (C-2), 150.76 (C-4), 149.35 (C-8'), 147.14 (C-19), 141.76 (C-20), 136.56 (C-16), 128.89 (C-26), 128.66 (C-28), 128.61 (C-27), 127.67 (C-7), 124.59 (C-5), 124.52 (C-6), 117.76 (C-4', C-17), 114.42 (C-8), 99.08 (C-3), 70.95 (C-24), 58.18 (C-15), 54.84 (C-13), 46.80 (C-10), 42.38 (C-22, C-23), 41.03 (C-12), 29.28 (C-11), 25.98 (C-21). ***V*max (KBr)** cm^{-1}**:** 3434 (N-H), 3054 (Ar C-H), 2976 (Alkyl C-H), 1607 (C=O), 1454 (C=C), 1372 (C=N), 1251 (C-O), 747 (C-Cl).

7.1.3.8 Synthesis of 5-(benzyloxy)-2-(((6-((7-chloroquinolin-4-yl)amino)hexyl)amino)methyl)-1-isopropylpyridin-4(1H)-one (1h)

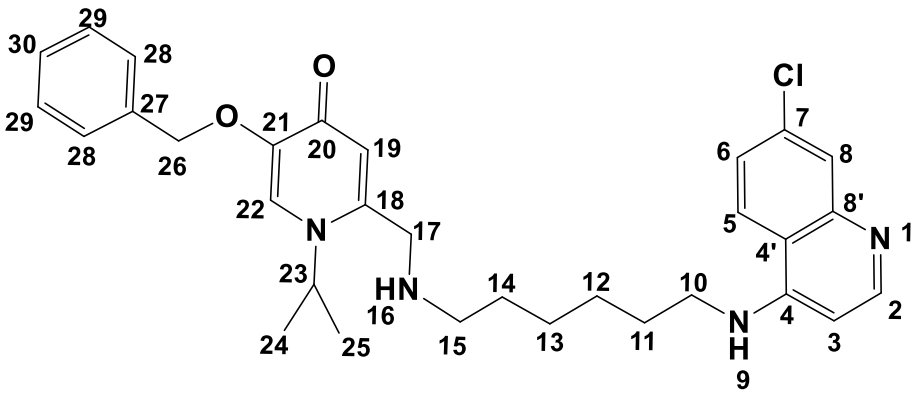

To a solution of **6g** (0.25g, 9.00mmol) in 3mL DMF, 0.125mL Et_3N (0.09g, 9.00mmol) and anhydrous Na_2CO_3 (0.19g, 18.00 mmol) was added **3b** (0.26g, 9.00mmol) and refluxed at 80°C for 24 hours to yield a brown oil, $C_{31}H_{37}ClN_4O_2$: 533.10g/mol (1.2g, 25%). **^{1}H NMR (400 MHz, DMSO-d_6) δ** 8.41 (s, 1H, NH-9), 8.35 – 8.17 (m, 2H, H-5, H-2), 8.03 (s, 1H, H-6), 7.79 (d, *J* = 6.0 Hz, 2H, H6, H-8), 7.54 – 7.29 (m, 5H, H-28, H-29, H-30), 6.49 (d, *J* = 5.2 Hz, 1H, H-3), 6.20 (s, 1H, H-19), 4.90 (s, 2H, H-26), 3.66 (s, 2H, H-15), 3.38 (s, 2H, H-10), 3.24 (s, 2H, H-14), 2.93 (s, 1H, H-12), 2.77 (s, 1H, H-17), 2.17 (s, 1H, H-23), 2.09 (s, 6H, H-24, h-25), 1.97 – 1.80 (m, 4H, H-12, H-13). **^{13}C NMR (101 MHz, DMSO-d_6) δ** 171.68 (C-20), 152.15 (C-2), 150.69 (C-4), 149.00 (C-8), 147.57 (C-21), 146.21 (C-22), 137.42 (C-18), 133.90 (C-7), 129.69 (C-30), 128.76 (C-29), 128.42 (C-28), 127.74 (C-19),124.65 (C-5), 124.56 (C-6), 118.75 (C-4'), 117.76 (C-19), 99.45 (C-3), 70.99 (C-26), 59.03 (C-17), 54.54 (C-15), 46.81 (C-10), 41.90 (C-24, C-25), 40.95 (C-14), 39.71 (C-11), 39.50 (C-13), 34.43 (C-12). ***V*max (KBr)** cm^{-1}**:** 3330 (N-H), 3100 (Ar C-H), 2935 (Alkyl C-H), 1657 (C=O), 1512 (C=C), 1473 (C=N), 1306 (C-O), 512 (C-Cl).

7.1.3.9 Synthesis of 5-(benzyloxy)-2-(((7-chloroquinolin-4-yl)(methyl)amino)methyl)-1-cyclopropylpyridin-4(1H)-one (1i)

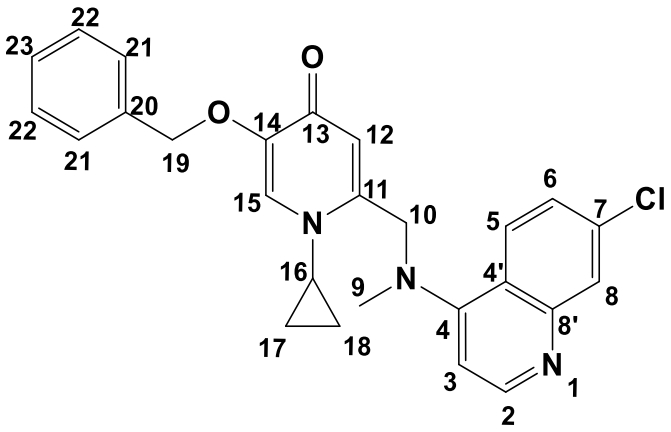

To a solution of **6a** (0.45g, 2.34mmol) in 3mL DMF, 0.33mL Et_3N (0.24g, 2.34mmol) and anhydrous Na_2CO_3 (0.50g, 4.70 mmol) was added **3c** (0.79g, 3.mmol) and refluxed at 80°C for 24 hours to yield a brown oil, $C_{26}H_{24}ClN_3O_2$: 445.94g/mol (0.71g, 68%).

^{1}H NMR (400 MHz, DMSO-d_6) δ 7.99 (s, 1H, NH-9), 7.81 (d, *J* = 9.0 Hz, 2H, H-5, H2), 7.70 (s, 1H, H-15), 7.37 (s, 2H, H-6, H-8), 7.22 – 6.80 (m, 5H, H-21, H-22, H-23), 6.06 (d, *J* = 5.1 Hz, 1H, H-3), 5.96 (s, 1H, H-12), 4.46 (s, 2H, H-19), 3.01 (s, 3H, H-9), 2.88 (d, *J* = 5.7 Hz, 4H, H-17, H-18), 2.35 (s, 1H, H-16), 2.09 (s, 2H, H-10).**^{13}C NMR (101 MHz, DMSO-d_6) δ** 170.72 (C-13), 152.50 (C-2), 150.72 (C-4), 149.35 (C-8), 134.55 (C-14, C-20), 128.24 (C-21), 127.55 (C-22), 127.17 (C-23), 125.46 (C-7, C-11), 124.76 (C-5, C-6), 118.44 (C-12), 117.39 (C-4'), 99.11 (C-3), 42.67 (C-19), 41.22 (C-10), 37.80 (C-16), 36.18 (C-17, C-18), 31.23 (C-9).

***Vmax* (KBr)** cm^{-1}**:** 3325 (N-H), 3282 (Ar C-H), 2927 (Alkyl C-H), 1666 (C=O), 1557 (C=C), 1539 (C=N), 1432 (C-O), 855 (C-Cl).

7.1.3.10 Synthesis of 5-(benzyloxy)-2-(((2-((7-chloroquinolin-4-yl)amino)ethyl)amino)methyl)-1-cyclopropylpyridin-4(1H)-one (1j)

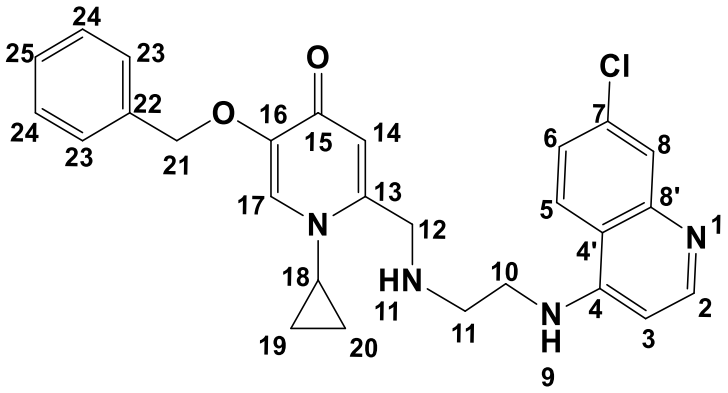

To a solution of **6b** (0.8g, 3.61mmol) in 3mL DMF, 0.50mL Et_3N (0.37g, 3.61mmol) and anhydrous Na_2CO_3 (0.76g, 7.22 mmol) was added **3c** (1.05g, 3.61mmol) and refluxed at 80°C for 24 hours to yield a brown solid, $C_{27}H_{27}ClN4O_2$: 474.98g/mol (0.86g, 85%); **mp.** 124-130°C.

^{1}H NMR (400 MHz, DMSO-d_6) δ 8.56 – 8.23 (m, 3H, NH-9, H-5, H-2), 8.07 (s, 1H, H-8), 7.95 (s, 1H, H-17), 7.62 – 7.36 (m, 6H, H-6, H-23, H-24, H-25), 7.19 (s, 1H, H-14), 6.60 (d, *J* = 5.4 Hz, 1H, H-3), 6.47 (s, 1H, H-14), 3.37 – 3.11 (m, 4H, H-11, H-10), 2.72 (s, 2H, H-12), 1.51 – 1.10 (m, 1H, H-18), 1.11 – 0.69 (m, 5H, H-18, H-19, H-20). **^{13}C NMR (101 MHz, DMSO-d_6) δ** 169.95 (C-15), 152.75 (C-2), 150.77 (C-4), 149.00 (C-16), 134.40 (C-22), 134.09 (C-7, C-13), 127.48 (C-23, C-25), 127.03 (C-26),124.62 (C-5), 124.48 (C-6), 117.83 (C-14, C-4'), 99.06 (C-3), 36.24 (C-21), 35.54 (C-18), 31.22 (C-11), 28.21 (C-19, C-20), 28.15 (C-10). ***Vmax* (KBr)** cm^{-1}**:** 3300 (N-H), 3125 (Ar C-H), 2880 (Alkyl C-H), 1666 (C=O), 1535 (C=C), 1429 (C=N), 1234 (C-O), 736 (C-Cl).

7.1.3.11 Synthesis of 5-(benzyloxy)-2-(((3-((7-chloroquinolin-4-yl)amino)propyl)amino)methyl)-1-cyclopropylpyridin-4(1H)-one (1k)

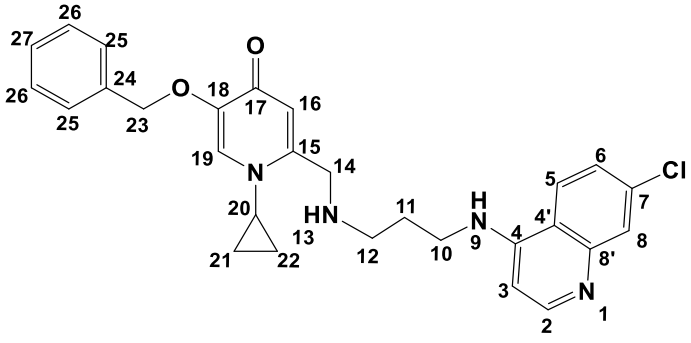

To a solution of **6d** (1.5g, 2.00mmol) in 3mL DMF, 0.28mL Et_3N (0.20g, 2.00mmol) and anhydrous Na_2CO_3 (0.024g, 4.00 mmol) was added **3c** (0.58g, 2.00mmol) and refluxed at 80°C for 24 hours to yield a brown oil, $C_{28}H_{29}ClN_4O_2$: 489.19/mol (0.97g, 71%).

1H NMR (400 MHz, DMSO-d_6) δ 8.37 (d, *J* = 5.2 Hz, 1H, H-2), 8.28 (d, *J* = 9.1 Hz, 1H, H-5), 8.17 (t, *J* = 5.4 Hz, 1H, NH-9), 7.78 (d, *J* = 1.7 Hz, 1H, H-8), 7.58 (d, *J* = 8.4 Hz, 2H, H-6, H-19), 7.49 – 7.36 (m, 4H, H-25, H-26, H-27), 7.32 (t, *J* = 4.9 Hz, 1H, H-14), 6.63 (d, *J* = 15.8 Hz, 1H, H-16), 6.45 (d, *J* = 5.4 Hz, 1H, H-3), 3.31 – 3.22 (m, 2H, H-12), 3.21 – 3.13 (m, 2H, H-10), 1.73 – 1.58 (m, 2H, H-11), 1.54 – 1.27 (m, 5H,H-20, H-21, H-22), 1.21 (s, 2H, H-13). **13C NMR (101 MHz, DMSO-d_6) δ** 171.61 (C-17), 152.28 (C-2), 150.63 (C-4), 149.8 (C-8'), 142.91 (C-19), 133.90 (C-7), 128.84 (C-24), 128.78 (C25), 128.75(C-26), 128.50 (C-27), 128.24 (C-16), 128.19 (C-8), 124.56 (C-5), 124.49 (C-6), 117.83 (C-4'), 99.06 (C-3), 71.84 (C-23), 63.33 (C-17), 47.80 (C-15), 42.77 (C-10), 32.35 (C-14), 31.12 (C-23), 30.26 (C-12), 30.08 (C-11), 23.99 (C-13), 7.87 (C-21, C-22). ***V*max (KBr)** cm^{-1}**:** 3339 (N-H), 2930 (Ar C-H), 2925 (Alkyl C-H), 1639 (C=O), 1506 (C=C), 1442 (C=N), 1124 (C-O), 633 (C-Cl).

7.1.3.12 Synthesis of 5-(benzyloxy)-2-(((6-((7-chloroquinolin-4-yl)amino)hexyl)amino)methyl)-1-cyclopropylpyridin-4(1H)-one (1l)

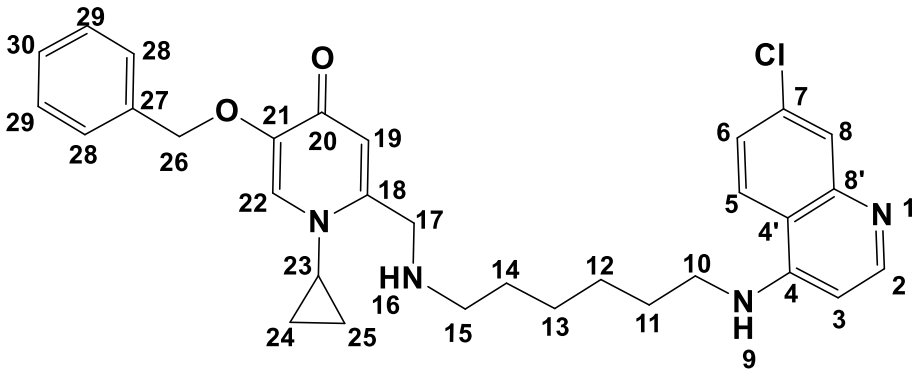

To a solution of **6g** (0.72g, 2.56mmol) in 3mL DMF, 0.36mL Et_3N (0.26g, 2.56mmol) and anhydrous Na_2CO_3 (0.55g, 5.18 mmol) was added **3c** (0.75g, 2.56mmol) and refluxed at 80°C for 24 hours to yield a brown oil, $C_{31}H_{35}ClN_4O_2$: 531.09g/mol (0.62g, 45%).

^{1}H NMR (400 MHz, DMSO-d_6) δ 8.42 – 8.25 (m, 3H, H-5, H-2, NH-9), 7.78 (d, *J* = 2.1 Hz, 1H, H-22), 7.61 (d, *J* = 7.5 Hz, 1H, H-6), 7.50 – 7.23 (m, 5H, H-28, H-29, H-30), 6.45 (d, *J* = 5.1 Hz, 1H, H-3), 6.15 (s, 1H, H-6), 5.02 (s, 2H, H-26), 3.85 (t, *J* = 11.5 Hz, 1H, H-15), 3.25 (dd, *J* = 11.8, 6.0 Hz, 1H, H-10, H-14), 2.73 (d, *J* = 7.5 Hz, 1H, H-17), 1.85 (s, 1H, H-23), 1.61 (ddd, *J* = 21.7, 13.7, 6.7 Hz, 4H, H-11, H-13), 1.49 – 1.20 (m, 4H, H-24, H-25). **^{13}C NMR (101 MHz, DMSO-d_6) δ** 172.31 (C-20), 152.34 (C-2), 150.61 (C-4), 149.51, 145.64, 141.18, 139.92, 138.13, 133.84, 128.97, 128.60, 128.26, 127.82, 124.75, 124.71, 124.41, 116.38 C-19), 99.03

(C-3), 72.19 (C-26), 42.73 (C-17), 39.30 (C-15), 31.14 (C-10), 30.48 (c-14), 28.05 (C-11), 26.60 (C-12), 26.13 (C-13), 25.92 (C-24, C-25), 12.32 (C-23). ***V*max (KBr)** cm^{-1}**:** 3328 (N-H), 3179 (Ar C-H), 2923 (Alkyl C-H), 1666 (C=O), 1533 (C=C), 1488 (C=N), 1224 (C-O), 761 (C-Cl).

7.1.4 General Synthesis Procedure of Maltol-Derived Conjugates

1.0 equiv. benzyl-maltol **(10a or 10b)** and 1.5 equiv N-(7- chloroquinoline 4yl) alkyl-diamine **(6a-6g)** were dissolved in 25mL ethanol (EtOH), then water (25ml) was added to the mixture to obtain a 50% aqueous EtOH solution. The pH of the solution was ad*j*usted to 13 (2M NaOH) before refluxing at 110°C for 24h. Afterwards, the pH was ad*j*usted to 1 (2M HCl) before washing with diethyl ether (50mLx2). On ad*j*ustment of the pH to 7 (2M NaOH), precipitates were formed which were filtered, washed with distilled water, and air dried. Target compounds were purified by column chromatography on silica gel (eluant: methanol/ethyl acetate) and excess solvent was removed by rotary evaporation. Compounds **2a-2h** were synthesized using a similar procedure[193]

7.1.4.1 Synthesis of 3-(benzyloxy)-1-(2-((7-chloroquinolin-4-yl)amino)ethyl)-2-methylpyridin-4(1H)-one (2a)

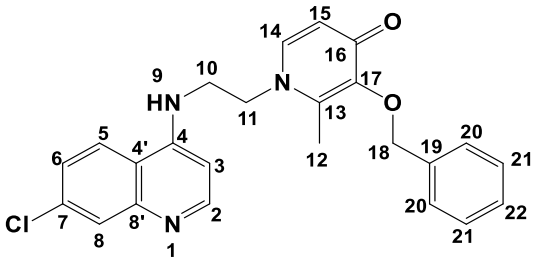

10a (1.43g, 6.62mmol) and **6b** (2.2g, 9.923mmol) in 50% aqueous EtOH solution were refluxed at 110°C for 24 hours to yield a brown solid (1.6g, 58%); **mp.** 158-159°C. Expected mass: 419.90g/mol. Obtained mass: 419 g/mol

^{1}H NMR (400 MHz, DMSO-d_6 and CD_3OD) δ 8.35 (s, 1H, NH-9), 8.21 (d, *J* = 8.9 Hz, 1H, H-5), 8.14 (d, *J* = 9.0 Hz, 1H, H-2), 7.80 (d, *J* = 8.8 Hz, 1H, H-14), 7.56 (d, *J* = 7.3 Hz, 1H, H-6), 7.40 (dd, *J* = 19.1, 9.1 Hz, 1H, H-8), 7.25 (tt, *J* = 29.8, 6.9 Hz, 5H, H-20, H-21, H-22), 6.45 (d, *J* = 5.4 Hz, 1H, H-3), 6.19 (d, *J* = 7.4 Hz, 1H, H-15), 4.87 (s, 2H, H-18), 3.44 – 3.32 (m, 2H, H-11), 2.83 (t, *J* = 6.0 Hz, 2H, H-10), 2.17 (s, 3H, H-12). **^{13}C NMR (101 MHz, DMSO-d_6 and CD_3OD) δ** 172.85 (C-16), 152.11 (C-2), 150.26 (C-4), 149.14 (C-8'), 145.92 (C-13), 142.04 (C-17) , 140.31 (C-14), 137.91 (C-19), 134.36 (C-7), 128.70 (C-20), 128.52 (C-21), 128.18 (C-22), 127.58 (C-8), 124.56 (C-5), 124.29 (C-6), 117.75 (C-4'), 116.41 (C-15), 98.89 (C-3), 72.68 (C-18), 46.74 (C-11), 42.44 (C-10), 12.37 (C-12). ***V*max (KBr)** cm^{-1}**:** 3280 (N-H), 3000 (Ar C-H), 2900 (Alkyl C-H), 1623 (C=O), 1610 (C=C), 1558m (C=N), 1222 (C-O), 707 (C-Cl).

7.1.4.2 Synthesis of 3-(benzyloxy)-1-(3-((7-chloroquinolin-4-yl)amino)propyl)-2-methylpyridin-4(1H)-one (2b)

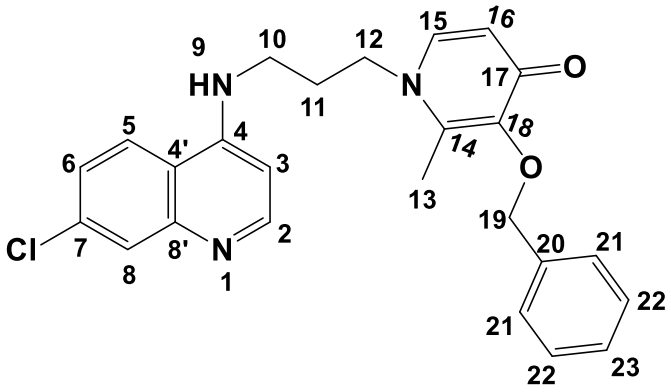

10a (1.22g, 5.67mmol) and **6d** (2.00g, 8.49mmol) in 50% aqueous EtOH solution were refluxed at 110°C for 24 hours to yield a yellow solid (1.2g, 36%); **mp.** 128-130°C. Expected mass ($C_{25}H_{24}ClN_3O_2$): 433.93 g/mol. Obtained mass: 434.93 g/mol.

^{1}H NMR (400 MHz, DMSO-d_6) δ 9.30 (s, 1H, NH-9), 8.47 (d, *J* = 9.1 Hz, 1H, H-5), 8.33 (d, *J* = 6.8 Hz, 1H, H-2), 7.82 (s, 1H, H-8), 7.54 (dd, *J* = 27.4, 8.1 Hz, 2H, H-6, H-15), 7.20 – 7.10 (m, 5H, H-21, H-22, H-23), 6.66 (d, *J* = 6.9 Hz, 1H, H-3), 6.03 (d, *J* = 7.4 Hz, 1H, H-16), 4.78 (s, 2H, H-19), 3.91 – 3.86 (m, 2H, H-12), 3.35 (d, *J* = 5.1 Hz, 2H, H-10), 1.98 (s, 3H, H-13), 1.91 – 1.81 (m, 2H, H-11). **^{13}C NMR (101 MHz, DMSO-d_6) δ** 172.31 (C-17), 155.51 (C-14), 145.75 (C-4), 143.83 (C-2), 141.40 (C-8'), 140.05 (C-15), 139.59 (C-18), 138.11 (C-20), 138.07 (C-7), 128.89 (C-21), 128.65 (C-22), 128.28 (C-23), 127.01 (C-5), 126.57 (C-6), 119.90 (C-8), 116.49 (C-4'), 116.48 (C-16), 99.07 (C-3), 72.31 (C-19), 50.97 (C-12), 40.63 (C-10), 28.98 (C-11), 12.43 (C-13). ***V*max (KBr)** cm^{-1}**:** 3300 (N-H), 3100 (Ar C-H), 2924 (Alkyl C-H), 1663 (C=O), 1614 (C=C), 1537m (C=N), 1257 (C-O), 798 (C-Cl).

7.1.4.3 Synthesis of 3-(benzyloxy)-1-(4-((7-chloroquinolin-4-yl)amino)butyl)-2-methylpyridin-4(1H)-one (2c)

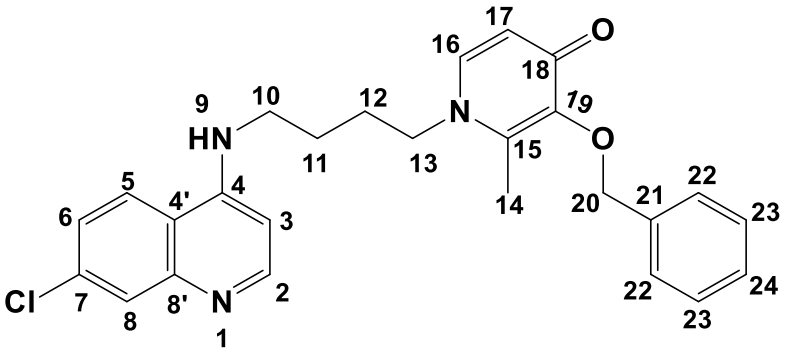

10a (0.93g, 4.29mmol) and **6f** (1.8g, 6.43mmol) in 50% aqueous EtOH solution were refluxed at 110°C for 24 hours to yield a yellow solid (1.2g, 63%); **mp.** 135-138°C**.** Expected mass: 447.96 g/mol. Obtained mass: 478 g/mol

^{1}H NMR (400 MHz, DMSO-d_6) 9.84 (s, 1H, NH-9), 8.81 (d, *J* = 9.1 Hz, 1H, H-5), 8.51 (d, *J* = 7.0 Hz, 1H, H-2), 8.45 (d, *J* = 7.1 Hz, 1H, H-6), 8.06 (s, 1H, H-8), 7.70 (d, *J* = 8.9 Hz, 1H, H-16), 7.38 (dt, *J* = 18.3, 8.9 Hz, 5H, H-22, H-23, H-24), 7.24 (d, *J* = 7.0 Hz, 1H, H-17), 6.87 (d, *J* = 7.0 Hz, 1H, H-3), 5.05 (s, 2H, H-20), 4.33 (d, *J* = 6.7 Hz, 2H, H-13), 2.44 (s, 3H, H-14), 1.83 (s, 2H, H-12), 1.73 (d, *J* = 6.2 Hz, 2H, H-11). **^{13}C NMR (101 MHz, DMSO-d_6) δ** 165.43 (C-18), 155.81 (C-15), 148.65 (C-4), 143.63 (C-2), 143.08 (C-8'), 142.22 (C-16), 138.91 (C-19), 138.40 (C-21), 136.74 (C-7), 129.13 (C-22), 128.91 (C-23), 127.18 (C-24), 126.64, 119.36 (C-8), 115.92 (C-4'), 113.54 (C-17), 99.08 (C-3), 74.34 (C-20), 55.53 (C-13), 42.80 (C-10), 27.34 (C-12), 24.49 (C-11), 13.43 (C-14). ***V*max (KBr)** cm^{-1}**:** 3328 (N-H), 3188 (Ar C-H), 2921 (Alkyl C-H), 1664 (C=O), 1621 (C=C), 1568m (C=N), 1299 (C-O), 805 (C-Cl).

7.1.4.4 Synthesis of 3-(benzyloxy)-1-(6-((7-chloroquinolin-4-yl)amino)hexyl)-2-methylpyridin-4(1H)-one (2d)

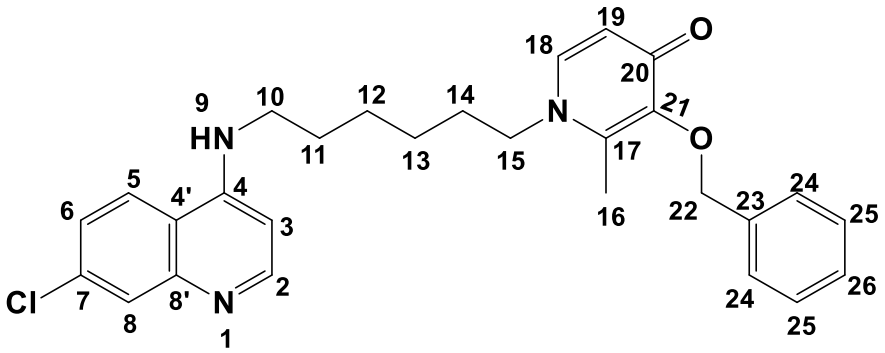

10a (1.56g, 7.20mmol) and **6g** (3g, 10.80mmol) in 50% aqueous EtOH solution were refluxed at 110°C for 24 hours to yield a brown solid (2.25g, 66%); **mp.** 88-90°C. Expected mass (: 476.01 g/mol. Obtained mass: 475 g/mol

^{1}H NMR(400 MHz, $CDCl_3$) δ 8.31 (d, *J* = 4.6 Hz, 1H, H-5, H-2), 7.89 (d, *J* = 8.5 Hz, 1H, H-8), 7.77 (s, 2H, H, H-6, H-18), 7.03 – 7.23 (m, 5H, H-24, H-25, H-26), 6.37 (s, 1H, NH-9), 6.26 (d, *J* = 7.4 Hz, 1H, H-3), 6.19 (d, *J* = 5.6 Hz, 1H, H-19), 5.05 (s, 2H, H-22), 3.54 (s, 1H, H-15), 3.13 (s, 2H, H-10), 1.93 (s, 3H, H-16), 1.56 (d, *J* = 6.4 Hz, 2H, H-14), 1.42 (d, *J* = 6.8 Hz, 2H, H-11), 1.33 – 1.23 (m, 2H, H-13), 1.15 (dd, *J* = 14.1, 6.7 Hz, 2H, H-12). **^{13}C NMR (101 MHz, $CDCl_3$) δ** 173.20 (C-20), 151.25 (C-2), 150.56 (C-4), 148.50 (C-8'), 146.05 C-17), 141.26 (C-21), 138.51 C-18), 137.25 (C-23), 134.88 (C-7), 128.84 (C-24), 128.26 (C-25), 128.06 (C-26), 127.60 (C-8), 125.05 (C-5), 122.54 (C-6), 117.36 (C-4'), 116.98 (C-19), 98.66 (C-3), 72.98 (C-

22), 53.77 (C-15), 42.95 (C-10), 30.51 (C-14), 28.28 (C-11), 26.69 (C-13), 26.05 (C-12), 12.37 (C-16). ***V*max (KBr)** cm^{-1}**:** 3300 (N-H), 3200 (Ar C-H), 2851 (Alkyl C-H), 1666 (C=O), 1610 (C=C), 1530m (C=N), 1164 (C-O), 797 (C-Cl).

7.1.4.5 Synthesis of 3-(benzyloxy)-1-(2-((7-chloroquinolin-4-yl)amino)ethyl)-2-ethylpyridin-4(1H)-one (2e)

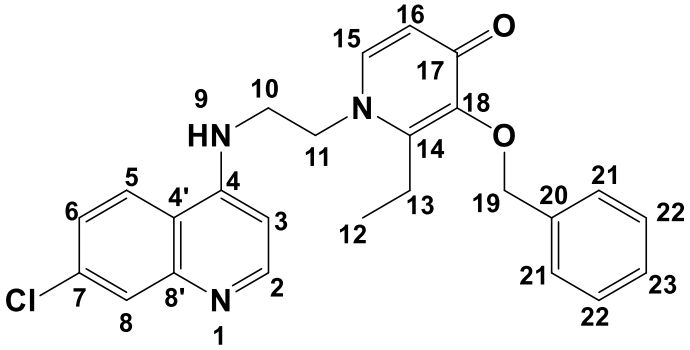

10a (1.14g, 4.94mmol) and **6b** (2g, 7.41mmol) in 50% aqueous EtOH solution were refluxed at 110°C for 24 hours to yield yellow oil (1.47g, 69%). Expected mass: 433.93 g/mol. Obtained mass: 434 g/mol. **^{1}H NMR (400 MHz, DMSO-d_6) δ** 8.37 (d, *J* = 5.3 Hz, 1H, H-5), 8.33 (d, *J* = 11.5 Hz, 1H, H-2), 8.24 (d, *J* = 8.9 Hz, 1H, H-15), 7.78 (d, *J* = 11.1 Hz, 1H, H-6), 7.60 (s, 1H, NH-9), 7.48 – 7.40 (m, 1H, H-8), 7.32 – 7.21 (m, 5H, H-21, H-22, H-23), 6.45 – 6.42 (m, 2H, H-3, H-16), 4.50 (s, 2H, H-19), 3.31 (s, 2H, H-12), 3.04 (d, *J* = 5.6 Hz, 2H, H-13), 2.66 (t, *J* = 6.4 Hz, 2H, H-11), 1.74 – 1.71 (m, 2H, H-10). **^{13}C NMR (101 MHz, DMSO-d_6) δ** 163.75 (C-17), 152.33 (C-2), 150.72 (C-14), 149.39 (C-4), 142.91 (C-8'), 133.89 (C-7), 128.65 (C-22), 128.50 (C-21), 127.89 (C-8), 127.78 (C-23), 127.09 (C-5), 126.88 (C-6), 124.49 (C-15), 117.90 (C-4'), 99.02 (C-3), 63.34 (C-19), 41.06 (C-11), 39.91 (C-10), 31.62 (C-13), 20.79 (C-12). ***V*max (KBr)** cm^{-1}**:** 3300 (N-H), 3180 (Ar C-H), 2900 (Alkyl C-H), 1666 (C=O), 1613 (C=C), 1582m (C=N), 1287 (C-O), 762 (C-Cl).

7.1.4.6 Synthesis of 3-(benzyloxy)-1-(3-((7-chloroquinolin-4-yl)amino)propyl)-2-ethylpyridin-4(1H)-one (2f)

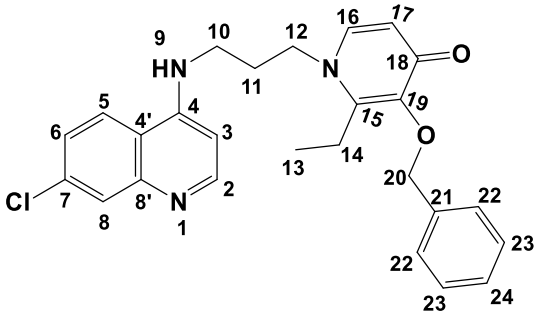

10b (0.97g, 4.24mmol) and **6d** (1.5g, 6.36mmol) in 50% aqueous EtOH solution were refluxed at 110°C for 24 hours to yield a light brown solid, (0.79g, 42%); **mp.** 128-135°C. Expected mass: 447.96 g/mol. Obtained mass: 448 g/mol

^{1}H NMR (400 MHz, DMSO-d_6) δ ^{1}H NMR (400 MHz, DMSO) δ 8.38 (d, *J* = 5.4 Hz, 1H, H-5), 8.27 (d, *J* = 9.0 Hz, 1H, H-2), 7.78 (d, *J* = 1.9 Hz, 1H, H-8), 7.43 (dd, *J* = 8.9, 2.0 Hz, 1H, H-6), 7.37 (d, *J* = 5.5 Hz, 1H, H-16), 7.42 – 7.21 (m, 5H, H-22, H-23, H-24),7.21 (d, *J* =, 1H, H-17), 6.45 (d, *J* = 5.5 Hz, 1H, H-3), 3.68 (s, 2H, H-20), 3.28 – 3.23 (m, 2H, H-14), 3.18 (s, 3H, H-13), 2.54 (d, *J* = 7.0 Hz, 2H, H-12), 1.70 (dt, *J* = 14.3, 7.0 Hz, 2H, H-10), 1.55 (dt, *J* = 14.0, 7.0 Hz, 2H, H-11). **^{13}C NMR (101 MHz, DMSO-d_6) δ** 152.36 (C-2), 150.57 (C-4), 149.55 (C-8'), 141.53 (C-15, C-16, C-19), 133.80 (C-21, C-7), 128.50 (C-22), 128.34 (C-23), 127.90 (C-24), 126.88 (C-8), 124.59 (C-5), 124.40 (C-6), 117.92 (C-4', C-17), 99.08 (C-3), 53.53 (C-20), 49.05 (C-13), 48.84 (C-14), 42.83 (C-12), 27.51 (C-10), 26.13 (C-11). ***V*max (KBr)** cm^{-1}**:** 3400 (N-H), 3300 (Ar C-H), 2928 (Alkyl C-H), 1661 (C=O), 1623 (C=C), 1535m (C=N), 1169 (C-O), 791 (C-Cl).

7.1.4.7 Synthesis of 3-(benzyloxy)-1-(4-((7-chloroquinolin-4-yl)amino)butyl)-2-ethylpyridin-4(1H)-one (2g)

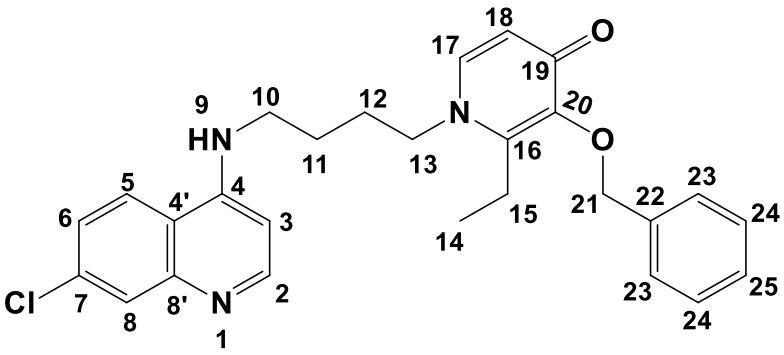

10b (0.98g, 4.27mmol) and **6f** (1.6g, 6.41mmol) in 50% aqueous EtOH solution were refluxed at 110°C for 24 hours to yield a light brown solid, (1.23g, 62%); **mp.** 126-128°C.

Expected mass: 461.98 g/mol. Obtained mass: 462 g/mol

^{1}H NMR (400 MHz, DMSO-d_6) δ 8.37 (d, *J* = 5.3 Hz, 1H, H-2), 8.33 (d, *J* = 11.5 Hz, 1H, H-5), 8.24 (d, *J* = 8.9 Hz, 1H, H-8), 7.78 (d, *J* = 11.1 Hz, 1H, H-6), 7.60 (s, 1H, NH-9), 7.45 - 7.40 (m, 1H, H-14), 7.31 - 7.19 (m, 6H, H-14, H-21, H-22, H-23), 6.45 (d, *J* = 5.4 Hz, 1H, H-3), 4.52 (s, 1H, H-19), 3.31 (d, *J* = 5.8 Hz, 2H, H-13), 2.63 (m, Hz, 2H, H-10), 2.1 (s, 3H, (H-20), 1.73 (m, 4H, H-11, H-12). **^{13}C NMR (101 MHz, DMSO-d_6) δ** 169.84 (C-16), 152.34 (C-2), 150.61 (C-4), 149.51 (C-8'), 145.64 (C-15), 141.18 (C-18), 139.92 (C-14), 133.84 (C-7), 128.97 (C-22),128.60 (C-23), 128.26 (C-24, C-25), 127.82 (C-8), 124.76 (C-15), 124.71 (C-6), 124.42 (C-5),117.92 (C-4'), 99.03 (C-3), 72.19 (C-21), 53.17 (C-19), 42.69 (C-13), 39.30 (C-10),

30.48 (C-11), 28.02 (C-12), 12.32 (C-20). ***V*max (KBr)** cm^{-1}**:** 3390 (N-H), 3284 (Ar C-H), 2923(Alkyl C-H), 1667 (C=O), 1615 (C=C), 1588m (C=N), 1198 (C-O), 817 (C-Cl).

7.1.4.8 Synthesis of 3-(benzyloxy)-1-(6-((7-chloroquinolin-4-yl)amino)hexyl)-2-ethylpyridin-4(1H)-one (2h)

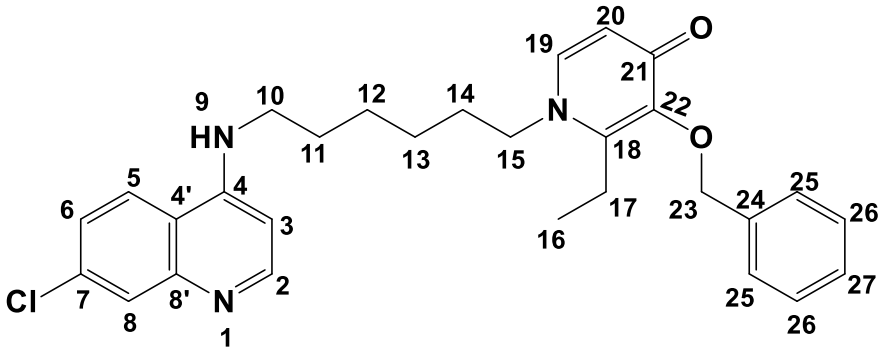

10b (1.66g, 7.20mmol) and **6g** (3g, 10.80mmol) in 50% aqueous EtOH solution were refluxed at 110°C for 24 hours to yield a brown solid (2.81g, 80%); **mp.** 165-168°C. Expected mass: 490.04 g/mol. Obtained mass: 490 g/mol

^{1}H NMR (400 MHz, DMSO-d_6) δ 8.38 (s, 1H, NH-9), 8.28 (d, *J* = 8.9 Hz, 2H, H-5, H-2), 7.78 (s, 1H, H-8), 7.60 (dd, *J* = 7.4, 4.2 Hz, 1H, H-6), 7.52 – 7.18 (m, 6H, H-19, H-25, H-26, H-27), 6.45 (d, *J* = 5.2 Hz, 1H, H-3), 6.16 (t, *J* = 7.4 Hz, 1H, H-20), 5.06 (d, *J* = 29.1 Hz, 1H, H-23), 3.30 – 3.19 (m, 3H, H-16), 2.13 (s, 2H, H-17), 1.76 – 1.14 (m, 12H, H-16, H-10, H-15, H-11, H-13, H-12). **^{13}C NMR (101 MHz, DMSO-d_6) δ** 172.28 (C-20), 152.27 (C-2), 150.61 (C-4), 149.42 (C-8'), 145.64 (C-18), 141.13 (C-22), 139.90 (C-19), 138.28 (C-24), 133.88 (C-7), 128.97 (C-25), 128.71 (C-26), 128.61 (C-27), 127.80 (C-8), 124.59 (C-5), 124.47 (C-6), 117.88 (C-4'), 116.39 (C-20), 99.05 (C-3), 72.17 (C-23), 53.16 (C-15), 42.72 (C-10), 40.14 (C-17), 30.49 (C-14), 28.07 (C-11), 26.66 (C-13), 25.94 (C-12), 13.80 (C-16). ***V*max (KBr)** cm^{-1}**:** 3400 (N-H), 3300 (Ar C-H), 2910 (Alkyl C-H), 1667 (C=O), 1615 (C=C), 1513m (C=N), 1198 (C-O), 770 (C-Cl).

7.2 In Vitro Anti-HIV Assay Methods

7.2.1 General information

In all the assays, sterility was maintained. Decontamination was achieved by spraying hands and all materials on the exterior with 70% ethanol. All operations were strictly carried out inside a sterile cabinet in aseptic conditions. The incubator used was set at 37°C, 5% CO_2.

7.2.2 Experimental Procedures

7.2.2.1 Cell thawing

Many cultures obtained from a culture collection, will arrive frozen and to use the cells they must be thawed and put into culture. A typical cell thawing protocol usually begins with retrieving cryovials from the liquid nitrogen storage (-80˚C). The cryovials containing 1 mL of TZM-bl cells, HEPG2 cells and Hela Cells preserved in 10% DMSO in Fetal Bovine Serum (FBS) were transferred into a 37°C water bath until all the ice had completely dissolved.

It is of great importance to thaw cells correctly to maintain the viability of the culture and enable the culture to recover more quickly. This is because cryoprotectants such as DMSO is toxic above 4 °C. Therefore, it is crucial that cultures are thawed immediately and diluted in culture medium to minimize the toxic effects[322][323].

The thawed cells were pipetted into sterile 50mL centrifuge tubes and thawing media (20% FBS in Dulbecco's Modified Eagle Medium (DMEM) media) supplemented with the appropriate constituents was added to dilute the DMSO. The mixtures were centrifuged at 1200 rotations per minute (rpm) for 5 minutes. The supernatants were discarded, and the pellets (cells) were resuspended in 15mL thawing media. These cells were then transferred into culturing flasks, and they were cultured at 37°C, 5% CO_2 for at least 24 hours before processing the cells for downstream experiments[322].

7.2.2.3 Cell harvesting

Because the growth rate or proliferation of cells is not the same, affected by the weather, type of the cell line etc, the flasks were continually monitored and changing the growing media (10% FBS in DMEM) whenever there is a need. Mostly the media is changed when it starts to turn yellowish, this is a clear indication that the nutrients are running out. When the cells have grown to 100% confluency, they are harvested for seeding. The quickest cells to grow to 100% confluency were the HeLa cells which are cancer cells, followed by the HEPG2 cells (also cancer cells) and lastly the TZM-bl cells (HIV Cells).

Harvesting is the separation of the cell culture from the growing medium. Firstly, the growing media was discarded and 3mL trypsin was added to detach the cells from the culture flasks. The flasks were incubated for 10mins, and the cells were transferred into centrifuge flasks. 7mL of growing media was added into the three tubes to neutralize the trypsin. The mixture was centrifuged at 1200rpm for 5mins. The supernatants were discarded, and the pellets were resuspended in growing media for cell counting.

7.2.2.4 Cell counting

To determine the viable cell density, trypan blue was used. 90µL of trypan blue and 10µL of the suspended cells were mixed gently in an eppendorf. 10µL of the mixture was then transferred onto the hemocytometer and the cells were counted under a microscope using the formula below:

$$\frac{\text{Total number of cells}}{\text{Number of squares}} \text{ x dilution factor x } 10^4$$

For example:

$$\frac{162 \text{ cells}}{4} \text{ x } 10 \text{ x } 10^4 = 4\,050\,000 \text{ cells/ml}$$

NB: for cell seeding, at least 1 000 000 cells are required.

7.2.2.5 Cell seeding

Cell seeding is usually the first protocol step and a standard procedure in cell-based experiments. A correct and standardized cell seeding protocol is a critical factor for reproducible experimental results.

100µL of $1x10^5$ cells/ml is required to seed one 96 well plate.

From the suspended cells, to determine the volume required for seeding, the formula below was used:

$$V_1 = \frac{C_2 V_2}{C_1}$$

For example, to seed 3 plates with 100µL of $1x10^5$ cells/ml

$$V_{required} = \frac{(1x10^5)(30ml)}{4\,050\,000} = 0.74ml\ cells$$

These cells were incubated at 37° C for 24hrs.

Treatment of the seeded cells with the selected compounds.

To prepare the compounds used for treating the cells, the first step was to weigh about 1-2mg of each compound and then dissolve them in ultra DMSO (the exact masses of the selected compound are shown in the table below). Compound **2b** will be used as any example in the calculations.

The amount of solvent required to dissolve the compounds was determined by the formular below:

Mass of the compound in mg x 50 X 1000 = volume of the solvent in µL

2mg x 50 x 1000 = 80µL

Second, was to determine the concentrations of these compounds so as to prepare a stock solution of 800µM in 500µL of each compound.

$$Concentration\ of\ the\ compound\ in\ \mu M = \frac{mass}{Molecular\ Mass\ x\ Volume\ of\ DMSO\ added}\ x10^6$$

$$Concentration\ = \frac{2x10^{-6}g}{\frac{433.93g}{mol}x\ 100\mu L}\ x10^6 = 46000\mu M$$

The third step was to determine the amount of the compound dissolved in DMSO required to make a stock solution of 800µM in 500µL of each compound. This was determined using the formula below:

$$C_1V_1 = C_2V_2$$

$$V_1 = \frac{C_2V_2}{C_1} = \frac{800\mu M\ x\ 500\mu L}{46000\mu M} = 8.695\mu L$$

Now to make a solution of 500µL, the amount of media to be added was determined using the formula below:

Total volume of the mixture required – the amount of the compound dissolved in DMSO = number of media to be added

500µL – 8.695µL = 491.31µL of media was added

The above formulas were used to prepare the rest of the compounds and their respective figures are shown in the table 6.1 below.

Table 6.1: Compound Concentrations

Compound	Quantity/mg	DMSO added/µL	Initial Concentration(µM)	Sample in Media (µL)	Media Added (µL)
2b	2.0	100	46000	8.695	491.40
2d	1.6	80	44600	8.968	491.03
1e	1.7	85	45000	8.889	491.11
1g	1.9	95	44600	8.968	491.032
1b	2.0	100	44500	8.987	491.013
1f	1.6	80	31600	12.658	487.34
1a	1.4	70	47600	8.403	491.597

These compounds were further diluted to 200µM which was required to treat the cells. This was achieved by:

1. Wells in 3 ninety-six well plates were divided and labelled in replica of the 3 plates which were being used to culture the cells.
2. 150µL of was media into each well and 150µL of the compound (from the stock solution prepared) was added to the first row of the 3 columns of wells allocated for each compound.
3. A pipette was used to mix and dilute going down the columns, drawing portions of 150µL to the next well. The last 150µL was discarded and 100µL was drawn from the last row of wells onto the corresponding last row with cells. Now the dilution was done going up.
4. To the wells allocated for controls, only media was added.
5. The plates were incubated for 48hrs at 37˚C.

7.2.2.6 MTT Assay

After incubating the plates for 48hrs, they were centrifuged at 1200 rotations per minute (rpm) for 5 minutes. 200µL of media was removed from each well and 200µL of PBS was added to the wells. The wells were centrifuged again at 1200 rpm for 5 minutes. Afterwards the PBS was removed for all the wells.

MTT Preparation

200mg MTT powder was dissolved in 40ml of sterile PBS(x1) solution to make a solution of concentration of 5mg/mL. The solution was filtered and sterilized through a 0.2µm syringe filter and collected in a sterile container. The MTT was store at 4˚C in a dark container.

MTT Buffer

10µL MTT/ 100µL cells = 1 well

So, for 96 wells = 96 x 10µL = 960µL of MTT

1mL MTT + 9mL of plain DMEM Media = 10mL of MTT buffer

100µL of MTT was added to each well, and the plates were incubated for 4-24hrs, light protected.

Solubilization of MTT Assays

The solubilization buffer was prepared by the ratio: 1mL of 1N HCL (was added) to 9mL Isopropanol.

100µL of the solubilization was buffer added to each well, and the plates were incubated at room temperature for at least 15 minutes. Readings were taken at 540nm and 690nm backgrounds.

7.2.2.7 Nitric oxide assay

Materials

1. HeLa cells' supernatants
2. 0.1% N-1-napthathylene-diamine dichloride (NED) in water
   Molecular Weight of NED = 259.17g/mol. Therefore 0.1% = 0.1g of NED diluted to 100ml with triple distilled water (dddH_2O)
3. 1% Sulfanilamide diluted in 5% phosphoric acid.
   1g of sulfanilamide was diluted to 100ml with 5% phosphoric acid.
   5% phosphoric acid = 5mL of phosphoric acid diluted to 100mL with dddH_2O.
4. Nitrate Standards – Nitrate ion standard solution (stock Solution = 0.1M)
   Working Solution:

$$C_1V_1 = C_2V_2$$

$$V_1 = \frac{C_2V_2}{C_1} = \frac{100x10^{-3}x\ 300\mu L}{0.1M} = 300\mu L \leftrightarrow 30\mu L\ (Nitric\ Oxide) + 270\ plain\ DMEM\ media$$

Using the formula $C_1V_1 = C_2V_2$, the nitrate oxide standard solutions prepared, whereby V_1 = 100µL were:

Table 7.2.2 Compound Concentrations

C_2/ µM	NO added from the working solution/µL	Plain Media Added/µL
100	200	0
50	100	100
25	50	150
10	20	180
5	10	190
0	0	200

Protocol

50mL of the supernatants from the treated Hela cells and nitric oxide solutions were transferred to each well of the 96 well plates. 50µL of 1% sulfanilamide solution was added to each well and the plates were incubated at room temperature (RT) for 10mins in the dark. The plate was covered with foil paper. 50µL NED solution was added to each well and the contents of each well were mixed well. The plates were incubated for 10minutes at RT in the dark. Again, the plate was covered with foil paper. Absorbance readings were measured at 520nm and 550nm.

7.2.2.8 Reverse transcriptase inhibition assay - ELISA assay

The Reverse Transcriptase assay kit was purchased from Sigma-Aldrich (catalog Number 11468120910. Storage Temperature –20 °C). The kit contained sufficient reagents 224 tests which are:

- HIV-1 reverse transcriptase (Bottle 1), Incubation buffer (Bottle 2), Reaction mixture (Bottles 2, 3, and 4), Lysis buffer (Bottle 5), Anti-DIG-POD (Bottle 6), Washing buffer, 1xconc. (Bottle 7), ABTS substrate solution (Bottles 9 and 10), ABTS substrate solution containing substrate enhancer (Bottle 11), Conjugate dilution buffer (Bottle 8), Microplate modules and Polyethylene glycol (PEG).

Table 7.2.3: Test Compounds which were prepared as follows:

Compound	Mass/gram	DMSO added/µL
2b	0.0029	145
1e	0.0049	245
1g	0.0038	190
1b	0.0037	185
1f	0.0031	155

Table 7. 2.4 Working concentrations of the test compounds:

Working Concentration/ µM	Volumed of test compound	Lysis Buffer added/µL
100	18.00	42.00
50	9.000	51.00
25	4.500	55.50
12.5	2.250	57.25
6.25	1.125	58.875

Procedure:

Firstly all the buffers were equilibrated to room temperature and the working solutions were prepared as instructed in the kit protocol[293].

Table 7.2.5: Mixture Contents in each tube

Experiment Tubes	Positive Control Tube	Negative Control Tube
Test Compound 60µL Enzyme 60µL Nucleotide 60µL	Lysis Buffer 60µL Enzyme 60µL Nucleotide 60µL	Lysis Buffer 60µL Lysis Buffer 60µL Nucleotide 60µL

All the tubes were incubated for an hour. The contents of the tubes were then transferred into their respective-designated microplate modules (60µL to each well) and incubated for 1 hour. The solutions were removed from the modules and the well were washed five times with 250µL wash buffer. 200µL of anti-Dig-POD solution was added to each well and the modules were incubated for an hour. The solutions were removed from the modules and the well were washed five times with 250µL wash buffer. 200µL of ABTS substrate (4 tablets dissolved in 20mL substrate buffer) was added to each well and the modules were incubated for 30minutes at room temperature before taking readings with a microplate reader at 405nm.

7.2.2.9 HIV protease activity detection assay

The HIV protease activity detection kit was purchased from Sigma-Aldrich (catalog Number APPA014. Storage Temperature –20 °C)[324]. The contained sufficient reagents for one 96 well plate (96 assays) which are:

1. 1.0mL Constrained Substrate (ready to use solution)
2. 20mL Detector (S1-10) Complementary GFP fragment (ready to use solution)
3. 500µL Positive Control Reagent (ready to use solution)

Procedure:

Table 7.2.6: Contents in each well

Experimental Wells		Negative Controls		Positive Controls	
Master Mixture	20µL	Master Mixture	20µL	Master Mixture	20µL
Compound	10µL	TE Buffer	10µL	Positive Control	10µL
Enzyme	0.5µL	Enzyme	0.5µL	Enzyme	0.5µL

Firstly, all the kit components were equilibrated to room temperature whilsting preparing TE buffer (2.07 pH). A 1:1 master mixture of the constrained substrate (1mL) and TE buffer (1mL) was prepared. Pipette 20 mL of the master mix into each microplate well. 0.5 mL each of HIV protease enzyme was added to the reaction control wells. 10 mL of each compound was added to experimental reaction wells. The plate was incubated overnight at 37 °C in a humidified incubator whilst wrapped with foil. 200 mL of Detector (S1-10) to test and controls was added to all wells and the plate was incubated again for 8 hours. GFP excitation and fluorescence were measured at 485nm and 538nm respectively[324].

7.2.2.10 Antioxidant (DPPH) assay

Materials

1. 1.77mg of 2, 2-diphenyl-1-picrylhydrazyl (DPPH) dissolved in 50mL 100% ethanol – 35.4ug/mL.
2. 2mg Ascorbic acids dissolved in 1mL 100% ethanol (starting concentration swas supposed to be 100µg/mL)
   MW = 176.12g/mol

$$Concentration = \frac{mass}{MW\ x\ Volume} = \frac{0.002g}{\frac{176.12g}{mol} x 0.001L} = 11\ 356\mu M$$

3. 2mg of each compound + 200µL of 100% ethanol (starting concentration was supposed to be 500µg/mL)
4. Preparation of Compounds used:
   Table 7.2.7: Contents in each well

Compound Name	Mass/ gram	100% Ethanol Added/µL
2b	0.00211	211
1e	0.00269	270
1g	0.00345	345
1b	0.00245	245
1f	0.00302	302
Vitamin C	0.00319	320

Protocol

Figure 7.2: The 96 well plating design layout for DPPH Assay

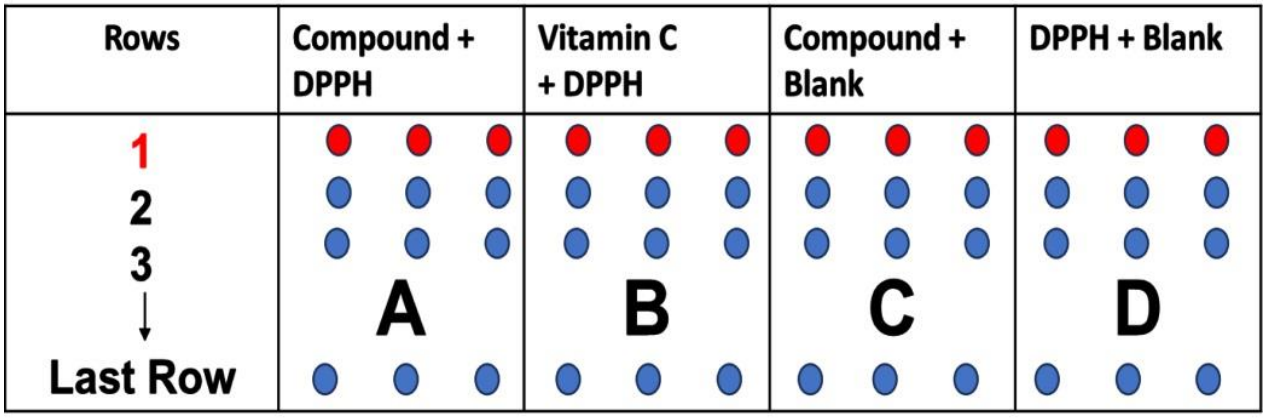

200µL of $dddH_2O$ was added to all the first-row wells (marked in red) using a multichannel pipette. 110µL of $dddH_2O$ was added to the rest of the wells. 20µL of each diluted compound was added to the first-row wells (**A**) and (**C**). 20µL of Vitamin C solution was added to the first-row wells of **B** – positive control. 20µL of 100% ethanol was added to the first row of **D** – solvent control.

Serial dilution (with 110µL) was done from the first-row wells downwards, the 110µL from the last row wells was discarded. After the serial dilution, a final volume of 110µL was left in all the wells.

In the dark, the DPPH solution was prepared by dissolving the1.77mg of DPPH in 50mL of 100% ethanol. 90µL of this DPPH solution was added to all triplicate wells expect for column **C** which was the compound control (compound + blank) whereby 90µL $dddH_2O$ was added instead. The plates were covered with foil as DPPH is light sensitive. These plates were incubated in the dark at room temperature for 30 minutes before reading the plates at 492nm.

7.3 *In Vitro* Antiplasmodial Assay Method

The test samples were prepared to a 10 mmol/L stock solution in 100% solvent. Samples were tested as a suspension if not completely dissolved. Further dilutions to the desired starting concentration were freshly prepared in growth media on each occasion of the experiment. The standard antimalarial drugs chloroquine (CQ) and artesunate (Arts) were used as the reference drug in all experiments. A full dose response was performed for all compounds in a 96-well plate to determine the concentration inhibiting 50% of parasite growth (IC_{50}–value). Test samples were tested at a starting concentration of 3 µmol/L, which was then serially diluted 2-fold in growth medium to generate the tested concentration range. The same dilution technique was used for all samples. CQ and Arts were tested from a starting concentration of 1µg/mL. The highest concentration of solvent to which the parasites were exposed was approximately 1% and had no measurable effect on the parasite viability (data not shown).

The assay plate was incubated at 37°C for 72 hours in a sealed gas chamber under 3% O_2 and 4% CO_2, with the balance being nitrogen.

After 72 hours, the wells in the assay plate were gently resuspended, and 15µL from each well was transferred to a duplicate plate containing 100µL of Malstat reagent and 25µL of nitroblue tetrazolium solution in each well. Plates were left to develop for 20 minutes in the dark, and then the absorbance of each well was quantified using a spectrophotometer at 620nM wavelength.

The remaining population of parasites at each concentration of the test compound was determined by comparing the absorbance of each well to the absorbance of a well containing the drug-free control. Survival was plotted against concentration, and the IC_{50} values were obtained using a non-linear dose-response curve fitting analysis via the Dotmatics software platform.

References

[1] World Health Organization, World Health Statistics 2023: Monitoring Health for the Sdgs, Sustainable Development Goals. **2023**, *27*.

[2] World malaria report 2021. WHO.int. https://www.who.int/teams/global-malaria-programme/reports/world-malaria-report-2021 (accessed 2024-08-05).

[3] Kwenti, T. E. Malaria and HIV Coinfection in Sub-Saharan Africa: Prevalence, Impact, and Treatment Strategies. *Res. Rep. Trop. Med.* **2018**, *9*, 123–136. https://doi.org/10.2147/rrtm.s154501.

[4] German Advisory Committee Blood (Arbeitskreis Blut), Subgroup 'Assessment of Pathogens Transmissible by Blood'. Human Immunodeficiency Virus (HIV). *Transfus. Med. Hemother.* **2016**, *43* (3), 203–222. https://doi.org/10.1159/000445852.

[5] Masenga, S. K.; Mweene, B. C.; Luwaya, E.; Muchaili, L.; Chona, M.; Kirabo, A. HIV–Host Cell Interactions. *Cells* **2023**, *12* (10), 1351. https://doi.org/10.3390/cells12101351.

[6] Williams, A.; Menon, S.; Crowe, M.; Agarwal, N.; Biccler, J.; Bbosa, N.; Ssemwanga, D.; Adungo, F.; Moecklinghoff, C.; Macartney, M.; Oriol-Mathieu, V. Geographic and Population Distributions of Human Immunodeficiency Virus (HIV)–1 and HIV-2 Circulating Subtypes: A Systematic Literature Review and Meta-Analysis (2010–2021). *J. Infect. Dis.* **2023**, *228* (11), 1583–1591. https://doi.org/10.1093/infdis/jiad327.

[7] Sharp, P. M.; Hahn, B. H. Origins of HIV and the AIDS Pandemic. *Cold Spring Harb. Perspect. Med.* **2011**, *1* (1), a006841. https://doi.org/10.1101/cshperspect.a006841.

[8] Vidya Vijayan, K. K.; Karthigeyan, K. P.; Tripathi, S. P.; Hanna, L. E. Pathophysiology of CD4+ T-Cell Depletion in HIV-1 and HIV-2 Infections. *Front. Immunol.* **2017**, *8*. https://doi.org/10.3389/fimmu.2017.00580.

[9] Center for Drug Evaluation and Research, U.S. Department of Health and Human Services, Food and Drug Administration (FDA). Guidance for Industry: Human Immunodeficiency Virus-1 Infection: Developing Antiretroviral Drugs for Treatment; Revision 1; **2015**; 1–39. Available online:http://www.fda.gov/Drugs/GuidanceComplianceRegulatoryInformation/Guidances/default.htm. (accessed 2024-08-05).

[10] Spach, D. H. Antiretroviral Medications and Initial Therapy HIV Life Cycle and Antiretroviral Drug Targets. *Natl. HIV Curric.* **2020**, *3* (1), 36. Available online:

https://cdn.hiv.uw.edu/pdf/antiretroviral-therapy/general-information/core-concept/all.

[11] Menéndez-Arias, L.; Delgado, R. Update and Latest Advances in Antiretroviral Therapy. *Trends Pharmacol. Sci.* **2022**, *43* (1), 16–29. https://doi.org/10.1016/j.tips.2021.10.004.

[12] Related C3 Roles. HIV Care Continuum. Targethiv.org. https://targethiv.org/sites/default/files/supporting-files/chw-00-HIV-Knowledge-Base-Manual.pdf (accessed 2024-08-07).

[13] Doitsh, G.; Greene, W. C. Dissecting How CD4 T Cells Are Lost during HIV Infection. Cell Host Microbe **2016**, *19* (3), 280–291. https://doi.org/10.1016/j.chom.2016.02.012.

[14] Cowling, B. J.; Ip, D. K. M.; Fang, V. J.; Suntarattiwong, P.; Olsen, S. J.; Levy, J.; Uyeki, T. M.; Leung, G. M.; Malik Peiris, J. S.; Chotpitayasunondh, T.; Nishiura, H.; Mark Simmerman, J. Aerosol Transmission Is an Important Mode of Influenza A Virus Spread. *Nat. Commun.* **2013**, *4* (1), 1935. https://doi.org/10.1038/ncomms2922.

[15] Centers for Disease Control & Prevention. HIV and Its Transmission, 1999 *1*. Available online: http://img.thebody.com/cdc/pdfs/transmission.pdf. (accessed 2024-08-07).

[16] Mohapatra, A.; Sahoo, D. Review on HIV AIDS. *Int. J. Psychosoc. Rehabil.* **2019**, *23* (6), 521–527. https://doi.org/10.37200/IJPR/V23I6/PR190803.

[17] Unaids.org. https://www.unaids.org/sites/default/files/media_asset/jc180-hiv-infantfeeding-3_en_0.pdf (accessed 2024-08-07)

[18] Njom Nlend, A. E. Mother-to-Child Transmission of HIV through Breastfeeding Improving Awareness and Education: A Short Narrative Review. *Int. J. Womens Health* **2022**, *14*, 697–703. https://doi.org/10.2147/ijwh.s330715.

[19] Joint United Nations Programme on HIV/AIDS. A Review of HIV Transmission Through Breastfeeding; UNICEF-UNAIDS-WHO HIV and Infant Feeding; World Health Organization: 1998. Available online: https://data.unaids.org/publications/irc-pub03/hivmod3_en.pdf (accessed 2024-08-07).

[20] Remien, R. H.; Higgins, J. A.; Correale, J.; Bauermeister, J.; Dubrow, R.; Bradley, M.; Steward, W. T.; Seal, D. W.; Sikkema, K. J.; Kerndt, P. R *et al.,* Lack of Understanding of Acute HIV Infection among Newly-Infected Persons—Implications for Prevention and Public Health: The NIMH Multisite Acute HIV Infection Study: II. *AIDS Behav*. **2009**, *13* (6). https://doi.org/10.1007/s10461-009-9581-7.

[21] Forsythe, S. S.; McGreevey, W.; Whiteside, A.; Shah, M.; Cohen, J.; Hecht, R.; Bollinger, L. A.; Kinghorn, A. Twenty Years of Antiretroviral Therapy for People Living

with HIV: Global Costs, Health Achievements, Economic Benefits. *Health Aff. (Millwood)* **2019**, *38* (7), 1163–1172. https://doi.org/10.1377/hlthaff.2018.05391.

[22] Iftikhar, S.; Ghias, M.; Shahid, S.; Ali, M. R.; Hassan, M. U.; Numan, A. Clinical and Biochemical Indicators of Disease Severity and Neurological Findings in COVID-19: A Study of King Edward Medical University (KEMU), Pakistan. *Pak. J. Pharm. Sci.* **2021**, *34* (1(Supplementary)), 275–281.

[23] Chang, C. C.; Crane, M.; Zhou, J.; Mina, M.; Post, J. J.; Cameron, B. A.; Lloyd, A. R.; Jaworowski, A.; French, M. A.; Lewin, S. R. HIV and Co-infections. *Immunol. Rev.* **2013**, *254* (1), 114–142. https://doi.org/10.1111/imr.12063

[24] Who.int. https://cdn.who.int/media/docs/default-source/hq-hiv-hepatitis-and-stis-library/j0294-who-hiv-epi-factsheet-v7.pdf (accessed 2024-08-07).

[25] UNAIDS data 2021. Unaids.org. https://www.unaids.org/en/resources/documents/2021/2021_unaids_data (accessed 2024-08-07).

[26] Dufour, I.; Fougère, Y.; Goetghebuer, T.; Hainaut, M.; Mbiya, B.; Kakkar, F.; Yombi, J. C.; Van der Linden, D. Gen Z and HIV—Strategies for Optimizing the Care of the next Generation of Adolescents Living with HIV. *Viruses* **2023**, *15* (10), 2023. https://doi.org/10.3390/v15102023.

[27] Nzengui-Nzengui, G. F.; Mourembou, G.; M'boyis-Kamdem, H.; Kombila-Koumavor, A. C.; Ndjoyi-Mbiguino, A. HIV Protease Resistance Mutations in Patients Receiving Second-Line Antiretroviral Therapy in Libreville, Gabon. *BMC Infect. Dis*. **2024***, 24* (1). https://doi.org/10.1186/s12879-024-09156-9.

[28] Brown, T.; Peerapatanapokin, W. Evolving HIV Epidemics: The Urgent Need to Refocus on Populations with Risk. *Curr. Opin. HIV AIDS* **2019,** *14* (5), 337–353. https://doi.org/10.1097/coh.0000000000000571.

[29] Richter, F. 10 countries account for almost half of new HIV infections. Statista. https://www.statista.com/chart/2477/new-hiv-infections-by-country/ (accessed 2024-08-07).

[30] *New HIV survey highlights progress and ongoing disparities in South Africa's HIV epidemic - HSRC*. HSRC - Human Sciences Research Council. https://hsrc.ac.za/press-releases/hsc/new-hiv-survey-highlights-progress-and-ongoing-disparities-in-south-africas-hiv-epidemic/ (accessed 2024-08-05).

[31] Pre-exposure prophylaxis (PrEP). Cdc.gov. https://www.cdc.gov/hiv/risk/prep/index.html (accessed 2024-08-07).

[32] Ochodo, E. A.; Olwanda, E. E.; Deeks, J. J.; Mallett, S. Point-of-Care Viral Load Tests to Detect High HIV Viral Load in People Living with HIV/AIDS Attending Health Facilities. *Cochrane Libr.* **2022**, *2022* (3). https://doi.org/10.1002/14651858.cd013208.pub2

[33] Lobritz, M. A.; Ratcliff, A. N.; Arts, E. J. HIV-1 Entry, Inhibitors, and Resistance. *Viruses* **2010**, *2* (5), 1069–1105. https://doi.org/10.3390/v2051069.

[34] Wang, T.; Ueda, Y.; Zhang, Z.; Yin, Z.; Matiskella, J.; Pearce, B. C.; Yang, Z.; Zheng, M.; Parker, D. D.; Yamanaka, G. A.; Gong, Y.-F.; Ho, H.-T.; Colonno, R. J.; Langley, D. R.; Lin, P.-F.; Meanwell, N. A.; Kadow, J. F. Discovery of the Human Immunodeficiency Virus Type 1 (HIV-1) Attachment Inhibitor Temsavir and Its Phosphonooxymethyl Prodrug Fostemsavir. *J. Med. Chem.* **2018**, *61* (14), 6308–6327. https://doi.org/10.1021/acs.jmedchem.8b00759.

[35] Moore, K.; Thakkar, N.; Magee, M.; Sevinsky, H.; Vakkalagadda, B.; Lubin, S.; Llamoso, C.; Ackerman, P. Pharmacokinetics of Temsavir, the Active Moiety of the HIV-1 Attachment Inhibitor Prodrug, Fostemsavir, Coadministered with Cobicistat, Etravirine, Darunavir/Cobicistat, or Darunavir/Ritonavir with or without Etravirine in Healthy Participants. *Antimicrob. Agents Chemother*. **2022**, *66* (4). https://doi.org/10.1128/aac.02251-21.

[36] Huet, T.; Kerbarh, O.; Schols, D.; Clayette, P.; Gauchet, C.; Dubreucq, G.; Vincent, L.; Bompais, H.; Mazinghien, R.; Querolle, O.; Salvador, A.; Lemoine, J.; Lucidi, B.; Balzarini, J.; Petitou, M. Long-Lasting Enfuvirtide Carrier Pentasaccharide Conjugates with Potent Anti-Human Immunodeficiency Virus Type 1 Activity. *Antimicrob. Agents Chemother.* **2010**, *54* (1), 134–142. https://doi.org/10.1128/aac.00827-09.

[37] Singh, V. K.; Mishra, R.; Kumari, P.; Som, A.; Yadav, A. K.; Ram, N. K.; Kumar, P.; Schols, D.; Singh, R. K. In Silico Design, Synthesis and Anti-HIV Activity of Quinoline Derivatives as Non-Nucleoside Reverse Transcriptase Inhibitors (NNRTIs). *Comput. Biol. Chem.* **2022**, *98* (107675), 107675. https://doi.org/10.1016/j.compbiolchem.2022.107675

[38] Zhao, A. V.; Crutchley, R. D.; Guduru, R. C.; Ton, K.; Lam, T.; Min, A. C. A Clinical Review of HIV Integrase Strand Transfer Inhibitors (INSTIs) for the Prevention and Treatment of HIV-1 Infection. *Retrovirology* **2022**, *19* (1). https://doi.org/10.1186/s12977-022-00608-1.

[39] Yang, H.; Nkeze, J.; Zhao, R. Y. Effects of HIV-1 Protease on Cellular Functions and Their Potential Applications in Antiretroviral Therapy. *Cell Biosci.* **2012**, *2* (1). https://doi.org/10.1186/2045-3701-2-32.

[40] Clinical trial of HIV vaccine begins in United States and South Africa. National Institutes of Health (NIH). https://www.nih.gov/news-events/news-releases/clinical-trial-hiv-vaccine-begins-united-states-south-africa (accessed 2024-08-07).

[41] Ng'uni, T.; Chasara, C.; Ndhlovu, Z. M. Major Scientific Hurdles in HIV Vaccine Development: Historical Perspective and Future Directions. *Front. Immunol.* **2020**, *11*. https://doi.org/10.3389/fimmu.2020.590780.

[42] Stieh, D. J.; Barouch, D. H.; Comeaux, C.; Sarnecki, M.; Stephenson, K. E.; Walsh, S. R.; Sawant, S.; Heptinstall, J.; Tomaras, G. D.; Kublin, J. G.; the ASCENT/HVTN118/HPX2003 Study Team *et al.*, Safety and Immunogenicity of Ad26-Vectored HIV Vaccine with Mosaic Immunogens and a Novel Mosaic Envelope Protein in HIV-Uninfected Adults: A Phase 1/2a Study. *J. Infect. Dis.* **2023**, *227* (8), 939–950. https://doi.org/10.1093/infdis/jiac445.

[43] Rosengarten, J. F.; Schatz, S.; Wolf, T.; Barbe, S.; Stitz, J. Components of a HIV-1 Vaccine Mediate Virus-like Particle (VLP)-Formation and Display of Envelope Proteins Exposing Broadly Neutralizing Epitopes. *Virology* **2022**, *568*, 41–48. https://doi.org/10.1016/j.virol.2022.01.008.

[44] Jnj.com. https://www.jnj.com/media-center/press-releases/janssen-and-global-partners-to-discontinue-phase-3-mosaico-hiv-vaccine-clinical-trial (accessed 2024-08-07).

[45] Barouch, D. H.; Stephenson, K. E.; Borducchi, E. N.; Smith, K.; Stanley, K.; McNally, A. G.; Liu, J.; Abbink, P.; Maxfield, L. F.; Seaman, M. S *et al.,* Protective Efficacy of a Global HIV-1 Mosaic Vaccine against Heterologous SHIV Challenges in Rhesus Monkeys. *Cell* **2013**, *155* (3), 531–539. https://doi.org/10.1016/j.cell.2013.09.061.

[46] L. G. Bekker *et al.*, "The complex challenges of HIV vaccine development require renewed and expanded global commitment," *Lancet*, vol. 395, no. 10221, pp. 384–388, 2020, doi: 10.1016/S0140-6736(19)32682-0.

[47] Sato, S. Plasmodium—a Brief Introduction to the Parasites Causing Human Malaria and Their Basic Biology. *J. Physiol. Anthropol.* **2021**, *40* (1). https://doi.org/10.1186/s40101-020-00251-9.

[48] Keleta, Y.; Ramelow, J.; Cui, L.; Li, J. Molecular Interactions between Parasite and

Mosquito during Midgut Invasion as Targets to Block Malaria Transmission. *NPJ Vaccines* **2021**, *6* (1). https://doi.org/10.1038/s41541-021-00401-9.

[49] Plasmodium Anatomy Structure Unicellular Parasite Vertebrates stock vector (royalty free) 1900768300. Shutterstock. https://www.shutterstock.com/image-vector/plasmodium-anatomy-structure-unicellular-parasite-vertebrates-1900768300 (accessed 2024-08-07).

[50] Lee, W.-C.; Cheong, F. W.; Amir, A.; Lai, M. Y.; Tan, J. H.; Phang, W. K.; Shahari, S.; Lau, Y.-L. Plasmodium Knowlesi: The Game Changer for Malaria Eradication. *Malar. J.* **2022**, *21* (1). https://doi.org/10.1186/s12936-022-04131-8.

[51] Looareesuwan, P.; Krudsood, S.; Lawpoolsri, S.; Tangpukdee, N.; Matsee, W.; Nguitragool, W.; Wilairatana, P. Gametocyte Prevalence and Risk Factors of P. Falciparum Malaria Patients Admitted at the Hospital for Tropical Diseases, Thailand: A 20-Year Retrospective Study. *Malar. J.* **2023**, *22* (1). https://doi.org/10.1186/s12936-023-04728-7

[52] Wassmer, S. C.; Taylor, T. E.; Rathod, P. K.; Mishra, S. K.; Mohanty, S.; Arevalo-Herrera, M.; Duraisingh, M. T.; Smith, J. D. Investigating the Pathogenesis of Severe Malaria: A Multidisciplinary and Cross-Geographical Approach. *Am. J. Trop. Med. Hyg.* **2015**, *93* (3_Suppl), 42–56. https://doi.org/10.4269/ajtmh.14-0841.

[53] Wiser, M. F. Knobs, Adhesion, and Severe Falciparum Malaria. *Trop. Med. Infect. Dis.* **2023**, *8* (7), 353. https://doi.org/10.3390/tropicalmed8070353.

[54] Aly, A. S. I.; Vaughan, A. M.; Kappe, S. H. I. Malaria Parasite Development in the Mosquito and Infection of the Mammalian Host. *Annu. Rev. Microbiol.* **2009**, *63* (1), 195–221. https://doi.org/10.1146/annurev.micro.091208.073403.

[55] Gregson, A.; Plowe, C. V. Mechanisms of Resistance of Malaria Parasites to Antifolates. *Pharmacol. Rev.* **2005**, *57* (1), 117–145. https://doi.org/10.1124/pr.57.1.4.

[56] Pegoraro, S.; Duffey, M.; Otto, T. D.; Wang, Y.; Rösemann, R.; Baumgartner, R.; Fehler, S. K.; Lucantoni, L.; Avery, V. M.; Moreno-Sabater, A.; Mazier, D.; Vial, H. J.; Strobl, S.; Sanchez, C. P.; Lanzer, M. SC83288 Is a Clinical Development Candidate for the Treatment of Severe Malaria. *Nat. Commun.* **2017**, *8* (1). https://doi.org/10.1038/ncomms14193

[57] Ouattara, A.; Laurens, M. B. Vaccines against Malaria. *Clin. Infect. Dis*. **2015**, *60* (6), 930–936. https://doi.org/10.1093/cid/ciu954.

[58] Su, X.-Z.; Zhang, C.; Joy, D. A. Host-Malaria Parasite Interactions and Impacts on Mutual Evolution. *Front. Cell. Infect. Microbiol.* **2020**, *10*. https://doi.org/10.3389/fcimb.2020.587933.

[59] Laurens, M. B. RTS,S/AS01 Vaccine (MosquirixTM): An Overview. *Hum. Vaccin. Immunother.* **2020**, *16* (3), 480–489. https://doi.org/10.1080/21645515.2019.1669415.

[60] Emeje, M.; Ogu, E.; Chidebe, I.; Roko, G.; Abdullahi, M.; Sule Bibinu, D. Therapeutic Potential of Medicinal Plants: Current Situation and Outlook. In Medicinal Plants - Harnessing the Healing Power of Plants for Health [Working Title]; IntechOpen, **2024.**

[61] Vaughan, A. M.; Aly, A. S. I.; Kappe, S. H. I. Malaria Parasite Pre-Erythrocytic Stage Infection: Gliding and Hiding. *Cell Host Microbe* **2008,** *4* (3), 209–218. https://doi.org/10.1016/j.chom.2008.08.010.

[62] Nicd.ac.za. https://www.nicd.ac.za/wp-content/uploads/2017/03/National-Guidelines-for-Malaria-Treatment-SEPTEMBER-2019-Update-WITH-FRONT.pdf (accessed 2024-08-07).

[63] Boudová, S.; Cohee, L. M.; Kalilani-Phiri, L.; Thesing, P. C.; Kamiza, S.; Muehlenbachs, A.; Taylor, T. E.; Laufer, M. K. Pregnant Women Are a Reservoir of Malaria Transmission in Blantyre, Malawi. *Malar. J.* **2014**, *13* (1). https://doi.org/10.1186/1475-2875-13-506

[64] Takem, E. N.; D'Alessandro, U. MALARIA IN PREGNANCY. *Mediterr. J. Hematol. Infect. Dis.* **2013**, *5* (1), e2013010. https://doi.org/10.4084/mjhid.2013.010.

[65] (226) Kourtis, A. P.; Read, J. S.; Jamieson, D. J. Pregnancy and Infection. *N. Engl. J. Med.* **2014**, *370* (23), 2211–2218. https://doi.org/10.1056/nejmra1213566.

[66] Cutts, J. C.; Agius, P. A.; Lin, Z.; Powell, R.; Moore, K.; Draper, B.; Simpson, J. A.; Fowkes, F. J. I. Pregnancy-Specific Malarial Immunity and Risk of Malaria in Pregnancy and Adverse Birth Outcomes: A Systematic Review. *BMC Med.* **2020**, *18* (1). https://doi.org/10.1186/s12916-019-1467-6.

[67] Sharma, L.; Shukla, G. Placental Malaria: A New Insight into the Pathophysiology. *Front. Med. (Lausanne)* **2017**, *4*. https://doi.org/10.3389/fmed.2017.00117.

[68] Uneke, C. J. Impact of Placental Plasmodium Falciparum Malaria on Pregnancy and Perinatal Outcome in Sub-Saharan Africa: II: Effects of Placental Malaria on Perinatal Outcome; Malaria and HIV. *The Yale Journal of Biology and Medicine* **2007**, *80* (3), 95.

[69] Malaria. Who.int. https://www.who.int/news-room/fact-sheets/detail/malaria (accessed

2024-08-07).

[70] G. M. P. World malaria report 2010. Who.int. https://www.who.int/publications/i/item/9789241564106 (accessed 2024-08-07).

[71] Shi, D.; Wei, L.; Liang, H.; Yan, D.; Zhang, J.; Wang, Z. Trends of the Global, Regional and National Incidence, Mortality, and Disability-Adjusted Life Years of Malaria, 1990–2019: An Analysis of the Global Burden of Disease Study 2019. *Risk Manag. Healthc. Policy* **2023**, *16*, 1187–1201. https://doi.org/10.2147/rmhp.s419616.

[72] Goodarzi, E.; Beiranvand, R.; Darvishi, I.; Naghibzadeh-Tahami, A.; Bechashk, S. M.; Naemi, H.; Khazaei, Z. Geographical Distribution of Falciparum Malaria in the World and Its Relationship with the Human Development Index (HDI): Countries Based on the WHO Report in 2017. *Z. Gesundh. Wiss.* **2022**, *30* (3), 655–664. https://doi.org/10.1007/s10389-020-01336-6.

[73] Liu, X.; Song, C.; Ren, Z.; Wang, S. Predicting the Geographical Distribution of Malaria-Associated Anopheles Dirus in the South-East Asia and Western Pacific Regions under Climate Change Scenarios. *Front. Environ. Sci.* **2022**, *10*. https://doi.org/10.3389/fenvs.2022.841966.

[74] Sousa, A.; Aguilar-Alba, M.; Vetter, M.; García-Barrón, L.; Morales, J. Spatiotemporal Distribution of Malaria in Spain in a Global Change Context. *Atmosphere (Basel)* **2020**, *11* (4), 346. https://doi.org/10.3390/atmos11040346.

[75] (Malaria - Annual Epidemiological Report for 2021. **2023.**

[76] Béguin, A.; Hales, S.; Rocklöv, J.; Åström, C.; Louis, V. R.; Sauerborn, R. The Opposing Effects of Climate Change and Socio-Economic Development on the Global Distribution of Malaria. *Glob. Environ. Change* **2011**, *21* (4), 1209–1214. https://doi.org/10.1016/j.gloenvcha.2011.06.001.

[77] Phbsa.ac.za. https://www.phbsa.ac.za/wp-content/uploads/2024/02/PHBSA-Malaria-vector-surveillance-report-2022.pdf (accessed 2024-08-07).

[78] Moonasar, D.; Nuthulaganti, T.; Kruger, P. S.; Mabuza, A.; Rasiswi, E. S.; Benson, F. G.; Maharaj, R. Malaria Control in South Africa 2000–2010: Beyond MDG6. *Malar. J.* **2012**, *11* (1). https://doi.org/10.1186/1475-2875-11-294

[79] Balmith, M.; Basson, C.; Brand, S. J. The Malaria Burden: A South African Perspective. *J. Trop. Med*. **2024**, 2024, 1–17. https://doi.org/10.1155/2024/6619010. [80] Na-Bangchang, K.; Karbwang, J. Pharmacology of Antimalarial Drugs, Current Anti-

Malarials. In *Encyclopedia of Malaria*; Springer New York: New York, NY, **2019**. 1–82. https://doi.org/10.1007/978-1-4614-8757-9_149-1.

[81] Nicd.ac.za. https://www.nicd.ac.za/wp-content/uploads/2019/03/National-Guidelines-for-prevention-of-Malaria_updated-08012019-1.pdf (accessed 2024-08-05)..

[82] Bowman, L. R.; Donegan, S.; McCall, P. J. Is Dengue Vector Control Deficient in Effectiveness or Evidence?: Systematic Review and Meta-Analysis. *PLoS Negl. Trop. Dis.* **2016**, *10* (3), e0004551. https://doi.org/10.1371/journal.pntd.0004551.

[83] Perko, N.; Kebede, T.; A. Mousa, S. Current and Future Directions in the Prevention and Treatment of Malaria. *J. Pharm. Pharmacol. Res.* **2022**, *06* (03). https://doi.org/10.26502/fjppr.058

[84] Kim, D.; Kramer, R.; Fedak, K. Reduction of Malaria Prevalence by Indoor Residual Spraying: A Meta-Regression Analysis. *Am. J. Trop. Med. Hyg.* **2012**, *87* (1), 117–124. https://doi.org/10.4269/ajtmh.2012.11-0620.

[85] Cairns, M.; Ceesay, S. J.; Sagara, I.; Zongo, I.; Kessely, H.; Gamougam, K.; Diallo, A.; Ogboi, J. S.; Moroso, D.; Van Hulle, S.; Eloike, T.; Snell, P.; Scott, S.; Merle, C.; Bojang, K.; Ouedraogo, J. B.; Dicko, A.; Ndiaye, J.-L.; Milligan, P. Effectiveness of Seasonal Malaria Chemoprevention (SMC) Treatments When SMC Is Implemented at Scale: Case–Control Studies in 5 Countries. *PLoS Med.* **2021**, *18* (9), e1003727. https://doi.org/10.1371/journal.pmed.1003727.

[86] Nicd.ac.za. https://www.nicd.ac.za/wp-content/uploads/2019/10/MALARIA-ELIMINATION-STRATEGIC-PLAN-FOR-SOUTH-AFRICA-2019-2023-MALARIA-ELIMINATION-STRATEGIC-PLAN-2019-2023.pdf (accessed 2024-08-07).

[87] Tan, K. R.; Magill, A. J.; Arguin, P. M.; Parise, M. E. Doxycycline for Malaria Chemoprophylaxis and Treatment: Report from the CDC Expert Meeting on Malaria Chemoprophylaxis. *Am. J. Trop. Med. Hyg.* **2011**, *84* (4), 517–531. https://doi.org/10.4269/ajtmh.2011.10-0285.

[88] Steyn, L. Don't Overlook Malaria: What the Pharmacist Needs to Know. *SA Pharm. J.* **2021**, *88* (6), 36–41.

[89] WHO. WHO Recommendation on Antenatal Care for a Positive Pregnancy Experience: Summary. *Lancet* **2018,** *387* (10017), 1–10. DOI: 10.1186/1742-4755-10-19.5.

[90] Gachelin, G.; Garner, P.; Ferroni, E.; Tröhler, U.; Chalmers, I. Evaluating *Cinchona* Bark and Quinine for Treating and Preventing Malaria. *J. R. Soc.*

Med. **2017**, *110* (1), 31–40. https://doi.org/10.1177/0141076816681421..

[91] Tse, E. G.; Korsik, M.; Todd, M. H. The Past, Present and Future of Anti-Malarial Medicines. *Malar. J.* **2019**, *18* (1). https://doi.org/10.1186/s12936-019-2724-z

[92] White, N. J. Severe Malaria. *Malar. J.* **2022**, *21* (1). https://doi.org/10.1186/s12936-022-04301-8.

[93] White, N. J. Anti-malarial Drug Effects on Parasite Dynamics in Vivax Malaria. *Malar. J.* **2021**, *20* (1). https://doi.org/10.1186/s12936-021-03700-7

[94] Okebe, J.; Bousema, T.; Affara, M.; Di Tanna, G. L.; Dabira, E.; Gaye, A.; Sanya-Isijola, F.; Badji, H.; Correa, S.; Nwakanma, D.; Van Geertruyden, J.-P.; Drakeley, C.; D'Alessandro, U. The Gametocytocidal Efficacy of Different Single Doses of Primaquine with Dihydroartemisinin-Piperaquine in Asymptomatic Parasite Carriers in The Gambia: A Randomized Controlled Trial. *EBioMedicine* **2016**, *13*, 348–355. https://doi.org/10.1016/j.ebiom.2016.10.032.

[95] Bradley, J.; Soumaré, H. M.; Mahamar, A.; Diawara, H.; Roh, M.; Delves, M.; Drakeley, C.; Churcher, T. S.; Dicko, A.; Gosling, R.; Bousema, T. Transmission-Blocking Effects of Primaquine and Methylene Blue Suggest Plasmodium Falciparum Gametocyte Sterilization Rather than Effects on Sex Ratio. *Clin. Infect. Dis.* **2019**, *69* (8), 1436–1439. https://doi.org/10.1093/cid/ciz134

[96] Macintyre, F.; Ramachandruni, H.; Burrows, J. N.; Holm, R.; Thomas, A.; Möhrle, J. J.; Duparc, S.; Hooft van Huijsduijnen, R.; Greenwood, B.; Gutteridge, W. E.; Wells, T. N. C.; Kaszubska, W. Injectable Anti-Malarials Revisited: Discovery and Development of New Agents to Protect against Malaria. *Malar. J.* **2018**, *17* (1). https://doi.org/10.1186/s12936-018-2549-1.

[97] Wu, T.; Nagle, A.; Kuhen, K.; Gagaring, K.; Borboa, R.; Francek, C.; Chen, Z.; Plouffe, D.; Goh, A.; Lakshminarayana, S. B *et al.,* Imidazolopiperazines: Hit to Lead Optimization of New Antimalarial Agents. *J. Med. Chem*. **2011**, *54* (14), 5116–5130. https://doi.org/10.1021/jm2003359.

[98] Ogutu, B.; Yeka, A.; Kusemererwa, S.; Thompson, R.; Tinto, H.; Toure, A. O.; Uthaisin, C.; Verma, A.; Kibuuka, A.; Lingani, M et al., Ganaplacide (KAF156) plus Lumefantrine Solid Dispersion Formulation Combination for Uncomplicated Plasmodium Falciparum Malaria: An Open-Label, Multicentre, Parallel-Group, Randomised, Controlled, Phase 2 Trial. *Lancet Infect. Dis.* **2023**, *23* (9), 1051–1061. https://doi.org/10.1016/s1473-3099(23)00209-8.

[99] White, N. J.; Duong, T. T.; Uthaisin, C.; Nosten, F.; Phyo, A. P.; Hanboonkunupakarn, B.; Pukrittayakamee, S.; Jittamala, P.; Chuthasmit, K.; Cheung, M. S.; Feng, Y.; Li, R.; Magnusson, B.; Sultan, M.; Wieser, D.; Xun, X.; Zhao, R.; Diagana, T. T.; Pertel, P.; Leong, F. J. Antimalarial Activity of KAF156 in Falciparum and Vivax Malaria. *N. Engl. J. Med.* **2016**, *375* (12), 1152–1160. https://doi.org/10.1056/nejmoa1602250.

[100] Case Medical Research. Pharmacokinetics, Safety, Tolerability and Efficacy of a New Artemether-Lumefantrine Dispersible Tablet in Infants and Neonates <5 Kg Body Weight with Acute Uncomplicated Plasmodium Falciparum Malaria. Case Medical Research **2020**. https://doi.org/10.31525/ct1-nct04300309..

[101] Who.int. https://cdn.who.int/media/docs/default-source/immunization/mvip/full-evidence-report-on-the-rtss-as01-malaria-vaccine-for-sage-mpag-(sept2021).pdf (accessed 2024-08-07).

[102] The RTS,S Clinical Trials Partnership. A Phase 3 Trial of RTS,S/AS01 Malaria Vaccine in African Infants. *N. Engl. J. Med.* **2012**, *367* (24), 2284–2295. https://doi.org/10.1056/nejmoa1208394.

[103] Schmit, N.; Topazian, H. M.; Natama, H. M.; Bellamy, D.; Traoré, O.; Somé, M. A.; Rouamba, T.; Tahita, M. C.; Bonko, M. D. A.; Sourabié, A *et al.*, The Public Health Impact and Cost-Effectiveness of the R21/Matrix-M Malaria Vaccine: A Mathematical Modelling Study. *Lancet Infect. Dis*. **2024**, *24* (5), 465–475. https://doi.org/10.1016/s1473-3099(23)00816-2.

[104] Polhemus, M. E.; Remich, S. A.; Ogutu, B. R.; Waitumbi, J. N.; Otieno, L.; Apollo, S.; Cummings, J. F.; Kester, K. E.; Ockenhouse, C. F.; Stewart, A.; Ofori-Anyinam, O.; Ramboer, I.; Cahill, C. P.; Lievens, M.; Dubois, M.-C.; Demoitie, M.-A.; Leach, A.; Cohen, J.; Ballou, W. R.; Heppner, D. G. Evaluation of RTS,S/AS02A and RTS,S/AS01B in Adults in a High Malaria Transmission Area. *PLoS One* **2009**, *4* (7), e6465. https://doi.org/10.1371/journal.pone.0006465.

[105] Efficacy and Safety of RTS,S/AS01 Malaria Vaccine with or without a Booster Dose in Infants and Children in Africa: Final Results of a Phase 3, Individually Randomised, Controlled Trial. *Lancet* **2015**, 386 (9988), 31–45. https://doi.org/10.1016/s0140-6736(15)60721-8..

[106] Datoo, M. S.; Natama, M. H.; Somé, A.; Traoré, O.; Rouamba, T.; Bellamy, D.; Yameogo, P.; Valia, D.; Tegneri, M.; Ouedraogo, F *et al*., Efficacy of a Low-Dose Candidate Malaria Vaccine, R21 in Adjuvant Matrix-M, with Seasonal Administration to Children in Burkina Faso: A Randomised Controlled Trial. *Lancet* **2021**, *397* (10287),

1809–1818. https://doi.org/10.1016/s0140-6736(21)00943-0.

[107] Datoo, M. S.; Natama, H. M.; Somé, A.; Bellamy, D.; Traoré, O.; Rouamba, T.; Tahita, M. C.; Ido, N. F. A.; Yameogo, P.; Valia, D *et al.,* Efficacy and Immunogenicity of R21/Matrix-M Vaccine against Clinical Malaria after 2 Years' Follow-up in Children in Burkina Faso: A Phase 1/2b Randomised Controlled Trial. *Lancet Infect. Dis.* **2022**, *22* (12), 1728–1736. https://doi.org/10.1016/s1473-3099(22)00442-x..

[108] 18 million doses of first-ever malaria vaccine allocated to 12 African countries for 2023–2025: Gavi, WHO and UNICEF. Who.int. https://www.who.int/news/item/05-07-2023-18-million-doses-of-first-ever-malaria-vaccine-allocated-to-12-african-countries-for-2023-2025--gavi--who-and-unicef (accessed 2024-08-07).

[109] Datoo, M. S.; Dicko, A.; Tinto, H.; Ouédraogo, J.-B.; Hamaluba, M.; Olotu, A.; Beaumont, E.; Ramos Lopez, F.; Natama, H. M.; Weston, S.; Chemba, M.; Compaore, Y. D.; Issiaka, D.; Salou, D.; Some, A. M.; Omenda, S.; Lawrie, A.; Bejon, P.; Rao, H.; Chandramohan, D.; Roberts, R.; Bharati, S.; Stockdale, L.; Gairola, S.; Greenwood, B. M.; Ewer, K. J.; Bradley, J.; Kulkarni, P. S.; Shaligram, U.; Hill, A. V. S.; Mahamar, A.; Sanogo, K *et al.,* Safety and Efficacy of Malaria Vaccine Candidate R21/Matrix-M in African Children: A Multicentre, Double-Blind, Randomised, Phase 3 Trial. *Lancet* **2024**, *403* (10426), 533–544. https://doi.org/10.1016/s0140-6736(23)02511-4.

[110] Tsoumani, M. E.; Voyiatzaki, C.; Efstathiou, A. Malaria Vaccines: From the Past towards the mRNA Vaccine Era. *Vaccines (Basel)* **2023,** *11* (9), 1452. https://doi.org/10.3390/vaccines11091452.

[111] Genton, B. R21/Matrix-MTM Malaria Vaccine: A New Tool to Achieve WHO's Goal to Eliminate Malaria in 30 Countries by 2030? *J. Travel Med.* **2023**, *30* (8). https://doi.org/10.1093/jtm/taad140.

[112] Hill, S. A.; Datoo, M.; Stockdale, L. Oxford R21/Matrix-MTM malaria vaccine receives WHO recommendation for use paving the way for global roll-out. Ox.ac.uk. https://www.ox.ac.uk/news/2023-10-02-oxford-r21matrix-m-malaria-vaccine-receives-who-recommendation-use-paving-way-global (accessed 2024-08-07).

[113] Genton, B. R21/Matrix-MTM Malaria Vaccine: A New Tool to Achieve WHO's Goal to Eliminate Malaria in 30 Countries by 2030? *J. Travel Med.* **2023**, 30 (8). https://doi.org/10.1093/jtm/taad140.

[114] Silk, S. E.; Kalinga, W. F.; Mtaka, I. M.; Lilolime, N. S.; Mpina, M.; Milando, F.; Ahmed, S.; Diouf, A.; Mkwepu, F.; Simon, B. *et al.*, Superior Antibody Immunogenicity of a Viral-

Vectored RH5 Blood-Stage Malaria Vaccine in Tanzanian Infants as Compared to Adults. *Med (N. Y.)* **2023**, *4* (10), 668-686.e7. https://doi.org/10.1016/j.medj.2023.07.003.

[115] Rausch, K. M.; Barnafo, E. K.; Lambert, L. E.; Muratova, O.; Gorres, J. P.; Anderson, C.; Narum, D. L.; Wu, Y.; Morrison, R. D.; Zaidi, I.; Duffy, P. E. Preclinical Evaluations of Pfs25-EPA and Pfs230D1-EPA in AS01 for a Vaccine to Reduce Malaria Transmission. *iScience* **2023**, *26* (7), 107192. https://doi.org/10.1016/j.isci.2023.107192.

[116] Singh, N.; Chaturvedi, N.; Bharti, P.; Tiwari, A. Strategies & Recent Development of Transmission-Blocking Vaccines against Plasmodium Falciparum. *Indian J. Med. Res*. **2016**, *143* (6), 696. https://doi.org/10.4103/0971-5916.191927.

[117] Ejigu, S.; Haile, D.; Solomon, Y. Effect of Malaria and HIV/AIDS Co-Infection on Red Blood Cell Indices and Its Relation with the CD4 Level of Patients on HAART in Bench Sheko Zone, Southwest Ethiopia. *PLoS One* **2022**, *17* (3), e0263865. https://doi.org/10.1371/journal.pone.0263865.

[118] Saracino, A.; Nacarapa, E. A.; da Costa Massinga, É. A.; Martinelli, D.; Scacchetti, M.; de Oliveira, C.; Antonich, A.; Galloni, D.; Ferro, J. J.; Macome, C. A. Prevalence and Clinical Features of HIV and Malaria Co-Infection in Hospitalized Adults in Beira, Mozambique. *Malar. J*. **2012**, *11* (1). https://doi.org/10.1186/1475-2875-11-241.

[119] Roberds, A.; Ferraro, E.; Luckhart, S.; Stewart, V. A. HIV-1 Impact on Malaria Transmission: A Complex and Relevant Global Health Concern. *Front. Cell. Infect. Microbiol*. **2021**, *11*. https://doi.org/10.3389/fcimb.2021.656938.

[120] Hochman, S.; Kim, K. The Impact of HIV and Malaria Coinfection: What Is Known and Suggested Venues for Further Study. *Interdiscip. Perspect. Infect. Dis*. **2009**, *2009*, 1–8. https://doi.org/10.1155/2009/617954.

[121] Figueroa-Romero, A.; Saura-Lázaro, A.; Fernández-Luis, S.; González, R. Uncovering HIV and Malaria Interactions: The Latest Evidence and Knowledge Gaps. *Lancet HIV* **2024**, *11* (4), e255–e267. https://doi.org/10.1016/s2352-3018(24)00035-3.

[122] R. W.; Guerra, C. A.; Noor, A. M.; Myint, H. Y.; Hay, S. I. The Global Distribution of Clinical Episodes of Plasmodium Falciparum Malaria. *Nature* **2005**, *434* (7030), 214-217. DOI: 10.1038/nature03342.

[123] Polyak, C. S.; Yuhas, K.; Singa, B.; Khaemba, M.; Walson, J.; Richardson, B. A.; John-Stewart, G. Cotrimoxazole Prophylaxis Discontinuation among Antiretroviral-Treated

HIV-1-Infected Adults in Kenya: A Randomized Non-Inferiority Trial. *PLoS Med*. **2016**, *13* (1), e1001934. https://doi.org/10.1371/journal.pmed.1001934.

[124] Di Gennaro, F.; Marotta, C.; Pizzol, D.; Chhaganlal, K.; Monno, L.; Putoto, G.; Saracino, A.; Casuccio, A.; Mazzucco, W. Prevalence and Predictors of Malaria in Human Immunodeficiency Virus Infected Patients in Beira, Mozambique. *Int. J. Environ. Res. Public Health* **2018**, *15* (9), 2032. https://doi.org/10.3390/ijerph15092032..

[125] Alfonso, Y.; Monzote, L. HIV Protease Inhibitors: Effect on the Opportunistic Protozoan Parasites. *Open Med. Chem. J*. **2011**, *5*, 40–50. https://doi.org/10.2174/1874104501105010040.

[126] Currie, G. M. Pharmacology, Part 2: Introduction to Pharmacokinetics. *J. Nucl. Med. Technol*. **2018**, *46* (3), 221–230. https://doi.org/10.2967/jnmt.117.199638.

[127] Dalvie, D. K.; Testa, B. Principles of Drug Metabolism. *Burger's Medicinal Chemistry and Drug Discovery*. Wiley April 26, **2021**, 1–139. https://doi.org/10.1002/0471266949.bmc033.pub3.

[128] Li, Y.; Meng, Q.; Yang, M.; Liu, D.; Hou, X.; Tang, L.; Wang, X.; Lyu, Y.; Chen, X.; Liu, K.; Yu, A.-M.; Zuo, Z.; Bi, H. Current Trends in Drug Metabolism and Pharmacokinetics. *Acta Pharm. Sin. B*. **2019**, *9* (6), 1113–1144. https://doi.org/10.1016/j.apsb.2019.10.001.

[129] Kulsharova, G.; Kurmangaliyeva, A. Liver Microphysiological Platforms for Drug Metabolism Applications. *Cell Prolif.* **2021**, *54* (9). https://doi.org/10.1111/cpr.13099.

[130] Zhao, M.; Ma, J.; Li, M.; Zhang, Y.; Jiang, B.; Zhao, X.; Huai, C.; Shen, L.; Zhang, N.; He, L.; Qin, S. Cytochrome P450 Enzymes and Drug Metabolism in Humans. *Int. J. Mol. Sci*. **2021**, *22* (23), 12808. https://doi.org/10.3390/ijms222312808.

[131] Guengerich, F. P. Cytochrome P450 Research and the Journal of Biological Chemistry. *J. Biol. Chem*. **2019**, *294* (5), 1671–1680. https://doi.org/10.1074/jbc.tm118.004144.

[132] Zaal, E. A.; Berkers, C. R. The Influence of Metabolism on Drug Response in Cancer. *Front. Oncol*. **2018**, *8*. https://doi.org/10.3389/fonc.2018.00500..

[133] Gabay, M.; Spencer, S. H. Drug interactions: Scientific and clinical principles. *Accp.com*.https://www.accp.com/docs/bookstore/psap/p2021b3_sample.pdf (accessed 2024-08-05).

[134] Kinirons, M. T.; O'Mahony, M. S. Drug Metabolism and Ageing. *Br. J. Clin. Pharmacol*. **2004**, *57* (5), 540–544. https://doi.org/10.1111/j.1365-2125.2004.02096.x..

[135] Guieu, B.; Jourdan, J.-P.; Dreneau, A.; Willand, N.; Rochais, C.; Dallemagne, P. Desirable Drug–Drug Interactions or When a Matter of Concern Becomes a Renewed Therapeutic Strategy. *Drug Discov. Today.* **2021**, *26* (2), 315–328. https://doi.org/10.1016/j.drudis.2020.11.026.

[136] Zanger, U. M.; Schwab, M. Cytochrome P450 Enzymes in Drug Metabolism: Regulation of Gene Expression, Enzyme Activities, and Impact of Genetic Variation. *Pharmacol. Ther.* **2013**, 138 (1), 103–141. https://doi.org/10.1016/j.pharmthera.2012.12.007.

[137] Hakkola, J.; Hukkanen, J.; Turpeinen, M.; Pelkonen, O. Inhibition and Induction of CYP Enzymes in Humans: An Update. *Arch. Toxicol*. **2020**, *94* (11), 3671–3722. https://doi.org/10.1007/s00204-020-02936-7.

[138] Fichtenbaum, C. J.; Gerber, J. G. Interactions between Antiretroviral Drugs and Drugs Used for the Therapy of the Metabolic Complications Encountered during HIV Infection. *Clin. Pharmacokinet*. **2002**, *41* (14), 1195–1211. https://doi.org/10.2165/00003088-200241140-00004.

[139] Pham, H. T.; Xiao, M. A.; Principe, M. A. V.; Wong, A.; Mesplède, T. Pharmaceutical, Clinical, and Resistance Information on Doravirine, a Novel Non-Nucleoside Reverse Transcriptase Inhibitor for the Treatment of HIV-1 Infection. *Drugs Context.* **2020**, *9*, 1–11. https://doi.org/10.7573/dic.2019-11-4.

[140] Xing, J.; Kirby, B. J.; Whittington, D.; Wan, Y.; Goodlett, D. R. Evaluation of P450 Inhibition and Induction by Artemisinin Antimalarials in Human Liver Microsomes and Primary Human Hepatocytes. *Drug Metab. Dispos*. **2012**, *40* (9), 1757–1764. https://doi.org/10.1124/dmd.112.045765.

[141] Prestinaci, F.; Pezzotti, P.; Pantosti, A. Antimicrobial Resistance: A Global Multifaceted Phenomenon. *Pathog. Glob. Health* **2015**, *109* (7), 309–318. https://doi.org/10.1179/2047773215y.0000000030.

[142] Eggleston, K.; Zhang, R.; Zeckhauser, R. J. The Global Challenge of Antimicrobial Resistance: Insights from Economic Analysis. I*nt. J. Environ. Res. Public Health*. **2010**, *7* (8), 3141–3149. https://doi.org/10.3390/ijerph7083141.

[143] Laxminarayan, R.; Heymann, D. L. Challenges of Drug Resistance in the Developing World. *BMJ* **2012**, *344* (apr03 2), e1567–e1567. https://doi.org/10.1136/bmj.e1567.

[144] Cohen, M. L. Epidemiology of Drug Resistance: Implications for a Post—Antimicrobial Era. *Science*. **1992**, *257* (5073), 1050–1055. https://doi.org/10.1126/science.257.5073.1050.

[145] Davies, J. Bacteria on the Rampage. *Nature* **1996**, *383* (6597), 219–220. https://doi.org/10.1038/383219a0.

[146] National Institute on Drug Abuse. *Summary of misuse of prescription drugs*. National Institute on Drug Abuse. https://nida.nih.gov/publications/research-reports/misuse-prescription-drugs/overview (accessed 2024-08-05).

[147] Albarqouni, L.; Palagama, S.; Chai, J.; Sivananthajothy, P.; Pathirana, T.; Bakhit, M.; Arab-Zozani, M.; Ranakusuma, R.; Cardona, M.; Scott, A *et al.*, Overuse of Medications in Low- and Middle-Income Countries: A Scoping Review. *Bull. World Health Organ*. **2023**, *101* (1), 36-61D. https://doi.org/10.2471/blt.22.288293.

[148] Meid, A. D.; Lampert, A.; Burnett, A.; Seidling, H. M.; Haefeli, W. E. The Impact of Pharmaceutical Care Interventions for Medication Underuse in Older People: A Systematic Review and Meta-analysis. *Br. J. Clin. Pharmacol*. **2015**, *80* (4), 768–776. https://doi.org/10.1111/bcp.12657.

[149] Cui, X.; Lü, Y.; Yue, C. Development and Research Progress of Anti-Drug Resistant Bacteria Drugs. *Infect. Drug Resist*. **2021**, *14*, 5575–5593. https://doi.org/10.2147/idr.s338987.

[150] C Reygaert, W.; Department of Biomedical Sciences, Oakland University William Beaumont School of Medicine, Rochester, MI, USA. An Overview of the Antimicrobial Resistance Mechanisms of Bacteria. *AIMS Microbiol*. **2018**, *4* (3), 482–501. https://doi.org/10.3934/microbiol.2018.3.482.

[151] de Souza, N. B.; Carmo, A. M. L.; da Silva, A. D.; França, T. C. C.; Krettli, A. U. Antiplasmodial Activity of Chloroquine Analogs against Chloroquine-Resistant Parasites, Docking Studies, and Mechanisms of Drug Action. *Malar. J*. **2014**, *13*, 1-12. DOI: 10.1186/1475-2875-13-469.

[152] (117) Butler, A. R.; Khan, S.; Ferguson, E. A Brief History of Malaria Chemotherapy. *J. R. Coll. Physicians Edinb*. **2010**, *40* (2), 172–177. https://doi.org/10.4997/jrcpe.2010.216.

[153] Mucklow, J. C. Adverse Drug Reactions. *Br. J. Clin. Pharmacol*. **2001**, *52* (4), 461–461. https://doi.org/10.1046/j.0306-5251.2001.01462.x.

[154] Aguiar, A. C. C.; Murce, E.; Cortopassi, W. A.; Pimentel, A. S.; Almeida, M. M. F. S.; Barros, D. C. S.; Guedes, J. S.; Meneghetti, M. R.; Krettli, A. U. Chloroquine Analogs as Antimalarial Candidates with Potent in Vitro and in Vivo Activity. *Int. J. Parasitol. Drugs Drug Resist.* **2018**, *8* (3), 459–464. https://doi.org/10.1016/j.ijpddr.2018.10.002.

[155] Counihan, N. A.; Modak, J. K.; de Koning-Ward, T. F. How Malaria Parasites Acquire Nutrients from Their Host. *Front. Cell Dev. Biol*. **2021**, *9*. https://doi.org/10.3389/fcell.2021.649184.

[156] Talman, A. M.; Ouologuem, D. T. D.; Love, K.; Howick, V. M.; Mulamba, C.; Haidara, A.; Dara, N.; Sylla, D.; Sacko, A.; Coulibaly, M. M. *et al.,* Uptake of Plasmodium Falciparum Gametocytes during Mosquito Bloodmeal by Direct and Membrane Feeding. *Front. Microbiol.* **2020**, *11*. https://doi.org/10.3389/fmicb.2020.00246.

[157] Olafson, K. N.; Ketchum, M. A.; Rimer, J. D.; Vekilov, P. G. Mechanisms of Hematin Crystallization and Inhibition by the Antimalarial Drug Chloroquine. *Proc. Natl. Acad. Sci. U. S. A*. **2015**, *112* (16), 4946–4951. https://doi.org/10.1073/pnas.1501023112.

[158] Bolarin, J. A.; Oluwatoyosi, M. A.; Orege, J. I.; Ayeni, E. A.; Ibrahim, Y. A.; Adeyemi, S. B.; Tiamiyu, B. B.; Gbadegesin, L. A.; Akinyemi, T. O.; Odoh, C. K.; Umeobi, H. I.; Adeoye, A. B.-E. Therapeutic Drugs for SARS-CoV-2 Treatment: Current State and Perspective. *Int. Immunopharmacol.* **2021**, *90* (107228), 107228. https://doi.org/10.1016/j.intimp.2020.107228.

[159] Solomon, V. R.; Haq, W.; Smilkstein, M.; Srivastava, K.; Puri, S. K.; Katti, S. B. 4-Aminoquinoline Derived Antimalarials: Synthesis, Antiplasmodial Activity and Heme Polymerization Inhibition Studies. *Eur. J. Med. Chem.* **2010**, *45* (11), 4990–4996. https://doi.org/10.1016/j.ejmech.2010.07.068.

[160] Olafson, K. N.; Nguyen, T. Q.; Rimer, J. D.; Vekilov, P. G. Antimalarials Inhibit Hematin Crystallization by Unique Drug–Surface Site Interactions. *Proc. Natl. Acad. Sci. U. S. A.* **2017**, *114* (29), 7531–7536. https://doi.org/10.1073/pnas.1700125114.

[161] Soto, S. M. Role of Efflux Pumps in the Antibiotic Resistance of Bacteria Embedded in a Biofilm. *Virulence* **2013**, *4* (3), 223–229. https://doi.org/10.4161/viru.23724.

[162] Sidhu, A. B. S.; Verdier-Pinard, D.; Fidock, D. A. Chloroquine Resistance in Plasmodium Falciparum Malaria Parasites Conferred by Pfcrt Mutations. *Science* **2002**, *298* (5591), 210–213. https://doi.org/10.1126/science.1074045.

[163] Agnello, S.; Brand, M.; Chellat, M. F.; Gazzola, S.; Riedl, R. A Structural View on Medicinal Chemistry Strategies against Drug Resistance. Angew. *Chem. Int. Ed Engl*. **2019**, *58* (11), 3300–3345. https://doi.org/10.1002/anie.201802416.

[164] Pereira, M.; Vale, N. Saquinavir: From HIV to COVID-19 and Cancer Treatment. *Biomolecules* **2022**, *12* (7), 944. https://doi.org/10.3390/biom12070944.

[165] Sajeb.org. http://sajeb.org/index.php/sajeb/article/view/13431 (accessed 2024-08-07).

[166] Edition, 2021 •. 9th. of HIV/AIDS-Related Terms. Hiv.gov. https://clinicalinfo.hiv.gov/sites/default/files/glossary/Glossary-English_HIVinfo.pdf (accessed 2024-08-05).

[167] Pennings, P. S. HIV Drug Resistance: Problems and Perspectives. *Infect. Dis. Rep*. **2013**, *5* (11), e5. https://doi.org/10.4081/idr.2013.s1.e5.

[168] Xavier RUIZ, F.; Arnold, E. Evolving Understanding of HIV-1 Reverse Transcriptase Structure, Function, Inhibition, and Resistance. *Curr. Opin. Struct. Biol.* **2020**, *61*, 113–123. https://doi.org/10.1016/j.sbi.2019.11.011.

[169] Pokorná, J.; Machala, L.; Řezáčová, P.; Konvalinka, J. Current and Novel Inhibitors of HIV Protease. *Viruses* **2009**, *1* (3), 1209–1239. https://doi.org/10.3390/v1031209.

[170] Tamma, P. D.; Cosgrove, S. E.; Maragakis, L. L. Combination Therapy for Treatment of Infections with Gram-Negative Bacteria. *Clin. Microbiol. Rev.* **2012**, *25* (3), 450–470. https://doi.org/10.1128/cmr.05041-11.

[171] Singh, A. K.; Kumar, A.; Singh, H.; Sonawane, P.; Paliwal, H.; Thareja, S.; Pathak, P.; Grishina, M.; Jaremko, M.; Emwas, A.-H *et al.,* Concept of Hybrid Drugs and Recent Advancements in Anticancer Hybrids. *Pharmaceuticals (Basel)* **2022**, *15* (9), 1071. https://doi.org/10.3390/ph15091071.

[172] Domalaon, R.; Idowu, T.; Zhanel, G. G.; Frank Schweizer. Antibiotic Hybrids: The next Generation of Agents and Adjuvants against Gram-Negative Pathogens? *Clin. Microbiol. Rev.* 2018, *31* (2). https://doi.org/10.1128/cmr.00077-17.

[173] Meunier, B. Hybrid Molecules with a Dual Mode of Action: Dream or Reality? *Acc. Chem. Res.* **2008**, *41* (1), 69–77. https://doi.org/10.1021/ar7000843.

[174] Long, D. D.; Aggen, J. B.; Christensen, B. G.; Judice, J. K.; Hegde, S. S.; Kaniga, K.; Krause, K. M.; Linsell, M. S.; Moran, E. J.; Pace, J. L. A Multivalent Approach to Drug Discovery for Novel Antibiotics. J. *Antibiot. (Tokyo)* **2008**, *61* (10), 595–602. https://doi.org/10.1038/ja.2008.79.

[175] Hu, Y.-Q.; Gao, C.; Zhang, S.; Xu, L.; Xu, Z.; Feng, L.-S.; Wu, X.; Zhao, F. Quinoline Hybrids and Their Antiplasmodial and Antimalarial Activities. *Eur. J. Med. Chem.* **2017**, *139*, 22–47. https://doi.org/10.1016/j.ejmech.2017.07.061.

[176] Szumilak, M.; Wiktorowska-Owczarek, A.; Stanczak, A. Hybrid Drugs—A Strategy for Overcoming Anticancer Drug Resistance? *Molecules* **2021**, *26* (9), 2601.

https://doi.org/10.3390/molecules26092601.

[177] Morphy, R.; Kay, C.; Rankovic, Z. From Magic Bullets to Designed Multiple Ligands. *Drug Discov. Today* **2004**, *9* (15), 641–651. https://doi.org/10.1016/s1359-6446(04)03163-0.

[178] Alkhzem, A. H.; Woodman, T. J.; Blagbrough, I. S. Design and Synthesis of Hybrid Compounds as Novel Drugs and Medicines. *RSC Adv*. **2022**, *12* (30), 19470–19484. https://doi.org/10.1039/d2ra03281c.

[179] Bargh, J. D.; Isidro-Llobet, A.; Parker, J. S.; Spring, D. R. Cleavable Linkers in Antibody–Drug Conjugates. *Chem. Soc. Rev*. **2019**, *48* (16), 4361–4374. https://doi.org/10.1039/c8cs00676h.

[180] (143) Załuski, M.; Karcz, T.; Drabczyńska, A.; Vielmuth, C.; Olejarz-Maciej, A.; Głuch-Lutwin, M.; Mordyl, B.; Siwek, A.; Satała, G.; Müller, C. E.; Kieć-Kononowicz, K. Xanthine–Dopamine Hybrid Molecules as Multitarget Drugs with Potential for the Treatment of Neurodegenerative Diseases. *Biomolecules* **2023**, *13* (7), 1079. https://doi.org/10.3390/biom13071079.

[181] Berger, G. K.; McBride, A.; Lawson, S.; Royball, K.; Yun, S.; Gee, K.; Bin Riaz, I.; Saleh, A. A.; Puvvada, S.; Anwer, F. Brentuximab Vedotin for Treatment of Non-Hodgkin Lymphomas: A Systematic Review. *Crit. Rev. Oncol. Hematol.* **2017,** *109*, 42–50. https://doi.org/10.1016/j.critrevonc.2016.11.009.

[182] Peddi, P. F.; Hurvitz, S. A. Trastuzumab Emtansine: The First Targeted Chemotherapy for Treatment of Breast Cancer. *Future Oncol*. **2013**, *9* (3), 319–326. https://doi.org/10.2217/fon.13.7.

[183] Chu, X. Y.; Zhang, C. C.; Zhang, R. X.; Zhang, J. F.; Xia, B.; Wu, J. W. Identification of Dacinostat as a Potential Anti-Obesity Compound through Transcriptional Activation of Adipose Thermogenesis in Mice. *Biochim. Biophys. Acta Mol. Basis Dis.* **2021**, *1867* (9), 166-169. https://doi.org/10.1016/j.bbadis.2021.166169.

[184] Sun, D.; Gao, W.; Hu, H.; Zhou, S. Why 90% of Clinical Drug Development Fails and How to Improve It? *Acta Pharm. Sin. B*. **2022**, *12* (7), 3049–3062. https://doi.org/10.1016/j.apsb.2022.02.002.

[185] Macchiarulo, A. Drug Selectivity: An Evolving Concept in Medicinal Chemistry. Edited by Norbert Handler and Helmut Buschmann. *ChemMedChem* **2018**, *13* (18), 2009–2010. https://doi.org/10.1002/cmdc.201800493.

[186] Pawełczyk, A.; Sowa-Kasprzak, K.; Olender, D.; Zaprutko, L. Molecular Consortia—Various Structural and Synthetic Concepts for More Effective Therapeutics Synthesis. *Int. J. Mol. Sci*. **2018**, *19* (4), 1104. https://doi.org/10.3390/ijms19041104.

[187] Merk, D.; Schubert-Zsilavecz, M. The Linker Approach in Drug Conjugates. In *Methods and Principles in Medicinal Chemistry*; Handler, N., Buschmann, H., Eds.; Wiley-VCH: Weinheim, 2017; Chapter 8. https://doi.org/10.1002/9783527674381.ch8.

[188] Alkhzem, A. H.; Woodman, T. J.; Blagbrough, I. S. Design and Synthesis of Hybrid Compounds as Novel Drugs and Medicines. *RSC Adv*. **2022**, *12* (30), 19470–19484. https://doi.org/10.1039/d2ra03281c.

[189] Yang, X.; Pan, Z.; Choudhury, M. R.; Yuan, Z.; Anifowose, A.; Yu, B.; Wang, W.; Wang, B. Making Smart Drugs Smarter: The Importance of Linker Chemistry in Targeted Drug Delivery. *Med. Res. Rev*. **2020**, *40* (6), 2682–2713. https://doi.org/10.1002/med.21720.

[190] Thelingwani, R.; Bonn, B.; Chibale, K.; Masimirembwa, C. Physicochemical and Drug Metabolism Characterization of a Series of 4-Aminoquinoline-3-Hydroxypyridin-4-One Hybrid Molecules with Antimalarial Activity. *Expert Opin. Drug Metab. Toxicol.* **2014**, *10* (10), 1313–1324. https://doi.org/10.1517/17425255.2014.954547.

[191] Andayi, W. A.; Egan, T. J.; Gut, J.; Rosenthal, P. J.; Chibale, K. Synthesis, Antiplasmodial Activity, and β-Hematin Inhibition of Hydroxypyridone–Chloroquine Hybrids. *ACS Med. Chem. Lett*. **2013**, *4* (7), 642–646. https://doi.org/10.1021/ml4001084.

[192] Andayi, W. A.; Egan, T. J.; Chibale, K. Kojic Acid Derived Hydroxypyridinone–Chloroquine Hybrids: Synthesis, Crystal Structure, Antiplasmodial Activity and β-Haematin Inhibition. *Bioorg. Med. Chem. Lett*. **2014**, *24* (15), 3263–3267. https://doi.org/10.1016/j.bmcl.2014.06.012.

[193] Andayi, W. A. *Synthesis, Antimalarial Evaluation, β-Hematin Inhibition, and In Silico and In Vitro ADMET Profiling of 4-Aminoquinoline-Hydroxypyridinone Hybrids*; Ph.D. Thesis, University of Cape Town, Department of Chemical Engineering, Faculty of Engineering and the Built Environment, 2007. Available online: http://hdl.handle.net/11427/14824. (accessed 2024-08-05)

[194] Matada, B. S.; Pattanashettar, R.; Yernale, N. G. A Comprehensive Review on the Biological Interest of Quinoline and Its Derivatives. *Bioorg. Med. Chem.* **2021**, *32* (115973), 115973. https://doi.org/10.1016/j.bmc.2020.115973.

[195] Mishra, P.; Kumar, A.; Sharma, U. C.; Saxena, A.; Prabahar, A. E.; Gupta, S.; Verma,

A. K. Quinoline Derivative and Their Pharmacological & Medicinal Potential. *Int. J. Health Sci. (IJHS)* **2022**, 2016–2040. https://doi.org/10.53730/ijhs.v6ns3.5918.

[196] Musiol, R. An Overview of Quinoline as a Privileged Scaffold in Cancer Drug Discovery. *Expert Opin. Drug Discov*. **2017**, *12* (6), 583–597. https://doi.org/10.1080/17460441.2017.1319357.

[197] Kaur, R.; Kumar, K. Synthetic and Medicinal Perspective of Quinolines as Antiviral Agents. *Eur. J. Med. Chem.* **2021**, *215* (113220), 113220. https://doi.org/10.1016/j.ejmech.2021.113220.

[198] Mondal, S. UNIT –V Heterocyclic Chemistry Quinoline, Isoquinoline and Indole. Unpublished **2018**. https://doi.org/10.13140/RG.2.2.10944.43524.

[199] Kumar, N.; Khanna, A.; Kaur, K.; Kaur, H.; Sharma, A.; Bedi, P. M. S. Quinoline Derivatives Volunteering against Antimicrobial Resistance: Rational Approaches, Design Strategies, Structure Activity Relationship and Mechanistic Insights. *Mol. Divers.* **2023**, *27* (4), 1905–1934. https://doi.org/10.1007/s11030-022-10537-y.

[200] Raj, R.; Land, K. M.; Kumar, V. 4-Aminoquinoline-Hybridization En Route towards the Development of Rationally Designed Antimalarial Agents. *RSC Adv.* **2015**, *5* (101), 82676–82698. https://doi.org/10.1039/c5ra16361g.

[201] Fakhfakh, M. A.; Fournet, A.; Prina, E.; Mouscadet, J.-F.; Franck, X.; Hocquemiller, R.; Figadère, B. Synthesis and Biological Evaluation of Substituted Quinolines: Potential Treatment of Protozoal and Retroviral Co-Infections. *Bioorg. Med. Chem*. **2003**, *11* (23), 5013–5023. https://doi.org/10.1016/j.bmc.2003.09.007.

[202] Silva, A. T.; Bento, C. M.; Pena, A. C.; Figueiredo, L. M.; Prudêncio, C.; Aguiar, L.; Silva, T.; Ferraz, R.; Gomes, M. S.; Teixeira, C.; Gomes, P. Cinnamic Acid Conjugates in the Rescuing and Repurposing of Classical Antimalarial Drugs. *Molecules* **2019**, *25* (1), 66. https://doi.org/10.3390/molecules25010066.

[203] Solomon, V.; Haq, W.; Smilkstein, M.; Srivastava, K.; Rajakumar, S.; Puri, S.; Katti, S. Synthesis and Antimalarial Activity of Novel Side Chain Modified Antimalarial Agents Derived from 4-Aminoquinoline. *Med. Chem*. **2008**, *4* (5), 446–456. https://doi.org/10.2174/157340608785700207.

[204] Wang, R.; Xu, K.; Shi, W. Quinolone Derivatives: Potential anti-HIV Agent—Development and Application. *Arch. Pharm. (Weinheim)* **2019**, *352* (9). https://doi.org/10.1002/ardp.201900045.

[205] Smith, M. B. Organic Synthesis, 4th ed.; Elsevier: Amsterdam, **2017**; pp. 1–1083. https://doi.org/10.1016/B978-0-12-800720-4.09991-8.

[206] Agrawal, A.; DeSoto, J.; Fullagar, J. L.; Maddali, K.; Rostami, S.; Richman, D. D.; Pommier, Y.; Cohen, S. M. Probing Chelation Motifs in HIV Integrase Inhibitors. *Proc. Natl. Acad. Sci. U. S. A*. **2012**, *109* (7), 2251–2256. https://doi.org/10.1073/pnas.1112389109.

[207] Lin, S.; Liu, C.; Zhao, X.; Han, X.; Li, X.; Ye, Y.; Li, Z. Recent Advances of Pyridinone in Medicinal Chemistry. *Front. Chem*. **2022**, *10*. https://doi.org/10.3389/fchem.2022.869860.

[208] Jiang, X.; Zhou, T.; Bai, R.; Xie, Y. Hydroxypyridinone-Based Iron Chelators with Broad-Ranging Biological Activities. *J. Med. Chem*. **2020**, *63* (23), 14470–14501. https://doi.org/10.1021/acs.jmedchem.0c01480.

[209] Khan, N.; Chen, X.; Geiger, J. D. Role of Divalent Cations in HIV-1 Replication and Pathogenicity. *Viruses* **2020**, *12* (4), 471. https://doi.org/10.3390/v12040471.

[210] Xiao, M.; Li, H.; Wang, Y.; Wang, X.; Wang, W.; Peng, J.; Chen, J.; Li, B. Characterization of the N-Terminal Domain of Classical Swine Fever Virus RNA-Dependent RNA Polymerase. *J. Gen. Virol.* **2006**, *87* (2), 347–356. https://doi.org/10.1099/vir.0.81385-0.

[211] Dias, A.; Bouvier, D.; Crépin, T.; McCarthy, A. A.; Hart, D. J.; Baudin, F.; Cusack, S.; Ruigrok, R. W. H. The Cap-Snatching Endonuclease of Influenza Virus Polymerase Resides in the PA Subunit. *Nature* **2009**, *458* (7240), 914–918. https://doi.org/10.1038/nature07745.

[212] Debnath, U.; Verma, S.; Jain, S.; Katti, S. B.; Prabhakar, Y. S. Pyridones as NNRTIs against HIV-1 Mutants: 3D-QSAR and Protein Informatics. *J. Comput. Aided Mol. Des.* **2013**, *27* (7), 637–654. https://doi.org/10.1007/s10822-013-9667-1.

[213] Andayi, W. A.; Egan, T. J.; Gut, J.; Rosenthal, P. J.; Chibale, K. Synthesis, Antiplasmodial Activity, and β-Hematin Inhibition of Hydroxypyridone–Chloroquine Hybrids. *ACS Med. Chem. Lett*. **2013**, *4* (7), 642–646. https://doi.org/10.1021/ml4001084.

[214] Zhang, Y.; Luo, M.; Wu, P.; Wu, S.; Lee, T.-Y.; Bai, C. Application of Computational Biology and Artificial Intelligence in Drug Design. *Int. J. Mol. Sci.* **2022,** *23* (21), 13568. https://doi.org/10.3390/ijms232113568.

[215] Brogi, S.; Ramalho, T. C.; Kuca, K.; Medina-Franco, J. L.; Valko, M. Editorial: In Silico Methods for Drug Design and Discovery. *Front. Chem*. **2020**, *8*. https://doi.org/10.3389/fchem.2020.00612.

[216] Shaker, B.; Ahmad, S.; Lee, J.; Jung, C.; Na, D. In Silico Methods and Tools for Drug Discovery. *Comput. Biol. Med*. **2021**, *137* (104851), 104851. https://doi.org/10.1016/j.compbiomed.2021.104851.

[217] N'Da, D. D.; Smith, P. J. Synthesis, in Vitro Antiplasmodial and Antiproliferative Activities of a Series of Quinoline–Ferrocene Hybrids. *Med. Chem. Res.* **2014**, *23* (3), 1214–1224. https://doi.org/10.1007/s00044-013-0748-4.

[218] Egan, T. J. Haemozoin (Malaria Pigment): A Unique Crystalline Drug Target. *TARGETS* **2003**, *2* (3), 115–124. https://doi.org/10.1016/s1477-3627(03)02310-9.

[219] Chang, Y.; Hawkins, B. A.; Du, J. J.; Groundwater, P. W.; Hibbs, D. E.; Lai, F. A Guide to in Silico Drug Design. *Pharmaceutics* **2022**, *15* (1), 49. https://doi.org/10.3390/pharmaceutics15010049.

[220] Dhamane, M. V.; Dhakane, P. A.; Merekar, S. A. In Silico Methods for Drug Designing and Drug Discovery. *World J. Pharm. Med. Res.* **2023**, *9* (5), 170-178

[221] Jia, C.-Y.; Li, J.-Y.; Hao, G.-F.; Yang, G.-F. A Drug-Likeness Toolbox Facilitates ADMET Study in Drug Discovery. *Drug Discov. Today* **2020**, *25* (1), 248–258. https://doi.org/10.1016/j.drudis.2019.10.014.

[222] Mishra, S.; Dahima, R. In-Vitro ADME Studies of TUG-891, a GPR-120 Inhibitor Using Swiss ADME Predictor. *J. Drug Delivery Ther*. **2019**, *9* (2-s), 266-369. Available online: http://jddtonline.info.

[223] Veber, D. F.; Johnson, S. R.; Cheng, H.-Y.; Smith, B. R.; Ward, K. W.; Kopple, K. D. Molecular Properties That Influence the Oral Bioavailability of Drug Candidates. *J. Med. Chem*. **2002**, *45* (12), 2615–2623. https://doi.org/10.1021/jm020017n.

[224] Vinarov, Z.; Abdallah, M.; Agundez, J. A. G.; Allegaert, K.; Basit, A. W.; Braeckmans, M.; Ceulemans, J.; Corsetti, M.; Griffin, B. T.; Grimm, M *et al.,* Impact of Gastrointestinal Tract Variability on Oral Drug Absorption and Pharmacokinetics: An UNGAP Review. *Eur. J. Pharm. Sci.* **2021**, *162* (105812), 105812. https://doi.org/10.1016/j.ejps.2021.105812.

[225] Lobo, S. Is There Enough Focus on Lipophilicity in Drug Discovery? *Expert Opin. Drug Discov.* **2020**, *15* (3), 261–263. https://doi.org/10.1080/17460441.2020.1691995.

[226] Gallego, R. A.; Edwards, M. P.; Montgomery, T. P. An Update on Lipophilic Efficiency as an Important Metric in Drug Design. *Expert Opin. Drug Discov.* **2024**, *19* (8), 917–931. https://doi.org/10.1080/17460441.2024.2368744.

[227] Sluga, J.; Venko, K.; Drgan, V.; Novič, M. QSPR Models for Prediction of Aqueous Solubility: Exploring the Potency of Randić-Type Indices. *Croat. Chem. Acta* **2020**, *93* (4). https://doi.org/10.5562/cca3776.

[228] Sorkun, M. C.; Khetan, A.; Er, S. AqSolDB, a Curated Reference Set of Aqueous Solubility and 2D Descriptors for a Diverse Set of Compounds. *Sci. Data* **2019**, *6* (1). https://doi.org/10.1038/s41597-019-0151-1.

[229] Sareen, S.; Joseph, L.; Mathew, G. Improvement in Solubility of Poor Water-Soluble Drugs by Solid Dispersion. *Int. J. Pharm. Investig.* **2012**, *2* (1), 12. https://doi.org/10.4103/2230-973x.96921.

[230] Scheler, S.; Fahr, A.; Liu, X. Linear Combination Methods for Prediction and Interpretation of Drug Skin Permeation. *ADMET DMPK* **2015**, *2* (4). https://doi.org/10.5599/admet.2.4.147.

[231] European Food Safety Authority (EFSA); Buist, H.; Craig, P.; Dewhurst, I.; Hougaard Bennekou, S.; Kneuer, C.; Machera, K.; Pieper, C.; Court Marques, D.; Guillot, G.; Ruffo, F.; Chiusolo, A. Guidance on Dermal Absorption. *EFSA J.* **2017,** *15* (6). https://doi.org/10.2903/j.efsa.2017.4873.

[232] Daina, A.; Zoete, V. A BOILED-Egg to Predict Gastrointestinal Absorption and Brain Penetration of Small Molecules. *ChemMedChem* **2016**, *11* (11), 1117–1121. https://doi.org/10.1002/cmdc.201600182.

[233] Orrego-Lagarón, N.; Martínez-Huélamo, M.; Vallverdú-Queralt, A.; Lamuela-Raventos, R. M.; Escribano-Ferrer, E. High Gastrointestinal Permeability and Local Metabolism of Naringenin: Influence of Antibiotic Treatment on Absorption and Metabolism. *Br. J. Nutr*. **2015**, *114* (2), 169–180. https://doi.org/10.1017/s0007114515001671.

[234] Wessler, J. D.; Grip, L. T.; Mendell, J.; Giugliano, R. P. The P-Glycoprotein Transport System and Cardiovascular Drugs. *J. Am. Coll. Cardiol*. **2013**, *61* (25), 2495–2502. https://doi.org/10.1016/j.jacc.2013.02.058.

[235] Daina, A.; Michielin, O.; Zoete, V. SwissADME: A Free Web Tool to Evaluate Pharmacokinetics, Drug-Likeness and Medicinal Chemistry Friendliness of Small Molecules. *Sci. Rep*. **2017**, *7* (1). https://doi.org/10.1038/srep42717.

[236] Bickerton, G. R.; Paolini, G. V.; Besnard, J.; Muresan, S.; Hopkins, A. L. Quantifying the Chemical Beauty of Drugs. *Nat. Chem*. **2012**, *4* (2), 90–98. https://doi.org/10.1038/nchem.1243.

[237] Ivanović, V.; Rančić, M.; Arsić, B.; Pavlović, A. Lipinski's Rule of Five, Famous Extensions, and Famous Exceptions. Chem. *Naissensis* **2023**, *3* (1), 171-177. https://doi.org/10.46793/chemn3.1.171i

[238] Halder, S. K.; Elma, F. In Silico Identification of Novel Chemical Compounds with Anti-TB Potential for the Inhibition of InhA and EthR from Mycobacterium Tuberculosis. *bioRxiv,* **2020.** https://doi.org/10.1101/2020.12.04.411967.

[239] Vlad, I. M.; Nuta, D. C.; Chirita, C.; Caproiu, M. T.; Draghici, C.; Dumitrascu, F.; Bleotu, C.; Avram, S.; Udrea, A. M.; Missir, A. V.; Marutescu, L. G.; Limban, C. In Silico and in Vitro Experimental Studies of New Dibenz[b,e]Oxepin-11(6H)One O-(Arylcarbamoyl)-Oximes Designed as Potential Antimicrobial Agents. *Molecules* **2020**, *25* (2), 321. https://doi.org/10.3390/molecules25020321.

[240] Craciun, D.; Modra, D.; Isvoran, A. ADME-Tox Profiles of Some Food Additives and Pesticides. *In AIP Conference Proceedings*; AIP Publishing LLC, **2015**.

[241] Ekins, S.; Mestres, J.; Testa, B. In Silico Pharmacology for Drug Discovery: Methods for Virtual Ligand Screening and Profiling. *Br. J. Pharmacol*. **2007**, *152* (1), 9–20. https://doi.org/10.1038/sj.bjp.0707305..

[242] Yadav, R.; Imran, M.; Dhamija, P.; Chaurasia, D. K.; Handu, S. Virtual Screening, ADMET Prediction and Dynamics Simulation of Potential Compounds Targeting the Main Protease of SARS-CoV-2. *J. Biomol. Struct. Dyn.* **2021**, *39* (17), 6617–6632. https://doi.org/10.1080/07391102.2020.1796812.

[243] Wang, H.; Wei, G. Introduction to Retrosynthesis: Strategies and Approaches. *E3S Web Conf.* **2023**, *385*, 04008. https://doi.org/10.1051/e3sconf/202338504008.

[244] Liu, L.; Zheng, J. Retrosynthesis-Introduction to the Analysis and Mechanism. *Applied and Computational Engineering* **2023**, *3* (1), 143–160. https://doi.org/10.54254/2755-2721/3/20230391.

[245] Fatima, G. N.; Paliwal, S. K.; Saraf, S. K. Synthesis and Antimicrobial Activity of Some Novel 7-Chloro-4-Aminoquinoline Derivatives. *Russ. J. Gen. Chem.* **2021**, *91* (2), 285–293. https://doi.org/10.1134/s1070363221020171..

[246] Thakur, A.; Gupta, P. R. S.; Pathak, P.; Kumar, A. Design, Synthesis, SAR, Docking

and Antibacterial Evaluation: Aliphatic Amide Bridged 4-Aminoquinoline Clubbed 1,2,4-Triazole Derivatives. *Int. J. ChemTech Res*. **2016**, *9* (3), 575-588.

[247] Bbosa, L. S. *Measurement of Impact Breakage Properties of Ore Particles Using a Series of Devices*; Master's Thesis, University of Cape Town, Department of Chemical Engineering, Faculty of Engineering and the Built Environment, **2007**. Available online: http://hdl.handle.net/11427/5346. (accessed 2024-08-05).

[248] Gutiérrez, J. E.; Fernandez-Moreira, E.; Rodríguez, M. A.; Mijares, M. R.; De Sanctis, J. B.; Gurská, S.; Džubák, P.; Hajdůch, M.; Bruno-Colmenarez, J.; Rojas, L *et al.,* Novel 7-Chloro-(4-Thioalkylquinoline) Derivatives: Synthesis and Antiproliferative Activity through Inducing Apoptosis and DNA/RNA Damage. *Pharmaceuticals (Basel)* **2022**, *15* (10), 1234. https://doi.org/10.3390/ph15101234.

[249] Kulkarni, A. A.; King, C.; Butcher, R. J.; Fortunak, J. M. D. 4,7-Dichloroquinoline. *Acta Crystallogr. Sect. E Struct. Rep. Online* **2012**, *68* (5), o1498–o1498. https://doi.org/10.1107/s1600536812014924.

[250] Babij, N. R.; McCusker, E. O.; Whiteker, G. T.; Canturk, B.; Choy, N.; Creemer, L. C.; Amicis, C. V. D.; Hewlett, N. M.; Johnson, P. L.; Knobelsdorf, J. A *et al.,* NMR Chemical Shifts of Trace Impurities: Industrially Preferred Solvents Used in Process and Green Chemistry. *Org. Process Res. Dev*. **2016**, *20* (3), 661–667. https://doi.org/10.1021/acs.oprd.5b00417.

[251] Um, I.-H.; Hong, J.-Y.; Kim, J.-J.; Chae, O.-M.; Bae, S.-K. Regioselectivity and the Nature of the Reaction Mechanism in Nucleophilic Substitution Reactions of 2,4-Dinitrophenyl X-Substituted Benzenesulfonates with Primary Amines. *J. Org. Chem.* **2003**, *68* (13), 5180–5185. https://doi.org/10.1021/jo034190i.

[252] Dehkordi, L. S.; Liu, Z. D.; Hider, R. C. Basic 3-Hydroxypyridin-4-Ones: Potential Antimalarial Agents. *Eur. J. Med. Chem.* **2008**, *43* (5), 1035–1047. https://doi.org/10.1016/j.ejmech.2007.07.011.

[253] Mohs, R. C.; Greig, N. H. Drug Discovery and Development: Role of Basic Biological Research. *Alzheimers Dement. (N. Y.)* **2017**, *3* (4), 651–657. https://doi.org/10.1016/j.trci.2017.10.005.

[254] Bioassay and its types. Pharmastate.academy. https://pharmastate.academy/courses/bioassay-and-its-types/ (accessed 2024-08-05).

[255] Panuganti, S. J. Principles Involved in Bioassay by Different Methods: A Mini-Review. *Res. Rev.: Res. J. Biol*. **2015**, *3* (2), 1–18.

[256] Indrayanto, G.; Putra, G. S.; Suhud, F. Validation of In-Vitro Bioassay Methods: Application in Herbal Drug Research. In *Profiles of Drug Substances, Excipients and Related Methodology*; Elsevier, **2021**; 273–307.

[257] Medina-Cleghorn, D.; Nomura, D. K. Exploring Metabolic Pathways and Regulation through Functional Chemoproteomic and Metabolomic Platforms. *Chem. Biol.* **2014**, *21* (9), 1171–1184. https://doi.org/10.1016/j.chembiol.2014.07.007.

[258] Berrouet, C.; Dorilas, N.; Rejniak, K. A.; Tuncer, N. Comparison of Drug Inhibitory Effects (IC_{50}) in Monolayer and Spheroid Cultures. *Bull. Math. Biol.* **2020**, *82* (6), 1–18. https://doi.org/10.1007/s11538-020-00746-7

[259] Nordin, M. L.; Abdul Kadir, A.; Zakaria, Z. A.; Abdullah, R.; Abdullah, M. N. H. In Vitro Investigation of Cytotoxic and Antioxidative Activities of Ardisia Crispa against Breast Cancer Cell Lines, MCF-7 and MDA-MB-231. *BMC Complement. Altern. Med.* **2018**, *18* (1). https://doi.org/10.1186/s12906-018-2153-5.

[260] B. A. Coull and L. M. Ryan, “Biological Assay,” *Encycl. Environmetrics*, **2012**. https://doi.org/10.1002/9780470057339.vab015.

[261] Rosso, A. Statistical Analysis of Experimental Designs Applied to Biological Assays, 2010, pp. 1–42.

[262] Yu, B.; Yang, H. Evaluation of Different Estimation Methods for Accuracy and Precision in Biological Assay Validation. PDA J. *Pharm. Sci. Technol*. **2017**, *71* (4), 297–305. https://doi.org/10.5731/pdajpst.2016.007088.

[263] Ramirez, C. N.; Antczak, C.; Djaballah, H. Cell Viability Assessment: Toward Content-Rich Platforms. *Expert Opin. Drug Discov*. **2010**, *5* (3), 223–233. https://doi.org/10.1517/17460441003596685.

[264] Buckner, C. A.; Lafrenie, R. M.; Dénommée, J. A.; Caswell, J. M.; Want, D. A.; Gan, G. G.; Leong, Y. C.; Bee, P. C.; Chin, E.; Teh, A. K. H et al., We Are IntechOpen, the World’s Leading Publisher of Open Access Books Built by Scientists, for Scientists. In Advanced Biometric Technologies; IntechOpen, **2016**, 1, p. 13. Available online: https://www.intechopen.com/books/advanced-biometric-technologies/liveness-detection-in-biometrics.

[265] Ghasemi, M.; Turnbull, T.; Sebastian, S.; Kempson, I. The MTT Assay: Utility, Limitations, Pitfalls, and Interpretation in Bulk and Single-Cell Analysis. *Int. J. Mol. Sci.* **2021**, *22* (23), 12827. https://doi.org/10.3390/ijms222312827.

[266] Hammerstein, A. F.; Wylie, P. G. Accurate Cytotoxicity and Proliferation Determination: Advantages of a High-Throughput Phenotypic Approach over ATP Luminescence Assays. *Assay Drug Dev. Technol*. **2016**, *14* (7), 407–415. https://doi.org/10.1089/adt.2016.735.

[267] Xing, J.-Y.; Song, G.-P.; Deng, J.-P.; Jiang, L.-Z.; Xiong, P.; Yang, B.-J.; Liu, S.-S. Antitumor Effects and Mechanism of Novel Emodin Rhamnoside Derivatives against Human Cancer Cells in Vitro. *PLoS One* **2015**, *10* (12), e0144781. https://doi.org/10.1371/journal.pone.0144781.

[268] Becit, M.; Aydın Dilsiz, S.; Başaran, N. Interaction of Curcumin on Cisplatin Cytotoxicity in HeLa and HepG2 Carcinoma Cells. *Istanb. J. Pharm*. **2020**, *50* (3). https://doi.org/10.26650/istanbuljpharm.2020.0039.

[269] Strober, W. Trypan Blue Exclusion Test of Cell Viability. *Curr. Protoc. Immunol.* **2015**, *111* (1). https://doi.org/10.1002/0471142735.ima03bs111.

[270] Wan, C. P.; Sigh, R. V.; Lau, B. H. S. A Simple Fluorometric Assay for the Determination of Cell Numbers. *J. Immunol. Methods* **1994**, *173* (2), 265–272. https://doi.org/10.1016/0022-1759(94)90305-0.

[271] Sapan, C. V.; Lundblad, R. L.; Price, N. C. Colorimetric Protein Assay Techniques. *Biotechnol. Appl. Biochem.* **1999**, *29* (2), 99-108.

[272] Riss, T. L.; Moravec, R. A.; Niles, A. L.; Duellman, S.; Benink, H. A.; Worzella, T. J.; Minor, L. Cell Viability Assays; Eli Lilly & Company and the National Center for Advancing Translational Sciences, **2016**. Available online: https://www.ncbi.nlm.nih.gov/books/NBK144065/

[273] Genotoxicity - A Predictable Risk to Our Actual World. InTech July 11, **2018.** https://doi.org/10.5772/intechopen.69556.

[274] Supino, R. MTT Assays. In In Vitro Toxicity Testing Protocols; Humana Press: Totowa, NJ, **1995**; 137–149.

[275] Sigmaaldrich.com. https://www.sigmaaldrich.com/deepweb/assets/sigmaaldrich/product/documents/191/466/11465007001.pdf (accessed 2024-08-06).

[276] Stemcell.com.https://www.stemcell.com/clonacell-hy-96-well-plate-protocol.html,%E2%80%9D%20p.%202023,%202023. (accessed 2024-08-06).

[277] Vanderbilt.edu. https://www.vanderbilt.edu/viibre/CellCultureBasicsEU.pdf (accessed

2024-08-06).

[278] Gold, J. M.; Raja, A. Cisplatin; StatPearls Publishing, **2023**. (222) 1–9

[279] Ma, H. Hela Cells and Immortality. *Cancer Biology* **2017**, *7*(3), 71–78. ISSN: 2150-1041 (print); ISSN: 2150-105X (online). Available at http://www.cancerbio.net. https://doi.org/10.7537/marscbj070317.11.

[280] Saghaie, L.; Sadeghi-Aliabadi, H.; Ashaehshoar, M. Synthesis, Analysis, and Cytotoxic Evaluation of Some Hydroxypyridinone Derivatives on HeLa and K562 Cell Lines. *Res. Pharm. Sci*. **2013**, *8* (3), 185-195.

[281] Arzumanian, V. A.; Kiseleva, O. I.; Poverennaya, E. V. The Curious Case of the HepG2 Cell Line: 40 Years of Expertise. *Int. J. Mol. Sci.* **2021**, *22* (23), 13135. https://doi.org/10.3390/ijms222313135.

[282] Schulz, C.; Kammerer, S.; Küpper, J. H. NADPH-Cytochrome P450 Reductase Expression and Enzymatic Activity in Primary-Like Human Hepatocytes and HepG2 Cells for In Vitro Biotransformation Studies. *Clin. Hemorheol. Microcirc.* **2019**, *73* (1), 249-260. https://doi.org/10.3233/CH-199226.

[283] Gaikwad, S. Y.; Phatak, P.; Mukherjee, A. Cutting-Edge Strategies for Screening of Novel Anti-HIV Drug Candidates against HIV Infection: A Concise Overview of Cell-Based Assays. *Heliyon* **2023**, *9* (5), e16027. https://doi.org/10.1016/j.heliyon.2023.e16027.

[284] Morozov, V.; Lagaye, S.; Morozov, A. The TZM-bl Reporter Cell Line Expresses Kynureninase That Can Neutralize 2F5-Like Antibodies in the HIV-1 Neutralization Assay. *Int. J. Mol. Sci*. **2022**, *23* (2), 641. https://doi.org/10.3390/ijms23020641.

[285] Alluri, S. S.; Ganguly, A. K. Design and Synthesis of HIV-1 Protease Inhibitors. In *Frontiers in Clinical Drug Research - HIV*; BENTHAM SCIENCE PUBLISHERS, **2019**; 1–33. https://doi.org/10.2174/9781681085265119040003

[286] Wang, Y.; Lv, Z.; Chu, Y. HIV Protease Inhibitors: A Review of Molecular Selectivity and Toxicity. *HIV AIDS (Auckl.)* **2015**, *95*. https://doi.org/10.2147/hiv.s79956.

[287] Ghosh, A. K.; Osswald, H. L.; Prato, G. Recent Progress in the Development of HIV-1 Protease Inhibitors for the Treatment of HIV/AIDS. *J. Med. Chem.* **2016**, *59* (11), 5172–5208. https://doi.org/10.1021/acs.jmedchem.5b01697.

[288] Holec, A. D.; Mandal, S.; Prathipati, P. K.; Destache, C. J. Nucleotide Reverse Transcriptase Inhibitors: A Thorough Review, Present Status and Future Perspective

as HIV Therapeutics. *Curr. HIV Res.* **2018**, *15* (6). https://doi.org/10.2174/1570162x1566617112011.

[289] Ercan, S.; Şenyiğit, B.; Şenses, Y. Dual Inhibitor Design for HIV-1 Reverse Transcriptase and Integrase Enzymes: A Molecular Docking Study. *J. Biomol. Struct. Dyn.* **2020**, *38* (2), 573–580. https://doi.org/10.1080/07391102.2019.1700166.

[290] Bastos, M. M.; Costa, C. C. P.; Bezerra, T. C.; da Silva, F. de C.; Boechat, N. Efavirenz a Nonnucleoside Reverse Transcriptase Inhibitor of First-Generation: Approaches Based on Its Medicinal Chemistry. *Eur. J. Med. Chem.* **2016**, *108*, 455–465. https://doi.org/10.1016/j.ejmech.2015.11.025.

[291] Dharmaratne, H.; Wanigasekera, W.; Mata-Greenwood, E.; Pezzuto, J. Inhibition of Human Immunodeficiency Virus Type 1 Reverse Transcriptase Activity by Cordatolides Isolated fromCalophyllum Cordato-Oblongum. *Planta Med.* **1998**, *64* (05), 460–461. https://doi.org/10.1055/s-2006-957483.

[292] Wang, Y.; De Clercq, E.; Li, G. Current and Emerging Non-Nucleoside Reverse Transcriptase Inhibitors (NNRTIs) for HIV-1 Treatment. *Expert Opin. Drug Metab. Toxicol.* **2019**, *15* (10), 813–829. https://doi.org/10.1080/17425255.2019.1673367.

[293] Sigmaaldrich.com. https://www.sigmaaldrich.com/deepweb/assets/sigmaaldrich/product/documents/380/565/11468120910.pdf **2020**. 1–18 (accessed 2024-08-06).

[294] Cada, D. J.; Levien, T.; Baker, D. E. Emtricitabine. *Hosp. Pharm*. **2003**, *38* (12), 1151–1160. https://doi.org/10.1177/001857870303801206.

[295]Hiv.gov.https://clinicalinfo.hiv.gov/sites/default/files/guidelines/documents/adult-adolescent-arv/guidelines-adult-adolescent-arv.pdf (accessed 2024-08-06).

[296] Fda.gov. https://www.accessdata.fda.gov/drugsatfda_docs/pepfar/077411PI.pdf (accessed 2024-08-06).

[297] Man, A.; Chaichana, C.; Wicharuck, S.; Rinchumphu, D. Predicting Sunlight Availability for Vertical Shelves Using Simulation. *IOP Conf. Ser. Earth Environ. Sci.* **2022**, *1094* (1), 012011. https://doi.org/10.1088/1755-1315/1094/1/012011.

[298] Matsunaga, S.; Masaoka, T.; Sawasaki, T.; Morishita, R.; Iwatani, Y.; Tatsumi, M.; Endo, Y.; Yamamoto, N.; Sugiura, W.; Ryo, A. A Cell-Free Enzymatic Activity Assay for the Evaluation of HIV-1 Drug Resistance to Protease Inhibitors. *Front. Microbiol.* **2015**, *6*. https://doi.org/10.3389/fmicb.2015.01220.

[299] Mahdi, M.; Mótyán, J. A.; Szojka, Z. I.; Golda, M.; Miczi, M.; Tőzsér, J. Analysis of the Efficacy of HIV Protease Inhibitors against SARS-CoV-2′s Main Protease. *Virol. J.* **2020**, *17* (1). https://doi.org/10.1186/s12985-020-01457-0.

[300] Hilton, B. J.; Wolkowicz, R. An Assay to Monitor HIV-1 Protease Activity for the Identification of Novel Inhibitors in T-Cells. *PLoS ONE* **2010**, *5* (6), e10940. https://doi.org/10.1371/journal.pone.0010940.

[301] Windsor, I. W.; Raines, R. T. Fluorogenic Assay for Inhibitors of HIV-1 Protease with Sub-Picomolar Affinity. *Sci. Rep*. **2015**, *5* (1). https://doi.org/10.1038/srep11286.

[302] Jones, M. B. *Disarming a Deadly Virus: Proteases and Their Inhibitors*; National Academy of Sciences: February **2000.**

[303] (239) Hosseinzadeh, E.; Banaee, N.; Nedaie, H. A. Cancer and Treatment Modalities. *Curr. Cancer Ther. Rev.* **2017**, *13* (1). https://doi.org/10.2174/1573394713666170531081818.

[304] Bonavida, B.; Khineche, S.; Huertayepez, S.; Garban, H. Therapeutic Potential of Nitric Oxide in Cancer. *Drug Resist. Updat*. **2006**, *9* (3), 157–173. https://doi.org/10.1016/j.drup.2006.05.003.

[305] Anggraini, T.; Wilma, S.; Syukri, D.; Azima, F. Total Phenolic, Anthocyanin, Catechins, DPPH Radical Scavenging Activity, and Toxicity of Lepisanthes Alata (Blume) Leenh. *Int. J. Food Sci*. **2019**, *2019*, 1–7. https://doi.org/10.1155/2019/9703176.

[306] Chekuri, S.; Arunjyothi, B.; Anupalli, R. R. Radical Scavenging Activity (2,2-Diphenyl-1-Picrylhydrazyl) of Acalypha Indica Linn. (Euphorbiaceae Family). *Int. J. Pharm. Sci. Res*. **2018**, *9* (1), 313. https://doi.org/10.13040/IJPSR.0975-8232.9(1).313-17.

[307] Lalhminghlui, K.; Jagetia, G. C. Evaluation of the Free-Radical Scavenging and Antioxidant Activities of Chilauni, Schima wallichii Korth in Vitro. *Futur. Sci. OA* **2018**, *4* (2). https://doi.org/10.4155/fsoa-2017-0086.

[308] Lourenço, S. C.; Moldão-Martins, M.; Alves, V. D. Antioxidants of Natural Plant Origins: From Sources to Food Industry Applications. *Molecules* **2019**, *24* (22), 4132. https://doi.org/10.3390/molecules24224132.

[309] Santos, M. A.; Irto, A.; Buglyó, P.; Chaves, S. Hydroxypyridinone-Based Metal Chelators towards Ecotoxicity: Remediation and Biological Mechanisms. *Molecules* **2022**, *27* (6), 1966. https://doi.org/10.3390/molecules27061966.

[310] Baartzes, N.; Stringer, T.; Smith, G. S. Targeting Sensitive-Strain and Resistant-Strain

Malaria Parasites through a Metal-Based Approach. In *Advances in Bioorganometallic Chemistry*; Elsevier, **2019**; 193–213.

[311] Maji, A. Drug Susceptibility Testing Methods of Antimalarial Agents. *Trop. Parasitol.* **2018**, *8* (2), 70. https://doi.org/10.4103/2229-5070.248695.

[312] Platten, J. D.; Cobb, J. N.; Zantua, R. E. Criteria for Evaluating Molecular Markers: Comprehensive Quality Metrics to Improve Marker-Assisted Selection. *PLoS One* **2019**, *14* (1), e0210529. https://doi.org/10.1371/journal.pone.0210529..

[313] Zhang, W.; Zhao, X. Y.; Wu, J.; Jin, L.; Lv, J.; Gao, B.; Liu, P. Screening and Verification of Molecular Markers and Genes Related to Salt-Alkali Tolerance in Portunus Trituberculatus. *Front. Genet*. **2022**, *13*. https://doi.org/10.3389/fgene.2022.755004.

[314] Kang, J.-S.; Lee, M.-H. Overview of Therapeutic Drug Monitoring. *Korean J. Intern. Med*. **2009**, *24* (1), 1. https://doi.org/10.3904/kjim.2009.24.1.1.

[315] Buzibye, A.; Musaazi, J.; von Braun, A.; Nanzigu, S.; Sekaggya-Wiltshire, C.; Kambugu, A.; Fehr, J.; Lamorde, M.; Gutteck, U.; Muller, D *et al.,* Antiretroviral Concentration Measurements as an Additional Tool to Manage Virologic Failure in Resource Limited Settings: A Case Control Study. *AIDS Res. Ther.* **2019**, *16* (1). https://doi.org/10.1186/s12981-019-0255-x.

[316] H. J. Huber and H. B. Mistry, “Explaining in-vitro to in-vivo efficacy correlations in oncology pre-clinical development via a semi-mechanistic mathematical model,” *J. Pharmacokinet. Pharmacodyn.* **2023***,* 7. https://doi.org/10.1007/s10928-023-09891-7.

[317] Palano, G.; Foinquinos, A.; Müllers, E. In Vitro Assays and Imaging Methods for Drug Discovery for Cardiac Fibrosis. *Front. Physiol*. **2021**, *12*. https://doi.org/10.3389/fphys.2021.697270.

[318] Price, E.; Gesquiere, A. J. Author Correction: An in Vitro Assay and Artificial Intelligence Approach to Determine Rate Constants of Nanomaterial-Cell Interactions. *Sci. Rep*. **2019**, *9* (1). https://doi.org/10.1038/s41598-019-56347-5.

[319] Nzila, A.; Mwai, L. In Vitro Selection of Plasmodium Falciparum Drug-Resistant Parasite Lines. *J. Antimicrob. Chemother*. **2010**, *65* (3), 390–398. https://doi.org/10.1093/jac/dkp449..

[320] Dale, T. Evaluation of Anti-Plasmodial Activity of UV2402MB Efficacy Report (Unpublished); H3D, University of Cape Town: February **2024**.

[321] Pandey, S.; Agarwal, P.; Srivastava, K.; RajaKumar, S.; Puri, S. K.; Verma, P.; Saxena,

J. K.; Sharma, A.; Lal, J.; Chauhan, P. M. S. Synthesis and Bioevaluation of Novel 4-Aminoquinoline-Tetrazole Derivatives as Potent Antimalarial Agents. *Eur. J. Med. Chem*. **2013**, 66, 69–81. https://doi.org/10.1016/j.ejmech.2013.05.023..

[322] Sigmaaldrich.com. https://www.sigmaaldrich.com/ZA/en/technical-documents/protocol/cell-culture-and-cell-culture-analysis/mammalian-cell-culture/thawing-of-frozen-cell-lines (accessed 2024-08-06).

[323] Long-term storage in liquid nitrogen: Should I keep frozen cells in the liquid phase or in the vapor phase?. Eppendorf.com. https://www.eppendorf.com/ca-en/lab-academy/life-science/cell-biology/long-term-storage-in-liquid-nitrogen-should-i-keep-frozen-cells-in-the-liquid-phase-or-in-the-vapor-phase/ (accessed 2024-08-06).

[324] Jin, Q.; Wu, J.; Wu, Y.; Li, H.; Finel, M.; Wang, D.; Ge, G. Optical Substrates for Drug-Metabolizing Enzymes: Recent Advances and Future Perspectives. *Acta Pharm. Sin. B*. **2022**, *12* (3), 1068–1099. https://doi.org/10.1016/j.apsb.2022.01.009.